Taking Artemisinin to Clinical Anticancer Applications: Design, Synthesis and Characterization of pH-responsive Artemisinin Dimer Derivatives in Lipid Nanoparticles

Yitong Zhang

A dissertation

submitted in partial fulfillment of the

requirements for the degree of

Doctor of Philosophy

University of Washington

2015

Reading Committee:

Tomikazu Sasaki, Chair

Rodney J.Y. Ho

Champak Chatterjee

Program Authorized to Offer Degree:
Chemistry

University of Washington

Abstract

Taking Artemisinin to Clinical Anticancer Applications:

Design, Synthesis and Characterization of pH-responsive Artemisinin Dimer Derivatives in Lipid Nanoparticles

Yitong Zhang

Chair of the Supervisory Committee:

Professor Tomikazu Sasaki

Chemistry

Abstract

Qinghaosu or Artemisinin is an active sesquiterpene lactone isolated from *Artemisia annua* L. The natural product and its derivatives are known as a first line treatment for malaria. Investigations have also reported that the compound exhibits anti-cancer activities both on cell lines and in animal models. The remarkably stable endoperoxide bridge under ambient conditions is believed to be responsible for the selectivity as well as potency against cells that are rich in iron content. Dimeric derivatives where two artemisinin units are covalently bonded through lactone carbon (C10) show superior efficacies against both malaria parasites and cancer cells. Artemisinin dimer succinate derivative demonstrates a 100-fold enhancement in potency, compared to the natural product, with IC_{50} values in the low micromolar range.

This work focuses on the development of artemisinin dimer derivatives to facilitate their clinical development. Novel pH-responsive artemisinin dimers were synthesized to enhance the aqueous solubility of the pharmacophore motif. Compounds with promising potency against human breast cancer cell lines were selected for lipid and protein based nanoparticle formulations for delivery of the derivatives without the need of organic co-solvents into animal models. To improve the efficiency in designing appropriate lipid-nanoparticles as drug delivery systems, a geometrical flit model based on the drug binding pocket hypothesis was introduced. Finally, to lay a foundation for understanding *in vivo* behaviors of artemisinin dimer derivatives and their nanoparticle formulations, the first analytical method for preparation of biological tissue samples and quantification of artemisinin dimer derivative using liquid chromatography-tandem mass spectrometry was developed.

Table of Contents

CHAPTER 1

CHAPTER 2

CHAPTER 3

CHAPTER 4

CHAPTER 5

CHAPTER 6

CHAPTER 7

CHAPTER 8

CHAPTER 9

CHAPTER 1

Introduction

Artemisinin: A Brief History and Overview

Artemisia annua L. is an annual plant that was first documented in the Wushi'er Bingfang of ancient China in 200 B.C[1]. The plant has long been used to treat fever[2] and malaria-associated symptoms[3] in Traditional Chinese Medicine remedies. The plant's active agent, Qinghaosu or Artemisinin (ART), was identified to be effective against malaria in the early 1970s[4]. While clinical studies in China soon began to validate the efficacy and safety of the active compound, the West did not start to adopt the idea of artemisinin being highly specific and effective for treating malaria until a decade later[5]. In the late 1970s, a number of multicenter clinical trials were completed in China, involving 2,255 cases of malarial infections with impressive results. The World Health Organization (WHO) was intrigued by the data presented by Dr. Tu in 1981, but it was not until 2006 that the WHO finally modified its guidelines to recommend artemisinin as a first line treatment, as monotherapy and later combinational therapy with chloroquine, against malaria parasites[5, 6] after studies in Thailand and Vietnam confirmed the high potency and low toxicity of the drug.

While the natural product could be obtained from the plant at between 0.25-3% of dry mass weight[7], investigations were carried out to improve the chemical-physical properties of the molecule for enhanced bioavailability after administration. During this time, several derivatives of ART were also synthesized to improve the efficacy of the compound. One notable derivative is artesunate, a water-soluble derivative that allows intravenous administration of the compound to allow rapid and effective delivery of the active drug into blood[5, 8]. Other monomeric derivatives that have also been applied clinically include dihydroartemisinin, artemether and artemisone[9].

ART-based anti-malarial drugs have excellent safety profiles[10] while demonstrating extraordinary activity. Lai et al reported that rats could be dosed with 8 mg/kg/day of artemisinin

mixed in food for 40 weeks without any adverse effects[11]. In 2003, Posner et al reported that malaria in a mouse model can be cured with a single dose of an ART-dimer derivative [12]. Mechanistically, the specificity of ART is attributed to the endoperoxide bridge (R-O-O-R') of the sequiterpene lactone, and the labile O-O sigma bond is believed to be required for its anti-malarial activity[13, 14]. Malaria parasites digest hemoglobin as a carbon source, and accumulate a large amount of heme iron [15]. When ART encounters heme iron, the endoperoxide group undergoes homolysis, and decomposes to form carbon-based free radicals. These carbon-based radicals, when formed within a malaria parasite, alkylate proteins and lipids and can lead to cellular damage and cell death[14, 16]. Cancer cells grow quickly and uncontrollably. The increased metabolism means enhanced intracellular heme content and thus allowing for selectivity of ART derivatives[17].

While the world slowly came to know artemisinin as a malarial chemotherapy, a number of scientists also explored the anti-cancer effects observed with artemisinins. Since the late 1980s, numerous studies have suggested anti-proliferative, anti-angiogenic and anti-inflammatory properties of artemisinin-derived compounds[18]. Among the artemisinin derivatives, Posner's ART-isobutylene dimers, with two artemisinin motifs linked at the C10 position spaced by 3 carbons, have been shown to be more potent than their monomeric analogues against various types of human cancer cell lines[19]. Artemisinin dimer succinate, for example, is over 100 fold more potent than its monomer analogue, Artesunate, against a panel of human breast cancer cell lines (mean $LogGI_{50}$ of -7.01[20] and -4.7[21] respectively).

While artemisinin dimer derivatives have been shown to possess activity against malaria parasites *in vivo* and rodent xenograft tumor models[22], limited solubility and bioavailability pose challenges for this class of hydrophobic compounds for clinical development. Limited water

solubility of the drug often requires an organic co-solvent, such as DMSO, as a delivery vehicle. Organic solvents, however, are not suitable for use in parenteral dosage forms in human at high concentrations. Thus, to develop dosage forms of artemisinin dimers that will not require co-solvents that cause irritation and allow delivery of enough compounds to the disease site, one can turn to nanotechnology and seek biopolymer or synthetic polymer based nanoparticle formulations.

Since the early 1990s, nanoparticles (NPs) have drawn attention as drug delivery vehicles from researchers across multiple disciplines[23,24,25]. Association of artemisinin to nano- or microparticles has been shown to improve *in vitro* solubility and *in vivo* pharmacokinetic profiles[31]. The idea of a drug-loaded particle made with biomolecule or amphiphilic polymer material is: the increased solubility of the compounds can improve the bioavailability and pharmacokinetics of the loaded compound, both of which are crucial to the efficacy of the drug in the body[23, 26, 27]. When the size of the nanoparticles is under 200 nm, these carriers, circulating in blood, can pass through the blood microvasculature into the tumor sites due to the enhanced permeability and retention (EPR) effect and accumulate to form a microresevior of the anti-tumor agent at the local site[23, 28]. The fate of the nanoparticle-bound drugs after administration depends on the route by which they are given. When injected intravenously, 100% of the drug becomes immediately available in the blood and circulates throughout body until extravasated via EPR effect or metabolized and cleared from the body[32]. On the other hand, to target the lymphatic system, where metastatic cancer cells tend to reside and travel through, subcutaneous administration may be employed[33].

To achieve the promised advantages of nanoparticle drug delivery systems, several factors should be considered, namely the material of choice, the size range of the particles – dependent

on targeted organ, and ability of the particles to load and release drug molecules[25, 27, 29, 30]. Biomolecules represent one of the most suitable groups of material for nanoparticle delivery system formulations, due to their biocompatibility as well as ease of degradation inside a living system[34]. Lipid nanoparticles are among the more mature and most commonly utilized drug delivery systems to serve such purposes, with a number of commercialized products[35]. One example for anti-cancer therapy is Doxil®, a liposome formulation of the chemotherapeutic compound doxorubicin, showed reduced cardiotoxicity and uncompromised efficacy, thus widening the therapeutic window compared to the free drug[36]. Liposome nanoparticles are characterized by an intact lipid membrane that encloses an internal aqueous compartment. Because of this unique structure, liposomes are especially attractive as a drug delivery system for combinational therapy development.

A second class of biomolecules that recently caught attention is protein-based nanoparticles. Abraxane®, a serum albumin-bound paclitaxel aggregate was recently approved by the FDA to treat a number cancers including breast cancer, lung cancer and pancreatic cancer[30, 37-39]. Protein-based nanoparticles can be degraded by proteases present in lysosomes of cells or in appropriate biological milieu, and thus releasing the loaded therapeutic[38]. Unmodified protein aggregates form when hydrophobic compounds are bound to hydrophobic pockets of the proteins under slightly denaturing conditions to help "staple" the small units together[39, 40]. These proteins behave much like micelles, which fall apart into the smaller units carrying drug molecules once diluted in high protein-content medium such as blood. Surface modification after during or after preparation of these protein nanoparticles may help to improve the stability, but may also retard the degradation of the particle and thus release of the drug molecule.

Loading of therapeutics into nanoparticles are largely dependent on the physical-chemical properties of the compound of interest and the vehicle. Commonly explored properties include hydrophobicity, charge and labile bonds. In terms of release, much of recent literature has focused on stimuli-responsive release of cargo from nanoparticle systems. External factors that trigger release include pH or temperature change, or application of electricity, light or ultrasound[41]. All of these mechanisms require a built-in chemical moiety that is sensitive to the applied stimuli. In context of a pH-dependent releasing nanoparticle, for instance, a pH-responsive polymer material or drug compound that is able to destabilize particle formation is required to achieve disintegration of the particles under the desired condition[42].

The challenge with the present investigational efforts in bringing artemisinin dimer derivatives into clinical anti-cancer applications is their poor aqueous solubility. To the best of our knowledge, no systematic study has been carried out to develop injectable dosage forms of ART dimer derivatives, nor are there methods for quantification of the *in vivo* concentrations of the molecules to shed light on their pharmacokinetic behaviors. Thus, in this work, efforts were made to advance the development of artemisinin dimer derivatives toward clinical anti-cancer applications.

To install a switch that allows stimuli-responsive solubility of artemisinin dimers, novel classes of artemisinin dimers that possess pH-dependent aqueous solubility profile are synthesized. The most potent compounds, tested by cell cytotoxicity assay against human breast cancer cell lines, are selected for development of nanoparticle formulations for delivery of the compounds to biological milieu without irritating co-solvents. We demonstrate with a pH-responsive artemisinin dimer-Lipid nanoparticle formulation and a fluorescent artemisinin dimer bodipy-

albumin nanoparticle formulation, that these natural product derivatives are potent against mice human breast cancer xenograft models.

Furthermore, in optimization of liposomal formulation design, we propose a hydrophobic drug binding pocket hypothesis that can be used for rational design of lipid composition to give enhanced drug retention and minimized nonspecific drug release. The model advocates the geometrical complementarity of the drug binding pocket to 3-dimensional structures of the drug molecules. The validated hypothesis and design model may potentially improve the success rates of advancing hydrophobic small molecule drugs into clinical applications.

Finally, to gain insight into the *in vivo* pharmacokinetic behaviors of the artemisinin dimers or nanoparticle forms of these derivatives, we describe the first sample preparation and analytical method for quantifying ART dimer-NP from biological tissues. We demonstrate good sensitivity, selectivity and reproducibility of the assay in a number of tissues including rat whole blood, solid tumor, liver and brain. The analytical method described in this thesis can be adapted to similar artemisinin dimer derivatives and help to gain a deeper understanding of the class of compound as cancer chemotherapy.

Reference

1. Harper, D. J., *Early Chinese Medical Literature: The Mawangdui Medical Manuscripts*. Kegan Paul International: London and New York, 1998; Ferreira, J. F. S. In *Artemisia annua L.: The hope against malaria and cancer.* , Proceedings of the 2nd Annual Symposium, Appalachian Opportunities, Medicinal and Aromatic Plants: Production, Business & Applications., Mountain State University/USDA, ARS, Appalachian Farming Systems Research Center, Mountain State University/USDA, ARS, Appalachian Farming Systems Research Center, **2004**; pp 56-61.

2. Klayman, D. L., Qinghaosu (Artemisinin) - An Antimalarial Drug from China. *Science* **1985,** *228* (4703), 1049-1055.

3. Wilcox, M.; Bodeker, G.; Bourdy, G.; Dhingra, V.; Falquet, J.; Ferreira, J.; Graz, B.; Hirt, H.; Hsu, E.; Melillo de Magalhaes, R.; Provendier, D.; Wright, C., *Artemisia annua* as a traditional herbal antimalarial. In *Traditional herbal medicines for modern times*, Wilcox, M.; Bodeker, G.; Rasoanaivo, P., Eds. CRC Press: Boca Raton, FL, **2004**; pp 43-60.

4. Miller, L. H.; Su, X. Z., Artemisinin: Discovery from the Chinese Herbal Garden. *Cell* **2011,** *146* (6), 855-858; Hsu, E., Reflections on the 'discovery' of the antimalarial qinghao. *British Journal of Clinical Pharmacology* **2006,** *61* (6), 666-670.

5. Maude, R. J.; Woodrow, C. J.; White, L. J., Artemisinin Antimalarials: Preserving the "Magic Bullet". *Drug Development Research* **2010,** *71* (1), 12-19.

6. White, N. J., Qinghaosu (Artemisinin): The price of success. *Science* **2008,** *320* (5874), 330-334.

7. Quennoz, M.; Bastian, C.; Simonnet, X.; Grogg, A. F., Quantification of the Total Amount of Artemisinin in Leaf Samples by Thin Layer Chromatography. *Chimia* **2010,** *64* (10), 755-757.

8. Dondorp, A. M.; Fanello, C. I.; Hendriksen, I. C. E.; Gomes, E.; Seni, A.; Chhaganlal, K. D.; Bojang, K.; Olaosebikan, R.; Anunobi, N.; Maitland, K.; Kivaya, E.; Agbenyega, T.; Nguah, S. B.; Evans, J.; Gesase, S.; Kahabuka, C.; Mtove, G.; Nadjm, B.; Deen, J.; Amumpaire, J. M.; Nansumba, M.; Karema, C.; Umulisa, N.; Uwimana, A.; Mokuolu, O. A.; Adedoyin, O. T.; Johnson, W. B. R.; Tshefu, A. K.; Onyamboko, M. A.; Sakulthaew, T.; Ngum, W. P.; Silamut, K.; Stepniewska, K.; Woodrow, C. J.; Bethell, D.; Wills, B.; Oneko, M.; Peto, T. E.; von Seidlein, L.; Day, N. P. J.; White, N. J.; Grp, A., Artesunate versus quinine in the treatment of severe falciparum malaria in African children (AQUAMAT): an open-label, randomised trial. *Lancet* **2010,** *376* (9753), 1647-1657.

9. Haynes, R. K., From artemisinin to new artemisinin antimalarials: Biosynthesis, extraction, old and new derivatives, stereochemistry and medicinal chemistry requirements. *Current Topics in Medicinal Chemistry* **2006,** *6* (5), 509-537.

10. Taylor, W. R. J.; White, N. J., Antimalarial drug toxicity - A review. *Drug Safety* **2004,** *27* (1), 25-61; Maude, R. J.; Plewes, K.; Faiz, M. A.; Hanson, J.; Charunwatthana, P.; Lee, S. J.; Taerning, J.; Bin Yunus, E.; Hoque, M. G.; Hasan, M. U.; Hossain, A.; Lindegardh, N.; Day, N. P. J.; White, N. J.; Dondorp, A. M., Does Artesunate Prolong the Electrocardiograph QT Interval in Patients with Severe Malaria? *American Journal of Tropical Medicine and Hygiene* **2009,** *80* (1), 126-132.

11. Lai, H.; Singh, N. P., Oral artemisinin prevents and delays the development of 7,12-dimethylbenz a anthracene (DMBA)-induced breast cancer in the rat. *Cancer Letters* **2006,** *231* (1), 43-48.

12. Posner, G. H.; Paik, I.-H.; Chang, W.; Borstnik, K.; Sinishtaj, S.; Rosenthal, A. S.; Shapiro, T. A., Malaria-infected mice are cured by a single dose of novel artemisinin derivatives. *Journal of Medicinal Chemistry* **2007,** *50* (10), 2516-2519.

13. Meshnick, S. R.; Taylor, T. E.; Kamchonwongpaisan, S., Artemisinin and the antimalarial endoperoxides: From herbal remedy to targeted chemotherapy. *Microbiological Reviews* **1996,** *60* (2), 301-+.

14. Meshnick, S. R., Artemisinin: mechanisms of action, resistance and toxicity. *International Journal for Parasitology* **2002,** *32* (13), 1655-1660.

15. Carter, M. D.; Hoang, A. N.; Wright, D. W., Hemozoin: A paradigm for biominerals in disease. *Wiley Encyclopedia of Chemical Biology* **2009,** *2*, 11; Meunier, B.; Robert, A., Heme as Trigger and Target for Trioxane-Containing Antimalarial Drugs. *Accounts of Chemical Research* **2010,** *43* (11); Weissbuch, I.; Leiserowitz, L., Interplay Between Malaria, Crystalline Hemozoin Formation, and Antimalarial Drug Action and Design. *Chemical Reviews* **2008,** *108* (11).

16. Haynes, R. K.; Cheu, K.-W.; N'Da, D.; Coghi, P.; Monti, D., Considerations on the Mechanism of Action of Artemisinin Antimalarials: Part 1-The 'Carbon Radical' and 'Heme' Hypotheses. *Infectious Disorders - Drug Targets* **2013,** *13* (4), 217-277.

17. Singh, N. P.; Lai, H. C., Artemisinin induces apoptosis in human cancer cells. *Anticancer Research* **2004,** *24* (4), 2277-2280; Zhang, S.; Gerhard, G. S., Heme Mediates Cytotoxicity from Artemisinin and Serves as a General Anti-Proliferation Target. *Plos One* **2009,** *4* (10).

18. Posner, G. H.; Ploypradith, P.; Parker, M. H.; O'Dowd, H.; Woo, S. H.; Northrop, J.; Krasavin, M.; Dolan, P.; Kensler, T. W.; Xie, S. J.; Shapiro, T. A., Antimalarial, antiproliferative, and antitumor activities of artemisinin-derived, chemically robust, trioxane dimers. *Journal of Medicinal Chemistry* **1999,** *42* (21), 4275-4280; Sun, W. C.; Han, J. X.; Yang, W. Y.; Deng, D. A.; Yue, X. F., Antitumor Activities of 4 Derivatives of Artemisic Acid and Artemisinin-B *in vitro*. *Acta Pharmacologica Sinica* **1992,** *13* (6), 541-543; Lai, H.; Singh, N. P., Selective Cancer Cell Cytotoxicity from Exposure to Dihydroartemisinin and Holotransferrin. *Cancer Letters* **1995,** *91* (1), 41-46.

19. Posner, G. H.; Northrop, J.; Paik, I. H.; Borstnik, K.; Dolan, P.; Kensler, T. W.; Xie, S.; Shapiro, T. A., New chemical and biological aspects of artemisinin-derived trioxane dimers. *Bioorganic & Medicinal Chemistry* **2002,** *10* (1), 227-232; Posner, G. H.; Paik, I. H.; Sur, S.; McRiner, A. J.; Borstnik, K.; Xie, S. J.; Shapiro, T. A., Orally active, antimalarial, anticancer, artemisinin-derived trioxane dimers with high stability and efficacy. *Journal of Medicinal Chemistry* **2003,** *46* (6), 1060-1065.

20. Posner, G. H.; Shapiro, T. A.; Sur, S.; Labonte, T.; Borstnik, K.; Paik, I.-H.; McRiner, A. J. Orally Active, Antimalarial, Anticancer, Artemisinin-derived Trioxane Dimers with High Selectively, Stability and Efficacy and Methods of Making the Same. 2006.

21. Efferth, T.; Dunstan, H.; Sauerbrey, A.; Miyachi, H.; Chitambar, C. R., The anti-malarial artesunate is also active against cancer. *International Journal of Oncology* **2001,** *18* (4), 767-773.

22. Posner, G. H.; McRiner, A. J.; Paik, I. H.; Sur, S.; Borstnik, K.; Xie, S. J.; Shapiro, T. A.; Alagbala, A.; Foster, B., Anticancer and antimalarial efficacy and safety of artemisinin-derived trioxane dimers in rodents. *Journal of Medicinal Chemistry* **2004,** *47* (5), 1299-1301; Singh, N. P.; Lai, H. C.; Park, J. S.; Gerhardt, T. E.; Kim, B. J.; Wang, S.; Sasaki, T., Effects of Artemisinin Dimers on Rat Breast Cancer Cells In Vitro and In Vivo. *Anticancer Research* **2011,** *31* (12), 4111-4114; Gao, N.; Budhraja, A.; Cheng, S.; Liu, E. H.; Huang, C.; Chen, J.; Yang, Z.; Chen, D.; Zhang, Z.; Shi, X., Interruption of the MEK/ERK signaling cascade promotes dihydroartemisinin-induced apoptosis in vitro and in vivo. *Apoptosis* **2011,** *16* (5), 511-523; Tan, W. F.; Shen, F.; Luo, X. J.; Su, C. Q.; Qiu, Z. Q.; Zeng, H. Z.; Yan, P. N.; Yu, Y.; Wu, M. C.; Jiang, X. Q.; Lau, W. Y., Artemisinin inhibits in vitro and in vivo invasion and metastasis of human hepatocellular carcinoma cells. *Phytomedicine* **2011,** *18* (2-3), 158-162.

23. Allen, T. M.; Cullis, P. R., Drug delivery systems: Entering the mainstream. *Science* **2004,** *303* (5665), 1818-1822.

24. Allen, T. M.; Cullis, P. R., Liposomal drug delivery systems: From concept to clinical applications. *Advanced Drug Delivery Reviews* **2013,** *65* (1), 36-48.

25. Kreuter, J., Nanoparticle-based Drug Delivery Systems. *Journal of Controlled Release* **1991,** *16* (1-2), 169-176.

26. Li, Y.; Wang, J.; Wientjes, M. G.; Au, J. L. S., Delivery of nanomedicines to extracellular and intracellular compartments of a solid tumor. *Advanced Drug Delivery Reviews* (0).

27. De Jong, W. H.; Borm, P. J. A., Drug delivery and nanoparticles: Applications and hazards. *International Journal of Nanomedicine* **2008,** *3* (2), 133-149.

28. *Medical Applications of Liposomes*. Elsevier Science B.V.: The Netherlands, 1998; p 779.

29. Bertrand, N.; Wu, J.; Xu, X. Y.; Kamaly, N.; Farokhzad, O. C., Cancer nanotechnology: The impact of passive and active targeting in the era of modern cancer biology. *Advanced Drug Delivery Reviews* **2014,** *66*, 2-25; Manzoor, A. A.; Lindner, L. H.; Landon, C. D.; Park, J. Y.; Simnick, A. J.; Dreher, M. R.; Das, S.; Hanna, G.; Park, W.; Chilkoti, A.; Koning, G. A.; ten Hagen, T. L. M.; Needham, D.; Dewhirst, M. W., Overcoming Limitations in Nanoparticle Drug Delivery: Triggered, Intravascular Release to Improve Drug Penetration into Tumors. *Cancer Research* **2012,** *72* (21), 5566-5575.

30. Dawidczyk, C. M.; Kim, C.; Park, J. H.; Russell, L. M.; Lee, K. H.; Pomper, M. G.; Searson, P. C., State-of-the-art in design rules for drug delivery platforms: Lessons learned from FDA-approved nanomedicines. *Journal of Controlled Release* **2014,** *187*, 133-144.

31. Chen, Y.; Lin, X.; Park, H.; Greever, R., Study of artemisinin nanocapsules as anticancer drug delivery systems. *Nanomedicine-Nanotechnology Biology and Medicine* **2009,** *5* (3), 316-322; Wang, S.; Wang, H.; Liang, W. Q.; Huang, Y. Z., An injectable hybrid nanoparticle-in-oil-in-water submicron emulsion for improved delivery of poorly soluble drugs. *Nanoscale Research Letters* **2012,** *7*, 7; Chadha, R.; Gupta, S.; Pathak, N., Artesunate-loaded chitosan/lecithin nanoparticles: Preparation, characterization, and in vivo studies. *Drug Development and Industrial Pharmacy* **2012,** *38* (12), 1538-1546; Isacchi, B.; Arrigucci, S.; la Marca, G.; Bergonzi, M. C.; Vannucchi, M. G.; Novelli, A.; Bilia, A. R., Conventional and long-circulating liposomes of artemisinin: preparation, characterization, and pharmacokinetic profile in mice. *Journal of Liposome Research* **2011,** *21* (3), 237-244.

32. Hacker, M.; Messer II, W. S.; Bachmann, K. A., *Pharmacology: Principles and Practice*. Academic Press: Burlington, MA USA, 2009.

33. Oussoren, C.; Zuidema, J.; Crommelin, D. J. A.; Storm, G., Lymphatic uptake and biodistribution of liposomes after subcutaneous injection: I. Influence of the anatomical site of injection. *Journal of Liposome Research* **1997,** *7* (1), 85-99.

34. Nagavarma, B.; Yadav, H. K. S.; Ayaz, A.; L.S., V.; H.G., S., Different Techniques for Preparation of Polymeric Nanopartiles - A Review. *Asian Journal of Pharmaceutical and Clinical Research* **2012,** *5* (3), 16-23; Kratz, F.; Warnecke, A., Finding the optimal balance: Challenges of improving conventional cancer chemotherapy using suitable combinations with nano-sized drug delivery systems. *Journal of Controlled Release* **2012,** *164* (2), 221-235.

35. *Liposomes: Rational Design*. Marcel Dekker, Inc: New York, USA, 1999; p 451.

36. Torchilin, V. P., Recent advances with liposomes as pharmaceutical carriers. *Nature Reviews Drug Discovery* **2005,** *4* (2), 145-160; Golla, K.; Cherukuvada, B.; Ahmed, F.; Kondapi, A. K., Efficacy, Safety and Anticancer Activity of Protein Nanoparticle-Based Delivery of Doxorubicin through Intravenous Administration in Rats. *Plos One* **2012,** *7* (12); Mohanraj, V.; Chen, Y., Nanoparticle - A Review. *Tropical Journal of Pharmaceutical Research* **2006,** *5* (1), 561-573; Immordino, M. L.; Dosio, F.; Cattel, L., Stealth liposomes: review of the basic science, rationale, and clinical applications, existing and potential. *International Journal of Nanomedicine* **2006,** *1* (3), 297-315.

37. Zhang, Z.; Mei, L.; Feng, S.-S., Paclitaxel drug delivery systems. *Expert Opinion on Drug Delivery* **2013,** *10* (3), 325-340.

38. Elsadek, B.; Kratz, F., Impact of albumin on drug delivery - New applications on the horizon. *Journal of Controlled Release* **2012,** *157* (1), 4-28.

39. Hoy, S. M., Albumin-Bound Paclitaxel: A Review of Its Use for the First-Line Combination Treatment of Metastatic Pancreatic Cancer. *Drugs* **2014,** *74* (15), 1757-1768.

40. Langer, K.; Balthasar, S.; Vogel, V.; Dinauer, N.; von Briesen, H.; Schubert, D., Optimization of the preparation process for human serum albumin (HSA) nanoparticles. *International Journal of Pharmaceutics* **2003,** *257* (1-2), 169-180; Zhang, J. Y.; He, B.; Qu, W.; Cui, Z.; Wang, Y. B.; Zhang, H.; Wang, J. C.; Zhang, Q., Preparation of the albumin nanoparticle system loaded with both paclitaxel and sorafenib and its evaluation in vitro and in vivo. *Journal of Microencapsulation* **2011,** *28* (6), 528-536.

41. Paliwal, S. R.; Paliwal, R.; Agrawal, G. P.; Vyas, S. P., Liposomal nanomedicine for breast cancer therapy. *Nanomedicine* **2011,** *6* (6), 1085-1100.

42. Bahadur, K. C. R.; Thapa, B.; Xu, P. S., pH and Redox Dual Responsive Nanoparticle for Nuclear Targeted Drug Delivery. *Molecular Pharmaceutics* **2012,** *9* (9), 2719-2729; Gao, W.; Chan, J. M.; Farokhzad, O. C., pH-Responsive Nanoparticles for Drug Delivery. *Molecular Pharmaceutics* **2010,** *7* (6), 1913-1920; Choi, S. U.; Bui, T.; Ho, R. J. Y., pH-dependent interactions of indinavir and lipids in nanoparticlies and their ability to entrap a solute. *Journal of Pharmaceutical Sciences* **2008,** *97* (2), 931-943; Kinman, L.; Bui, T.; Larsen, K.; Tsai, C. C.; Anderson, D.; Morton, W. R.; Hu, S. L.; Ho, R. J. Y., Optimization of lipid-indinavir complexes for localization in lymphoid tissues of HIV-infected macaques. *Jaids-Journal of Acquired Immune Deficiency Syndromes* **2006,** *42* (2), 155-161.

CHAPTER 2

Synthesis of pH-Responsive Artemisinin Derivatives that Inhibit Growth of Breast Cancer Cells *in vitro* and induce down-regulation of HER family members

Content of this Chapter was published as a research article in PLoS ONE, 2013, 8.

The manuscript was authored by:

Yitong J. Zhang[†], Byron Gallis[‡], Michio Taya[†], Shusheng Wang[†], Rodney J.Y. Ho[§], Tomikazu Sasaki[†]*

[†]Department of Chemistry, University of Washington, Seattle, Washington, 98195, United States
[‡]Department of Medicinal Chemistry and [§]Department of Pharmaceutics, School of Pharmacy, University of Washington, Seattle, Washington, 98195, United States.

Abstract

A new ART dimer was designed to become increasingly more water-soluble as pH declines. The new artemisinin dimer piperazine derivatives (ADPs) were synthesized in 4 steps from artemisinin in 50-80% yields. At neutral pH, the Artemisinin dimer remained tightly associated with liposomal nanoparticles (NPs) but were efficiently released at acidic pH's that are known to exist within solid tumors and organelles such as endosomes and lysosomes. ADPs incorporated into nanoparticles down regulated the anti-apoptotic protein, survivin, and cyclin D1 when incubated at low concentrations with breast cancer cell lines. We demonstrated for the first time, for any ART derivative, that ADP NPs can down regulate the oncogenic protein HER2, and its counterpart, HER3 in a HER2+ cell line. We also showed that the wild type epidermal growth factor receptor (EGFR or HER1) declines in a triple negative breast cancer (TNBC) cell line in response to ADP NPs. The declines in these proteins were achieved at concentrations of NP109 at or below 1 μM. Furthermore, the new artemisinin derivatives showed improved cell-proliferation inhibition effects compared to known dimer derivatives.

Introduction

Artemisinin is a natural product first discovered for treatment of malaria[1]. The mechanism of action, though not yet fully elucidated, is believed to involve activation of the endoperoxide bridge by heme iron and other iron species that are accumulated in the parasite's food vacuole[2]. Cancer cells have also been shown to be sensitive to ART due to their elevated iron uptake and metabolic activities[3]. Derivatives of ART have shown promising anticancer effects against multiple cell lines derived from various types of cancers[4-6]. Dimeric and oligomeric derivatives of ART show greatly enhanced efficacy[5-9]. ART derivatives induce apoptosis in human cancer cell lines[10] and simultaneously down-regulate proteins such as c-myc, cyclin D1, and survivin, which are known to be involved with oncogenesis, the cell cycle, and apoptotic resistance[11, 12] respectively. Both ART monomer and dimer derivatives have shown activity *in vivo* in mouse xenograft models[13], especially for breast cancer models[14].

Despite both the encouraging *in vitro* and animal model data, several key issues need to be addressed before further clinical development of ART derivatives as cancer chemotherapy can take place. ART derivatives, a class of sesquiterpene, generally possess poor aqueous solubility. Chemical approaches to solubilize the compound in an aqueous environment have only been probed briefly, such as the development of artesunate[15], a water-soluble derivative. For dimers, however, the succinate ester analogue does not possess sufficient water solubility for clinical development[9]. Alternative approaches, such as carrier conjugated ART derivatives, are also scarce in the literature, given the promising cytotoxicity results reported by numerous groups. Furthermore, the rapid clearance of the free drug molecules from blood circulation (artesunate < 15 minutes)[16] makes these compounds unsuitable to use in the free drug form for treatments of cancer.

The use of a nanoparticle (NP) carrier to deliver a drug to the target site is no foreign concept today. In the NP approach, drugs are incorporated or encapsulated into a suitable carrier to improve their bioavailability and pharmacokinetics[17]. Among the multitude of nanoparticle systems being studied, liposomal nanoparticles represent a class of better developed delivery vehicles[18]. Both classical liposomes composed of only lipids and cholesterol, and stealth liposomes containing PEGylated lipids have been developed as anti-fungal, anti-cancer, anti-HIV, etc. therapies. Doxil® is one example of commercialized liposomal cancer chemotherapeutics.

Nanoparticles of size less than 200 nm are able to pass through the solid tumor microvasculature due to the enhanced permeability and retention (EPR) effect at these sites [19]. As the NPs accumulate, they fors a local microresevior of drugs for an enhanced biodistribution [20]. The accumulation of drug-loaded nanoparticles, however, may not correlate with bioavailability when dug release at solid tumor sites is inefficient.

While there may be multiple potential solutions to this problem, we sought a pH-dependent loading-release mechanism in our approach with ART-containing NPs. The working principle of such delivery systems relies on the acidified tumor microenvironment (pH=6.5-7.0) compared to physiological pH of 7.4, and a further acidification to as low as pH 4.8 in the endosome/lysosome network after cellular uptake [21].

Here, we report the syntheses of four novel ART dimer piperazine conjugates (ADPs) that show pH-responsive aqueous solubility profiles (**Figure 1**), and one of the first liposome nanoparticle formulations of ART dimers for *in vitro* characterization. We also demonstrate that these nanoparticles down-regulate multiple proteins that maintain and contribute to malignant state in two types of human breast cancer cell lines.

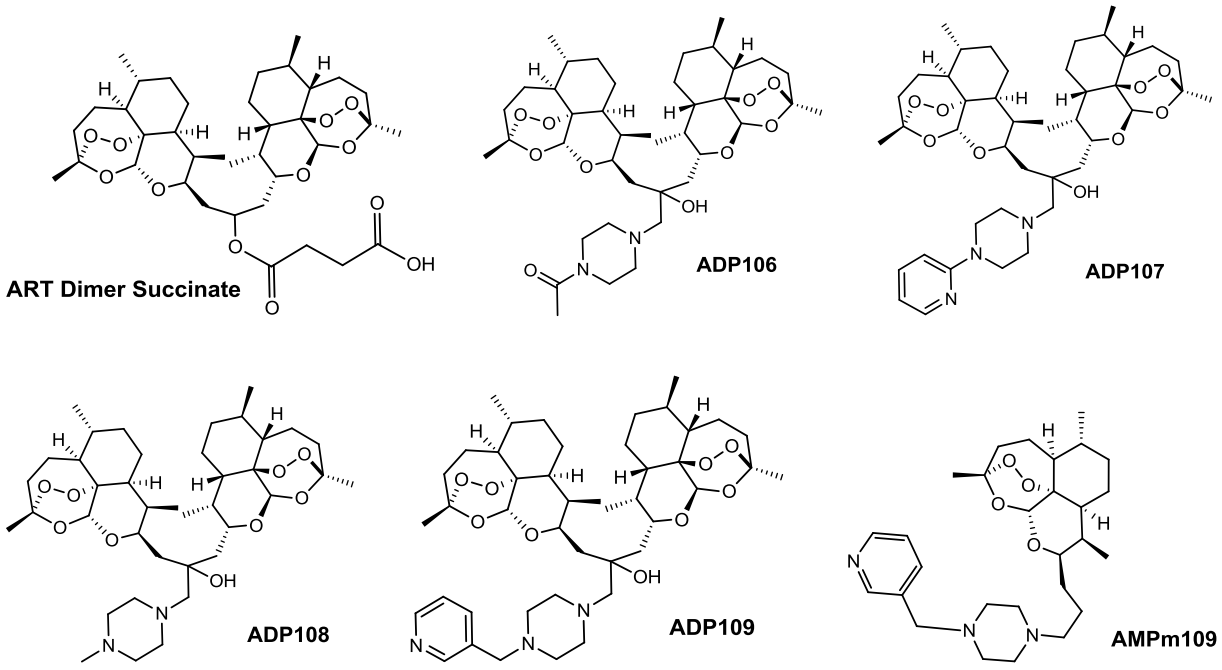

Figure 1. Structures of artemisinin dimer succinate, **ADPs 106-109** and **ADPm109** the monomer analogue of compound **ADP109**.

Results

Synthesizing pH-responsive Artemisinin Dimer Piperazine Conjugates (ADPs)

In synthesizing the ADPs (**Figure 2**), ART Isobutylene Dimer **2** was prepared according to the literature[8]. The double bond in **2** was then epoxidized with *meta*-chloroperbenzoic acid (mCPBA) to give **3** for the subsequent epoxide-opening reaction. Compound **3** and corresponding piperazine were reacted in the presence of lithium bromide at room temperature, affording final **ADP106-109** in 53-81% yield. The pH-responsive moieties of the ADPs draw analogy from indinavir, a potent HIV drug, which demonstrated pH-responsive properties in lipid nanoparticle formulations [22]. An ART-monomer piperazine conjugate (**AMPm109)** was also synthesized for comparison in characterizations. For the monomer derivative, the initial approach with epoxide ring-opening reaction produced inseparable diastereomers. Therefore, we utilized reductive amination of ART 10-β-propanal **9** to circumvent the complications with the hydroxyl group in the arm. The effect of the hydroxyl group was confirmed to be minimal by MTT assay (data not shown).

Table 1. Solubility of compounds **ADP106-109**, **AMPm109** in phosphate/citrate buffer with 5% DMSO, estimated from visual turbidity test.

	Aqueous Solubility with 5% DMSO (mM)		
	pH 7.4	pH 6	pH 4
ADP106	<<0.055	0.082	1.6
ADP107	<<0.048	<<0.048	0.14
ADP108	0.25	0.57	1.1
ADP109	0.034	0.19	1.5
AMPm109	1.4	>2	>2

ADP106-109 and **AMPm109** were characterized by ^{1}H-NMR and MALDI-TOF (See Chapter 9), and structures are shown in **Figure 1**. The solubilities of the compounds were estimated by visual turbidity test in phosphate/citrate buffer at various pH values (**Table 1**). Of the ADPs, **ADP109** showed the most desirable solubility profile with 0.034 mM at pH 7.4, 0.19 mM at pH 6 and 1.5 mM at pH 4. **ADP109** was thus chosen as the lead compound for nanoparticle formulation (**NP109**).

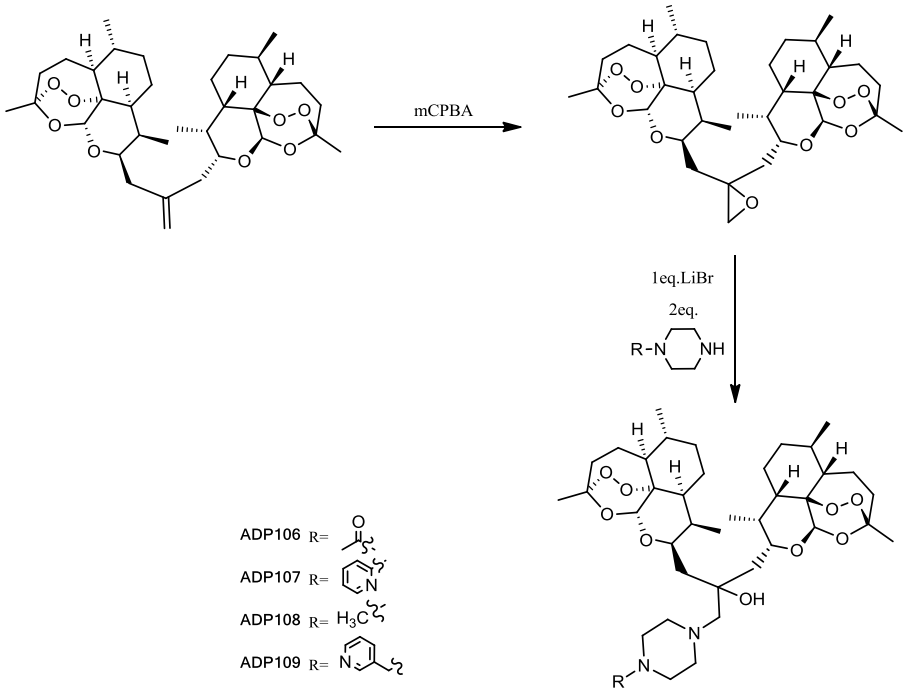

Figure 2. Schematic of synthesis of **ADPs 106-109**.

*Nanoparticle Formulation with **ADP109** and **AMPm109***

L-α-Phosphatidylcholine extracted from eggs (EPC) was used to construct the liposome formulation for our initial showcase formulations **NP109** (EPC + **ADP109**) and **NPm109** (EPC + **AMPm109**). We prepared the liposome nanoparticles with the liquid-hydration-sonication

method previously described [22]. Briefly, a 10-to-1 ratio of EPC and **ADP109**, both in chloroform, were mixed and dried down to form a thin film before rehydrated in 0.9X phosphate buffered saline (PBS) and sonicated to give a suspension of the nanoparticles at a concentration of 20 mM of lipid. Photon correlation spectroscopy showed that the sonicated suspension contained mono-dispersed nanoparticles with the size of 70 nm (±20 nm) in diameter for **NP109** and 50 nm (±20 nm) for the ART monomer analogue **NPm109**.

Table 2. Summary of loading and release efficiencies of the NPs. Values represent an average and standard deviation of three independent experiments read at λ=263nm.

	% Association	% Released (24hrs)		
		pH 7.6	pH 6	pH 4
NP109	91 (±9)	1 (±4)	14 (±14)	52 (±14)
NPm109	63 (±13)	13 (±3)	91 (±10)	96 (±7)

Loading efficiencies of ADP-NPs were determined by comparing the UV absorbance values measured at 263nm for the dialyzed and original samples (**Eq. 1**). An average of three independent experiments gave a loading efficiency of 91% (±9%) for NP109 and 63% (±13%) for **NPm109** (**Table 2**). The release of the drug from NPs was determined by equilibrium dialysis for 24 hours against buffers at various pH values and then comparing the UV absorbance values at 263 nm to that of time zero. **NP109** retained 99% of the bound drug at pH 7.6, released 14% at pH 6 and 52% at pH 4 after 24 hours. In contrast, NPm109 lost 13%, 91% and 96% of **AMPm109** at pH 7.6, 6 and 4 respectively (Spectra **Figure 3-4**). The loading and release profiles of both compounds effectively demonstrated the dependence on the environmental pH that was originally designed into the derivatives.

(a) (b)

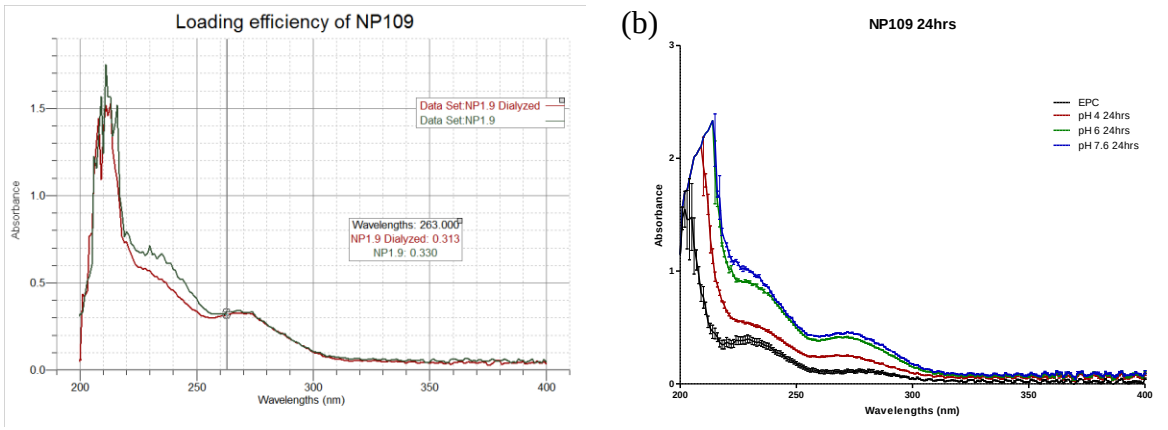

Figure 3. Typical UV spectra overlay of dialyzed and undialyzed (a) and retention of drug after 24-hrs dialysis in buffers at various pH values (b) of NP109. Spectrum (a) shown is the average and (b) the average and standard deviation graphed from three parallel readings.

(a) (b)

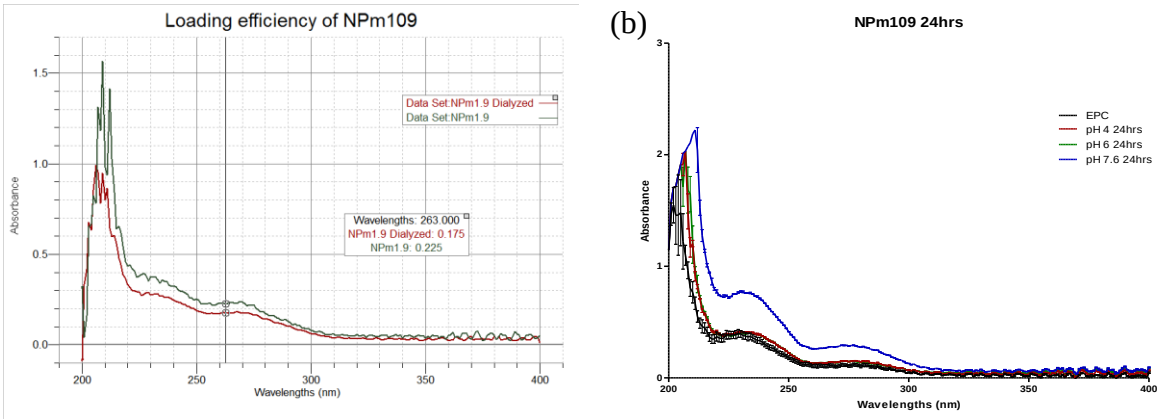

Figure 4. Typical UV spectra overlay of dialyzed and undialyzed (a) and retention of drug after 24-hrs dialysis in buffers at various pH values (b) of NPm109. Spectrum (a) shown is the average and (b) the average and standard deviation graphed from three parallel readings.

In vitro Cytotoxicity Study

Next, MTT assays were performed to evaluate the ability of **ADP106-109** to inhibit cell growth on BT474 (HER2+), and MDA-MB-231, ("triple-negative" or TNBC) human breast tumor cell lines (**Figure 5-6**).

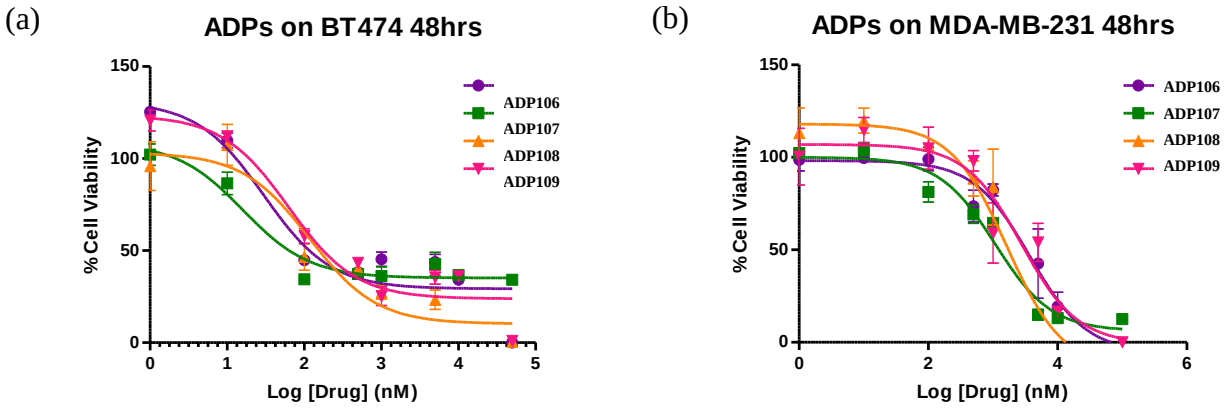

Figure 5. Overlay of typical cell viability data calculated from absorbance values at 570 nm of MTT assays of BT474 (a) and MDA-MB231(b) cells incubated with ADPs for 48hrs with 10%FBS in DMEM at 37°C, 5% CO_2 at various concentrations. IC_{50} values see **Table 3.**

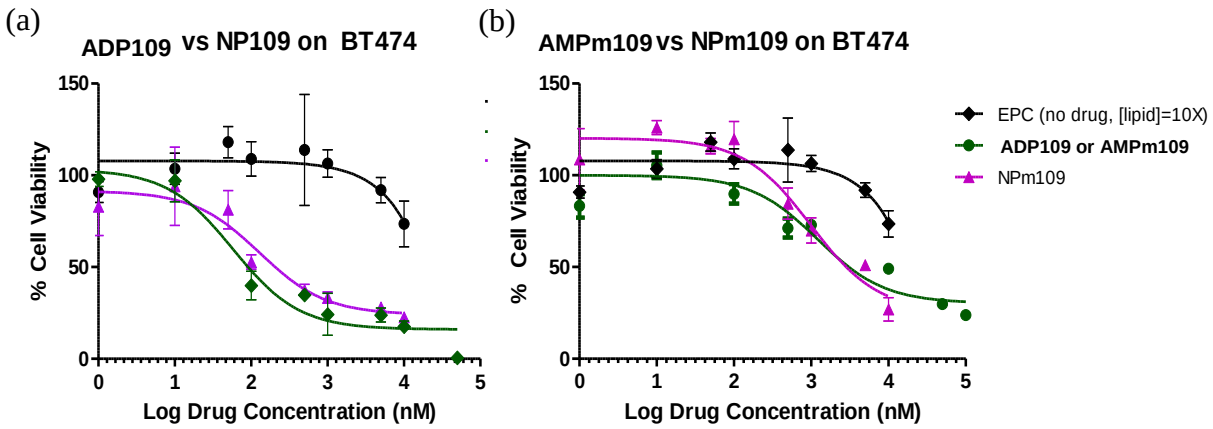

Figure 6. Overlay of typical cell viability data calculated from absorbance values at 570 nm of MTT assays of BT474 cells incubated with EPC empty liposome, free drug **ADP109**, NP109 (a),

or EPC empty liposome, free drug **AMPm109**, NPm109 (b) for 48hrs with 10%FBS in DMEM at 37°C, 5% CO_2 at various concentrations. IC_{50} values see **Table 3**.

Table 3 and **Table 4** show the IC_{50} values. All the compounds except for **AMPm109** showed sub-micromolar IC_{50} values on BT474 cells, consistent with high anti-proliferative effects reported in the literature for other artemisinin dimers. Monomeric artemisinin derivative, **AMPm109**, showed a comparable activity to that of artesunate (data not shown). The nanoparticle formulations retained the potency of the free drug, confirming that the drugs are efficiently loaded and released from liposomes.

Table 3. Summary of IC_{50} values calculated from MTT assays of ADPs and NPs on BT474 and MDA-MB-231 cells. Values represent average (±SD) calculated from three independent experiments.*Exceeded maximum concentration of assay.

	IC_{50} (μM)	
	BT474 (± S.D.)	**MDA-MB231** (± S.D.)
ART Dimer Succ.	0.39 (±0.27)	32 (±4)
ADP106	0.06 (±0.03)	8 (±3)
ADP107	0.022 (±0.009)	5 (±2)
ADP108	0.11 (±0.02)	3.3 (±0.7)
ADP109	0.07(±0.01)	10 (±3)
AMPm109	1.3 (±0.8)	>>100*
NP109	0.08 (±0.01)	7 (±2)
NPm109	1.3 (±0.4)	>>20*

Table 4. IC50 values of **ADP109** and **NP109** on SKBR3 and MDA-MB-468 cell lines, values reported as mean and standard deviation of triplicate independent experiments.

	IC_{50} (μM)	
	SKBR3 (± S.D.)	**MDA-MB468** (± S.D.)
ADP109	7 (±2)	2.6 (±0.4)
NP109	>10	>10

NP109 *down regulates proteins which support neoplasia in two breast cancer cell lines*

A closer look at the biochemical responses of BT474 and MDA-MB-231cells incubated with NP109 at nanomolar and low micromolar concentrations showed marked declines of both survivin, which causes resistance to apoptosis[23], and cyclin D1, a protein integral to cell replication[24]. Dose-response experiments showed that both survivin and cyclin D1 were decreased in the presence of 100 nM to 1 μM **NP109** in BT474 cells (**Figure 7a**) and 1μM **NP109** in MDA-MB-231 cells (**Figure 7d**).

Since survivin levels have been shown to be coupled to HER2 expression [23], we also observed that HER2 levels declined when BT474 cells were incubated with 100 nM-1 μM **NP109** (**Figure 7a**). In addition, the level of another mutated form of the epidermal growth factor receptor, ErbB3 (HER3), frequently expressed in HER2+ cell lines, was shown to decrease in BT474 cells in dose response (**Figure 7b**) and time course (**Figure 7c**) experiments with **NP109**. Epidermal growth factor receptor, EGFR (HER1), over-expressed in triple negative breast cancers [25], was down-regulated in MDA-MB-231 cells by **NP109** in the dose response (**Figure 7e**) and time course (**Figure 7f**) studies. In summary, we have shown that **NP109** was able to induce decline in the levels of the same proteins, survivin and cyclin D1, as well as over-expressed and mutated forms of EGFR in BT474 (HER2+) and MDA-MB-231 (EGFR) cells.

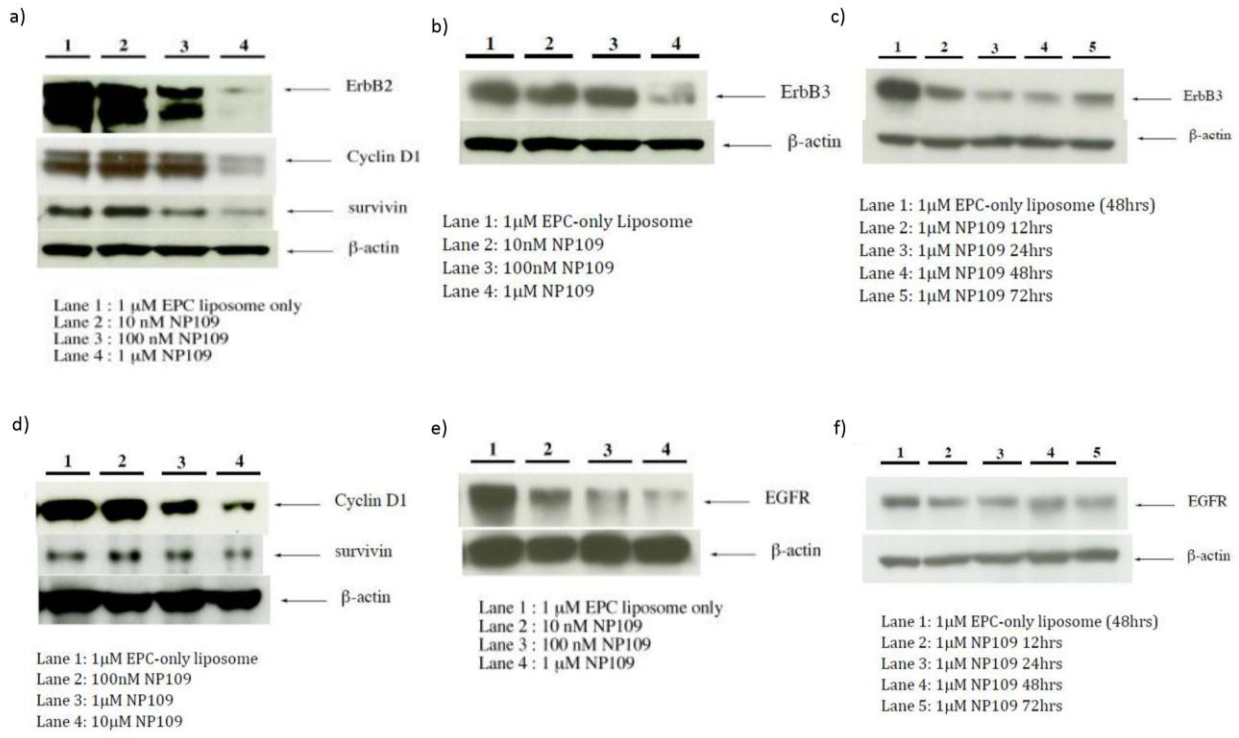

Figure 7. Responses to NP109 on selected proteins involved in cell proliferation, cell cycling, and apoptosis in BT474 (a-c) and MDA-MB-231 cells (d-f).

When the biochemical effects of **NP109** were determined for an additional HER2+ cell line, SKBR3, and another TNBC cell line, MDA-MB-468, survivin was strongly down regulated in both cell lines, but neither HER2/HER3 levels were altered in SKBR3 nor EGF levels changed in MDA-MB-468 cells (data not shown). Cyclin D1 levels were not examined.

Discussions

The ART Dimer piperazine conjugates (ADPs) designed here were synthesized using lithium bromide (LiBr) as a mild Lewis acid [26] for the epoxide ring opening reaction. This method allowed incorporation of the pH-responsive piperazine moiety while avoiding use of heavy metal. The novel ADPs preserved the active core of the artemisinin dimer while introducing multiple protonation sites to increase aqueous solubility as pH lowers from 7.4 under physiological conditions to below 5 in lysosomes [27].

In the absence of LiBr, the epoxide opening reaction hardly gave any product after overnight conditions. Reactions using tin(II) trifluoromethanesulfonate at both room temperature and under reflux conditions resulted in large amounts of decomposition and little desired products. The lower loading efficiency for **AMPm109** is likely due to its higher solubility at neutral pH.

The ADP-NPs described in this manuscript is the first liposomal nanoparticle formulation of artemisinin dimer derivatives, to the best of our knowledge. We were able to demonstrate efficient incorporation of the novel artemisinin derivatives **ADP109** and **AMPm109** at physiological pH and a pH-dependent release of the incorporated drugs, according to design. The data attest to the potential of the liposome-nanoparticle approach for selective *in vivo* delivery of the ADPs to tumor cells.

This study also examined selected biochemical changes in a $HER2^+$ (BT474) and a TNBC (MDA-MB-231) cell line in response to an ART derivative-containing NP. Both survivin and cyclin D1 were down-regulated in the two cell lines as they are in prostate cancer cell lines [11] by a different ART derivative. Other investigators have shown that ART-derivative-induced declines in survivin protein levels in cancer cell lines are accompanied by declines in survivin mRNA [28]. Survivin is an anti-apoptotic protein that is expressed in the majority of tumors in

most human cancers [29] and is correlated with poor prognosis in breast cancers [30]. It is, however, not detected in terminally differential healthy tissues. This differential expression has made it a target for potential cancer therapy [31]. Among the cyclin isoforms, cyclin D1 over-expression is most frequently associated with human cancers [32]. Since cyclin D1 is an important regulator of G1 to S-phase during the cell cycle, ART induced degradation of this protein may be sufficient to arrest cell growth in some cancers [33].

Known as a marker, the over-expression of HER2, a member of the epidermal growth factor receptor tyrosine kinase family, occurs in 25% of breast cancers, predict for poor clinical outcomes, and resistance to chemotherapies [34-36]. While it has no activating ligand, HER2 is activated by homo-and hetero-dimerization with wild type EGFR (HER1), HER3, or HER4. The poor prognosis for patients with tumors over-expressing HER2 is believed to be due to activation of the PI3-k/Akt family of kinases [37]. HER2 preferentially heterodimerizes with HER3, which while having no tyrosine kinase activity on its own contains six PI3-kinase docking sites, making the HER2/HER3 heterodimer a potent activator of this pathway [38]. The unique roles and properties of HER3 cause resistance to chemotherapies [35, 39]. Recent studies conclude that only combined blockade of HER2 and HER3 will be effective in treatment of HER2-mediated breast cancers [35, 36, 40]. Furthermore, the EGF receptor is over-expressed in 50% or more of triple negative breast cancers [25]. Presently, it is unclear what and how important a role EGFR amplification plays in the etiology of TNBC.

We have shown in our studies that **NP109** caused a decline of EGFR level in the TNBC cell line MDA-MB-231 and near elimination of HER2 level in the HER2+ cell line BT474. The ability of nanoparticles containing a pH sensitive ART derivative to down-regulate HER1, HER2, and

HER3, as well as other proteins linked to neoplasia, suggests that this approach has real therapeutic potential for treatment of specific breast cancer subtypes.

In conclusion, we designed and synthesized a series of pH-responsive artemisinin dimers and successfully incorporated a candidate derivative into liposomal nanoparticles without significantly compromising its *in vitro* efficacy. Our studies clearly show that ADP-NPs elicit a unique set of biological responses from breast cancer cells to ultimately induce cell death, potentially opening up new avenues for treatments of breast cancer. The optimization of the lipid composition for these NPs is ongoing in our lab using animal models to evaluate the *in vivo* characteristics of ADP-NPs for further clinical development.

Experimental Section

Materials

Artemisinin was purchased from Shaanxi Sciphar Hi-Tech Industry Co., LDT (Xi'an, China).Lithium Bromide, 1-acetylpiperazine, 1-(2-pyridyl)piperazine, 1-methylpiperazine were purchased from TCI America (Portland, OR), and 1-(3-pyridyl)methylpiperazine from Oakwood Products, Inc. (West Columbia, SC). All other chemicals and solvents used for synthesis were purchased from Sigma Aldrich (MO, USA) and were used without purification unless specified otherwise. L-α-phosphatidylcholine isolated from eggs (EPC) was purchased from Avanti Polar Lipids (Alabaster, AL). 10X PBS was purchase from Invitrogen (Eugene, OR).

Nuclear Magnetic Resonance (NMR) of compounds were recorded on Bruker's AVANCE AV 500 MHz in $CDCl_3$. MALDI-TOF mass spectra were recorded on a Bruker Autoflex II using 2,5-dihydroxy benzoic acid (DHB) and α-cyano-4-hydroxycinnamic acid (α-cyano) (2:1) matrix.

Cell cultures were generous gifts from Dr. N. Singh (MDA-MB-231) and Dr. B. Gallis (BT 474) for MTT assays. Thiazolyl blue tetrazolium bromide (MTT) was purchased from Sigma Aldrich (St. Louis, MO). Fetal bovine serum (FBS) and 0.25% trypsin-EDTA with phenol red were purchased from Invitrogen (Eugene, OR), and Dulbecco's Modified Eagle's Medium - high glucose (DMEM) and Dulbecco's Phosphate Buffered Saline (PBS) were from Sigma Aldrich (St. Louis, MO).

The following antibodies were used for Western blotting: actin (clone 15) from Sigma-Aldrich (St. Louis, MO), survivin and epidermal growth factor receptor (EGFR) from Cell Signaling, Inc (Danvers, MA), HER2, HER3, and cyclin D1 from Epitomic, Inc (Burlingame, CA). Western blotting was performed as previously described[5]

Synthesis of Trioxane Isobutylene Dimer 2.

Trioxane isobutylene dimer **2** was synthesized in two steps from artemisinin by following the procedure described by Posner et al[1].

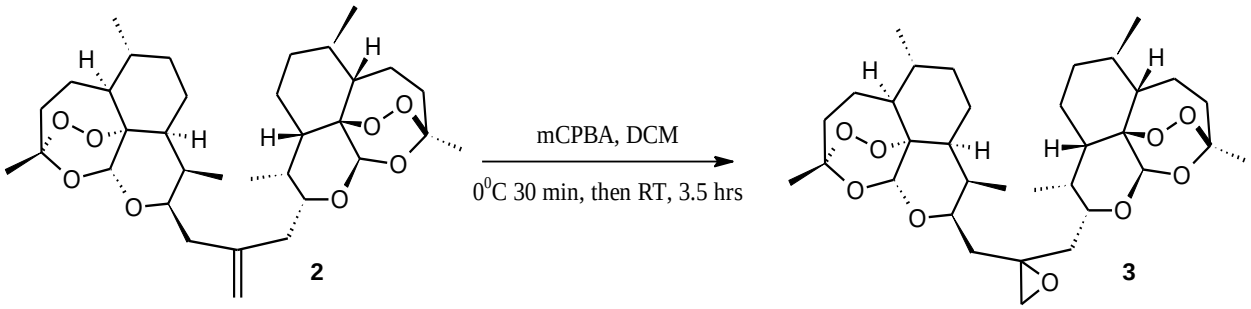

Synthesis of Bis-Trioxane Epoxide 3.

meta-Chloroperbenzoic acid (mCPBA) was purified by dissolving 0.5g of the commercial material (≤77%) in 5mL of diethyl ether and extracting twice with 1mL of 0.1M potassium phosphate buffer (KH_2PO_4/K_2HPO_4) at pH 7.2.The ether layer was dried over Na_2SO_4 and the solvent was removed *in vacuo* to obtain pure mCPBA.

To a 50mL round bottom flask under N_2 was charged 0.24g (0.4mmol) of **2** dissolved in 15mL of dry dichloromethane (DCM). The solution was cooled to 0°C before 0.14g (0.8mmol, 2 eq.) of mCPBA, dissolved in 10mL dry DCM was added dropwise under nitrogen. The reaction mixture was stirred at 0°C for 30 minutes before warming up to room temperature for additional 3 hours with stirring. The consumption of the reactant **2** was confirmed by TLC (30% ethylacetate (EA) in hexane (H)) before the reaction was quenched with a mixture of 4mL saturated sodium bicarbonate ($NaHCO_3$) and 4mL 0.1N disodium carbonate (Na_2CO_3). The reaction was stirred for 15 minutes. The organic layer was then extracted 3 times with 10mL saturated $NaHCO_3$,

dried over Na_2SO_4, concentrated under reduced pressure to obtain the epoxide. The product was used for subsequent reaction without further purification. Analytical data matched that reported in literature [8].

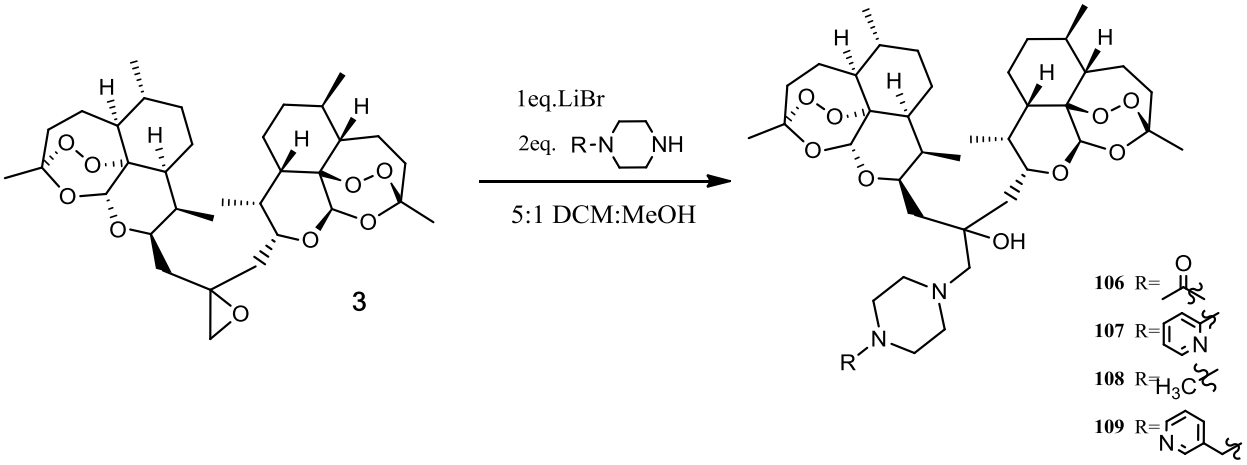

Synthesis of Bis-Trioxane Piperazine Conjugates (ADPs) 106-109.

ADPs **106-109** were synthesized by using the same general procedure described as follows. In a 1 dram glass vial with a magnetic stir bar were placed ca. 60mg (0.1mmol) of **3** and 8.6mg (0.1mmol, 1 eq.) of lithium bromide and then 200μL methanol:DCM (1:5). To the solution, 0.2mmol (2eq.) of piperazine derivatives were added to start the reaction. The vial was briefly purged under N_2, capped and stirred at room temperature for 16-40 hours depending on the compound (see below). Upon consumption of **3** monitored by TLC, the reaction mixture was diluted with 2mL of DCM, extracted 4 times with 1mL 0.1N Na_2CO_3, dried over Na_2SO_4. The solvent was then removed *in vacuo* to yield the crude products. Each product was purified by column chromatography as shown below.

1-Bis-Trioxane-4-acetylpiperazine (ADP106).

21.5μL of 1-acetylpiperazine was added to the reaction mixture. The reaction was run for 16 hours before quenching. The crude product was subjected to flash chromatography with first 50% EA in H, then 5% aqueous ammonium hydroxide(NH_4OH)-methanol (1:1) in DCM to give **ADP 106** as a white solid (39mg, 0.053mmol, 53%). ^{1}H NMR (500 MHz, $CDCl_3$) δ (ppm) 5.46 (s, 1H), 5.33 (s, 1H), 4.60 – 4.50 (m, 1H), 4.35 (dd, *J* = 11.1, 6.0 Hz, 1H), 3.54 (d, *J* = 30.7 Hz, 2H), 3.44 – 3.31 (m, 2H), 2.76 – 2.47 (m, 8H), 2.29 (ddd, *J* = 14.4, 9.5, 5.0 Hz, 2H), 2.13 (dd, *J* = 14.6, 11.8 Hz, 2H), 2.05 (s, 3H), 2.02 – 1.96 (m, 2H), 1.96 – 1.82 (m, 4H), 1.84 – 1.71 (m, 4H), 1.67 – 1.54 (m, 4H), 1.45 – 1.16 (m, 14H, including a doublet at 1.36, *J* = 5 Hz), 0.94 (dd, *J* = 5.6, 1.6 Hz, 6H), 0.95-0.86 (m, 2H), 0.88 (dd, *J* = 15.9, 8.0 Hz, 6H). MALDI-TOF *m/z* calcd for $C_{40}H_{64}N_2O_{10}$ 732.46 (M^+), found, 733.6 ($[M+H]^+$).

1-Bis-Trioxane-4-(2-pyridyl)piperazine (ADP107).

30.5μL of 1-(2pyridyl)piperazine was added to the reaction mixture. The reaction was run for 20 hours before quenching. The crude product was subjected to flash chromatography with gradient mobile system from 30% to 50% EA in H to give **ADP107** as a white solid (62mg, 0.081mmol, 81%). ^{1}H NMR (500 MHz, $CDCl_3$) δ (ppm) 8.19 – 8.15 (m, 1H), 7.45 (ddd, *J* = 8.7, 7.2, 2.0 Hz, 1H), 6.63 (d, *J* = 8.6 Hz, 1H), 6.60 – 6.56 (m, 1H), 5.49 (s, 0H), 5.37 (s,1H), 4.57 – 4.50 (m, 1H), 4.47 (d, *J* = 4.9 Hz, 1H), 3.48 (s, 4H), 2.90 – 2.82 (m, 2H), 2.70 – 2.65 (m, 2H), 2.64 – 2.56 (m, 2H), 2.76-2.56 (m, 2H), 2.31 (td, *J* = 14.0, 3.8 Hz, 2H), 2.08 (dd, *J* = 22.4, 10.8 Hz, 1H), 2.01 (d, *J* = 14.4 Hz, 2H), 1.95 – 1.75 (m, 8H), 1.68 – 1.57 (m, 4H), 1.45 – 1.19 (m, 14H, including a doublet at 1.36, *J* = 15.0 Hz), 0.95 (dd, *J* = 13.1, 6.2 Hz, 6H), 0.90 (dd, *J* = 7.5, 3.5 Hz, 6H), 0.97-0.85, (m, 2H). MALDI-TOF *m/z* calcd for $C_{43}H_{65}N_3O_9$ 767.49 (M^+), found, 768.5 ($[M+H]^+$).

1-Bis-Trioxane-4-methylpiperazine (ADP108).

22.2μL of 1-methylpiperazine was added to the reaction mixture. The reaction was run for 30 hours before quenching. The crude product was subjected to flash chromatography with first 25% EA in H, then 25% methanol in DCM to give **ADP108** as a white solid (50mg, 0.071mmol, 71%). ^{1}H NMR (500 MHz, $CDCl_3$) δ (ppm) 5.49 (s, 1H), 5.36 (s, 1H), 4.49 (d, *J* = 9.1 Hz, 2H), 2.68 (d, *J* = 13.5 Hz, 1H), 2.60 (dd, *J* = 11.4, 6.4 Hz, 2H), 2.54 (d, *J* = 13.4 Hz, 1H), 2.37 – 2.27 (m, 2H), 2.25 (s, 3H), 1.94 (ddd, *J* = 29.1, 22.9, 13.2 Hz, 8H), 1.81 – 1.71 (m, 4H), 1.69 – 1.54 (m, 12H), 1.45 – 1.17 (m, 14H, including a doublet at 1.39, *J* = 18.7 Hz), 0.98 – 0.95 (m, 6H), 0.91 – 0.88 (m, 6H), 0.98-0.89 (m, 2H). MALDI-TOF *m/z* calcd for $C_{39}H_{64}N_2O_9$ 704.46 (M^+), found, 705.4 ($[M+H]^+$).

1-Bis-Trioxane-4-(3-pyidyl)methylpiperazine (ADP109).

33.5μL of 1-(3-pyridyl)methyl-piperazine was added to the reaction mixture. The reaction was run for 40 hours before quenching. The crude product was subjected to flash chromatography with first 30% EA in H, then 5% aqueous ammonium hydroxide(NH_4OH)-methanol (1:1) in DCM to give **ADP109** as a white solid (56mg, 0.071mmol, 71%). ^{1}H NMR (500 MHz, $CDCl_3$) δ (ppm) 8.50 (m, 2H), 7.67 (m, 1H), 7.24 (m, 1H), 5.47 (s, 1H), 5.35 (s, 1H), 4.47 (d, *J* = 37.4 Hz, 2H), 3.47 (s, 2H), 2.84 – 2.21 (m, 10H), 2.14 – 1.55 (m, 16H), 1.52 – 1.16 (m, 14H, including a doublet at 1.37, *J* = 13.0Hz), 0.96 – 0.94 (m, 6H), 0.88 – 0.86 (m, 6H), 1.06-0.82 (m, 2H). MALDI-TOF *m/z* calcd for $C_{44}H_{67}N_3O_9$ 781.49 (M^+), found, 782.6 ($[M+H]^+$).

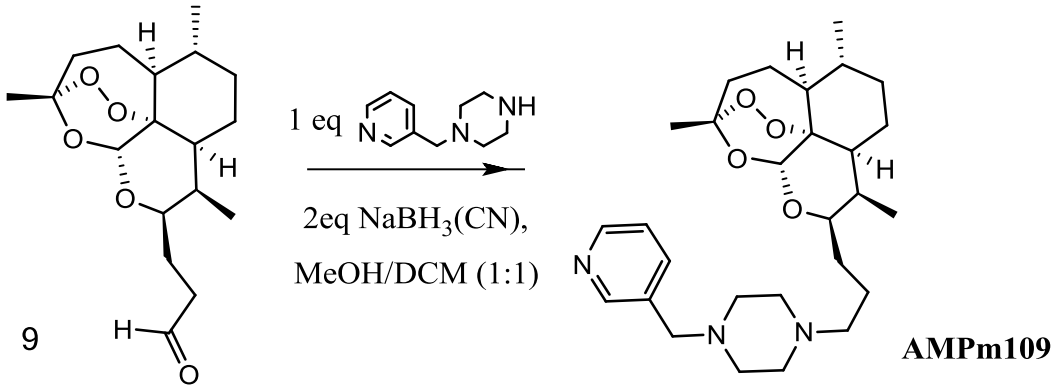

Synthesis of 10β-[(1-(3-pyidyl)methylpiperazyl)propyl]deoxoartemisinin (AMPm109).

Compound **9** was synthesized according to the literature[41-6]. 69 mg (0.2 mmol) of **9** was dissolved in 1mL of dry DCM:methanol (1:1) in a 10 mL 2-neck round bottom flask (Flask A) under N_2 atmosphere and cooled to 0°C. In a separate 10 mL round bottom flask, 28mg (0.44 mmol, 2.2 eq.) of sodium cyanoborohydride was dissolved in 1mL of dry DCM:methanol (1:1) under N_2 before transferred to Flask A. 38 μL (0.2 mmol, 1 eq.) of 1-(3-pyridyl)-methylpiperazine was added to the reaction flask (A). The reaction mixture was warmed up to room temperature and stirred for 1 hour. TLC (30% EA in H) was used to check the consumption of **9** before 1 mL of deionized water was added dropwise at 0°C to quench the reaction. The emulsion was then stirred for additional 30 minutes before organic solvents were removed under reduced pressure. The residue was redissolved in 2 mL of DCM and extracted with 1 mL of deionized water. The aqueous layer was extracted 3 times with 2mL DCM. The combined organic layer was then extracted with 5 mL 0.1N Na_2CO_3 twice. The organic layer was dried over Na_2SO_4 and concentrated under reduced pressure. The product was purified by flash chromatography with 30% EA in H followed by 30% MeOH in DCM to give **AMPm109** as a white solid (20.3 mg, 0.042 mmol, 20%). ^{1}H NMR (500 MHz, $CDCl_3$) δ (ppm) 8.60 – 8.48 (m, 2H), 7.68 (d, *J* = 7.7 Hz, 1H), 7.34 – 7.21 (m, 1H), 5.31 (s, 1H), 4.16 (dd, *J* = 8.7, 4.9 Hz, 1H),

3.54 (s, 2H), 2.75 – 2.27 (m, 13H), 2.08 – 1.99 (m, 1H), 1.97 – 1.75 (m, 3H), 1.66-1.52 (m Hz, 4H), 1.49 – 1.21 (m, 7H, including a singlet at 1.42), 0.98 (d, *J* = 6.0 Hz, 3H), 0.87 (d, *J* = 7.5 Hz, 3H), 0.98-0.86 (m, 1H). MALDI-TOF *m/z* calcd for $C_{28}H_{43}N_3O_4$ 485.33 (M^+), found, 786.5 ($[M+H]^+$).

Aqueous Solubility Test.

Buffers at pH 7.4, 6 and 4 were prepared from titration of 0.2M disodium hydrogen phosphate (Na_2HPO_4) with 0.1M citric acid solution to the desired pH without addition of other salts.

In five labeled 1.5 mL eppendorf tubes was measured out 1mg of compounds **ADP106-109, AMPm109** and dissolved in 50 μL of DMSO to make the stock solutions. 5 μL of each of the stock solutions was pipetted into 5 separate small glass test tubes. 95μL of buffer was added to the test tubes, and mixture was vortexed for 10 seconds. The mixtures in the test tubes were allowed to settle and were observed for undissolved solids. If solids remained, 5 μL DMSO and 95 μL buffer were then added and process repeated until the mixture becomes a clear solution with no observable solid particles. For compounds **ADP106-108**, the process was stopped when there are still considerable amounts of particles in mixture after a total of 3 mL of liquid were added.

*Egg Phosphatidylcholine 1-Bis-Trioxane-4-(3-pyidyl)methylpiperazine Liposome Nanoparticle (**NP109**) Preparation.*

General procedure follows that of previously published protocol[42]. Compound **7** was dissolved in chloroform to make a 10 mg/mL stock solution. The EPC solution was purchased at the concentration of100 mg/ml. 31.3 μL of **7** stock solution and 30.4 μL of EPC solution were added to a screw-capped glass test tube, dried under a gentle stream of N_2 followed by *in vacuo* to form

a thin film on the inner wall. The film was rehydrated with 200 μL of 0.9X PBS at 40°C for 10 minutes to give a liposome suspension at 20mM lipid concentration. The mixture was then sonicated for 5 minutes 3 times to give a translucent suspension without observable particles, to afford the desired nanometer sized liposomes. 50 μL of the liposome suspension was diluted with 450 μL of 0.9X PBS in a test tube for size measurements on Zetasizer 5000 (Malvern Instrument, Worcestershire, UK) with argon laser at 633.0 nm at room temperature. Liposome populations generally show narrow distribution (peak width less than 20 nm) with occasionally 1% of peak at ~300 nm by intensity (but not visible by volume or number). Mean particle size reported in manuscript represents average and standard deviation calculated from number measurements of at least 3 sizing experiments.

*Egg Phosphatidylcholine-10β-[(1-(3-pyidyl)methylpiperazyl)propyl]deoxoartemisinin Liposome Nanoparticle (**NPm109**) Preparation.*

Procedure was the same as that described above. 19.4 μL of 10 mg/mL stock of **AMPm109** in chloroform was added for making 200 μL of 20 mM liposome at 10:1 lipid:drug ratio.

Loading and Release Efficiencies.

pH 7.6 buffer was made by diluting a 10X PBS buffer to 0.9X PBS, the same as used for preparing NPs. pH 6 and pH 4 buffers were made by titrating 0.95 mM citric acid monohydrate with 2.67 mM trisodium citrate dehydrate. Sodium chloride was then added to make buffer solutions containing 0.81% sodium chloride. The osmotic pressures of the buffers were tested to ensure that there's no significant variation.

For loading efficiency studies, after the liposomes were made, 500 μL out of 600 μL of the liposome suspension were placed into a dialysis tubing (MWCO 6000-8000 Da) and dialyzed

against 500 mL of 0.9X PBS buffer for 16 hours at room temperature. 30 μL of both dialyzed and undialyzed samples were collected in separate 5mL glass test tubes. The liposome samples were diluted to 100 μL with 0.9X PBS buffer, and extracted with 1 mL of spectroscopy-grade DCM by pipetting in and out 10 times with a 150 mm disposable glass transfer pipet. After extraction, 0.8mL of the organic layer was collected in a clean test tube. The extraction process was repeated for a total of 3 times, and the combined organic layer was dried over Na_2SO_4. The solvent was then removed *in vacuo*. The dried solids were redissolved in 900 μL of acetonitrile (HPLC grade), divided into three 300 μL portion and each portion used for the UV absorbance measurement from 200 to 400 nm by DU 640 spectrophotometer (Beckman Culter, USA).

The percent loaded was calculated according to the following equation (**Eq. S1**):

$$\text{Loading Efficiency (\%)} = \frac{\text{A263 (D) -A263 (EPC)}}{\text{A263 (UD) - A263 (EPC)}} \times 100\%$$

Where A_{263} (D) is th absorbance at 263 nm of the dialyzed sample, A_{263} (UD) is that of the undialyzed sample, and A_{263} (EPC) is that of EPC alone. Values used for calculation for a single experiment are the average of triplicate readings.

For the release efficiency studies 150 μL of 20 mM dialysis-purified liposome suspensions were placed in dialysis tubing and dialyzed against 500 mL of buffers of different pHs for 24 hours at room temperature. 30 μL of dialyzed samples were collected afterward for UV studies with the same workup procedure as that of the loading efficiency studies.

The percent released was calculated according to **Eq.2** :

$$\text{Release Efficiency (\%)} = 100\% - \left(\frac{\text{A263 (pH) -A263 (EPC)}}{\text{A263 (D) - A263 (EPC)}} \times 100\% \right)$$

Where A_{263} (pH) is the absorbance at 263 nm of the sample dialyzed for 24 hours at various pH values, A_{263} (D) is that of the dialysis-purified sample, and A_{263} (EPC) is that of EPC alone. Values used for calculation for a single experiment are the average of triplicate readings.

Cell Cytotoxicity MTT Assays.

In a 96 well plate was seeded ca. 2000 cells/well for BT474 or 7000 cells/well for MDA-MB-231 and incubated for 18 hours at 5% CO_2 in DMEM containing 10% FBS (Complete Medium) at 37°C. Serial dilutions of ADP stock solutions at 20 mM in DMSO were made to 8 appropriate concentrations ranging from1nM to100μM, depending on the specific compound, in Complete Medium with 1% DMSO. 200 μL of the compound containing medium were added to each well after removal of the original exhausted medium. NP concentrations were calculated assuming 100% loading for both formulations. Three wells were run in parallel for any given compound and concentration. The negative control was 1% DMSO containing Complete Medium and positive control employed 100 μM ART dimer succinate. The cells were incubated with the drugs for 48 hours at 37°C before the medium was replaced with 90 μL of fresh Complete Medium plus 10 μL of MTT solution at 5mg/mL concentration and incubated further for 4 hours. At the end of incubation time, exhausted medium was gently removed and the purple formazan crystals were dissolved in 50 μL of DMSO, incubated for 10 minutes before the absorbance at 570 nm was read on microplate reader model 680 (Bio-Rad, California, USA).

Western Blots.

Western blots were performed as described [10]. Primary antibodies used in Western blots were rabbit monoclonal antibodies (rabmabs) to cyclin D1, HER2, and HER3 from Epitomics, Inc (Burlingame, CA), rabmabs to survivin and HER1 from Cell Signaling Technology, Inc

(Danvers, MA) and mouse mab to actin, clone AC-15 (Sigma, St. Louis, MO). Three independent experiments were performed for all Western blots.

Protein Assay Cell Culture.

BT474 and MDA-MB-231 cells were obtained from the American Type Culture Collection (Manassas, VA) and maintained in DMEM with L-glutamine (Invitrogen Corporation) and supplemented with 10% fetal bovine serum (Atlanta Biologicals, Lawrenceville, GA) and penicillin/streptomycin. Liposomes and drug containing NPs were suspended in PBS and diluted into cell culture media.

Reference

1. Hsu, E., Reflections on the 'discovery' of the antimalarial qinghao. *British Journal of Clinical Pharmacology* **2006,** *61* (6), 666-670; Miller, L. H.; Su, X. Z., Artemisinin: Discovery from the Chinese Herbal Garden. *Cell* **2011,** *146* (6), 855-858.

2. Carter, M. D.; Hoang, A. N.; Wright, D. W., Hemozoin: A paradigm for biominerals in disease. *Wiley Encyclopedia of Chemical Biology* **2009,** *2*, 11; Haynes, R. K.; Cheu, K.-W.; N'Da, D.; Coghi, P.; Monti, D., Considerations on the Mechanism of Action of Artemisinin Antimalarials: Part 1-The 'Carbon Radical' and 'Heme' Hypotheses. *Infectious Disorders - Drug Targets* **2013,** *13* (4), 217-277; Weissbuch, I.; Leiserowitz, L., Interplay Between Malaria, Crystalline Hemozoin Formation, and Antimalarial Drug Action and Design. *Chemical Reviews* **2008,** *108* (11).

3. Karin, M.; Mintz, B., Receptor-mediated Endocytosis of Transferrin in Developmentally Totipotent Mouse Tetraocarcinoma Stem-cells. *Journal of Biological Chemistry* **1981,** *256* (7); Das, S. K.; Subbaiyan, N. K.; D'Souza, F.; Sandanayaka, A. S. D.; Wakahara, T.; Ito, O., Formation and photoinduced properties of zinc porphyrin-SWCNT and zinc phthalocyanine-SWCNT nanohybrids using diameter sorted nanotubes assembled via metal-ligand coordination and pi-pi stacking. *Journal of Porphyrins and Phthalocyanines* **2011,** *15* (9-10), 1033-1043; May, W. S.; Cuatrecasas, P., Transferrin Receptor - Its Biological Significance. *Journal of Membrane Biology* **1985,** *88* (3); Raaf, H.; Jacobsen, D.; Savon, S.; Green, R., Serum transferrin receptor level is not altered in invasive adenocarcinoma of the breast. *American Journal of Clinical Pathology* **1993,** *99*, 6; Reizenstein, P., Iton, Free-Radicals and Cancer. *Medical Oncology and Tumor Pharmacotherapy* **1991,** *8* (4).

4. Chaturvedi, D.; Goswami, A.; Saikia, P. P.; Barua, N. C.; Rao, P. G., Artemisinin and its derivatives: a novel class of anti-malarial and anti-cancer agents. *Chemical Society Reviews* **2010,** *39* (2), 435-454; Gravett, A. M.; Liu, W. M.; Krishna, S.; Chan, W. C.; Haynes, R. K.; Wilson, N. L.; Dalgleish, A. G., In vitro study of the anti-cancer effects of artemisone alone or in combination with other chemotherapeutic agents. *Cancer Chemotherapy and Pharmacology* **2011,** *67* (3), 569-577; Stockwin, L. H.; Han, B. N.; Yu, S. X.; Hollingshead, M. G.; ElSohly, M. A.; Gul, W.; Slade, D.; Galal, A. M.; Newton, D. L., Artemisinin dimer anticancer activity correlates with heme-catalyzed reactive oxygen species generation and endoplasmic reticulum stress induction. *International Journal of Cancer* **2009,** *125* (6), 1266-1275; Tan, W. F.; Shen, F.; Luo, X. J.; Su, C. Q.; Qiu, Z. Q.; Zeng, H. Z.; Yan, P. N.; Yu, Y.; Wu, M. C.; Jiang, X. Q.; Lau, W. Y., Artemisinin inhibits in vitro and in vivo invasion and metastasis of human hepatocellular carcinoma cells. *Phytomedicine* **2011,** *18* (2-3), 158-162; Yang, X. L.; Liu, D.; Wang, W.; Qu, L.; Jing, Y. K.; Zhao, L. X., Design, Synthesis and Antiproliferative Activities of Artemisinin Derivatives Containing a Substituted Piperazine. *Letters in Drug Design & Discovery* **2009,** *6* (8), 595-598; Singh, N. P.; Lai, H., Selective toxicity of dihydroartemisinin and holotransferrin toward human breast cancer cells. *Life Sciences* **2001,** *70* (1), 49-56.

5. He, R.; Mott, B. T.; Rosenthal, A. S.; Genna, D. T.; Posner, G. H.; Arav-Boger, R., An Artemisinin-Derived Dimer Has Highly Potent Anti-Cytomegalovirus (CMV) and Anti-Cancer Activities. *Plos One* **2011,** *6* (8); Ji, Y.; Zhang, Y. C.; Pei, L. B.; Shi, L. L.; Yan, J. L.; Ma, X. H., Anti-tumor effects of dihydroartemisinin on human osteosarcoma. *Molecular and Cellular Biochemistry* **2011,** *351* (1-2), 99-108; Jung, M.; Lee, S.; Ham, J.; Lee, K.; Kim, H.; Kim, S. K.,

Antitumor activity of novel deoxoartemisinin monomers, dimers, and trimer. *Journal of Medicinal Chemistry* **2003,** *46* (6), 987-994.

6. Hindley, S.; Ward, S. A.; Storr, R. C.; Searle, N. L.; Bray, P. G.; Park, B. K.; Davies, J.; O'Neill, P. M., Mechanism-based design of parasite-targeted artemisinin derivatives: Synthesis and antimalarial activity of new diamine containing analogues. *Journal of Medicinal Chemistry* **2002,** *45* (5), 1052-1063.

7. Posner, G. H.; Northrop, J.; Paik, I. H.; Borstnik, K.; Dolan, P.; Kensler, T. W.; Xie, S.; Shapiro, T. A., New chemical and biological aspects of artemisinin-derived trioxane dimers. *Bioorganic & Medicinal Chemistry* **2002,** *10* (1), 227-232.

8. Posner, G. H.; Paik, I. H.; Sur, S.; McRiner, A. J.; Borstnik, K.; Xie, S. J.; Shapiro, T. A., Orally active, antimalarial, anticancer, artemisinin-derived trioxane dimers with high stability and efficacy. *Journal of Medicinal Chemistry* **2003,** *46* (6), 1060-1065.

9. Posner, G. H.; McRiner, A. J.; Paik, I. H.; Sur, S.; Borstnik, K.; Xie, S. J.; Shapiro, T. A.; Alagbala, A.; Foster, B., Anticancer and antimalarial efficacy and safety of artemisinin-derived trioxane dimers in rodents. *Journal of Medicinal Chemistry* **2004,** *47* (5), 1299-1301.

10. Nakase, I.; Gallis, B.; Takatani-Nakase, T.; Oh, S.; Lacoste, E.; Singh, N. P.; Goodlett, D. R.; Tanaka, S.; Futaki, S.; Lai, H.; Sasaki, T., Transferrin receptor-dependent cytotoxicity of artemisinin-transferrin conjugates on prostate cancer cells and induction of apoptosis. *Cancer Letters* **2009,** *274* (2), 290-298.

11. Morrissey, C.; Gallis, B.; Solazzi, J. W.; Kim, B. J.; Gulati, R.; Vakar-Lopez, F.; Goodlett, D. R.; Vessella, R. L.; Sasaki, T., Effect of artemisinin derivatives on apoptosis and cell cycle in prostate cancer cells. *Anti-Cancer Drugs* **2010,** *21* (4), 423-432.

12. Firestone, G. L.; Sundar, S. N., Anticancer activities of artemisinin and its bioactive derivatives. *Expert Reviews in Molecular Medicine* **2009,** *11*.

13. Gao, N.; Budhraja, A.; Cheng, S.; Liu, E. H.; Huang, C.; Chen, J.; Yang, Z.; Chen, D.; Zhang, Z.; Shi, X., Interruption of the MEK/ERK signaling cascade promotes dihydroartemisinin-induced apoptosis in vitro and in vivo. *Apoptosis* **2011,** *16* (5), 511-523; Galal, A. M.; Gul, W.; Slade, D.; Ross, S. A.; Feng, S.; Hollingshead, M. G.; Alley, M. C.; Kaur, G.; ElSohly, M. A., Synthesis and evaluation of dihydroartemisinin and dihydroartemisitene acetal dimers showing anticancer and antiprotozoal activity. *Bioorganic & Medicinal Chemistry* **2009,** *17* (2), 741-751.

14. Singh, N. P.; Lai, H. C.; Park, J. S.; Gerhardt, T. E.; Kim, B. J.; Wang, S.; Sasaki, T., Effects of Artemisinin Dimers on Rat Breast Cancer Cells In Vitro and In Vivo. *Anticancer Research* **2011,** *31* (12), 4111-4114.

15. Augustijns, P.; Dhulst, A.; VanDaele, J.; Kinget, R., Transport of artemisinin and sodium artesunate in Caco-2 intestinal epithelial cells. *Journal of Pharmaceutical Sciences* **1996,** *85* (6), 577-579.

16. Morris, C. A.; Duparc, S.; Borghini-Fuhrer, I.; Jung, D.; Shin, C. S.; Fleckenstein, L., Review of the clinical pharmacokinetics of artesunate and its active metabolite dihydroartemisinin following intravenous, intramuscular, oral or rectal administration. *Malaria Journal* **2011,** *10*, 17.

17. Kreuter, J., Nanoparticle-based Drug Delivery Systems. *Journal of Controlled Release* **1991,** *16* (1-2), 169-176.

18. *Liposomes: Rational Design*. Marcel Dekker, Inc: New York, USA, 1999; p 451.

19. Allen, T. M.; Cullis, P. R., Drug delivery systems: Entering the mainstream. *Science* **2004,** *303* (5665), 1818-1822.

20. *Medical Applications of Liposomes*. Elsevier Science B.V.: The Netherlands, 1998; p 779.

21. Hashim, A. I.; Zhang, X. M.; Wojtkowiak, J. W.; Martinez, G. V.; Gillies, R. J., Imaging pH and metastasis. *Nmr in Biomedicine* **2011,** *24* (6), 582-591; Schindler, M.; Grabski, S.; Hoff, E.; Simon, S. M., Defective pH regulation of acidic compartments in human breast cancer cells (MCF-7) is normalized in adriamycin-resistant cells (MCF-7adr). *Biochemistry* **1996,** *35* (9), 2811-2817; Martinez, G. V.; Zhang, X.; García-Martín, M. L.; Morse, D. L.; Woods, M.; Sherry, A. D.; Gillies, R. J., Imaging the extracellular pH of tumors by MRI after injection of a single cocktail of T1 and T2 contrast agents. *NMR in Biomedicine* **2011**.

22. Choi, S. U.; Bui, T.; Ho, R. J. Y., pH-dependent interactions of indinavir and lipids in nanoparticlies and their ability to entrap a solute. *Journal of Pharmaceutical Sciences* **2008,** *97* (2), 931-943; Kinman, L.; Bui, T.; Larsen, K.; Tsai, C. C.; Anderson, D.; Morton, W. R.; Hu, S. L.; Ho, R. J. Y., Optimization of lipid-indinavir complexes for localization in lymphoid tissues of HIV-infected macaques. *Jaids-Journal of Acquired Immune Deficiency Syndromes* **2006,** *42* (2), 155-161.

23. Xia, W. L.; Bisi, J.; Strum, J.; Liu, L. H.; Carrick, K.; Graham, K. M.; Treece, A. L.; Hardwicke, M. A.; Dush, M.; Liao, Q. Y.; Westlund, R. E.; Zhao, S. M.; Bacus, S.; Spector, N. L., Regulation of survivin by ErbB2 signaling: Therapeutic implications for ErbB2-overexpressing breast cancers. *Cancer Research* **2006,** *66* (3), 1640-1647.

24. Velasco-Velazquez, M. A.; Li, Z.; Casimiro, M.; Loro, E.; Homsi, N.; Pestell, R. G., Examining the role of cyclin D1 in breast cancer. *Future Oncology* **2011,** *7* (6), 753-765.

25. de Ruijter, T. C.; Veeck, J.; de Hoon, J. P. J.; van Engeland, M.; Tjan-Heijnen, V. C., Characteristics of triple-negative breast cancer. *Journal of Cancer Research and Clinical Oncology* **2011,** *137* (2), 183-192.

26. Chakraborti, A. K.; Rudrawar, S.; Kondaskar, A., Lithium bromide, an inexpensive and efficient catalyst for opening of epoxide rings by amines at room temperature under solvent-free condition. *European Journal of Organic Chemistry* **2004,** (17), 3597-3600.

27. Huotari, J.; Helenius, A., Endosome maturation. *Embo Journal* **2011,** *30* (17), 3481-3500.

28. Mu, D.; Chen, W.; Yu, B.; Zhang, C.; Zhang, Y.; Qi, H., Calcium and survivin are involved in the induction of apoptosis by dihydroartemisinin in human lung cancer SPC-A-1 cells. *Methods and Findings in Experimental and Clinical Pharmacology* **2007,** *29* (1), 33-38; Li, L.-N.; Zhang, H.-D.; Yuan, S.-J.; Tian, Z.-Y.; Wang, L.; Sun, Z.-X., Artesunate attenuates the growth of human colorectal carcinoma and inhibits hyperactive Wnt/beta-catenin pathway. *International Journal of Cancer* **2007,** *121* (6), 1360-1365.

29. Yamamoto, H.; Ngan, C. Y.; Monden, M., Cancer cells survive with survivin. *Cancer Science* **2008,** *99* (9), 1709-1714.

30. Hinnis, A. R.; Luckett, J. C. A.; Walker, R. A., Survivin is an independent predictor of short-term survival in poor prognostic breast cancer patients. *British Journal of Cancer* **2007,** *96* (4), 639-645.

31. Nakahara, T.; Takeuchi, M.; Kinoyama, I.; Minematsu, T.; Shirasuna, K.; Matsuhisa, A.; Kita, A.; Tominaga, F.; Yamanaka, K.; Kudoh, M.; Sasamata, M., YM155, a novel small-molecule survivin suppressant, induces regression of established human hormone-refractory prostate tumor xenografts. *Cancer Research* **2007,** *67* (17), 8014-8021; Tolcher, A. W.; Mita, A.; Lewis, L. D.; Garrett, C. R.; Till, E.; Daud, A. I.; Patnaik, A.; Papadopoulos, K.; Takimoto, C.; Bartels, P.; Keating, A.; Antonia, S., Phase I and Pharmacokinetic Study of YM155, a Small-Molecule Inhibitor of Survivin. *Journal of Clinical Oncology* **2008,** *26* (32), 5198-5203.

32. Masamha, C. P.; Benbrook, D. M., Cyclin D1 Degradation Is Sufficient to Induce G(1) Cell Cycle Arrest despite Constitutive Expression of Cyclin E2 in Ovarian Cancer Cells. *Cancer Research* **2009,** *69* (16), 6565-6572.

33. Shan, J.; Zhao, W.; Gu, W., Suppression of Cancer Cell Growth by Promoting Cyclin D1 Degradation. *Molecular Cell* **2009,** *36* (3), 469-476.

34. Slamon, D. J.; Clark, G. M.; Wong, S. G.; Levin, W. J.; Ullrich, A.; McGuire, W. L., Human-Breast Cancer - Correlation of the Relaps and Survival with Amplification of the HER-2 NEU Oncogene. *Science* **1987,** *235* (4785), 177-182.

35. Garrett, J. T.; Olivares, M. G.; Rinehart, C.; Granja-Ingram, N. D.; Sanchez, V.; Chakrabarty, A.; Dave, B.; Cook, R. S.; Pao, W.; McKinely, E.; Manning, H. C.; Chang, J.; Arteaga, C. L., Transcriptional and posttranslational up-regulation of HER3 (ErbB3) compensates for inhibition of the HER2 tyrosine kinase. *Proceedings of the National Academy of Sciences of the United States of America* **2011,** *108* (12), 5021-5026.

36. Cook, R. S.; Garrett, J. T.; Sanchez, V.; Stanford, J. C.; Young, C.; Chakrabarty, A.; Rinehart, C.; Zhang, Y.; Wu, Y.; Greenberger, L.; Horak, I. D.; Arteaga, C. L., ErbB3 Ablation Impairs PI3K/Akt-Dependent Mammary Tumorigenesis. *Cancer Research* **2011,** *71* (11), 3941-3951.

37. Bacus, S. S.; Altomare, D. A.; Lyass, L.; Chin, D. M.; Farrell, M. P.; Gurova, K.; Gudkov, A.; Testa, J. R., AKT2 is frequently upregulated in HER-2/neu-positive breast cancers and may contribute to tumor aggressiveness by enhancing cell survival. *Oncogene* **2002,** *21* (22), 3532-3540.

38. Holbro, T.; Beerli, R. R.; Maurer, F.; Koziczak, M.; Barbas, C. F.; Hynes, N. E., The ErbB2/ErbB3 heterodimer functions as an oncogenic unit: ErbB2 requires ErbB3 to drive breast tumor cell proliferation. *Proceedings of the National Academy of Sciences of the United States of America* **2003,** *100* (15), 8933-8938.

39. Amin, D. N.; Campbell, M. R.; Moasser, M. M., The role of HER3, the unpretentious member of the HER family, in cancer biology and cancer therapeutics. *Seminars in Cell & Developmental Biology* **2010,** *21* (9), 944-960.

40. Garrett, J. T.; Arteaga, C. L., Resistance to HER2-directed antibodies and tyrosine kinase inhibitors. *Cancer Biology & Therapy* **2011,** *11* (9), 793-800.

41. Chadwick, J.; Mercer, A. E.; Park, B. K.; Cosstick, R.; O'Neill, P. M., Synthesis and biological evaluation of extraordinarily potent C-10 carba artemisinin dimers against P-

falciparum malaria parasites and HL-60 cancer cells. *Bioorganic & Medicinal Chemistry* **2009,** *17* (3), 1325-1338.

42. Kinman, L.; Brodie, S. J.; Tsai, C. C.; Bui, T.; Larsen, K.; Schmidt, A.; Anderson, D.; Morton, W. R.; Hu, S. L.; Ho, R. J. Y., Lipid-drug association enhanced HIV-1 protease inhibitor indinavir localization in lymphoid tissues and viral load reduction: A proof of concept study in HIV-2(287)-infected macaques. *Jaids-Journal of Acquired Immune Deficiency Syndromes* **2003,** *34* (4), 387-397.

CHAPTER 3

pH-Responsive Artemisinin Dimer in Lipid Nanoparticles are Effective Against Human Breast Cancer in a Xenograft Model

Content of this Chapter was published as a research article in Journal of Pharmaceutical Sciences, 2015, in press.

The manuscript was authored by:

Yitong J. Zhang[1], Xi Zhan[2], Liguo Wang[2], Rodney J.Y. Ho[3], Tomikazu Sasaki[1*]

[1]Department of Chemistry, [2]Department of Biological Structures, [3]Department of Pharmaceutics
University of Washington, Seattle, WA, 98105

Abstract

We previously reported a group of novel dimeric artemisinin piperazine conjugates (ADPs) possessing pH-dependent aqueous solubility and further improved potency in a proof-of-concept

lipid nanoparticle formulation based on natural egg phosphatidylcholine (EPC). EPC may induce allergic reactions in individuals sensitive to egg products. Therefore, the goal of this report is to develop ADP-synthetic lipid particles suitable for *in vivo* evaluation. We found that ADP binds to DPPC with >90% efficiency and forms drug-lipid particles (d ~80nm). Cryo-electron microscopy of the ADP drug-lipid particles revealed unilamellar vesicle-like structures when 10 mol% of ADP109 is incorporated. Detailed characterization studies show insertion of ADP lead compound, **ADP109,** into the DPPC membrane and presence of a core capable of carrying aqueous marker calcein. Over 50% of the **ADP109** was released in 48 hours at acidic pH compared to less than 20% at neutral. **ADP109**-lipid particles exhibited high potency against human breast cancer, but was tolerated well by non-tumorigenic cells. In MDA-MB-231 mouse xenograft, lipid-bound **ADP109** particles were more effective than paclitaxel in controlling tumor growth (29% smaller tumor at Day 15). Cellular uptake studies showed endocytosis of the nanoparticles and release of core-trapped marker throughout the cytosol at 37°C. These results demonstrate, for the first time, the *in vivo* feasibility of lipid-bound artemisinin dimer cancer chemotherapy.

Introduction

Previously, we reported a proof-of-concept study where the pH-responsive artemisinin dimer, **ADP109** (**Scheme 1**), was bound to egg phosphatidylcholine (EPC) liposome and the drug-lipid nanoparticles demonstrated equally high potency as the free drug in cell culture[1]. While EPC is useful in initial *in vitro* studies, it has a number of limitations for clinical use. Being a mixture of

phospholipids extracted from natural sources, EPC may have variation in fatty acyl chain compositions among batches, increasing the risk of poor reproducibility. In addition, patients who are allergic to egg products may be at risk of an immune response to the EPC. Thus, despite the gaining clinical use of liposomal drug therapeutics[2], few contain natural EPC lipids[3].

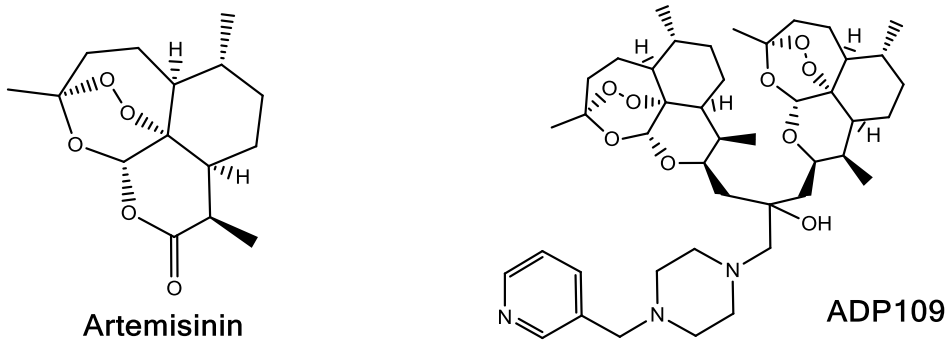

Scheme 1. Chemical Structure of Artemisinin and **ADP109**.

The goal of this study, thus, is to characterize the **ADP109**-lipid interactions and formulate nanoparticles using lipids with well-defined, saturated fatty acid chains for preclinical development. The **ADP109**-lipid particles in this study are based on a more robust synthetic lipid with saturated fatty acid chains, dipalmitoylphosphatidylcholine (DPPC) with a polyethylene glycol shell. The pH-responsive loading and release of ADP109 are confirmed with the new DPPC-based formulation by measuring the amount of drug association after dialysis under corresponding conditions. The drug-lipid interaction, specifically the effect of drug incorporation on lipid molecular packing, is studied by monitoring the fluorescence polarization of a planar probe, diphenylhexatriene (DPH)[4].

Furthermore, we examine the morphology of the **ADP109**-DPPC lipid nanoparticles with cryo-electron microscopy techniques. The presence of an aqueous core enclosed by a lipid membrane,

representative of liposomal structures, is confirmed by trapping a concentration-dependent self-quenching fluorescent dye, calcein, in the core[5].

Anticancer activities and selectivity of the **ADP109**-DPPC lipid nanoparticles are evaluated both *in vitro* and *in vivo*. Cytotoxicity of the formulation is tested against two types of human breast cancer cell lines, BT474 and MDA-MB-231 and a non-tumorigenic human epithelial cell line, MCF10A. The *in vivo* study is conducted on nude mice MDA-MB-231 xenograft model. Standard treatment regime of paclitaxel is used as a bench-mark control for comparison of the ADP109-DPPC nanoparticles.

Results and Discussion

The feasibility of substituting egg derived phosphatidylcholine with a well-defined synthetic lipid, DPPC, was validated by preparing **ADP109**-bound liposome composed of 95% DPPC and 5% polyethylene glycol-2000 (PEG_{2000}) at the same drug-to-lipid ratio as that of the EPC-liposomes for comparison of drug association efficiency and particle size (**Table 1**). PEG_{2000} was included at 5% (mole) to provide higher degree of hydration intended for *in vivo* stealth

(reduced nonspecific uptake by phagocytes) effect[6,7]. Our data in **Table 1** demonstrate that replacement of EPC with DPPC has no impact on percent drug loading or particle diameter. Therefore, all studies were performed with DPPC-based composition below.

Table 1. Comparison of size and incorporation efficiency of NP109 and NP209.

	Lipid Composition	Drug:Lipid Ratio	Average Size (d, nm)	% Drug Incorporation
NP109[1]	EPC	1:10	70(±20)	91(±9)%
NP209	95% DPPC : 5% DPPE-mPEG$_{2000}$	1:10	76(±10)	90(±6)%

Average Size and % Drug Incorporation values reported as average (±S.D.) of three independent experiments.

***ADP109** Liposome Nanoparticle Characterization and Optimization*

ADP109-bound lipid nanoparticles, **NP209**, were prepared by thin-film-rehydration method and particle size was reduced by bath sonication[8]. Particles with varied drug-to-lipid ratio (D:L) were prepared to study the loading capacity of bulky hydrophobic ART-dimers in liposomes and drug-lipid binding interactions. ART-dimer loading was optimum at D:L of 1:10. Insoluble **ADP109** precipitated when the D:L was 1:3 or 1:5. When the D:L was decreased to 1:7, no precipitates were observed but the efficiency of drug incorporation was only 50 ± 3%. These data suggest that there exists an upper limit to the amount of **ADP109** that is able to bind to the lipid membrane, either interacting with the surface of or incorporated into the hydrophobic membrane. Thus, **NP209** was prepared at D:L of 1:10 for further characterizations to most efficiently load the drug into the lipid particles that are under 100 nm in diameter.

Physical properties such as size, drug loading efficiency and aqueous core presence were characterized for the ART-dimer (**ADP109**)-lipid nanoparticle. At 1:10 ratio of **ADP109**:total

lipid, **NP209** sized at 76 ±10 nm in diameter with polydispersity index (PDI) of 0.205 ± 0.015. The drug loading efficiency was 90 ± 6% at lipid concentrations between 20 mM to 200 mM, with a maximum concentration of 15.6 mg of **ADP109** dissolved per milliliter with 200mM lipid in PBS (**Table 1**). The existence of an aqueous core within **NP209** was confirmed by trapping an aqueous soluble fluorescent marker, calcein. High concentrations of calcein result in self-quenching phenomenon. When 50 mM of calcein is stably encapsulated in the aqueous core of liposome particles, fluorescence is reduced due to self-quenching; when the core is unstable or the liposome is lysed, calcein escapes from the aqueous core and the concentration is diluted, resulting in regeneration of fluorescence. In **NP209**, calcein showed 98.5 (±0.5)% quenching, indicating a stable aqueous core capable of trapping small water-soluble marker at a **ADP109**:lipid ratio of 1:10.

Morphological characterization by cryo-electron microscopy (cryo-EM) showed spherical nanoparticles with an average particle size at 55.9 nm (n=468). Comparison between 0° and 45° tilted imaging proved that the **ADP109**-bound liposome particles are three-dimensional spheres. The **NP209** cryo-EM images are reflective of literature published unilamellar vesicles[9] (**Figure 1**), suggesting that these **NP209** nanoparticles exist as liposome-like structures with a single bilayer enclosing an aqueous core. Membrane inserted **ADP109** at 10 mol% does not seem to significantly impact the formation of these DPPC-based unilamellar vesicles.

(a)

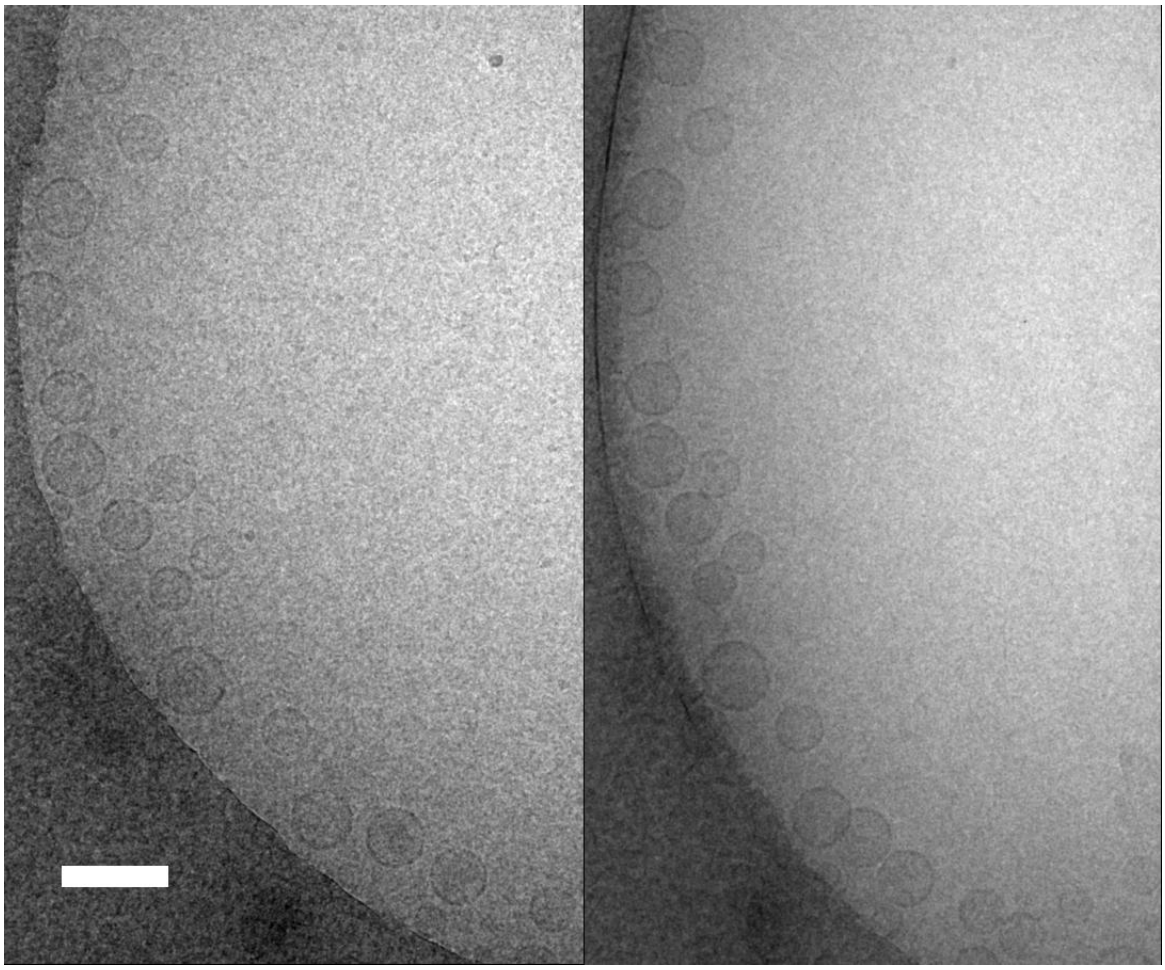

(b)

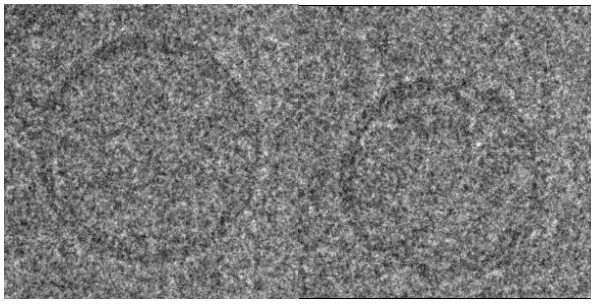

Figure 1. (a)Representative cryo-EM images of **NP209** liposomes viewed as untilted (left, 0°) and tilted (right, -45°). Scale bar = 100 nm. (b) Enlarged images showing individual particles selected from untilted view.

*Effect of **ADP109** Binding on Lipid Membrane Phase Transition Behavior*

While the above study denoted that **ADP109** was associated with the lipid membrane, it is not yet clear how the ART-dimer interacts with the membrane. Drug incorporation in the lipids alters membrane behavior, while encapsulation within the aqueous core may have minimal impact on membrane lipid organization. To study this lipid-drug interaction, a fluorescent polarization probe, diphenyl-1,3,5-hexatriene[4, 10] (DPH), was used to determine the effect of **ADP109** incorporation on the packing order of lipids. The rotational freedom of the inserted DPH corresponds to the viscosity of the membrane environment. Thus gel state, or high viscosity, membranes yield high fluorescence anisotropy values and depolarization are observed as membranes become more disordered during and after phase transition[5, 11]. Depolarization of DPH as particle membranes melt can be modeled to estimate the T_m. As shown in **Figure 2**, when **ADP109** was incorporated into the lipid membranes at 1:10 D:L ratio, fluorescence anisotropy of DPH in **NP209** at gel state (~23°C) was lower than that of control liposome without drug (**Blank NP209**), suggesting that **ADP109** presence resulted in less ordered packing of lipid molecules even when the particles were in solid phase (**Figure 2a**). Presence of **ADP109** lowered the T_m of the membrane system in **NP209** compared to **Blank NP209** by 3°C (**Figure. 2b**). Together, these data suggest that **ADP109** molecules insert into the lipid-membrane with sufficient depth such that the interactions impacted both the phase transition temperature and membrane packing or "order" in both gel and fluid phase.

(a)

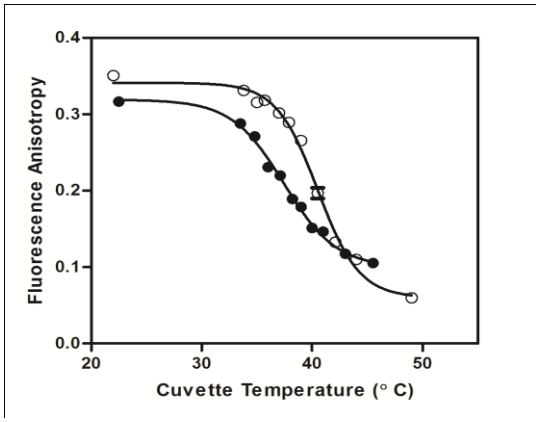

(b)

	T_m (°C)
Blank NP209	40.4 (±0.1)
NP209	37.4 (±0.1)

Figure 2. Effects of **ADP109** on phase transition behavior of lipids containing 95% DPPC and 5% $mPEG_{2000}$-DPPE, determined by DPH fluorescence anisotropy as a function of temperature. (a) Fluorescence anisotropy of DPH incorporated in lipid membranes of control **Blank NP209** (○) or drug-bound **NP209** (●) with change in temperature. (b) Gel-fluid phase transition temperatures calculated from fluorescence polarization studies. Values plotted and reported as average (± S.D.) of triplicate measurements.

*pH-Responsive Release of Lipid-bound **ADP109** and Aqueous Core Entrapped Calcein*

ADP109 possesses a pyridine-methyl-piperazine tail (**Scheme 1**) to allow pH-dependent aqueous solubility, as previously reported[1]. To evaluate pH-responsive drug release, **NP209** was exposed to pH 7.4, 6.0 and 4.0 to measure the ART-dimer release over time. **NP209** released **ADP109** more efficiently at pH 4 than physiological neutral. At pH 4, over 50% of the hydrophobic drug escaped from the liposomes by 48 hours while only 20% release was recorded at pH 7.4 in the same time period (**Figure 3**).

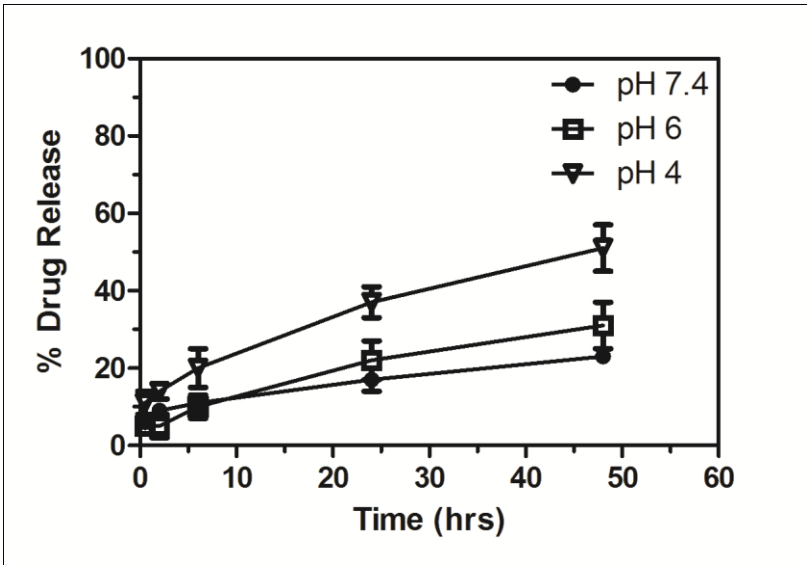

Figure 3. pH-dependent **ADP109** release from **NP209** (20 mM lipid) dialyzed under ambient temperature at pH 7.4, 6, and 4. Values plotted as average (±S.D.) of three independent experiments.

The protonation of **ADP109** incorporated in the liposome membrane resulted in perturbation of membrane and destabilization of the particle aqueous compartment, as measured by an increase in fluorescence generated by released calcein. The encapsulated calcein release profile, albeit also dependent on pH of the environment, were different from that of **ADP109**. The time course of fluorescence regeneration was recorded over 48 hours at indicated pH and 37°C (**Figure 4**). While drug-free **Blank NP209** showed little fluorescence regeneration regardless of pH, **NP209** released calcein in a clear pH-dependent manner (**Figure 4**). It should be noted that **NP209** regenerated 30% of calcein fluorescence after 24 hours even at pH 7.4 when the blank control regenerated less than 1% under the same conditions. This was likely due to the T_m of **NP209** (37.4°C) being close to the incubation temperature (37.0°C), resulting in the most leaky state of

the membrane during incubation[12]. Improvements in drug retention and particle stability under physiological conditions are being investigated and will be reported separately.

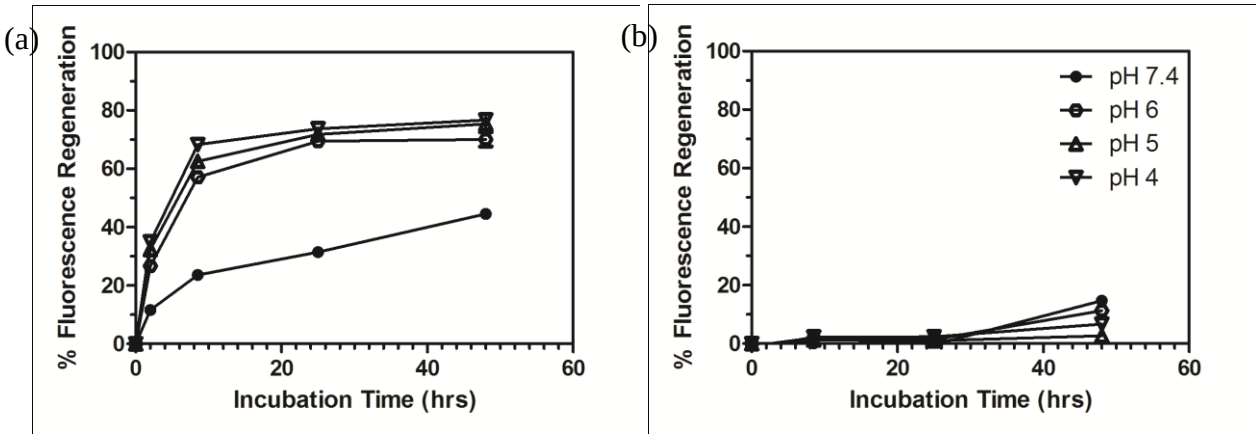

Figure 4. pH-dependent calcein fluorescence regeneration profiles of (a) **NP209** and (b) the drug-free **Blank NP209**. Values plotted as average with S.D. as error bars of triplicate readings, after adjustment of pH effect on calcein fluorescence.

*Effects of Liposome Association on **ADP109** in vitro Cytotoxicity against Human Breast Cancer Cells*

We assessed the potency of **NP209** on two human breast cancer cell lines with different degrees of drug resistance. BT474 is a $HER2^+$ cell line that has been shown to be susceptible towards the artemisinin pharmacophore; MDA-MB-231 is a Triple Negative Breast Cancer (TNBC) cell line (lacking estrogen receptor, progesterone receptor and HER2) that is more resistant toward artemisinin derivatives[13]. In addition, to evaluate selectivity and safety, a non-tumorigenic human breast epithelial cell line, MCF10A, was also used in the cytotoxicity assay. We found that lipid nanoparticle-bound **ADP109** exhibited similar potency to that of free **ADP109** (**Table**

2), with IC_{50} values in the low nanomolar range for BT474 and single digit micromolar range for MDA-MB-231. The **NP209** nanoparticles showed similar anti-cancer potency as free drug in 1% DMSO against BT474 cells, and a 3-fold reduction in the IC_{50} value (p = 0.03) on MDA-MB-231 cells.

Table 2. Calculated IC_{50} values of ADP109, NP109 and NP209 on BT474, MDA-MB-231 and MCF10A cell lines.

	IC_{50} (μM±SD)		
	BT474	MDA-MB-231	MCF10A
ADP109	0.07±0.01	10 (±3)	>10[†]
NP109	0.08±0.01[1]	7 (±2) [1]	>10[†]
NP209	0.105±0.003	3 (±1)*	>10[†]

Values reported as average (±S.D) of three independent experiments, with each experiment performed in triplicates. * Significantly different from IC_{50} of free ADP109 (p=0.03). [†] more than 50% cell living after 48-hour incubation with 10μM.

Although the exact mechanism leading to the anti-tumor effects of **ADP109** or **NP209** nanoparticles is not clear, our previous study with **NP109** showed down-regulation of proteins such as survivin and cyclin D1[1]. Survivin has been reported to correlate strongly with anti-apoptotic ability of cancer cells[14] and cyclin D1 with human cancer incidence[15]. The immortal non-tumorigenic human breast epithelial cell line, MCF10A, was less susceptible to both the free compound and its liposome formulations. In both **NP109**[1] and **NP209** assays, more than 50% of MCF10A cells were still viable after 48 hours of incubation at 10 μM **ADP109** concentration. We have yet to test concentrations higher than 10 μM on MCF10A cells. Under our experimental conditions, **NP209** was about 100 times more selective against BT474 cells than MCF10A cells, and 3 fold more potent against MDA-MB231 cells. While MCF10A is often used as a non-

tumorigenic control, it in fact differs from real healthy cells found *in vivo* as it has been induced to proliferate in culture. Thus, the selectivity recorded for **ADP109** and its lipid particles may represent underestimated values.

*Effect of **NP209** on Suppressing Tumor Growth in MDA-MB-231 Mice Xenograft*

Prior to the efficacy study, the *in vivo* safety of **NP209** was done to define a maximum tolerated dose (MTD). We found that a maximum dose of 40 mg/kg every 2 days (q2d) could be tolerated for at least 3 weeks without significant body weight loss in healthy mice. Therefore, a dose of 40 mg/kg q2d subcutaneous injection was chosen for the initial proof-of-concept efficacy study.

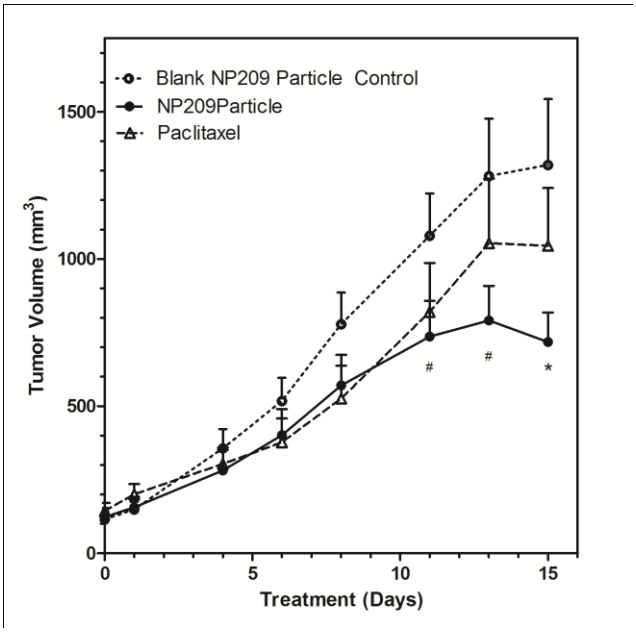

Figure 5. Average tumor volume measured of **NP209** (●) Test Group and **Blank NP209** (---) Control Group treated with 40 mg/kg drug every other day subcutaneous injection of nanoparticles from Day 0 to Day 15, and intravenous injection of Paclitaxel (△) once per day from Day 0 to Day 4 at 10 mg/kg. Day 0 is defined as 10 days after tumor implant. Values plotted as average with error bars as standard error of mean (SEM) of seven animals in each group. Significant difference was defined by the *t*-test where $p < 0.05$: $^{\#}$ $p < 0.1$, * $p < 0.05$

between **NP209** and **Blank NP209**. Paclitaxel group did not show significant difference compared with Control or Test groups.

Despite lower potency reported for **ADP109** compared to other breast cancer cells tested, MDA-MB-231 was chosen for the *in vivo* study. The use of TNBC cells, MDA-MB-231, in immune-compromised mice as xenograft models provide a more challenging treatment that addresses both drug resistance and drug sensitive scenarios. Currently, there are only a few treatment choices for TNBC patients. Standard cytotoxic agents such as taxanes, anthracyclines and platinum-based agents, either used as single or combination therapy control tumor growth with limited efficacy[16]. Thus, to explore the potency of our pH-responsive **ADP109**-bound lipid nanoparticle on TNBC *in vivo*, female athymic nude mice were implanted with MDA-MB-231 cells in the mammary pad and allowed 10 days for tumor development until solid volume reached approximately 100 mm^3. The mice were then randomly assigned into 3 groups: **NP209**, **Blank NP209**, or paclitaxel (positive control) at typically recommended dose and frequency. The **NP209** test group received a 40 mg **ADP109**/kg dose (q2d for 14d) in lipid nanoparticle formulation while the vehicle control group received equivalent dose of **Blank NP209**, both given subcutaneously on the back of the animal. As shown in **Figure 5**, although tumor size in all groups increased, the rate of tumor growth was suppressed significantly in mice receiving **NP209** compared to that of the lipid control ($p < 0.05$) on day 14. Furthermore, **NP209** outperformed paclitaxel, a standard chemotherapy for breast cancer[16], given under standard dose regimen for this TNBC xenograft mouse model. The apparent low efficacy of paclitaxel found in both our study and the literature[17, 18] is consistent with the fact that MDA-MB-231 cells are relatively insensitive to paclitaxel-induced mitotic arrest that leads to apopsotis[17]. While the

mechanism of action of ART-dimers' anti-proliferative effect is still a subject of active investigation, our results showed that MDA-MB-231 cells were susceptible to the ART-dimers both *in vitro* and *in vivo*. This initial xenograft efficacy study provided us with the first insight to support our continued effort of ART-dimer nanoparticle development.

Our finding on the effective growth suppression but not regression of the TNBC tumor by pH-responsive ART-dimer liposomes is consistent with literature consensus that the artemisinin pharmacophore is cytostatic but not cytotoxic at the concentrations used in these animal studies[19]. This suggests that ART-dimer based compounds may best be administered as adjuvant therapy to manage the disease progression. We showed that aqueous marker, calcein, can be effectively co-released with the membrane-incorporated **ADP109**. Therefore, one can design a water soluble cytotoxin encapsulated within the core of these **ADP109**-bound lipid nanoparticles to simultaneously deliver multiple drugs to cancer cells to achieve a maximal potency against hard-to-treat cancers such as TNBC. Dose dependent pharmacology and toxicology as well as pharmacokinetic and efficacy studies would be needed to confirm the potential of **ADP109**-bound lipid nanoparticles as a mono- or combination therapeutic candidate. Such studies are beyond the scope of this report and are part of our on-going effort to optimize the lipid-drug nanoparticle's properties for enhanced stability, safety and efficacy. The pH-responsive ART-dimer nanoparticle xenograft study reported here is the first *in vivo* experiment to deliver these hydrophobic dimer derivatives in aqueous solutions, to the best of our knowledge. We hope that the better understanding of drug-lipid interactions and promising potency shown in this report will enable further development of artemisinin based nanoparticle therapeutics.

*Cellular Uptake of Calcein-encapsulating **NP209** Shows Energy-dependent Uptake Mechanism*

To shed light on uptake mechanisms of **NP209** by human breast cancer cells, BT474 cells were incubated with 1mM **NP209** for 10 or 120 minutes at 37°C, at physiological temperature or 4°C, where no energy-dependent uptake was feasible[20]. Figure 6 shows representative fluorescence microscopy images of cells incubated with blank PBS for 120 minutes, 1mM **NP209** for 10 or 120 minutes and free calcein at a concentration equivalent to that released by 1mM **NP209** in 120 minutes. Intact calcein-trapped NP209 particles show up as punctated fluorescence whereas when particle membrane disintegrates and calcein is released, diffused fluorescence is observed throughout the cell. Only at 37°C were we able to see clear diffused calcein fluorescence inside the peripheral of the cell, suggesting release of the aqueous core-trapped content into intracellular compartments and cytosol of the cells. Longer incubation time afforded higher fluorescence intensity, correlating to greater amount of uptake and cargo release.

At 4°C, however, where all energy-dependent uptake pathways are inhibited, we no longer were able to observe diffused fluorescence inside the cell membranes. The rigidity of cell and drug-bound lipid membranes at lower temperature also likely resulted in less fusion of **NP209** to cell membranes, further decreasing amount of delivery to the cells. In case of 1mM **NP209** incubated for 120 minutes at 4°C, few of the faintly fluorescent **NP209** could be observed attached to cell surface under microscope. These cellular uptake results confirm our *in vitro* and *in vivo* data that the lipid-associated **ADP109** are being delivered into the cytoplasm and other organelles within breast cancer cells, thus leading to observed suppression of tumor cell growth.

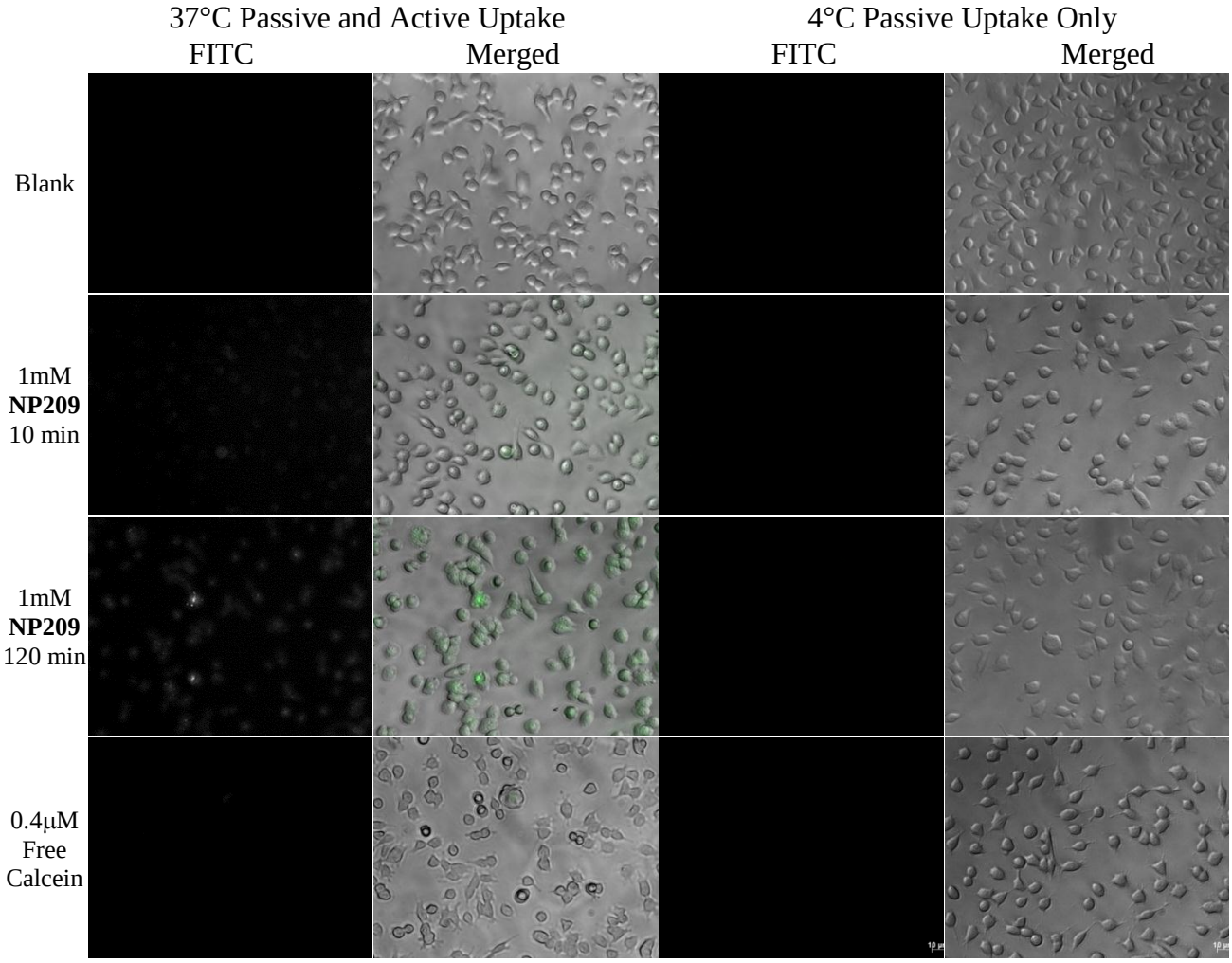

Figure 6. Representative fluorescence microscopy images of BT474 cells incubated at 37°C (left 2 panels) and 4°C (right 2 panels) with Blank PBS, **NP209** or free calcein concentration equivalent to that released by **NP209** in 120 minutes at 37°C. Energy-dependent uptake of intact particles and release of aqueous core-trapped calcein are observed at both 10 minutes and 120 minutes. Images taken with 40X magnification and scale bar = 10 μm.

Experimental Section

Materials

Lipids 1,2-dipalmitoyl-*sn*-glycero-3-phosphocholine (DPPC) and 1,2-dipalmitoyl-*sn*-glycero-3-phosphoethanolamine-N-[methoxy(polyethylene glycol)-2000 sodium salt ($mPEG_{2000}$-DPPE) were purchased from Genzyme (Cambridge, MA) in powder form. Chloroform (*hazardous volatile solvent, handle in ventilated hood)* was dried with molecular sieves for at least 24 hours before use. Calcein was purchased from TCI America (Portland, OR), dipheyl-1,3,5-hexatriene (DPH) was bought from Life Technologies (Formerly Invitrogen, Carlsbad, CA). Thiazolyl Blue Tetrazolium Bromide (MTT) powder was purchased from Sigma Aldrich (St.Louis, MO). Commercially prepared 1X phosphate buffered saline (PBS) solution was obtained from Thermo Scientific (Waltham, MA). Glow-discharged Quantifoil R-2/2 grid (300 mesh) for EM imaging was purchased from Electron Microscopy Sciences (Hatfield, PA). Mice experiments were conducted in the facility of Washington Biotechnology Inc. (Baltimore, MD). Animal protocol was reviewed and approved by the company's IACUC, approval number 12-002.

*Preparation and Size Characterization of DPPC-based Liposome (**NP209**) of Artemisinin-dimer-pyridylmethylperazine (**ADP109**)*

The general procedure followed that of the previously published protocol[8]. **ADP109** was dissolved in chloroform to make a 50mg/mL stock solution. The DPPC and $mPEG_{2000}$-DPPE were dissolved in chloroform at the concentration of 100 mg/mL. Aliquots of **ADP109**, DPPC and $mPEG_{2000}$-DPPE stock solutions were added to a screw-capped glass test tube. Organic solvent was removed under a gentle stream of nitrogen followed by further drying *in vacuo*

overnight to form a thin film on the inner wall. The thin film was rehydrated with 1X PBS at ~47°C for 1-3 hours, depending on concentration, to give a liposome suspension at desired lipid concentration (20-200 mM). The mixture was then sonicated at 45°C for 5 minutes 3 times to give a translucent suspension without observable particles and then gradually cooled down to well below the lipid phase transition temperature (4°C), to afford the desired nanometer-sized liposomes. **NP209** was diluted to 2 mM for sizing measurements on a Zetasizer Nano ZS (Malvern Instrument, Worcestershire, UK) with argon laser (λ=633.0 nm) at room temperature. Sizing data were reported as the average (± S.D.) of 5 measurements with 13 runs per measurement.

*Cryo-electron Microscopy Characterization of **NP209***

To prepare **NP209** nanoparticle samples for cryo-EM imaging, 4 μL of 1 mM liposome suspension was applied on a glow-discharged Quantifoil R-2/2 grid (300 mesh, Electron Microscopy Sciences, Hatfield, PA). The sample was blotted by a piece of filter paper to remove excess solution, and then plunged into liquid ethane, which was cooled by liquid nitrogen. Cryo-EM samples were stored in liquid nitrogen till observation. Cryo-EM images were recorded on an Eagle 4k×4k camera (FEI, OH) using a Tecnai G2 F20 microscope (FEI Inc., OR) at 200 kV with a 20 μm objective aperture at -180°C. The electron dose for each exposure was around 2,000 e^-/nm^2. Cryo-EM images were taken at -4 μm defocus, and the effective pixel size was 0.44 nm. The size of nanoparticles was analyzed using ImageJ[21] .

*Effects of **ADP109** on Membrane Phase Transition Behavior*

NP209 was diluted to 1 mM in 1X PBS and warmed to 60°C for 5 minutes. Stock solution of 1,6-Diphenyl-1,3,5-hexatriene (DPH), was prepared at 2 mM in tetrahydrofuran (THF). 0.05%

volume of the DPH Stock was mixed with the liposome suspensions, vortexed briefly, incubated at 60°C for 15 minutes in the dark, then cooled down to room temperature (21-24°C) for fluorescence polarization measurements on a Hitachi F4500 fluorescence spectrophotometer (Tokyo, Japan). A circulating water bath (Fischer Scientific model 800, Pittsburgh, PA) maintained stable temperature during measurements. A digital thermo probe (Fischer Scientific, Pittsburgh, PA) was used to monitor the exact temperature within the cuvette and ensure stability of temperature while the liposome sample was heated. Fluorescence measurements were taken as an average of 10 seconds of continuous reading. Triplicate measurements in each direction of emission polarization: 0° ($I_{/\!/}$) and 90° ($I_{\perp}$) with respect to 0° excitation, were measured with liposomes in 1X PBS. Curve fitting was based on average and standard deviation (S.D.) calculated from triplicate readings. The fluorescence anisotropy was calculated using **Eq. 1** below:

$$\text{Fluorescence Anisotropy} = \frac{I_{/\!/} - I_{\perp}}{I_{/\!/} + 2I_{\perp}}$$

ADP109 *Incorporation into Liposomes and pH-responsive Release Efficiencies*

Methods used for loading and release efficiencies were the same as described in the Experimental Section of Chapter 2. 1X PBS buffer was used for dialysis of **NP209** in this case.

The Loading Efficiency was calculated according to the following equation (**Eq. 2**) below:

$$\text{Loading Efficiency (\%)} = \frac{A_{263}\,(D)}{A_{263}\,(UD)} \times 100\%$$

Where A_{263} (D) is the absorbance at 263nm of the dialyzed sample, and A_{263} (UD) is that of the undialyzed sample.

For the release efficiency studies, aliquots of 300μL of 20mM dialysis-purified liposome suspensions were dialyzed against 500mL of pH 7.4 PBS, pH 6 citrate or pH 4 citrate buffers at ambient temperature. 30μL aliquots were removed from each dialysis at times t=0.5, 2, 6, 24 and 48 hours for UV studies with the same workup procedure as that of the loading efficiency studies. Values were plotted as the average (±S.D.) of three independent experiments.

The Release Efficiency was calculated according to **Eq.3** below:

$$\text{Release Efficiency (\%)} = 100\% - \left(\frac{A_{263}\ (\text{pH})}{A_{263}\ (\text{D})} \times 100\% \right)$$

Where A_{263} (pH) is the absorbance at 263 nm of the sample dialyzed at indicated pH, and A_{263} (D) is that of the initial dialysis-purified sample.

*Encapsulation of Calcein in **NP209** Nanoparticles*

Thin film of lipids with or without **ADP109** was generated as described above in the preparation of **NP209** lipid-drug particles. Aqueous calcein stock was prepared at 200 mM in double-deionized and 0.2 μm filtered water with pH adjusted to 7.8. The dried thin film was rehydrated with 50 mM calcein (diluted from stock with 2X PBS) for 1 hour at 47°C and sonicated 3 times at 45°C for 5 minutes each to yield a translucent suspension of nanoparticles at 20 mM lipid concentration. The suspension was gradually cooled to 25°C over duration of at least 2 hours, allowing membranes to anneal as described above. The calcein-trapped liposomes were then

separated from the free dye on a Sephadex G50 gel column with 2X PBS of matching osmolality, and stored at 4°C until use.

*pH-dependent Release of Encapsulated Aqueous Marker Calcein from **NP209** Nanoparticles*

In 96-well plates, calcein-trapped **NP209** was diluted 4 times with 2X PBS at indicated pH for pH-dependent fluorescence regeneration at 37°C. Positive control was generated by dilution with 2X PBS in presences of 0.15% sodium deoxycholate (DOC) for complete calcein release from aqueous core. All buffers used were tested for matching osmolality to prevent particle burst as a result of osmotic pressure. The fluorescence of calcein was measured using a Victor^{2}D fluorometer (Perkin Elmer, Waltham, MA) equipped with excitation and emission filter wavelengths of 495 nm and 515 nm respectively. The Quenching Efficiency was calculated according to **Eq. 4** below:

$$\text{Percent Quenching (\%)} = \left(1 - \frac{\text{F (NP)}}{\text{F (DOC)}}\right) \times 100\%$$

Where F (NP) is the fluorescence intensity of **NP209** and F (DOC) is that of **NP209** in 0.15% DOC.

The pH-dependent Fluorescence Regeneration was calculated according to **Eq. 5** below:

$$\text{Percent Fluorescence Regeneration (\%)} = \frac{\text{F}_{\text{NP}}\text{ (pH)}}{\text{F}_{\text{NP}}\text{ (DOC)}} \times \frac{\text{F}_{\text{Cal}}\text{ (DOC)}}{\text{F}_{\text{Cal}}\text{ (pH)}} \times 100\%$$

Where F_{NP} (pH) is the fluorescence intensity of **NP209** at various pH, F_{NP} (DOC) is that of **NP209** in 0.15% DOC, F_{Cal} (pH) is the fluorescence intensity of free calcein at various pH, and F_{Cal} (DOC) is that of free calcein in 0.15% DOC.

A calcein fluorescence-concentration standard curve was generated to define self-quenching threshold, and linear range was defined below the self-quenching concentration to estimate calcein concentrations trapped inside particles and to ensure data points collected fell within the linear range. Each fluorescence regeneration data point was performed as triplicates and values were reported as the average ± S.D.

*Effects of Lipid-association on **ADP109** Potency against Human Breast Cancer Cells*

In a 96 well plate were seeded ca. 5000 cells/well of BT474 or MDA-MB-231 cells and incubated until fully adhered (20-30 hours). The incubation condition was a humid chamber at 37°C with 5% CO_2 supply, and the culture medium was DMEM (high-glucose, with L-glutamine) containing 10% FBS (Complete Medium). For MCF10A, 15,000 cells/well were seeded. MCF10A culture medium and assay medium were prepared according to literature[22]. Serial dilutions of **ADP109** stock solution at 20 mM in DMSO were made to 8 appropriate concentrations ranging from 1 nM to100 μM, in Complete Medium for cancerous cell lines or assay medium for MCF10A, with 1% DMSO. 200μL of the compound-containing medium were added to each well after removal of the seeding medium. Sterile dialysis-purified **NP209** was diluted in Complete Medium or assay medium assuming 100% loading. Three wells were run in parallel for any given compound and concentration in one experiment. The cells were incubated with the drugs for 48 hours at 37°C before the medium was replaced with 90 μL of fresh Complete Medium plus 10 μL of MTT solution at 5mg/mL and incubated further for 4 hours. At the end of incubation time, exhausted medium was gently removed. The purple formazan crystals (MTT) were dissolved in 50 μL of DMSO, and incubated for 10 minutes before the absorbance at 570 nm was read on Microplate Reader model 680 (Bio-Rad, California, USA).

IC_{50} values were defined as drug concentration that resulted in 50% viability of cells compared to medium control (with or without 1% DMSO), and three independent experiments were performed to reported average IC_{50}.

*Effects of **NP209** Liposomes on Human Breast Cancer Mice Xenograft Model*

Animal experiments were carried out by Washington Biotechnology, Inc. (Baltimore, MD) under IACUC approved protocol. Maximum tolerated dose study was carried out on healthy 4-6 weeks old female Swiss-Webster mice. Dose range study of single injections, chronic dosing and intermittent studies were done with 5 mice in each group with subcutaneous injections. Body-weight and clinical adverse reactions (piloerection, signs of distress) were recorded to determine the dose regimen for the efficacy study.

In the single dose efficacy study, thirty female athymic nude mice (Harlan Sprague-Dawley, Inc.), 5-6 weeks old, were implanted with $1x10^6$ MDA-MB-231 cells (passage 24) in 20% Matrigel (BD Biosciences, San Jose, CA) subcutaneously in the right flank, and left to develop solid tumor for 10 days (Therapy Day -10 to Day 0). Animals were grouped into three groups: **Blank NP209** Vehicle, **NP209** and Paclitaxel Control. Starting from Day 0, mice were injected with 40 mg/kg drug of **NP209** or lipid equivalence of **Blank NP209** subcutaneously every other day for 2 weeks, or 10 mg/kg Paclitaxel (Hospira, Lake Forest, IL) intravenously every day until Day 4. All mice were weighed every Monday, Wednesday and Friday, and tumor sizes were estimated by calculating Tumor Volume according to **Eq. 6** below.

$$\text{Tumor Volume} = length \times width^2 \times \frac{1}{2}$$

Statistical comparison was evaluated by two-tail Student's *t* test. Data was presented as mean (±SEM) of 7 animals in each group. Extra animals were accounted for in each group in consideration of outliers and anomalies.

*Cellular Uptake Study of **NP209***

For cellular uptake studies, sterile calcein-trapped **NP209** liposomes were prepared and purified as described above in 1X PBS. Osmolality of the nanoparticle suspension was tested on a vapor pressure osmometer (Wescor Vapor®, model 5520, Princeton, NJ) to ensure biocompatibility. In 12-well plates were seeded $1.5X10^5$ cells/well of BT474, and cells were incubated for 24 hours at 37°C with Complete Medium under 5% CO_2. On the day of imaging experiment, Complete Medium was replaced by 0.5 mL of blank PBS (Blank), 1 mM calcein-trapping **NP209** or 0.4 μM free calcein in PBS. Two time points for **NP209** uptake were studied in different wells with varying start time so that the end of incubation time coincided. At the end of the incubation period, cells were washed 3 times with 1 mL PBS each, and imaged live with 0.5 mL PBS in each well. All images were taken on a Carl Zeiss Axiovert 200M inverted microscope equipped with XBO 75 light source and an AxioCam MRm Camera, using a FITC/GFP filter cube (EX/BP 485/20) and Plan Neofluar 40X/0.75 D objective (Göttingen, DE). Image analysis was performed with AxioVision V4.8 software. Image settings, exposure levels, brightness and contrast were held constant for all samples incubated under the same temperature for qualitative comparison.

Reference

1. Zhang, Y. T. J.; Gallis, B.; Taya, M.; Wang, S. S.; Ho, R. J. Y.; Sasaki, T., pH-Responsive Artemisinin Derivatives and Lipid Nanoparticle Formulations Inhibit Growth of Breast Cancer Cells In Vitro and Induce Down-Regulation of HER Family Members. *Plos One* **2013,** *8* (3).

2. Kraft, J. C.; Freeling, J. P.; Wang, Z. Y.; Ho, R. J. Y., Emerging Research and Clinical Development Trends of Liposome and Lipid Nanoparticle Drug Delivery Systems. *Journal of Pharmaceutical Sciences* **2014,** *103* (1), 29-52.

3. Chang, H.-I.; Cheng, M.-Y.; Yeh, M.-K., Clinically-Proven Liposome-Based Drug Delivery: Formulation, Characterization and Therapeutic Efficacy. *Open Access Scientific Reports* **2012,** *1* (3), 8.

4. Burton, J.; Litman, B. J.; Barenholz, Y., [91] Fluorescent Probe:Diphenylhexatriene. In *Methods in Enzymology*, Fleischer, S.; Packer, L., Eds. Academic Press: **1982**; Vol. 81, pp 678-685.

5. Choi, S. U.; Bui, T.; Ho, R. J. Y., pH-dependent interactions of indinavir and lipids in nanoparticlies and their ability to entrap a solute. *Journal of Pharmaceutical Sciences* **2008,** *97* (2), 931-943.

6. Howard, M. D.; Jay, M.; Dziublal, T. D.; Lu, X. L., PEGylation of nanocarrier drug delivery systems: State of the art. *Journal of Biomedical Nanotechnology* **2008,** *4* (2), 133-148.

7. Oussoren, C.; Storm, G., Lymphatic uptake and biodistribution of liposomes after subcutaneous injection .3. Influence of surface modification with poly(ethyleneglycol). *Pharmaceutical Research* **1997,** *14* (10), 1479-1484; Du, H.; Chandaroy, P.; Hui, S. W., Grafted poly-(ethylene glycol) on lipid surfaces inhibits protein adsorption and cell adhesion. *Biochimica Et Biophysica Acta-Biomembranes* **1997,** *1326* (2), 236-248.

8. Kinman, L.; Brodie, S. J.; Tsai, C. C.; Bui, T.; Larsen, K.; Schmidt, A.; Anderson, D.; Morton, W. R.; Hu, S. L.; Ho, R. J. Y., Lipid-drug association enhanced HIV-1 protease inhibitor indinavir localization in lymphoid tissues and viral load reduction: A proof of concept study in HIV-2(287)-infected macaques. *Jaids-Journal of Acquired Immune Deficiency Syndromes* **2003,** *34* (4), 387-397.

9. Wang, L.; Bose, P. S.; Sigworth, F. J., Using cryo-EM to measure the dipole potential of a lipid membrane. *Proceedings of the National Academy of Sciences of the United States of America* **2006,** *103* (49), 18528-18533.

10. Fuchs, P.; Parola, A.; Robbins, P. W.; Blout, E. R., Fluorescence Polarization and Viscosities of Membrane Lipids of 3T3 Cells. *Proceedings of the National Academy of Sciences of the United States of America* **1975,** *72* (9), 3351-3354.

11. Cogan, U.; Shinitzk.M; Weber, G.; Nishida, T., Microviscosity and Order in Hydrocarbon Region of Phospholipid and Phospholipid-Cholesterol Dispersions Determined with Fluorescent Probes. *Biochemistry* **1973,** *12* (3), 521-528.

12. Mills, J. K.; Needham, D., Lysolipid incorporation in dipalmitoylphosphatidylcholine bilayer membranes enhances the ion permeability and drug release rates at the membrane phase

transition. *Biochimica Et Biophysica Acta-Biomembranes* **2005,** *1716* (2), 77-96; Mouritsen, O. G.; Jorgensen, K.; Honger, T., Permeability of Lipid Bilayers Near the Phase Transition. In *Permeability and Stability of Lipid Bilayers*, Disalvo, E. A.; Simon, S. A., Eds. CRC Press: Boca Raton, **1995**; pp 137-160.

13. Bachmeier, B.; Fichtner, I.; Killian, P. H.; Kronski, E.; Pfeffer, U.; Efferth, T., Development of Resistance towards Artesunate in MDA-MB-231 Human Breast Cancer Cells. *Plos One* **2011,** *6* (5).

14. Yamamoto, H.; Ngan, C. Y.; Monden, M., Cancer cells survive with survivin. *Cancer Science* **2008,** *99* (9), 1709-1714.

15. Shan, J.; Zhao, W.; Gu, W., Suppression of Cancer Cell Growth by Promoting Cyclin D1 Degradation. *Molecular Cell* **2009,** *36* (3), 469-476.

16. Isakoff, S. J., Triple-Negative Breast Cancer Role of Specific Chemotherapy Agents. *Cancer Journal* **2010,** *16* (1), 53-61.

17. Flores, M. L.; Castilla, C.; Avila, R.; Ruiz-Borrego, M.; Saez, C.; Japon, M. A., Paclitaxel sensitivity of breast cancer cells requires efficient mitotic arrest and disruption of Bcl-xL/Bak interaction. *Breast Cancer Research and Treatment* **2012,** *133* (3), 917-928.

18. Yang, T.; Choi, M. K.; Cui, F. D.; Lee, S. J.; Chung, S. J.; Shim, C. K.; Kim, D. D., Antitumor effect of paclitaxel-loaded PEGylated immunoliposomes against human breast cancer cells. *Pharmaceutical Research* **2007,** *24* (12), 2402-2411.

19. Lai, H. C.; Singh, N. P.; Sasaki, T., Development of artemisinin compounds for cancer treatment. *Investigational New Drugs* **2013,** *31* (1), 230-246.

20. Khalil, I. A.; Kogure, K.; Akita, H.; Harashima, H., Uptake pathways and subsequent intracellular trafficking in nonviral gene delivery. *Pharmacological Reviews* **2006,** *58* (1), 32-45.

21. Schneider, C. A.; Rasband, W. S.; Eliceiri, K. W., NIH Image to ImageJ: 25 years of image analysis. *Nature Methods* **2012,** *9* (7), 671-675.

22. Debnath, J.; Muthuswamy, S. K.; Brugge, J. S., Morphogenesis and oncogenesis of MCF-10A mammary epithelial acini grown in three-dimensional basement membrane cultures. *Methods* **2003,** *30* (3), 256-268.

CHAPTER 4

Optimization of ADP109-Lipid Nanoparticles for Improved Drug Retention *in vitro*

Abstract

pH-responsive artemisinin dimer, **ADP109**, is an amphiphilic bulky compound that is poorly soluble in water. Previous Chapters described the early efforts of **ADP109**-lipid nanoparticle formulations we studied to suspend **ADP109** in aqueous solution without the aid of organic co-solvents. This Chapter further expands on exploring possible factors that will contribute to increased suspended concentration of the artemisinin dimer in aqueous environment and/or improved particle stability of the formulations. Three major questions were investigated in this section, 1) the drug-to-lipid ratio to maximize aqueous solubility in presence of lipid, 2) the effect of surface polyethylene glycol (PEG) content on the particle size, structure and cytotoxicity, and 3) correlation between phase transition temperature (T_m) and stability of drug-loaded particles. We confirmed that optimal drug loading in DPPC-based lipid nanoparticles is at 10 mole percent of **ADP109** with respect to total lipid. We found that high surface PEG content leads to formation of mixed micelles with size distributions that change with concentration. High PEG content also increased cytotoxicity of the drug-free particles when tested on human breast cancer cell line, BT474. Screening of lipid nanoparticles of different compositions led to the discovery of potential stabilization offered by lipid membranes consisting of mixture of lipids with saturated fatty acyl chain. The high degree of aqueous core stability observed in lipid nanoparticles composed of 50% DPPC and 50% DSPC, at 5% surface PEGylation, lay the foundation for the "Fatty Acyl Domain Drug Binding Pocket" Hypothesis described in Chapter 5.

Introduction

First and second generation **ADP109**-Lipid nanoparticles were good proof of concept formulations and sufficed for animal model studies. First generation formulation, **NP109**, which are based on egg phosphatidylcholine (EPC), is not ideal for human use due to potential irritations that may result from egg-product allergens. The second generation formulation based on dipalmytoylphosphatidylcholine (DPPC, **Figure 1B**) shows unsatisfactory drug retention ability under neutral pH at physiological temperature of 37°C. Thus, here we explore alternative formulations to maximize loading capacity of **ADP109** in lipid-based nanoparticles that will also allow stable retention of compound at neutral pH.

Initial drug loading of **ADP109** in the proof of concept EPC nanoparticles were artificially fixed at 10 mole percent (10%) due to the amount being a respectable loading capability for liposomal particles. The DPPC-based lipid particles initially prepared inherited the compound loading used for the proof of concept studies. In this section, we tried to increase the amount of hydrophobic compound that can be carried by the second generation DPPC particles or prove that 10% **ADP109** was the highest loading efficiency achievable with lipid nanoparticles based on saturated fatty acyl chain PCs. Thus, drug to lipid ratio is varied in a number of formulations and the prepared particles are subjected to visual observation for drug precipitation out of colloidal suspension as well as quantification of drug incorporation efficiency.

While lipid molecules with small head groups, such as phosphatidylcholines (PCs), spontaneously assemble into bilayer structures in aqueous environments, lipids with large head groups are more inclined to form mixed micelles where the surface curvature is much greater[1]. Formation of micelles is a highly concentration dependent phenomenon. At lipid concentrations

above the critical micelle concentration (CMC), lipid molecules with large head groups adopt a dandelion-like structure where the hydrophobic fatty acyl tails form a non-polar core for binding of lipophilic compounds, and the hydrophilic head groups shield the core from unfavorable intermolecular repulsions of the core with the polar aqueous environment[2]. As the lipid concentration is diluted to below the CMC, the aggregates then fall apart and release the loaded compound. Hence, micelle nanoparticles have been explored as a potential drug delivery system for *in vivo* trafficking of hydrophobic or amphiphilic compounds. In this section, we describe a number of mixed micelle formulations tested based on mixtures of DPPC and polyethylene glycol (PEG)-conjugated dipalmitoyl phosphatidylethanolamine ($mPEG_{2000}$-DPPE, **Figure 1C**). The particle sizes are measured by dynamic light scattering and the toxicity of these polymer coated particles is tested on human breast cancer cell line, BT474, *in vitro*.

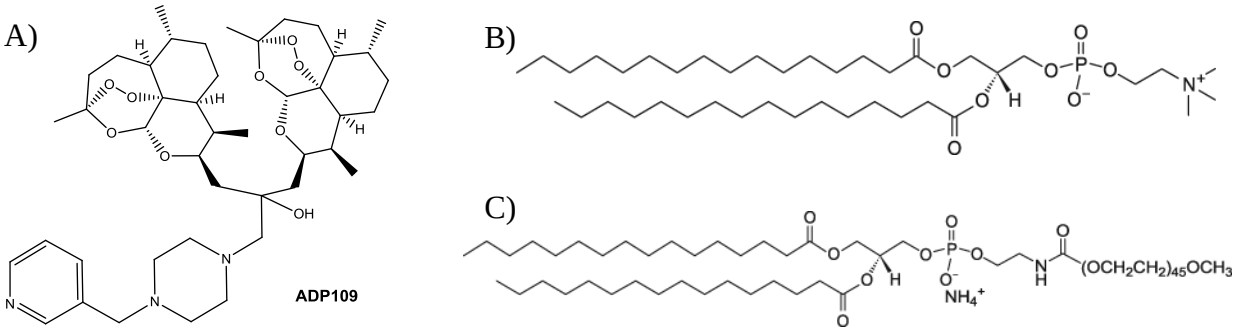

Figure 1. Chemical structures of A) **ADP109**, B) DPPC and C) DPPE-$mPEG_{2000}$.

Phase transition temperature (T_m) of DPPC is at 41°C[3], and with the addition of 10% **ADP109**, the T_m is further lowered to 37.4°C (Chapter 3). Lipid membranes are most permeable when they are near the phase transition[4], and so for *in vivo* delivery of **ADP109**-DPPC particles, the membrane may be too leaky for stable incorporation of core-trapped compounds at physiological temperature of 37°C. This would mean that the formulation, while may be suitable for delivering

ART dimer, does not suffice for combination therapy – one of the advantages of liposomal drug delivery system. Thus, to formulate more intact membranes for **ADP109**-Lipid formulations, two approaches were taken, addition of cholesterol or utilizing different lipid compositions.

Cholesterol is known to intercalate near the hydration surface of the bilayer, where it is able to hydrogen-bond with the head groups and the water molecules near the surface. Presence of cholesterol, thus helps to suppress the incompatibility during phase transition by filling in holes created at the interface of melted and gel-phase domains[4]. In this study, cholesterol is added to study the effect of this additive on incorporation and stability of the particle membrane.

Lipids with different fatty acyl chains show characteristic phase transition temperatures. Thus, to manipulate the T_m of the lipid nanoparticles incorporating 10% **ADP109**, we vary the nature of the fatty acyl (FA) tails of phosphotidylcholines to understand the effect of drug incorporation on intactness of the lipid membrane. The stability of the aqueous core is measured to reflect the tightness of the enclosing membrane.

Results and Discussion

*Optimization of drug to lipid ratio in DPPC-based **ADP109**-Lipid nanoparticles*

Table 1. Size measurements of lipid nanoparticles composed on various surface PEG content at 5 mM and 2.5 mM concentrations at room temperature. Measurements were recorded on Zetasizer (Malvern). Values reported as intensity average of 10 measurements, each with 13 runs, unless otherwise indicated.

Formulation	Diameter (nm) at 5 mM		Diameter (nm) 2.5 mM	
	Peak 1 (% Area)	Peak 2 (% Area)	Peak 1 (% Area)	Peak 2 (% Area)
5% PEG	N/A	N/A	86.9 (91.8%)	N/A
50% PEG	15.8 (56.9%)	668.1 (35.6%)	670.9 (71.8%)	15.4 (28.2%)
70% PEG	14.0 (54.0%)	593.1 (38.4%)	640.6 (59.2%)	14.6 (39.9%)
100% PEG	12.1 (53.7%)	582.2 (38.4%)	1037.1* (68.8%)	13.8* (29.9%)

*Average of 5 measurements

To maximize the amount of **ADP109** that can associate stably with the current DPPC based formulation, we optimized the drug to lipid ratio (D:L). For this study, lipid membrane composed of 5% DPPE-PEG_{2000} and 95% DPPC were kept at constant concentration, and various amount of **ADP109** was added to each sample. The D:L tested were: 1:10, 1:7, 1:5, 1:3, and the final lipid concentration was 20 mM in 1X PBS. In samples with D:L of 1:5 and 1:3, drug precipitates were observed after reduction of the initial vesicles by sonication. To conserve the synthesized **ADP109**, samples which show incomplete incorporation of the compound, as evident by presence of drug precipitates, were removed. With D:L at 1:10 and 1:7, liposome suspensions appear to be translucent with no visible precipitates (**Figure 2**). These samples were subjected to overnight dialysis to remove any unbound or loosely-bound **ADP109**. The dialyzed samples were collected for quantification with UV absorbance at λ=263 nm, characteristic of

ADP109. The D:L at 1:10 sample showed 90 ±6% loading efficiency, whereas 1:7 had only 50 (±3)%. Thus, 10% loading of the hydrophobic artemisinin dimer was likely near the maximum loading capacity of the 5% DPPE-mPEG$_{2000}$ in DPPC membrane system.

Effect of surface PEG composition on size and cell cytotoxicity of the formulations

To evaluate the effect of covalently bound surface PEGylation on the ability of the lipid nanoparticles to incorporate and release the hydrophobic compound **ADP109**, amount of DPPE-mPEG$_{2000}$ (**Figure 1**) in DPPC membrane was varied. Due to the high degree surface hydration brought by long PEG polymer chains, higher amount of surface PEG will lead to formation of mixed micelle structures rather than liposomes, which are characteristic of an intact lipid bilayer enclosing an aqueous core. In this section, DPPE-mPEG$_{2000}$ at a molar composition of 5%, 15%, 50%, 70% and 100% with total lipid to drug ratio of 10 to 1 were prepared.

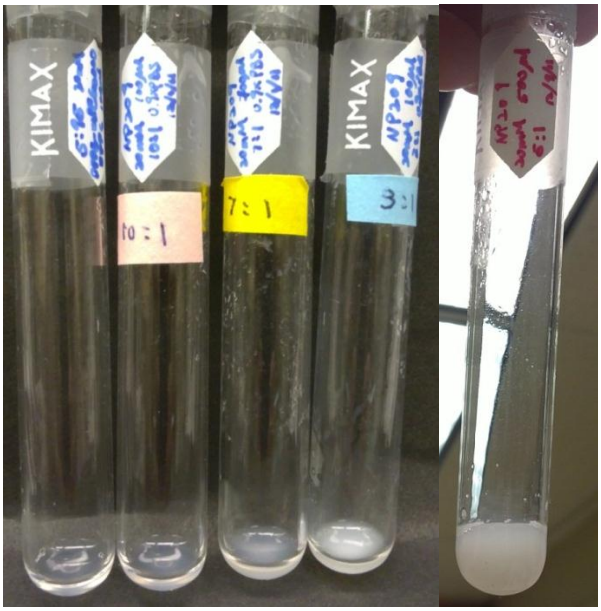

Figure 2. Representative photos of **ADP109**-DPPC particles prepared at various lipid to drug ratios after sonication and annealing. From left to right: lipid-only, D:L at 1:10, D:L at 1:7, D:L at 1:3 and D:L at 1:5. Total Lipid concentration was 20 mM in all samples.

All formulations, prepared via the thin film-rehydration-sonication method, appeared to be a homogeneous suspension with no visible drug precipitation. The particle sizes were measured by dynamic light scattering (DLS) to track the change in size as compositions of the particles are varied (**Table 1**). High PEG content formulations generally showed two populations in DLS measurement with the intensity of the two peaks changing upon dilution, alluding to a mixture of micelles of various diameters. The poorly defined size range of these particles may introduce complexity to understanding the *in vitro* and *in vivo* behavior of the particles in future development.

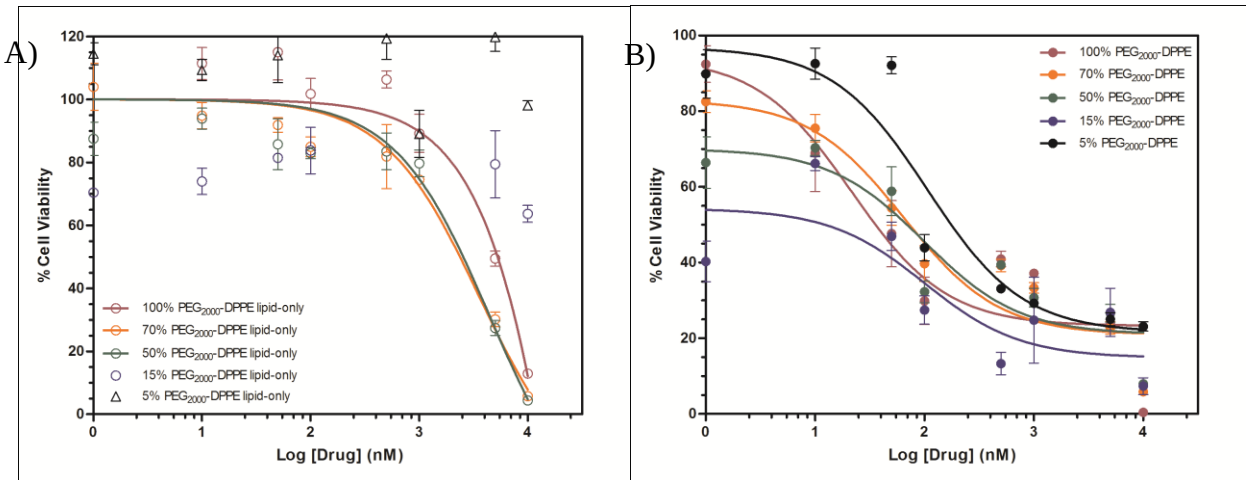

Figure 3. Cell viability inhibition curves of BT474 cells incubated with lipid formulations containing A) no drug or B) 10% **ADP109** and various surface PEGylation at indicated concentrations. Data represent average ± S.D. of triplicate wells for a single experiment.

To examine the effect of PEG content in lipid formulations on cell cytotoxicity, MTT assay was performed on BT474 cells to estimate the IC_{50} values of the liposomal or mixed micellar formulations, all containing 10% **ADP109** (**Table 2**). Increased PEG content or mixed micelle formulations seemed to inhibit cell growth at low concentrations more significantly, with the

largest difference observed at 1 nM **ADP109**, or 10 nM lipid. At higher drug concentration (> 50 nM), however, the effect of lipid becomes insignificant (**Figure 3**). It should be noted that at blank lipid particles with high PEG contents are also toxic to BT474 cells at concentrations above 1 μM, where only approximately 75% of cells remain viable after 48 hours of incubation (**Figure 3**).

Table 2. IC_{50} values of lipid nanoparticle compositions containing 10% **ADP109** or no drug (lipid-only) and various surface PEG content tested against BT474, a $HER2^+$ human breast cancer cell line. Values represent average ± S.D. of triplicates in a single experiment.

Formulation	IC_{50} (nM)
5% PEG	106.8 ± 1.4
15% PEG	77.1 ± 1.3
50% PEG	99.7 ± 1.7
70% PEG	64.4 ± 1.4
100% PEG	21.6 ± 1.7
5% PEG lipid-only	>10,000*
15% PEG lipid-only	>10,000*
50% PEG lipid-only	4,456± 1.5
70% PEG lipid-only	3,554± 1.4
100% PEG lipid-only	53,822± 13.1

*More than 60% viable at maximum concentration of the assay at 10 μM.

*Effect of phase transition temperature on stability of the **ADP109**-Lipid nanoparticles*

To study the effect of cholesterol on both incorporation of **ADP109** and the phase transition behavior of the drug-bound lipid nanoparticles, we prepared DSPC-based particles at 10% **ADP109** loading with different cholesterol contents. The cholesterol (Chol) to DSPC molar ratios were: 1:9, 1:6, 1:3 and 1:1. Cholesterol and DSPC together accounted for the total amount of lipid and **ADP109** concentration was kept constant.

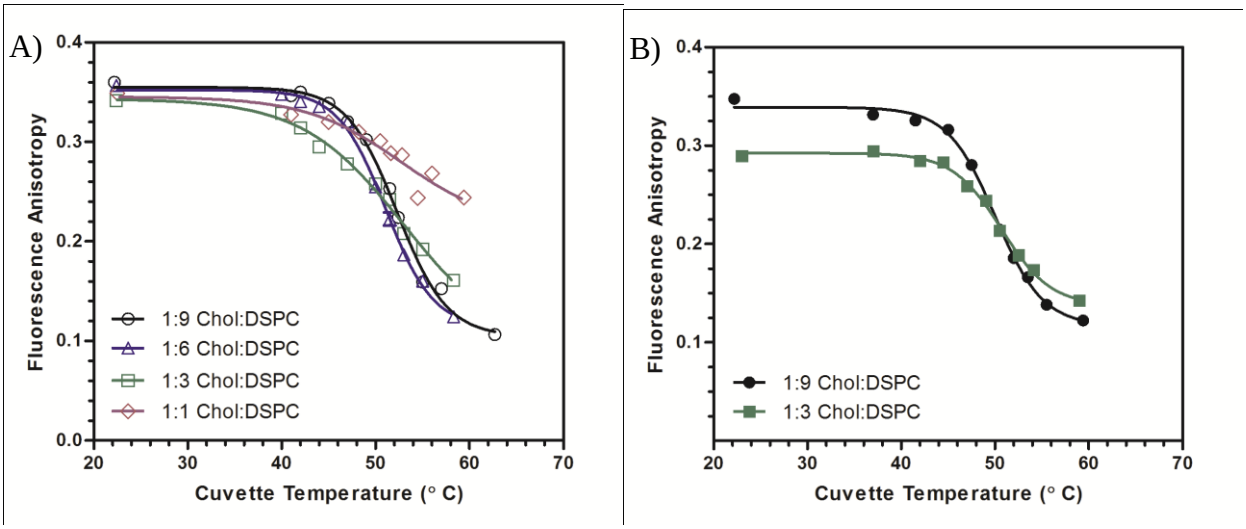

Figure 4. Phase Transition Curves of A) lipid only and B) 10% **ADP109** loaded DSPC-based lipid nanoparticles with various amounts of cholesterol embedded in lipid membrane with no surface PEG coating. Data points represent average ± S.D. of triplicate readings of a single experiment.

Blank DSPC-Cholesterol lipid particles were first prepared to examine the effect of cholesterol content on size and phase transition behavior (**Figure 4**). While no significant difference was observed in appearance or particle size, phase transition behavior was greatly suppressed when 50% of cholesterol is present. Formulations of 1:9 and 1:6 Chol:DSPC showed very similar melting curves in the lipid-only samples, and 1:3 Chol:DSPC formulation showed moderate phase transition suppression. Thus, for **ADP109** loading efficiency measurement and phase transition behavior monitor, only 1:9 and 1:3 Chol:DSPC formulations were prepared. The particle sizes of both formulations were within the range of all other **ADP109**-Lipid nanoparticles with number-weighted mean at 53 nm and 70 nm respectively (**Table 3**). The higher amount of cholesterol, however, competed with association of **ADP109** with the lipid membrane, resulting in a decreased loading efficiency in the case of 1:3 Chol:DSPC formulation.

The stability of the particles over 48 hours under dialysis conditions, improved only marginally, from 48% retention with no cholesterol to 57% with 30% cholesterol (**Table 3**). With these results, we concluded that cholesterol did not improve the stability of the **ADP109**-Lipid nanoparticle formulation.

Table 3. Summaries of particle size measurements, phase transition temperatures (T_m) in 1X PBS, drug incorporation efficiencies and drug retention efficiencies after 48 hours of dialysis for DSPC lipid nanoparticles and DSPC-based particles with various amounts of embedded cholesterol. All samples were prepared with 10% **ADP109** loading.

	Lipid Compositions (Chol : DSPC ratio)		
	0:10	**1:9**	**1:3**
Size[*] (d, nm)	91.5	52.5	78.5
T_m[#] (°C)	49.7 ±0.2	50.0 ±0.1	50.7 ±0.2
Incorporation Efficiency[†] (%)	101.1	94.3	74.9
Retention Efficiency[†] (%)	48.7	58.2	57.0

[*]Size were measured on NICOMP 380ZLS (Particle Sizing Systems) and reported as number-weighted average calculated based on 6 minutes of continuous measurement. Major peak reported has a peak area >99%.

[#]Values reported as average ±S.D. of triplicate readings.

[†]Values reported from a single point with all samples tested in parallel.

Cholesterol as an additive competed with the association of **ADP109** with the lipid membranes. We next manipulated the lipid membrane to study the effect of different fatty acyl chain on phosphotidylcholines (PCs) on drug-lipid interactions. The goal of this study was to screen for a formulation that would be able to keep the membrane intact when 10% of the hydrophobic ART dimer is loaded. While a leaky membrane does not necessarily correlate with release of the hydrophobic compound, which is thought to interact with the fatty acyl domain of the membrane based on the fluorescence polarization studies described in Chapter 3, an intact membrane is

confirmative for successful retention of membrane-bound **ADP109**. Thus, as a high throughput screening method, we prepared calcein trapped lipid-only or **ADP109** loaded particles, and monitored the fluorescence regeneration as a result of calcein release from the aqueous core of the liposomes. Particles composed of different lipid compositions were summarized in **Table 4**.

Table 4. Mixed lipid formulations nomenclature and their compositions. All formulations contained 10% ADP109 or no drug (Blank).

	Composition (mol%)		
	PC lipid	**mPEG$_{2000}$-PE**	**ADP109**
NP109	100 EPC	0	10
PEGNP109	95 EPC	5	10
NP209	95 DPPC	5	10
NP209Flex	85 DPPC + 10 POPC	5	10
NP309	95 DSPC	5	10
NP409	95 POPC	5	10
NP509	45 DPPC + 50 POPC	5	10
NP609	45 DPPC + 50 DSPC	5	10

mPEG$_{2000}$-PE:methyl-poly(ethylene glycol)$_{2000}$-Phoosphatidylethanolamine
EPC: Egg Phosphatidylcholine
DPPC: Dipalmitoyl Phosphatidylcholine
POPC: Palmitoyl-oleoyl Phosphatidylcholine
DSPC: Distearoyl Phosphatidylcholine

Figure 5 and **Figure 6** showed the time course of calcein release as a result of the various formulations when incubated at 37°C to simulate *in vivo* conditions of both lipid-only and drug-bound particles. We found that formulations that contain lipids of higher T_m regenerated lower fluorescence, implying a more stable intact membrane. Interesting, we also noticed that when 50% of DPPC were mixed with 50% of DSPC (NP609), the particles were highly stable both in PBS and serum incubations. The finding with this mixture of PCs with saturated fatty acyl tails laid the foundation for Chapter 5, where we developed the idea of a FA domain binding pocket design hypothesis.

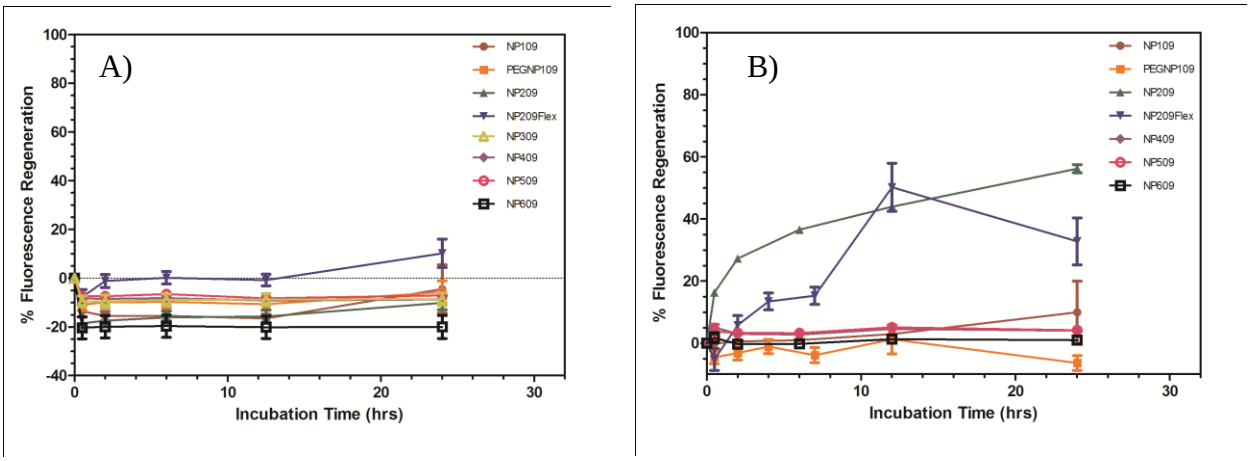

Figure 5. Calcein fluorescence regeneration profiles in phosphate buffered saline solution of A) lipid-only lipid nanoparticles and B) 10% **ADP109** loaded lipid nanoparticles of various compositions (See **Table 4**). Values plotted as average with S.D. as error bars of triplicate readings.

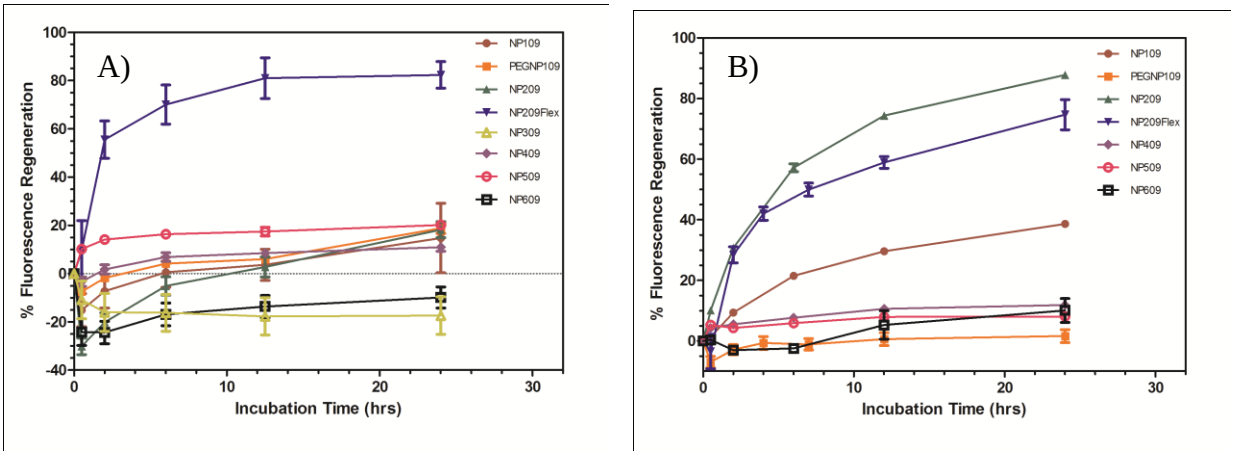

Figure 6. Calcein fluorescence regeneration profiles in 50% fetal bovine serum in phosphate buffered saline solution of A) lipid-only lipid nanoparticles and B) 10% **ADP109** loaded lipid nanoparticles of various compositions (See **Table 4**). Values plotted as average with S.D. as error bars of triplicate readings.

Experimental Section

Materials

Lipids 1,2-dipalmitoyl-*sn*-glycero-3-phosphocholine (DPPC), 1,2-distearoyl-*sn*-glycero-3-phosphocholine (DSPC), and 1,2-dipalmitoyl-*sn*-glycero-3-phosphoethanolamine-N-[methoxy(polyethylene glycol)-2000 sodium salt ($mPEG_{2000}$-DPPE) were purchased from Genzyme (Cambridge, MA) in powder form. Cholesterol was purchased from Invitrogen (Carlsbad, CA). Chloroform was dried with molecular sieves for at least 24 hours before use. Calcein was purchased from TCI America (Portland, OR), dipheyl-1,3,5-hexatriene (DPH) was bought from Life Technologies (Formerly Invitrogen, Carlsbad, CA). Thiazolyl Blue Tetrazolium Bromide (MTT) powder was purchased from Sigma Aldrich (St.Louis, MO). Commercially prepared 1X phosphate buffered saline (PBS) solution was obtained from Thermo Scientific (Waltham, MA).

*Preparation of **ADP109**-Lipid Nanoparticle Formulations*

Liposomes were prepared with a thin-film rehydration-sonication method outlined in previously published literature[5] and described in Chapter 2. Lipid stock solutions were prepared at 100 mg/ml and ADP109[6] stock solution was prepared at 50 mg/mL in chloroform. After addition of appropriate amounts of lipids and drug aliquots to a screw-cap test tube, organic solvent was removed under a gentle stream of N_2 followed by vacuum drying. The film was rehydrated with 1X PBS at 55°C for 1 hour for all formulations except DSPC liposomes (at 60°C), to give multilamellar vesicles at 20 mM lipid concentration. The mixture was then sonicated at 53°C for 5 minutes 3 times to give a translucent suspension without observable particulates and then gradually cooled down to well below the lipid phase transition temperature (4°C), to give

liposomes nanoparticles. The nanoparticle suspension was diluted to 2 mM for sizing measurements on a NICOMP 380ZLS (Particle Sizing Systems, Santa Barbara, CA), with argon laser at 633.0 nm at room temperature.

For micelle formulations, appropriate amounts of lipids and ADP109 were dried under a gentle stream of N_2 and in *vacuo* overnight. The thin films were rehydrated in 1X PBS at 50°C fir 50 minutes at lipid concentration of 10 mM with intermittent vigorous vortexing to give mixed micelle suspensions. The mixture was then cooled down to ~30°C over 15 minutes, vortexed again, and warmed up to 50°C for an additional 20 minutes and vortexed. The suspension was finally cooled down to room termpature for 2 hours and at 4°C overnight. Micelle mixtures were diluted to 5 mM and 2.5 mM for sizing measurements on a Zetasizer 5000 (Malvern Instrument, Worcestershire, UK) with argon laser at 633.0 nm at room temperature.

Preparation of Calcein Trapped Liposomal Nanoparticles

Preparation and characterization methods for calcein trapped liposomal nanoparticles follow that described in Chapter 3. Positive control was generated by dilution with PBS in presences of 0.15% sodium deoxycholate (DOC) for complete calcein release from aqueous core. All buffers used were tested for matching osmolality to prevent particle burst as a result of osmotic pressure. The fluorescence of calcein was measured using a Victor^{2}D fluorometer (Perkin Elmer, Waltham, MA) equipped with excitation and emission filter wavelengths of 495 nm and 515 nm respectively. The Quenching Efficiency was calculated according to **Eq. 1** below:

$$\text{Percent Quenching (\%)} = \left(1 - \frac{\text{F (NP)}}{\text{F (DOC)}}\right) \times 100\%$$

Where F (NP) is the fluorescence intensity of the lipid nanoparticles and F (DOC) is that of lipid nanoparticles in 0.15% DOC.

A calcein fluorescence-concentration standard curve was generated to define self-quenching threshold, and linear range was defined below the self-quenching concentration to estimate of calcein concentrations trapped inside particles and to ensure data points collected fell within the linear range. Each fluorescence regeneration data point was performed as triplicates and values were reported as the average ± S.D.

Drug Incorporation and Release Efficiencies

The Drug loading efficiency and release efficiency studies were carried out according to procedure described in Chapter 5.

Phase Transition Behavior Studied with Fluorescence Polarization Probe DPH

Procedure for phase transition behavior studies follow that described in Chapter 3. Fluorescence measurements were taken as an average of 10 seconds of continuous reading. Triplicate measurements in each direction of emission polarization: 0° ($I_{/\!/}$) and 90° ($I_{\perp}$) with respect to 0° excitation, were measured with liposomes in 1X PBS. Curve fitting was based on average and standard deviation (S.D.) calculated from triplicate readings. The fluorescence anisotropy was calculated using **Eq. 2** below:

$$\text{Fluorescence Anisotropy} = \frac{I_{/\!/} - I_{\perp}}{I_{/\!/} + 2I_{\perp}}$$

Cell Cytotoxicity Assay

Cell cytotoxicity assays were conducted according to that described in Chapter 2 on BT474 cells. 5000 cells/well of BT474 cells were seed on 96 well plates. **ADP109**-Lipid or lipid-only particles were administered to cells without organic solvents. Data represent average ± S.D. of a single experiment with each concentration run as triplicates. IC_{50} value is calculated by **Eq. 3** below:

$$\%\ \text{Cell Viability} = \frac{I_{\text{MTT (Test drug)}} - I_{\text{MTT (Blank)}}}{I_{\text{MTT (Negative control)}} - I_{\text{MTT (Blank)}}} \times 100\%$$

Reference

1. Ashok, B.; Arleth, L.; Hjelm, R. P.; Rubinstein, I.; Onyuksel, H., In vitro characterization of PEGylated phospholipid micelles for improved drug solubilization: Effects of PEG chain length and PC incorporation. *Journal of Pharmaceutical Sciences* **2004,** *93* (10), 2476-2487; Sugin, Z.; Yuksel, N.; Baykara, T., Preparation and characterization of polymeric micelles for solubilization of poorly soluble anticancer drugs. *European Journal of Pharmaceutics and Biopharmaceutics* **2006,** *64* (3), 261-268; Lin, W. J.; Chen, Y. C.; Lin, C. C.; Chen, C. F.; Chen, J. W., Characterization of pegylated copolymeric micelles and in vivo pharmacokinetics and biodistribution studies. *Journal of Biomedical Materials Research Part B-Applied Biomaterials* **2006,** *77B* (1), 188-194.

2. Kastantin, M.; Missirlis, D.; Black, M.; Ananthanarayanan, B.; Peters, D.; Tirrell, M., Thermodynamic and Kinetic Stability of DSPE-PEG(2000) Micelles in the Presence of Bovine Serum Albumin. *Journal of Physical Chemistry B* **2010,** *114* (39), 12632-12640.

3. Silvius, J. R., Thermotropic Phase Transitions of Pure Lipids in Model Membranes and Their Modifications by Membrane Proteins. In *Lipid-Protein Interactions*, John Wiley & Sons, Inc: New York, 1982; Vol. 2.

4. Mouritsen, O. G.; Jorgensen, K.; Honger, T., Permeability of Lipid Bilayers Near the Phase Transition. In *Permeability and Stability of Lipid Bilayers*, Disalvo, E. A.; Simon, S. A., Eds. CRC Press: Boca Raton, 1995; pp 137-160.

5. Kinman, L.; Brodie, S. J.; Tsai, C. C.; Bui, T.; Larsen, K.; Schmidt, A.; Anderson, D.; Morton, W. R.; Hu, S. L.; Ho, R. J. Y., Lipid-drug association enhanced HIV-1 protease inhibitor indinavir localization in lymphoid tissues and viral load reduction: A proof of concept study in HIV-2(287)-infected macaques. *Jaids-Journal of Acquired Immune Deficiency Syndromes* **2003,** *34* (4), 387-397.

6. Zhang, Y. T. J.; Gallis, B.; Taya, M.; Wang, S. S.; Ho, R. J. Y.; Sasaki, T., pH-Responsive Artemisinin Derivatives and Lipid Nanoparticle Formulations Inhibit Growth of Breast Cancer Cells In Vitro and Induce Down-Regulation of HER Family Members. *Plos One* **2013,** *8* (3).

CHAPTER 5

Differences in Fatty-acyl Chain Lengths Modulate the Stability of Hydrophobic Compound Integration into Lipid Bilayers: a Geometrical Fit Model for Phospholipid Nanoparticle Design

Content of this Chapter was submitted for publication as an original research article.

The manuscript was authored by:

Yitong J. Zhang[1], Josefin Koehn[2], Rodney J.Y. Ho[2]*, Tomikazu Sasaki[1]*

[1]Department of Chemistry and [2]Department of Pharmaceutics,
University of Washington, Seattle, WA 98105

Abstract

Hydrophobic and sterically bulky compounds are challenging to formulate into stable dosage forms, due to their poor aqueous solubility. Lipid-based formulations have been adopted to solubilize the hydrophobic drugs; but optimizing the incorporation and retention is often an empirical process, as association mechanisms of drug molecules are not well defined. Here, we propose a binding pocket hypothesis, where the hydrophobic compound is able to insert into a binding pocket in the fatty acyl (FA) domain of the lipid membrane that geometrically complements the structural dimensions of the molecule. A three-dimensional structure of the molecule defines the dimensions needed for complementary fit, and a mixture of phospholipids with different FA chain lengths allows the formation of drug binding pockets to intercalate compounds deep within the bilayer. The favorable drug-FA domain interactions result in stable integration and retention of the compound. The fitting of the bulky molecules into the binding pockets results in no perturbation of lipid molecular packing in the bilayer system, as reflected by the degree of polarization of the fluorescence probe. Our results show that when the model compound, an artemisinin dimer derivative, is loaded at 10 mol% in a mixture of 40 mol% C14PC (DMPC) in C18PC (DSPC) designed based on the hypothesis, more than 97% of the loaded drug remains associated with the phospholipid nanoparticles after 48 hours at room temperature with no compromised lipid packing order. The binding pocket hypothesis is further validated with two other challenging compounds, Darunavir and Curcumin, with particle membrane compositions designed to geometrically complement their molecular structures. With the binding pocket hypothesis and geometrical fit considerations outlined here, we lay the foundation for a systematic approach to phospholipid nanoparticle formulation design that may lead to higher rate of success for translating hydrophobic drug candidates to clinical applications.

Introduction

Parenteral injections of drug solutions or suspensions provide direct drug access to blood and often allow a much higher therapeutic effect per dose administered compared to alternative routes[1]. Yet, for hydrophobic drugs, an organic co-solvent or oil-based medium is required to enhance solubility, which may induce undesired effects at the site of injection. Lipid vesicles and lipid particles represent some of the most widely utilized drug delivery vehicles to address the solubility issue and alter the *in vivo* behavior and unwanted effects of therapeutic molecules[2, 3]. Over the last 20 years, complexity of liposomes and lipid-bound drug delivery systems have evolved significantly, from conventional phospholipid compositions, to long-circulating polymer-coated particles, and multifunctional nanoparticles with surface modifications such as targeting moiety or stimuli-responsive functional groups[4]. These added features of the liposomes, however, have not resulted in increased number of products that are clinically applied. To date, there are less than 20 liposomal formulations approved by the FDA for therapeutic use and the number of chemical entities prepared as lipid-bound particles remain in the single digits[3]. One reason for the small number of successful cases is the heavy reliance on empirical trial-and-error without an in-depth understanding of the drug-lipid interactions at the molecular level.

Liposome particles contain lipids assembled in an enclosed bilayer to entrap an aqueous core. The fatty acyl (FA) domain of the bilayer allows hydrophobic compounds to intercalate, while hydrophilic drugs can be encased inside the aqueous compartment. Thus, we use liposome particles as a model system to observe drug-lipid interaction in their native state. While incorporation of hydrophobic drugs into lipid membranes is potentially driven by the hydrophobicity of the compounds, the stability or retention of drug molecule in particle would depend on factors such as depth of drug binding within the hydrophobic domain (fatty acyl

chains) and impact of drug presence on lipid bilayer packing[9]. Therefore, to address the retention of drug molecules in lipid bilayers, a systematic approach to lipid composition design and drug integration is needed to minimize the release from drug-lipid complexes. In this paper, we propose to use a mixture of phospholipids with variation in FA chain lengths to allow formation of drug binding pocket for stable integration and retention of bulky hydrophobic compounds.

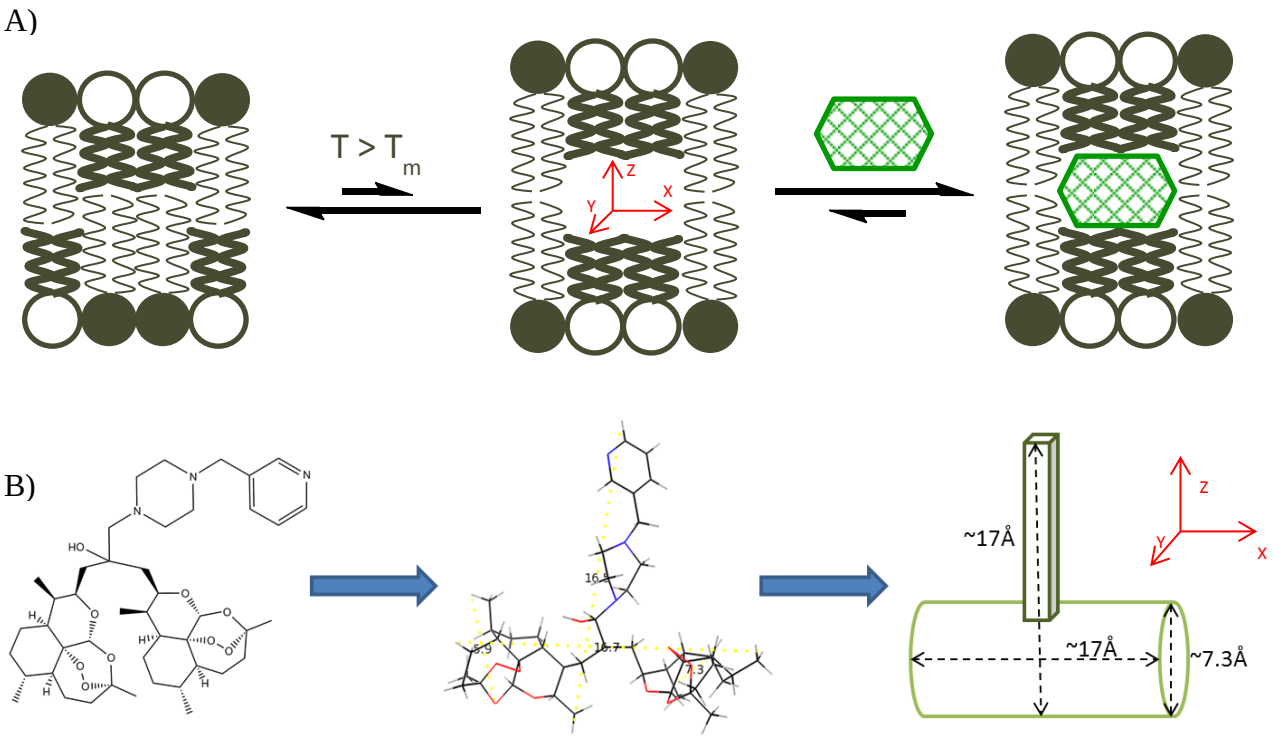

Figure 1. A) Schematic diagram to show a drug binding pocket in the fatty acyl domain with geometrical complementarity to the hydrophobic molecule that facilitate its stable membrane insertion. B) Schematic diagram demonstrating the molecular dimension estimation. This process involves 3D visualization of the molecule (left) based on known crystal structures[23] (middle), PyMOL software measured molecular dimensions and finally arriving at a simplified geometrical shape representing molecular geometry (right).

The phospholipid molecule contains a hydrophilic head-group and a hydrophobic FA tail. When suspended in solution, lipid molecules with small head groups, such as phosphatidylcholine (PC), spontaneously assemble into bilayer structures with the head-groups interacting with the aqueous environment, shielding the FA domain. Once assembled into bilayer, individual molecules can freely diffuse within the two dimensional plane of the leaflet with temperature-dependent kinetics[10]. We hypothesize that drug binding pockets can be transiently formed within the FA domain when lipid molecules of short FA chains in the two leaflets slide pass each other, in a bilayer composed of mixture of phospholipids that are only different in FA chain length. When hydrophobic molecules are present during the assembly of the bilayer, the drug binding pockets are established to allow drug insertion into the FA domain[11, 12]. These drug binding pockets allow hydrophobic compounds to bind deep inside the membrane, while having minimal impact on lipid packing (**Figure 1A**). If the dimensions of the binding pocket are complementary to the geometry of the hydrophobic compound, then the favorable hydrophobic interaction energy would be maximized with minimal entropic penalty of binding, resulting in more stable drug-bound membranes. Macroscopically, this stabilization would be reflected as improved retention of membrane-integrated compound as well as minimized effected on phase transition behavior of the particle membranes.

With the FA domain drug binding pocket hypothesis, we examined the lateral (X, Y axes) and vertical (Z-axis) dimensions of the binding pockets that best accommodate the model compound. A pH-responsive ART-dimer, **ADP109**, was used as a model compound to validate the existence of the binding pockets. Dimensions of the binding pockets were predicted with the geometrical fit model and confirmed experimentally with 10 mole percent (mol%) of **ADP109** integrated in Mixed-Lipid bilayer composed of phosphatidylcholines (PCs) with varying FA chain lengths. To

evaluate the drug retention of the formulation, we measured the initial incorporation efficiency and percent of retained compounds post dialysis. The effect of bulky hydrophobic molecule integration on lipid packing order was reflected by fluorescence anisotropy studies. Furthermore, to expand the scope of the model application, we demonstrate the enhanced drug association with two other hydrophobic drug molecules, Darunavir and Curcumin.

Results

We hypothesized that by driving interaction of lipophilic drug molecules into the hydrophobic drug binding pockets in the FA domains and by geometrically optimizing the fit of the binding pocket for compounds, bulky hydrophobic compounds can be stably integrated at high incorporation efficiency. To systematically evaluate whether the dimensions of the binding pocket can be manipulated to incorporate drug molecules, we changed the percent compositions of phospholipid mixtures with fixed head groups but different FA chain lengths, as well as varied the difference in FA chain tail lengths at an optimized percent composition. Common phosphatidylcholines (PCs) were used in this study. The drug retention ability was measured as amount of drug remaining associated with particles at 48 hours. To gain molecular-level understanding and rationalize the enhanced stability, we studied the gel-liquid phase transition behavior of the lipid membranes with or without ART-dimer embedded. Diphenylhexatriene (DPH) was used as a probe for measuring fluorescence anisotropy. Suppressed polarization in the gel phase and shifted phase transition point (T_m) were attributed to the presence of ART-dimer, which disrupts lipid packing. Finally, to validate the applicability of the geometry fit model for design of drug binding pocket, optimization of membrane composition was tested on two additional compounds, darunavir and curcumin.

We estimated molecular dimension based on the crystal structure of an ART-dimer similar to that of **ADP109**[5] for design of liposome composition, and assumed that the molecule would adopt the similar conformation in lipid bilayer (**Figure 1B**). Molecular dimensions of single lipids have been estimated by a number of techniques such as gravimetric x-ray method[10, 11]. **Table 1** summarizes the lipid cross-section area as measured by gravimetric x-ray and fatty acyl

chain length estimated based on simulation of electron density profile of common saturated synthetic PCs.

Table 1A. Summary of cross-section area and fatty acyl chain measures for common saturated synthetic phosphatidylcholine lipids.

Lipid	Area/Lipid (Å^2)	Fatty Acyl Chain	
		Carbon Count	Length (Å)
DSPC	52.3 (25°C)[11]	18	ca. 20.5[a]
DPPC	71.2 (50°C)[11]	16	17.3 (50°C)[25]
DMPC	65.2 (27°C)[11]	14	13.1 (30°C)[12]

Table 1B. Summary of values adopted for binding pocket dimension estimations in the mixed lipid nanoparticle design in this paper. Axes directions: Z = along lipid molecules through bilayer, X = perpendicular to fatty acyl chains, in plane of paper, Y = orthogonal to both lipid fatty acyl chain and plane of paper.

Composition	Pocket Z-direction dimension	Pocket X-direction dimension per Short Lipid
C16/C18	3.8 Å	~ 7.5-8 Å solid state
C15/C18	5.7 Å	~ 7.5-8 Å solid state
C14/C18	7.6 Å	~ 8.7 Å liquid state

[a] Calculated as phosphate group peak position reported by Kenworthy et al[26] subtracting ½ of Steric Headgroup Thickness reported by Nagle et al[12].

Varying Lipid Composition of Membrane does not Impact Particle Size and Initial Incorporation Efficiency

To compare mixed-lipid systems against pure lipid systems, we first need to confirm that variation in lipid composition of PCs with different fatty acyl chain length does not significantly impact size distribution and initial incorporation capacity of the liposomes at given drug loading. Pure lipid systems were composed of common PC and lipid mixtures contained a specified mole

percent (mol%) of lipid with short fatty acyl chain (hereon referred to as "Short Lipid") in C18 lipid. All formulations contain 5% PEG_{2000} on surface to provide reduced protein binding for future applications on biological studies and 10% **ADP109** incorporated in the membrane. Particles demonstrated comparable initial drug incorporation efficiencies and similar particle sizes regardless of composition (**Table 2**).

Table 2. Summary of Mixed Lipid Nanoparticle (MLNP) Composition with DPPC and DSPC. Particle diameters measured dynamic light scattering (DLS) are representative of number-weighted average of 6-minute measurement (peak intensity >99%) and initial drug incorporation efficiencies are reported as average and standard deviation of three independent batches.

	Composition (mol%)				Mean Size (d, nm)	Incorporation Efficiency (%)
	DPPC (C16)	DSPC (C18)	$mPEG_{2000}$-DPPE	ADP109		
DSPC	0	95	5 ($mPEG_{2000}$-DSPE)	10	58	94 ±2
MLNP20PS	15	80	5	10	55	94 ±4
MLNP40PS	35	60	5	10	53	92 ±1
MLNP60PS	55	40	5	10	56	91 ±3
MLNP80PS	75	20	5	10	47	91 ±1
DPPC	95	0	5	10	50	94 ±5

Optimization of X-direction Dimension Achieved by Variation of Short Lipid to DSPC ratio

Based on the estimated molecular dimension, we expected 40 mol% of Short Lipid in DSPC (C18 lipid) to offer the most accommodating binding pocket dimension along the x-axis for **ADP109**, and thus highest drug retention. Y-direction is assumed to require the same dimension that x-direction due to free rotation of the ART-dimer with respect to the piperazine tail. To confirm our hypothesis, ratio of C16 to C18 lipids was changed to determine the optimum ratio experimentally (**Table 2**). Ability of the membranes to retain the integrated **ADP109** was measured as drug association at 24 and 48 hours. The results show that at 24 hours, mixed lipid systems with 60 mol% or less short lipid retain comparable amounts of **ADP109** as pure DSPC

formulation (**Figure 2A**, **Figure 3**). At 48 hours, however, all mixed-lipid systems exhibited less than 6% change in drug association while pure-lipid systems continued to release the hydrophobic drug (**Figure 2B**). The absence of continuous-release phenomenon in the mixed-lipid systems alludes to a deeper binding of the extraneous compound in membrane and less disturbance on lipid packing caused by 10% **ADP109**. Our data agreed with the model estimate of 40 mol% Short Lipid composition offer the most accommodating fit to **ADP109**, with no steric clash or wasted cavity.

A)

	% ADP109 Retention	
	24 Hours	48 Hours
DSPC (C18)	93.6 ±1.2	81.7 ±4.8
MLNP40PS (C16:C18=4:6)	92.4 ±5.7	87.8 ±3.2
DPPC (C16)	85.0 ±1.4	75.6 ±4.1

B)

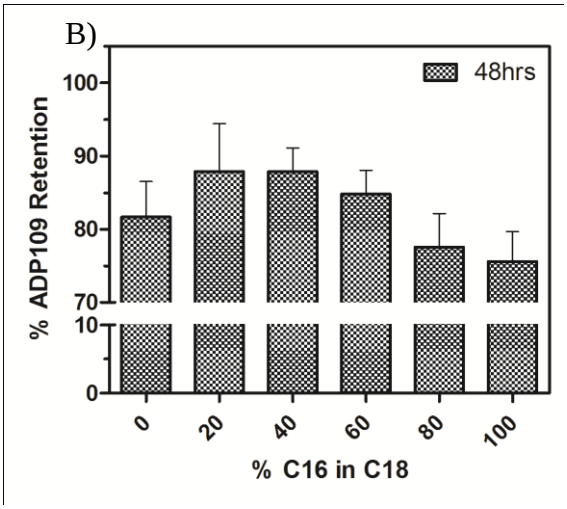

Figure 2. A) Summary Table comparing percent of **ADP109** retention over 24 and 48 hours of pure-lipid systems and MLNP40PS. B) **ADP109** retention in C16/C18 mixed liposome nanoparticles (MLNP-PS) measured 48 hours post dialysis using purified particles. The amount of **ADP109** retained in the liposomes were quantified by UV-Vis at λ=263 nm. All points represent average (±S.D.) of three independent experiments. Student's t-test comparing 40% C16 in C18 (MLNP40PS) and 100% C18 (DSPC) give p=0.14 at 48hours.

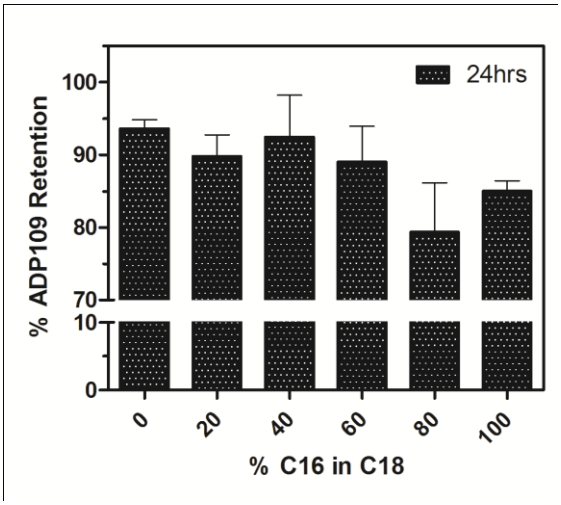

Figure 3. **ADP109** retention in C16/C18 mixed liposome nanoparticles (MLNP-PS) measured 24 hours post dialysis using purified particles. The amount of **ADP109** retained in the liposomes were quantified by UV-Vis at λ=263 nm. All points represent average (±S.D.) of three independent experiments.

Optimization of Z-direction Dimension Achieved by Variation of Short Lipid Fatty Acyl Chain Length

With the horizontal dimensions of the drug binding pocket optimized at 40 mol% Short Lipid in C18 lipid, we varied the number of methylene groups on the FA tails of the Short Lipid to examine the vertical depth, or the z-axis dimension, of the binding pocket. Geometrical considerations of **ADP109** suggest that optimal z-direction dimension is offered with a space of 8 missing methylene groups in the FA domain (**Table 1B**). Thus, membranes with carbon number difference of 4 (MLNP40PS, C16 in C18), 6 (MLNP40d(15)S, C15 in C18) and 8 (MLNP40MS, C14 in C18) were prepared at 40 mol% Short Lipid in C18 PC and the drug retention ability of the membranes was studied. MLNP40MS or 40 mol% C14 in C18 PC mixture was expected to show highest level of drug retention.

Table 3. Summary of Mixed Lipid Nanoparticle (MLNP) Composition at 40% short fatty acyl chain phosphatidylcholine in DSPC. Particle diameters measured dynamic light scattering (DLS) are representative of number-weighted average of 6-minute measurement (peak intensity >99%) and initial drug incorporation efficiencies are reported as average and standard deviation of three independent batches.

	Composition (mol%)				Mean Size (d, nm)	Incorporation Efficiency (%)
	Short Lipid	DSPC (C18)	$mPEG_{2000}$-DSPE	ADP109		
MLNP40PS	40 (C14)	55	5	10	53	92 ±1
MLNP40d(15)S	40 (C15)	55	5	10	59	95 ±1
MLNP40MS	40 (C16)	55	5	10	53	97 ±1

Measurement of drug association showed that as we increased the height of the binding pocket, more **ADP109** was able to integrate stably and remain associated with bilayer. After 48 hours, MLNP 40MS showed greater than 97% drug retention compared to 85% in the case of MLNP 40PS (**Figure 4**), both of which are improvements over the <75% retention with pure DPPC-**ADP109** or DSPC-**ADP109** particles.

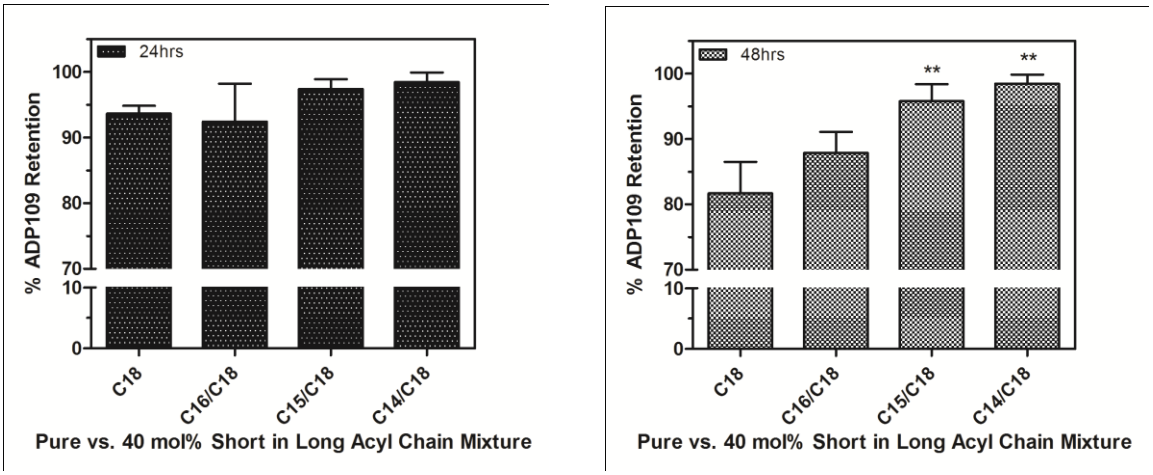

Figure 4. **ADP109** retention in liposome nanoparticles with 40% short chain lipid in DSPC, measured at 24 hours (left) and 48 hours (right) post dialysis using purified particles. The amount

of **ADP109** retained in the liposomes were quantified by UV-Vis at λ=263 nm. All points represent average (±S.D.) of three independent experiments. Student's *t*-test comparing 40% C14 in C18 (MLNP40MS) and 100% C18 (DSPC) give p=0.004 at 48hours. Statistical significance compared to pure C18 lipid is indicated by **.

*Mixed Lipid Systems Offering Optimal Geometrical Complementarity Show Least Defective Lipid Packing in Presence of **ADP109***

Next, to provide an explanation for the enhanced stability, we observed the depolarization of an inserted planar fluorescent probe, diphenyl-1,3,5-hexatriene (DPH), to delineate phase transition behaviors of the particle membranes. In a solid phase, planar hydrophobic fluorophore, DPH, aligns with the lipid fatty acyl chain and show high degree of polarization in emitted fluorescence when excited with polarized light. As the membrane undergoes phase transition with rising temperature, inserted fluorophores regain rotational freedom and result in fluorescence depolarization[12]. At 10% **ADP109**, particle membranes containing single type of PC show significantly disordered lipid packing compared to the drug-free blank control, as reflected by compromised anisotropy in the solid state in lower temperature region (**Figure 5A**). With the presence of a drug binding pocket to accommodate 10% **ADP109**, achieved by mixture of C14 and C18 PCs, the high anisotropy state becomes less perturbed and the melting curve of the drug-bound and drug-free membranes show smaller variation (**Figure 5B**). These results suggest that in mixed lipid systems with appropriate binding pocket size, drug molecule presence are considered "invisible" and thus have minimal effect on lipid molecular packing order.

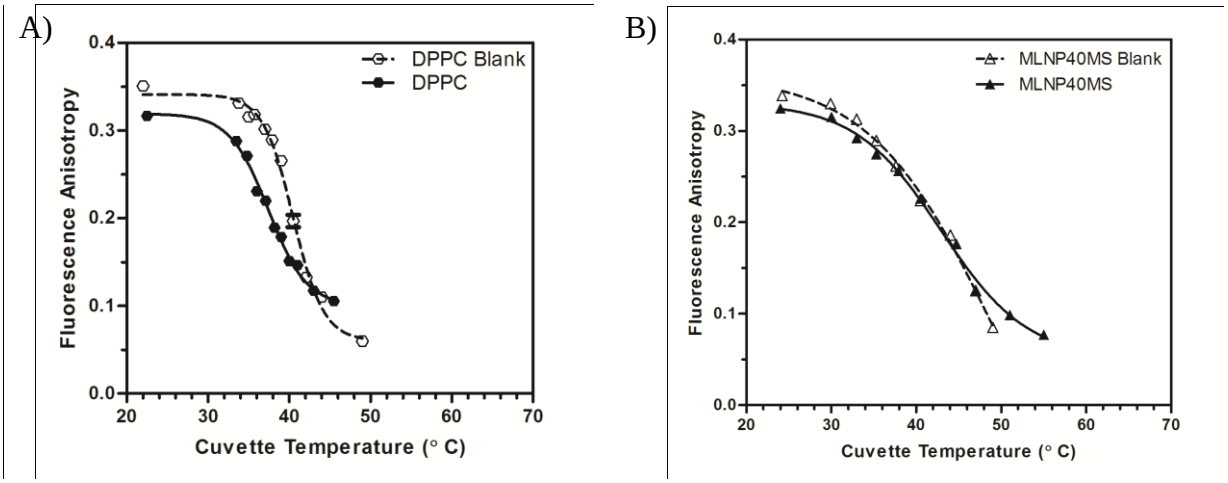

Figure 5. Liposome phase transition curve of A) C16 Lipid and B) 40% C14 in C18 lipid mixture membrane systems as measured by DPH fluorescence depolarization. Data points represent average (±S.D.) of triplicate readings.

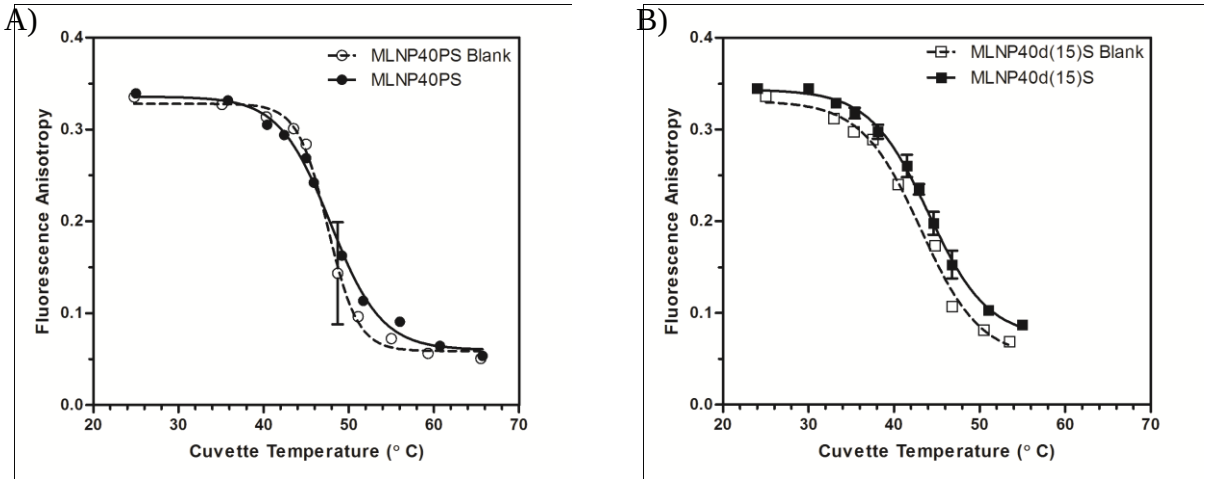

Figure 6. Liposome phase transition curve of A) 40% C16 in C18 lipid mixture and B) 40% C15 in C18 lipid mixture mixture membrane systems as measured by DPH fluorescence depolarization. Data points represent average (±S.D.) of triplicate readings.

*pH-dependent Release of **ADP109** in Mixed Lipid System MLNP 40MS*

ADP109 is an artemisinin dimer derivative we previously reported to possess pH-dependent solubility[5]. Thus, while the mixed lipid membranes were able to incorporate and stably retain the sterically bulky **ADP109**, we wanted to confirm that the pH-dependent release property was not compromised. Our 48 hour drug release results show that while the stability of drug-associated liposomes increased dramatically with the mixed lipid nanoparticles, **ADP109** was still released in a pH-dependent manner (**Figure 7**). The enhanced binding of drug molecules to lipid bilayer at neutral does not significantly compromise the pH-responsive drug release as we originally designed.

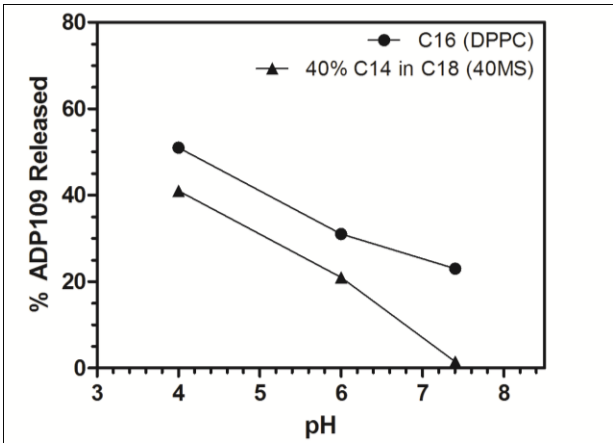

Figure 7. Representative pH-dependent release of **ADP109** at pH 7.4, pH 6 and pH 4 at 48 hours. 40MS data was collected in one experiment as proof of concept. DPPC data represent average value reported in previous publication[24].

Application of Geometry-Complementarity-Based Liposome Design to Darunavir and Curcumin

The fitting hypothesis based on geometrical complementarity model was supported with the systematic studies described above. To test that our approach is also applicable to other sterically

bulky compounds, we demonstrate below, the experimental data of two other drug molecules, darunavir and curcumin. The key characteristics of the two compounds along with **ADP109** are summarized in **Table 3** below. Binding pocket dimensions were designed based on the assumption that the compounds preferentially associate with hydrophobic region of the membrane. Simple PCs were used in lipid compositions tested.

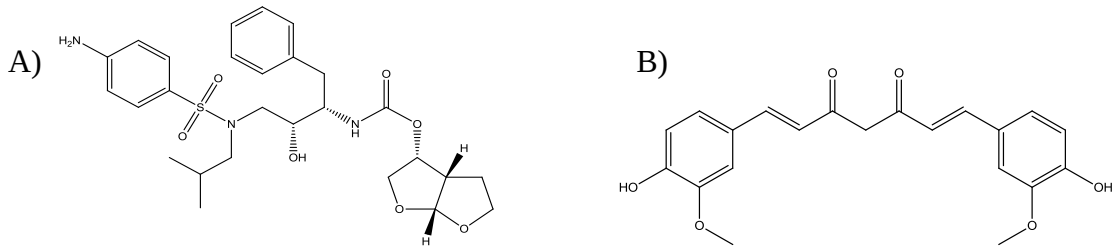

Figure 8. Chemical Structures of A) Darunavir and B) Curcumin.

Darunavir (**Figure 8A**) is a bulky compound that is more water-soluble than ADP109. We reasoned that the hydrophilic (aminophenyl)-sulfonyl tail preferentially associates with the lipid headgroups to maximize hydrogen-bonding stabilization. With this in mind, we hypothesize that a mixture of 3 lipids (10 mol% single-chain unsaturation C16-C18:1 lipid, 20 mol% C15, and 70 mol% C18 lipids) which allow for fitting of all greasy branches will be superior to the pure C18 lipid formulation in retaining the compound (**Table 4**).

For the flat hydrophobic molecule, Curcumin (**Figure 8B**), two scenarios may be assumed for interactions between the compound and lipid membrane systems. If the molecule inserts into the membrane along the Z-direction, aligning with fatty acyl chains, then we do not expect significant variation among different lipid compositions. If the drug molecule is driven to bind deep within the membrane, along the x-direction for example, then we expect a binding pocket formed with 60 mol% Short Lipid to offer complementarity for the molecule. **Table 4**

summarizes the key factors we considered in our hypothesis, the systematically designed liposome composition, and measured outcomes of incorporation efficiency and drug retention at 48 hours.

Table 4. Summary of key characteristics and drug retention of the optimal liposome composition obtained from geometry-based design.

	ADP109		**Darunavir**		**Curcumin**	
Molecular Weight (g/mol)	782.0		547.7		368.4	
Lipophilicity (LogP)[a]	5.24		1.89		3.62	
Water solubility (mg/mL)	0.027[6] (5% DMSO in PBS, RT)		0.15[27] (Ethanolate salt, 20°C)		<0.0011[22] (pH 5)	
Molecular Dimension[b] **(Z × X × Y)**	17Å × 17Å × 7.3 Å ~7.3Å cross section in hydrophobic region		16Å × 11Å × 5Å ~4.5 Å cross section in binding pocket, branch ~8.5Å from bilayer center		7.3Å × 19Å × 2Å Planar structure, align with fatty acyl chains or lay flat between leaflets	
Fatty-acyl Chain Composition for Drug Retention	100% C18	40% C14 +60% C18	100% C18	20% C15 +10% C16:0-C18:1 +70% C18	100% C18	60% C14 +40% C18
Incorporation Efficiency[c]	94(±2)%	97(±1)%	65%	56%	80%	99%
48-hour % Drug Retention[c]	82(±5)%	97(±2)%	15%	25%	86%	103%

[a] Predicted values on Virtual Computational Chemistry Laboratory (http://www.vcclab.org/lab/alogps/)[28]

[b] Estimated with structure visualization software based on known crystal structures of compounds, Axes directions: Z = along lipid molecules through bilayer, X = perpendicular to fatty acyl chains, in plane of paper, Y = orthogonal to both lipid fatty acyl chain and plane of paper

[c] Incorporation efficiency and Percent Drug Retention for ADP109 are reported as mean and standard deviation of three independent batches of particles, and those reported for Darunavir and Crucumin are mean of triplicate samples for the same batch of particles

Discussions

Hydrophobic drug molecules that are sterically bulky, such as ART-dimers, are challenging to solubilize and stabilize in aqueous solution. In this paper, we focus on development of a rational design approach that resulted in improvement of the drug retention in membranes through geometrical fitted drug binding pocket to integrate compounds into the lipid bilayers. We propose the importance of considering geometrical dimensions of compound and installing complementary binding pockets, achieved by mixture of lipids with fatty acyl chain incongruity, to enhanced colloidal stability. With this, we lay the foundation for selection of appropriate lipid compositions for stabilization and delivery of challenging hydrophobic drug molecules.

We validate, with bulky hydrophobic molecule, **ADP109**, that dimensions of the binding pockets can be manipulated by varying the percent composition and the FA tails of the lipids in mixture to accommodate drug molecules based on their 3D shapes. The geometry fit model provides systematic approach to lipid nanoparticle design that allows stable incorporation of challenging molecules at respectable loading efficiency, thus increasing the rate of success for delivering small molecule drugs to the targeted biological milieu in clinical applications.

In the gel state, lipid molecules with saturated fatty acyl chains optimize intermolecular interactions to achieve most stable packing. In doing so, membrane eventually expel compounds that interfere with the fatty acyl chain alignment, which destabilize the membrane structure. To minimize the negative impact of incorporating bulky hydrophobic drug, a binding pocket can be introduced in the bilayer with methods such as incorporating cholesterol or lyso-lipids and using unsaturated lipids[6]. The use of cholesterol, however, may compromise loading capacity of membrane due to competitive binding. In the case of lyso-lipids, misalignment of lipid molecules with different head-to-tail area ratio may result in membrane leakiness, lower rigidity, and

compromised aqueous core stability. Thus, we propose to use simple mixtures of common lipids, such as phosphatidylcholines, that result in binding pockets deep within the hydrophobic FA domain.

Theoretical values and extrapolated fluid phase data, however, are available to estimate the binding pocket size in order to rationalize the goodness of fit for **ADP109**. J.F.Nagle, in a 2000 review, summarized various membrane parameters based on experimental data[11]. Though limited gel-phase data are available, with reasonable assumptions such as thickness of membrane increases by approximately 20%[13] and equal spacing between each methylene groups in the fatty acyl chain, we estimate that a 2-carbon mismatch contributes to ~1.6 Å of leaflet thickness difference in the fluid phase and ~1.9Å in gel phase. Here, we refer to Gibbs-Luzzati bilayer thickness for DPPC at 50°C being 38.5Å and that of DMPC at 30°C being 36.9Å[11]. Thus, we approximate the binding pocket height, assuming matching of phosphate head group, to be 3.8Å for DPPC/DSPC, 5.7Å for d(15)PC/DSPC and 7.6Å for DMPC/DSPC at room temperature. It should be noted that T_m for DMPC is 24°C[14], and so binding pocket may be bigger than 7.6Å for the C14/C18 mixture as some of the DMPC micro-domains undergo phase transition. The maximum diameter of **ADP109**'s artemisinin core that embeds in the binding pocket is estimated to be 7.3Å, based on the x-ray structure of a similar artemisinin dimer derivative (**Table 3**, **Figure 1B**). With these approximations, 40 mol% C14 in C18 lipid mixture offers the least constrain when **ADP109** molecule is fitted in the binding pocket for the mixed lipid membranes, and thus expected to cause minimal disturbance to lipid packing. **Table 4** summarizes the values we used for approximation of the pocket dimensions for the 4, 6 and 8 carbon difference mixtures. We chose a pocket with Z-direction measuring slightly larger than that required by the

molecule and an x/y direction that would accommodate the molecule with the variation in dimension at no more than ~0.5Å.

Similar design processes may be applied to integrate other challenging compounds to improve their drug retention. We demonstrated the feasibility of the design process of liposomal nanoparticles as drug delivery vehicles with two other compounds of distinct lipophilicity and molecular geometry, Darunavir and Curcumin. Darunavir is a protease inhibitor that is approved as part of combination therapy for HIV treatment[15]. To maximize the co-delivery efficiency of the HIV cocktail therapy, a drug delivery vehicle that offers simultaneous loading of both hydrophobic and hydrophilic payload is desirable[16]. Darunavir-bound liposomes, for example, have been reported, but exhibited poor stability and drug retention[7]. Stabilization gained by drug-binding pocket complementarity contributed to twice the amount of drug retained after 48 hours with a minor compromise in the initial incorporation efficiency – obtaining higher absolute amount of drug in the mixed lipid system overall. Our Darunavir data suggest that while improvements can be obtained for these amphiphilic bulky compounds, the solubility of the compounds in water still play a critical role in drug-lipid association.

Curcumin is a bioactive agent found in turmeric that has a planar geometry. Although Curcumin has long been known for medicinal benefits, it suffers from low aqueous solubility and poor bioavailability. Nanoparticle forms of Curcumin have recently attracted significant attraction for clinical applications[17]. Because of its planar structure and high hydrophobicity, we can expect reasonable loading and retention of Curcumin for both the pure and mixed lipid systems. As demonstrated in Table 4, however, the presence of FA domain binding pocket in case of MLNP60MS (60 mol% C14 in C18) appears to increase the stability of the lipid-bound state of Curcumin, which results in the measurable increase in loading efficiency as well as retention.

The Curcumin data are consistent with our findings in the Darunavir and **ADP109** systems, further alluding to the advantage of installing binding pocket deep within the membrane as a means to increase incorporation efficiency.

Our findings suggest that geometrical complementarity, which historically has not been emphasized in drug formulation development, is an important consideration when designing suitable lipid-based drug delivery vehicles. In the current study, phosphatidylcholines with different lengths of FA tails were used to validate our hypothesis. Lipids with different head groups and asymmetric fatty acyl chains remain to be investigated to develop a more robust and comprehensive model. Through the understanding of geometrical fitting of hydrophobic molecules and incentivizing integration of bulky lipophilic compounds deep within the fatty acyl domain of the lipid membrane may change behavior of the drug-bound nanoparticles *in vivo*. Ultimately, the systematic approach to rational design of lipid-based drug delivery systems may lead to higher success rate in translation of hydrophobic drug candidates to clinical applications.

Experimental Section

Materials

Lipids 1,2-dipalmitoyl-*sn*-glycero-3-phosphatidylcholine (DPPC), 1,2-ditetradecanoyl-*sn*-glycero-3-phosphatidylcholine (DMPC), 1,2-dipentadecanoyl-*sn*-glycero-3-phosphatidylcholine (D(15)PC), 1,2-distearoyl-*sn*-glycero-3-phosphatidylcholine (DSPC), and pegylated phospholipids $mPEG_{2000}$-DSPE, $mPEG_{2000}$-DPPE and $mPEG_{2000}$-DMPE were purchased from Avanti Polar Lipids Inc. (Alabaster, AL) in powder form. Curcumin (natural) was bought from TCI America (Portland, OR) and Darunavir was provided by Waterstone Technology (Carmel, IN). Chloroform (*hazardous volatile solvent, handle in ventilated hood)* purchased from Avantor Performance Materials (Center Valley, PA) was dried with molecular sieves (4Å) for at least 24 hours before use. Calcein was purchased from TCI America (Portland, OR), dipheyl-1,3,5-hexatriene (DPH) was bought from Life Technologies (Formerly Invitrogen, Carlsbad, CA). Phosphate buffered saline (1X PBS) solution was diluted from commercially prepared 10X PBS (GE Healthcare HyClone, Thermo Fisher Scientific, Waltham, MA). Acetonitrile, LCMS grade, was purchased through Fisher Scientific (Pittsburg, PA) and acetic acid (HAc) from Avantor Performance Materials (Center Valley, PA). Molecule 3-dimensional structures were visualized using PyMOL Molecular Graphics Systems (Version 1.3, Schrodinger, LLC).

Preparation and Size Characterization of Liposomal Nanoparticles

Liposomes were prepared with a thin-film rehydration-sonication method outlined in previously published literature[18]. Lipid stock solutions were prepared at 100 mg/ml, **ADP109**[5] stock solution was prepared at 50 mg/mL and Darunavir stock was prepared at 100 mg/mL in chloroform. Curcumin stock solution was prepared at 8.33 mg/mL in 4:1 chloroform:methanol. After addition of appropriate amounts of lipids and drug aliquots to a screw-cap test tube,

organic solvent was removed under a gentle stream of N_2 followed by vacuum drying. The film was rehydrated with 1X PBS at 55°C for 1 hour for all formulations except DSPC liposomes (at 60°C), to give multilamellar vesicles at 20 mM lipid concentration with 10 mol% drug. The mixture was then sonicated at 53°C for 5 minutes 3 times to give a translucent suspension without observable particulates and then gradually cooled down to well below the lipid phase transition temperature (4°C), to give liposomes nanoparticles. The nanoparticle suspension was diluted to 2 mM for sizing measurements on a NICOMP 380ZLS (Particle Sizing Systems, Santa Barbara, CA) with argon laser at 633.0 nm at room temperature. Sizing data were reported as the average (± S.D.) of 3 batches of particles.

Analytical Methods for Drug Molecules

ADP109 and Curcumin were quantified according to UV-Vis absorbance. With **ADP109**-bound liposomes, 30 μL aliquots of both dialyzed and undialyzed samples were collected in separate Eppendorf tubes, crashed with 300 μL of cold acetonitrile, vortexed for 30 seconds and centrifuged at 14,000 rpm for 5 minutes. The supernatant of the centrifuged samples was collected for UV absorbance measurement from 200 to 400 nm by DU 640 spectrophotometer (Beckman Coulter, USA). Curcumin was prepared according to the sample method as described above and Visible light absorbance was measured at 405 nm on Victor^3 Multilabel Counter Reader (Model 1420, Perkin Elmer, Waltham, MA).

Darunavir was quantified using a liquid chromatography-tandem mass spectrometry (LCMS) method. 30 μL aliquots of both dialyzed and undialyzed samples were collected in separate Eppendorf tubes. Triplicates of 5 μL each of the sample were crashed with 495 μL of cold acetonitrile, vortexed for 30 seconds and centrifuged at 14,000 rpm for 5 minutes. The supernatant of the centrifuged samples were then further diluted 20 times (50 μL to 1 mL final

volume) for LCMS analysis. Specifically, samples were separated on a Phenomenex Synergi column (100 x 2.0 mm, 4 µm particle size, Torrance, CA) with a C_8 guard column (4.0 x 2.0 mm) (Phenomenex) on a Shimadzu HPLC system (Columbia, MA) and signals were detected with the coupled 3200 QTRAP mass spectrometer from Applied Biosystems (Grand Island, NY), equipped with an electrospray ionization (ESI) Turbo Ion Spray source. The mobile phase for the separations consisted of A: water with 0.1% HAc and B: acetonitrile with 0.1% HAc. The gradient program used was as follow: 50% B for 1 min, 100% B at 2 min to 3.5 min, 50% B at 3.75 min held until 5 min. The analyte was monitored in positive MRM mode at transition 548.3 → 392.3 m/z.

Drug Incorporation, Retention and pH-responsive Release Efficiencies

For loading efficiency studies, liposome suspensions in original concentrations were placed into dialysis tubing (MWCO 6000-8000 Da, Spectrum Labs, Rancho Dominguez, CA) and dialyzed against at least 1000X volume of 1X PBS buffer overnight (16-20 hours) at room temperature. The Loading Efficiency was calculated according to the following equation (**Eq. 1**) below:

$$\text{Loading Efficiency (\%)} = \frac{A_{max}\,(D)}{A_{max}\,(UD)} \times 100\%$$

Where A_{max} (D) is the sample signal of the dialyzed sample, and A_{max} (UD) is that of the undialyzed sample. For **ADP109**, A_{max} is defined as absorbance at λ_{max} of 263 nm, and that of Curcumin is 405 nm. For Darunavir, A_{max} is defined as peak area. Calibration curves of response versus concentration were defined to ensure that all signals obtained in assays were within the linear range.

Retention of the drugs in pH 7.4 at ambient temperature was studied using aliquots of dialysis-purified liposomes by dialysis method. Samples were taken at 24 and 48 hours and prepared for quantification analysis. The Retention Efficiency is given by equation (**Eq. 2**):

$$\text{Retention Efficiency (\%)} = \frac{A_{max}\,(t)}{A_{max}\,(D)} \times 100\%$$

Where A_{max} (t) is the sample signal of the dialyzed sample after *t* (t=24 or 48) hours of dialysis, and A_{max} (D) is that of the overnight dialyzed sample.

For the pH-dependent release efficiency study of **ADP109**, aliquots of at least 120 μL of 20 mM dialysis-purified liposome suspensions were dialyzed against 1000 mL of pH 7.4 PBS, pH 6 citrate or pH 4 citrate buffers at ambient temperature. 30 μL aliquots were removed from each dialysis at times t=24 and 48 hours for quantification. Values were plotted from one representative experiment as proof of concept.

The Release Efficiency was calculated according to **Eq.3** below:

$$\text{Release Efficiency (\%)} = 100\% - \left(\frac{A_{263}\,(\text{pH})}{A_{263}\,(D)} \times 100\%\right)$$

Where A_{263} (pH) is the sample signal of the dialyzed sample in buffer with different pH, and A_{263} (D) is that of the overnight dialyzed sample.

*Effects of **ADP109** on Membrane Phase Transition Behavior*

Liposome suspension was diluted to 1 mM in 1X PBS and warmed to 60°C for 5 minutes. Stock solution of 1,6-Diphenyl-1,3,5-hexatriene (DPH) was prepared at 1mM in tetrahydrofuran (THF). 0.1% volume of the DPH Stock was mixed with the liposome suspensions, vortexed briefly, incubated at 60°C for 15 minutes in the dark, then cooled down to room temperature (21-24°C)

for fluorescence polarization measurements on a Hitachi F4500 (Tokyo, Japan) fluorescence spectrophotometer. A circulating water bath (Fischer Scientific model 800, Pittsburgh, PA) maintained stable temperature during measurements. A digital thermo probe (Fischer Scientific, Pittsburgh, PA) was used to monitor the exact temperature within the cuvette and ensure stability of temperature while the liposome sample was heated. Fluorescence measurements were taken as an average of 10 seconds of continuous reading. Triplicate measurements in each direction of emission polarization: 0° ($I_{/\!/}$) and 90° ($I_{\perp}$) with respect to 0° excitation, were measured with liposomes in 1X PBS. Curve fitting was based on average and standard deviation (S.D.) calculated from triplicate readings. The fluorescence anisotropy was calculated using **Eq. 4** below:

$$\text{Fluorescence Anisotropy} = \frac{I_{/\!/} - I_{\perp}}{I_{/\!/} + 2I_{\perp}}$$

Where $I_{/\!/}$ is the fluorescence intensity in the plane parallel (0° rotation) to polarized excitation light and $I_{\perp}$ is that perpendicular (90° rotation) to excitation light.

Reference

1. Harvey, R. A.; Clark, M. A.; Finkel, R.; Rey, J. A.; Whalen, K., *Pharmacology*. 5 ed.; Lippincott Williams & Wilkins: China, 2012.

2. Immordino, M. L.; Dosio, F.; Cattel, L., Stealth liposomes: review of the basic science, rationale, and clinical applications, existing and potential. *International Journal of Nanomedicine* **2006,** *1* (3), 297-315; Chang, H.-I.; Cheng, M.-Y.; Yeh, M.-K., Clinically-Proven Liposome-Based Drug Delivery: Formulation, Characterization and Therapeutic Efficacy. *Open Access Scientific Reports* **2012,** *1* (3), 8.

3. Kraft, J. C.; Freeling, J. P.; Wang, Z. Y.; Ho, R. J. Y., Emerging Research and Clinical Development Trends of Liposome and Lipid Nanoparticle Drug Delivery Systems. *Journal of Pharmaceutical Sciences* **2014,** *103* (1), 29-52.

4. Torchilin, V. P., Recent advances with liposomes as pharmaceutical carriers. *Nature Reviews Drug Discovery* **2005,** *4* (2), 145-160.

5. Zhang, Y. T. J.; Gallis, B.; Taya, M.; Wang, S. S.; Ho, R. J. Y.; Sasaki, T., pH-Responsive Artemisinin Derivatives and Lipid Nanoparticle Formulations Inhibit Growth of Breast Cancer Cells In Vitro and Induce Down-Regulation of HER Family Members. *Plos One* **2013,** *8* (3).

6. Koudelka, S.; Turanek, J., Liposomal paclitaxel formulations. *Journal of Controlled Release* **2012,** *163* (3), 322-334.

7. Duan, J. H.; Freeling, J. P.; Koehn, J.; Shu, C. L.; Ho, R. J. Y., Evaluation of Atazanavir and Darunavir Interactions with Lipids for Developing pH-Responsive Anti-HIV Drug Combination Nanoparticles. *Journal of Pharmaceutical Sciences* **2014,** *103* (8), 2520-2529.

8. Anderson, M.; Omri, A., The effect of different lipid components on the in vitro stability and release kinetics of liposome formulations. *Drug Delivery* **2004,** *11* (1), 33-39.

9. Bagatolli, L. A.; Gratton, E., A correlation between lipid domain shape and binary phospholipid mixture composition in free standing bilayers: A two-photon fluorescence microscopy study. *Biophysical Journal* **2000,** *79* (1), 434-447; Muresan, A. S.; Diamant, H.; Lee, K. Y. C., Effect of temperature and composition on the formation of nanoscale compartments in phospholipid membranes. *Journal of the American Chemical Society* **2001,** *123* (28), 6951-6952.

10. Lis, L. J.; McAlister, M.; Fuller, N.; Rand, R. P.; Parsegian, V. A., Interactions Between Neutral Phospholipid-bilayers Membranes. *Biophysical Journal* **1982,** *37* (3), 657-665.

11. Nagle, J. F.; Tristram-Nagle, S., Structure of lipid bilayers. *Biochimica Et Biophysica Acta-Reviews on Biomembranes* **2000,** *1469* (3), 159-195.

12. Fuchs, P.; Parola, A.; Robbins, P. W.; Blout, E. R., Fluorescence Polarization and Viscosities of Membrane Lipids of 3T3 Cells. *Proceedings of the National Academy of Sciences of the United States of America* **1975,** *72* (9), 3351-3354; Burton, J.; Litman, B. J.; Barenholz, Y., [91] Fluorescent Probe:Diphenylhexatriene. In *Methods in Enzymology*, Fleischer, S.; Packer, L., Eds. Academic Press: **1982**; Vol. 81, pp 678-685.

13. Mouritsen, O. G.; Jorgensen, K.; Honger, T., Permeability and Stability of Lipid Bilayers. Disalvo, E. A.; Simon, S. A., Eds. CRC Press: Boca Raton, FL, **1995**.

14. Silvius, J. R., Thermotropic Phase Transitions of Pure Lipids in Model Membranes and Their Modifications by Membrane Proteins. In *Lipid-Protein Interactions*, John Wiley & Sons, Inc: New York, **1982**; Vol. 2.

15. Saskova, K. G.; Kozisek, M.; Rezacova, P.; Brynda, J.; Yashina, T.; Kagan, R. M.; Konvalinka, J., Molecular Characterization of Clinical Isolates of Human Immunodeficiency Virus Resistant to the Protease Inhibitor Darunavir. *Journal of Virology* **2009,** *83* (17), 8810-8818.

16. Morton, S. W.; Lee, M. J.; Deng, Z. J.; Dreaden, E. C.; Siouve, E.; Shopsowitz, K. E.; Shah, N. J.; Yaffe, M. B.; Hammond, P. T., A Nanoparticle-Based Combination Chemotherapy Delivery System for Enhanced Tumor Killing by Dynamic Rewiring of Signaling Pathways. *Science Signaling* **2014,** *7* (325).

17. Kurien, B. T.; Singh, A.; Matsumoto, H.; Scofield, R. H., Improving the solubility and pharmacological efficacy of curcumin by heat treatment. *Assay and Drug Development Technologies* **2007,** *5* (4), 567-576; Tonnesen, H. H., Solubility, chemical and photochemical stability of curcumin in surfactant solutions - Studies of curcumin and curcuminolds, XXVIII. *Pharmazie* **2002,** *57* (12), 820-824.

18. Kinman, L.; Brodie, S. J.; Tsai, C. C.; Bui, T.; Larsen, K.; Schmidt, A.; Anderson, D.; Morton, W. R.; Hu, S. L.; Ho, R. J. Y., Lipid-drug association enhanced HIV-1 protease inhibitor indinavir localization in lymphoid tissues and viral load reduction: A proof of concept study in HIV-2(287)-infected macaques. *Jaids-Journal of Acquired Immune Deficiency Syndromes* **2003,** *34* (4), 387-397.

CHAPTER 6

Sample Preparation and Liquid Chromatography-Tandem Mass Spectrometry Analysis of Artemisinin Dimer Liposome from Biological Tissues

Part of the content of this Chapter was submitted for publication as an original research article.

The manuscript was authored by:
Yitong J. Zhang[1], Dale Whittington[2], Tomikazu Sasaki[1]

[1]Department of Chemistry, [2]Department of Medicinal Chemistry Mass Spectrometry Center
University of Washington, Seattle, WA 98105

Abstract

Artemisinin dimer derivatives that are linked at C10 (**Figure 1**) with non- hydrolyzable carbon-carbon bonds are potent antimalarial and anti-proliferative chemotherapeutics. We've previously demonstrated promising tumor suppression efficacy in triple-negative human breast cancer mice xenograft models with lipid-nanoparticle (LNP) formulation of a pH-responsive artemisinin dimer derivative, **ADP109**. To further refine the chemical structure of the compound and optimize the drug delivery and formulation, we need an understanding of the behavior of these drug-bound lipid particles *in vivo*. We report here, the first sample preparation technique and analytical method for quantifying **ADP109**-LNP from whole blood using LC-MS/MS. The analytical assay has a dynamic range defined over two orders of magnitude from 10 ng/mL to 1000 ng/mL. The recovery efficiencies of the artemisinin dimer derivative from rat whole blood were 63 (±4)% and 76 (±3)% at 100 ng/mL and 1000 ng/mL, respectively. The method was validated with intraday and interday runs for accuracy, and the robustness and reproducibility of the assay was confirmed with intraday recovery efficiency studies. The robust and versatile sample preparation and LC-MS/MS quantification methods described here lay the foundation for future pharmacokinetic and tissue distribution studies to enhance the understanding of the *in vivo* behaviors of lipid-bound artemisinin dimer derivatives.

Introduction

Artemisinin is used as a first-line treatment for malaria and has been documented to possess anti-inflammatory effect[1]. In attempt to understand the pharmacokinetic profile and safety of artemisinin-derived drug molecules, a number of studies analyzing drug behavior from biological milieu have been reported for the natural product or simple derivatives[2]. In the early 1990's, Lai and other researchers independently reported potent anti-cancer effect of artemisinin derivatives[3]. Artemisinin contains an endoperoxide group that is activated by intracellular iron to exert the biological activity. Recently, Posner et al introduced a dimeric structure of artemisinin linked with an isobutylene at C10 that showed orders of magnitude improvement in efficacy against malaria parasite as well as promising anti-cancer effects[4].

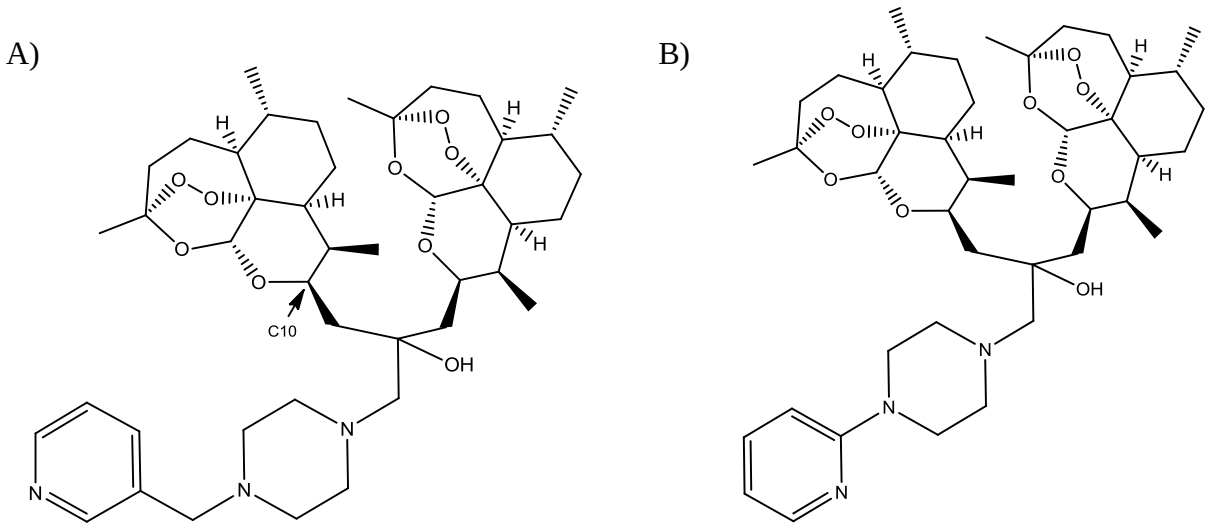

Figure 1. Chemical Structure of A) pH-responsive artemisinin dimer **ADP109**, and B) internal standard **ADP107**.

While enhancing the drug potency, the dimeric structure posed a number of challenges both in terms of delivery *in vivo* and concentration analysis in biological tissues. The class of C10-linked artemisinin dimers has poor aqueous solubility and requires organic co-solvent for delivery to cell culture. We previously reported a liposomal formulation of a pH-responsive dimer artemisinin that eliminated the need for organic solvent while maintaining the enhanced cytotoxicity of the pH-responsive derivative, **ADP109**, compared to the parent C10-isobutylene artermisinin dimer[5]. Our recent *in vivo* study using liposomal pH-responsive artemisinin dimer (**ADP109**-LNP) formulation showed promising efficacy when tested against MDA-MB-231 human breast cancer mice xenograft model[6]. To further refine the artemisinin dimer derivatives and their formulation, it is essential to understand the pharmacokinetics and tissue distribution of the drug. Unfortunately, no quantification method for artemisinin dimers in biological samples has been reported in literature. The highly hydrophobic nature of artemisinin dimers coupled with the sensitive peroxide group in the artemisinin core provide a unique challenge for the development of a robust analytical method for **ADP109**-LNP in biological samples.

In the decades of artemisinin research and clinical applications, a number of analytical methods have been developed to quantify blood or plasma drug concentration from clinical samples. Such methods employ a variety of chromatographic separation in tandem with potentiometric detection[7], on-line derivatization then UV detection[8], or more preferably tandem mass spectrometry[9]. To the best of our knowledge, however, no analogous analytical methods have been developed for either lipid-bound artemisinin or the class of more potent dimer derivatives. We report here the first liquid chromatography-tandem mass spectrometry (LC-MS/MS) method for analyzing concentration of the liposome-bound pH-responsive artemisinin dimer, **ADP109**-LNP, from rat whole blood and a number of organ tissues.

Results

Chromatograms of the Compounds of Interest and Matrix

The pH-responsive artemisinin dimer derivative, **ADP109**[9], is an amphiphilic compound that contains a highly hydrophobic artemisinin pharmacophore and a protonatable pyridyl-methyl-pipierazine tail (**Figure 1A**). We were able to quantify the dimer parent compound as well as the internal standard (**Figure 1B**), another artemisinin dimer with similar structure, from highly complex biological samples with high sensitivity and selectivity. The LC method provided clear separation of **ADP109** and the internal standard extracted from **ADP109**-Lipid nanoparticles spiked with internal standard. Blank whole blood extractions gave small peaks that overlap with the elution times corresponding to both compound of interest and the internal standard used for quantification, but the magnitude of these co-eluting peaks were confirmed to not interfere with quantification when whole blood extracted standard curve was used for calibration.

Table 1. A) Liquid chromatography mobile phase gradient for separation of **ADP109** and internal standard. B) Mass spectrometry settings for detection of parent and daughter ions of **ADP109** and internal standard.

A)

Time (min)	Flow Rate (mL/min)	% A	% B
0.00	0.5	70	30
1.00	0.5	70	30
4.00	0.5	0	100
5.00	0.5	0	100
5.10	0.5	70	30

B)

Cone Voltage (V)	**55**
Capillary Voltage (kV)	3.50
Desolvation Temperature (°C)	350
Desolvation Gas Flow (L/hr)	800
Collision Voltage	35
ADP109 Fragments (Da)	782.4 → 190.1
ADP107 Fragments (Da)	768.4 → 121.1

Representative chromatograms of **ADP109** extracted from **ADP109**-Lipid nanoparticles, from blood spiked **ADP109**-Lipid nanoparticles, and blank blood samples are shown below in **Figure 2**. Compound of interest (**ADP109**) is eluted at 2.7 (±0.1) minutes whereas the internal standard is eluted at 3.0 (±0.1) minutes.

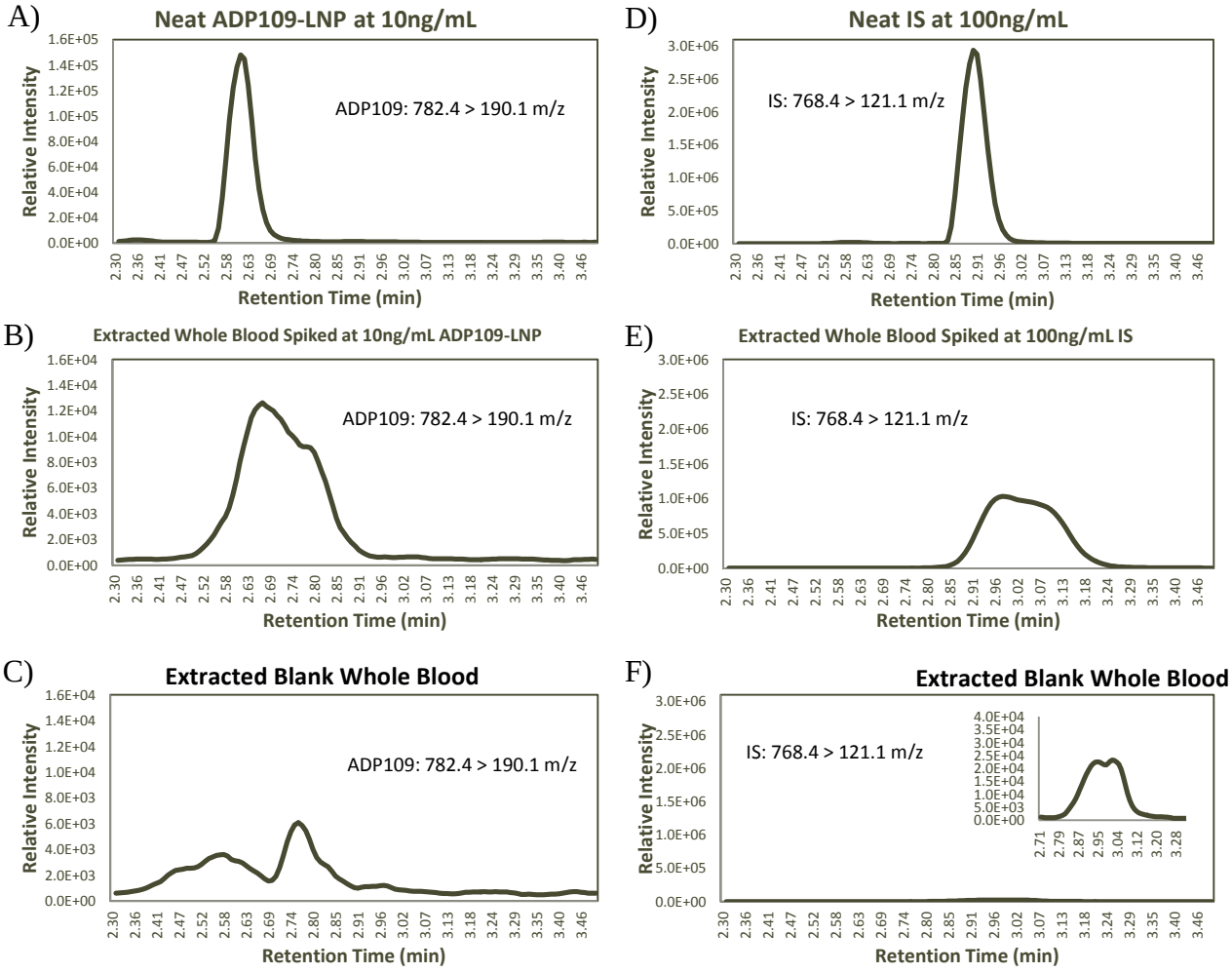

Figure 2. Representative chromatograms monitored by daughter ion channel for quantification: A), B, C) at ADP109: 782.4 > 190.1 m/z, and D), E), F) at IS: 768.4 > 121.1 m/z).

__ADP109__-LNP Spiked Whole Blood Sample Preparation

Upon spiking whole blood with **ADP109**-Lipid nanoparticles, we found that extraction of **ADP109** from separated plasma alone was not feasible and so sample preparation methods were developed for **ADP109** from whole blood. Furthermore, the rapid degradation of artemisinin pharmacophore in the presence of heme and free ferrous ions (Fe^{2+}) present challenges in recovery of parent drug molecule from whole blood.

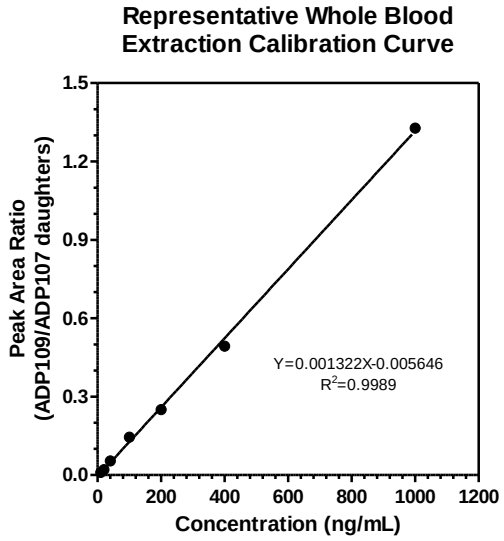

Figure 3. Representative standard curve of spiked whole blood extractions at 7 different concentrations. Values plotted for single run and linearity is representative of all spiked whole blood samples.

Conventional extraction methods failed in recovering compounds of interest from whole blood with the best result being 1% of recovery efficiency when whole blood was treated with first $HClO_4$ followed by 10% methanol in DCM liquid-liquid extraction in presence of 4M KOH. Under the experimental conditions, hemoglobin was quickly denatured and released free heme that likely destroyed the artemisinin core during sample preparation.

A number of factors affected the recovery efficiency of **ADP109** from spiked **ADP109**-Lipid nanoparticles, specifically the pH of the sample, the chemical properties of the solid phase, and the composition and pH of the solvents used for final elution of the compounds of interest. We found that 0.1N hydrochloric acid at pH 1 resulted in highest amount of compound recovery (58%) compared to either lower concentrations of HCl or various concentrations of the weak acid, acetic acid. 0.01M HCl (pH 2) gave 22% recovery efficiency and 1% acetic acid (pH 3) yielded 47%. In terms of solid phase cartridge, we found that mixed-mode cation-exchange (MCX) resins allowed higher recovery compared to both hydrophobic-lipophilic balanced (HLB) and weak cation-exchange (WCX) solid phases. Finally, the elution solvents were optimized to be 1 : 4 : 6 $NH_4OH_{(aq)}$: MeOH : ACN to wash off **ADP109** and internal standard under basic conditions. Sample preparation optimization was based on LCMS results comparing neat and spiked extracted samples (**Figure 4**).

The endoperoxide moiety on artemisinin is unstable in the presence of strongly reducing metal ions such as ferrous ion in lysed red blood cells[16-18]. In our hands, initial attempts at extracting **ADP109** from whole blood confirmed the rapid loss of the parent compound when blood was lysed with organic solvents such as methanol. Thus, we deactivated heme groups with excess strong oxidizing reagent, potassium dichromate, in the sample preparation step to covert released ferrous ions to the non-reactive ferric ion upon lysis of red blood cells in whole blood. With potassium dichromate, we were able to significantly enhance extraction efficiency of **ADP109** from blood samples spiked with **ADP109**-Lipid nanoparticles. We achieved an average recovery efficiency of at 63 (±4)%, at 100 ng/mL spiked concentration of **ADP109**-Lipid nanoparticles, and 76 (±3)% at 1000 ng/mL from whole blood among three independent experiments. The concentrations reflect middle and high values on the standard curve and relatively low

concentrations relative to expected concentrations in biological tissues given that the maximum tolerated dose of **ADP109**-LNP was determined to be 40 mg/kg on mice via subcutaneous injection[10].

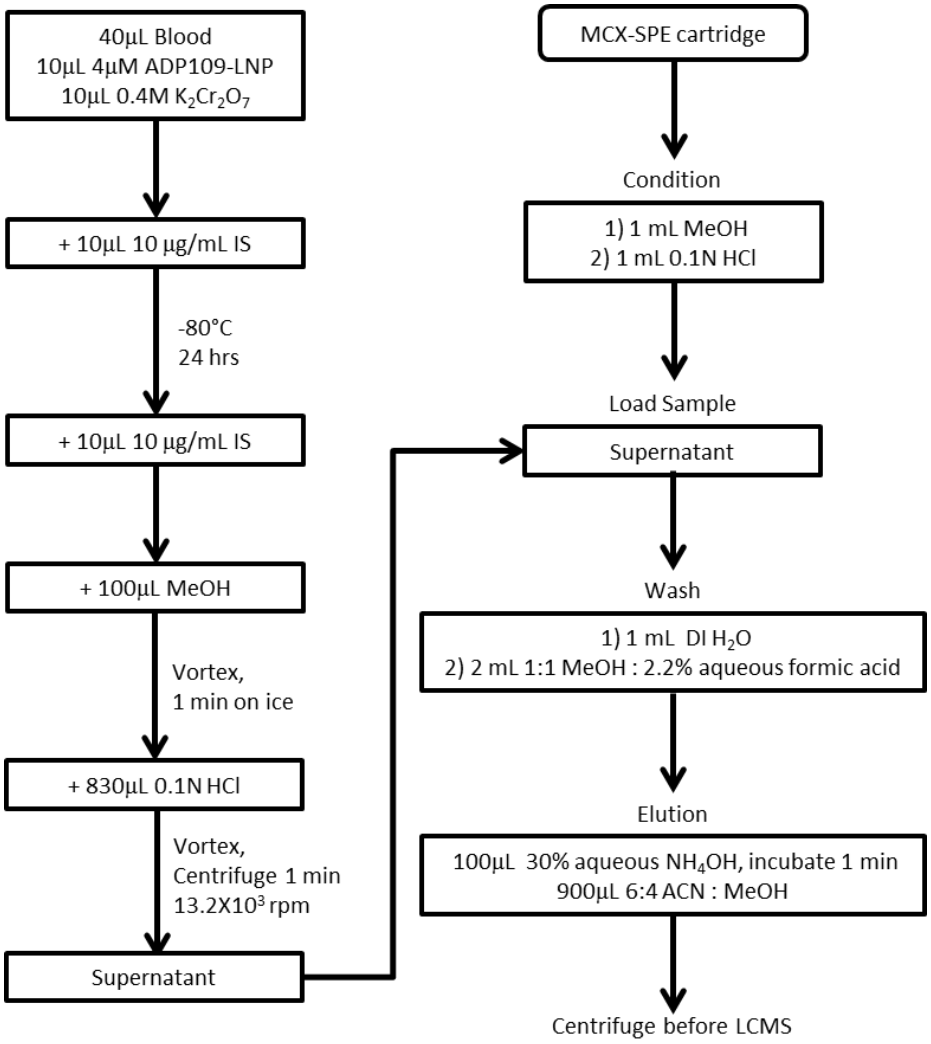

Figure 4. Schematic describing extraction procedure of **ADP109** from spiked whole blood for LCMS analysis.

The relatively consistent recovery efficiency at different concentrations suggests that our sample preparation protocol is a robust method for extracting artemisinin dimer derivatives from whole blood. The reproducibility of the method is further confirmed with the small standard deviation among three independent extractions at the same concentration.

__ADP109__-LNP Spiked Tissue Sample Preparation

The solid phase extraction (SPE) methods worked well for extraction of spiked **ADP109**-LNP from whole blood, it was not the optimal method for tissue sample preparations. We found that liquid-liquid extractions under basic condition after perchloric acid protein denaturation yielded higher recovery efficiency, as well as cheaper and easier to perform. The liquid-liquid extraction method was able to recover higher amount of parent **ADP109** from spiked tissue samples that contain higher amount of lipid, such as brain tissue, compared to tissues where iron content is relatively high, such as liver. At a spiked concentration of 50 ng/mL of **ADP109**, 49% of the compound was recovered from liver and 90% could be recovered from brain, in a trial run. Standard curves of liver, brain and tumor were conducted using the optimized liquid-liquid extraction method (**Figure 5**).

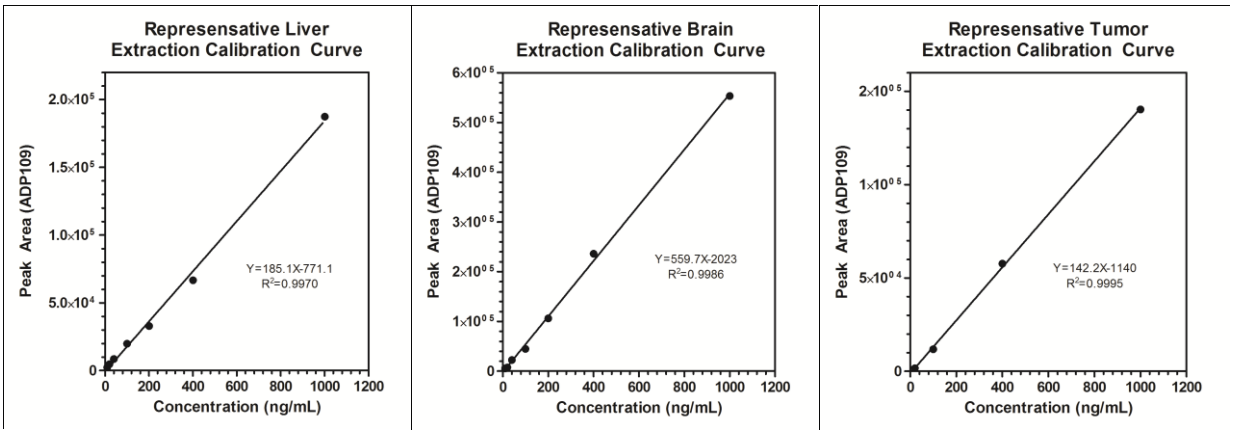

Figure 5. Representative standard curves of spiked tissue extractions to define linear range of the assay. Single run standard curves representative of all spiked whole blood samples are plotted.

Validation of Quantification Method

Sensitivity of the assay was determined by the limit of quantification (LOQ). While neat **ADP109** was detectable at 10 pg on-column. The complex matrix of whole blood resulted in an increase in baseline noise, pushing the limit of quantification to 100 pg on column in order to ensure a clear delineation between noise and analyte of interest. The LOQ of current assay was determined to be 100 pg on column.

Linearity was measured over 7 concentrations from 10 ng/mL to 1000 ng/mL (at 10 μL injection volume) with correlation coefficients (r^2) at 0.99 or higher for **ADP109** (**Figure 3, 5**).

Table 2. Intraday and interday accuracy of assay to detect **ADP109** demonstrated with three representative low, medium and high concentrations on the calibration curve.

	Intraday (n=2)			**Interday (n=2)**		
Concentration (ng/mL)	10	100	1000	10	100	1000
Average	10.1	99.8	999.1	11.0	100.3	996.4
Accuracy %	101.3%	99.8%	99.9%	110.4%	100.3%	99.6%

Table 3. Intraday accuracy and precision for assay validation on QC samples at indicated concentrations.

	Intraday (n=3)	
Concentration (ng/mL)	50	800
Average	59.9	884.4
SD	1.1	37.5
Accuracy %	120%	111%
% CV	1.86%	4.24%

Discussion

While the detection of natural product artemsinin and simple derivatives of artemisinin, such as artesunate and dihydroartemisinin, have been developed and utilized in clinical settings, there lacks a quantification method for the class of more potent artemisinin dimer derivatives. A reliable analytical method for quantifying C10-linked artemisinin dimer derivatives from whole blood will facilitate the development of this class of more potent compounds clinically for treatment of malaria and cancer.

In 2011, Lindegardh et al reported a robust sample preparation and quantification method for artemisinin derivatives that overcomes the endoperoxide degradation problem when red blood cells are lysed in whole blood[13]. We adapted the use of strong oxidizing reagent, potassium dichromate, in converting the highly reactive ferrous (Fe^{2+}) ion into ferric (Fe^{3+}) ion that is much less reactive toward the endoperoxide bridge. The sample preparation and LC-MS/MS method developed here is the first report of quantification of artemisinin dimers, specifically lipid-bound artemsinin dimer derivatives, from whole blood. In our method, the inclusion of oxidizing reagent in addition to mixed cationic solid phase extraction in our protocol afforded decent recovery efficiencies. A chelating reagent may have helped to further improve stability of the endoperoxide in hemolyzed blood, as reported in Lindegardh's paper[13]. However, we infer from trial experiments that the neutral or basic condition required for chelating of ferric ion results in loss of charge on **ADP109**, thus a compromised recovery efficiency overall.

Optimization was carried out for sample preparation method in order to consistently achieve desire recovery efficiency prior to solid phase extraction. The ADP compounds contain a weak base, N-pyridylmethylpiperazine, which allows binding and separation on the mixed-cationic exchange cartridge at acidic pH. While at pH 4, ADP compounds show significantly enhanced

aqueous solubility, we found that lowering the pH further to pH 1 afforded even higher recovery post solid phase cartridge. The pKa values for N,N'-dimethylpiperazine are 8.38 and 3.81[19], and that of 3-methylpyridine is 5.63[20]. Thus, the ADP compounds were likely triply protonated at pH 1, which ionic strength of the sample mixture was key to both cleaner separation of **ADP109** from whole blood matrix and higher recovery efficiency. Comparing 0.01N HCl (pH 2) and 1% acetic acid (pH 3), the latter case resulted in twice the amount of recovered sample as the former. This phenomenon may be explained by reduced non-specific binding of matrix components to the SPE resin and so higher retention of the compounds of interest.

The LCMS method developed and validated in this report can be applied to a number of other tissues such as solid tumor, tumor-infiltrated lymph node, liver, kidney and brain. Albeit, a simple liquid-liquid extraction of tissue homogenate under alkaline pH with dichloromethane may suffice for tissues were heme-content is low. The lack of high concentrations of reactive heme in the tissue samples means that we do not have to subject the samples to numerous steps of work-up and so the chance of losing material is diminished, giving higher overall yield. While the specificity of the liquid-liquid extraction may be lower, it is much simpler to conduct and the LCMS runs did not show interferences within the linear range defined.

ART-dimer derivatives represent an attractive class of medicinally important compounds because of their high potency and relative safety demonstrated on cell lines and animal models[1]. The novel sample preparation and LCMS quantification method described here lay the foundation for more detailed understanding of the drug and drug-lipid particle behaviors *in vivo* and further development of ART-dimer based chemotherapy.

Experimental Section

Materials

ADP109, **ADP107** and **ADP109**-Lipid nanoparticles were synthesized according to previous publications[5, 6]. Acetonitrile (ACN), water, methanol (MeOH) and trifluoroacetic acid (TFA), all Optima® LC/MS grade and dichloromethane (DCM, analytical grade) were purchased from Fisher Scientific (Pittsburgh, PA). Formic acid Certified ACS grade was obtained from Fischer Scientific (Pittsburgh, PA). Hydrochloric acid (HCl, AR, 36.5-38%) was purchased from Mallinckrodt Chemicals (St. Louis, MO), perchloric acid ($HClO_4$, AR, 70%) and ammonium hydroxide (NH_4OH, Baker Analyzed, 30%) were from J.T.Baker (Center Valley, PA). Rat whole blood (with K_3EDTA) was bought from Lampire Biological Laboratories Inc. (Pipersville, PA). Potassium hydroxide (KOH) and potassium dichromate ($K_2Cr_2O_7$) were purchased from J.T.Baker (Center Valley, PA). Chromatograms were processed with MassLynx V4.1 (Waters Informatics Laboratory), and standard curves were graphed using GraphPad Prism 5.0.

Chromatographic and Mass Spectrometry Conditions

Quantification analysis was carried out using Waters Premier XE UPLC – tandem mass spectrometer. a Waters ACQUITY UPLC BEH phenyl column (2.1 X 50 mm, 1.7 μm, Milford, MA) was used as solid phase for chromatographic separation with a gradient mobile phase composed 30% to 100% acetonitrile (ACN) in water, with water containing 0.05% trifluoroacetic acid, over a 4-minute run. Each injection contained 10 μL volume.

Multiple-reaction-monitoring (MRM) mode for positive ions was used to detect analytes. Parent compound was fragmented into daughter ions to afford additional selectivity beyond separation on column. For ADP109: m/z 782.4 → 190.1, and for internal standard ADP107: m/z 768.4 >

121.1, were monitored. The detector parameters were as follows: cone voltage 55 V, capillary voltage 3.50 kV, desolvation temperature 350°C, desolvation gas flow 800 (L/hr), Collision voltage 35.

Preparation of Standard and Quality Control Samples, Preparation of Biological Samples

Conventional methods such as protein precipitation (PP) with acetonitrile and various liquid-liquid extractions (LLE) with organic solvents under denaturing conditions were first tried, to extract **ADP109** from plasma or whole blood. For protein precipitation, 100 μL of spiked plasma or whole blood was crashed with 380 μL of cold ACN, vortexed for 15 minutes and centrifuged at $14X10^3$ rpm for 5 minutes before the supernatant was removed for LCMS analysis. For liquid-liquid extractions, several different methods were tried (**Table 2**). Simple LLE was performed by vortex mixing of 100 μL of spiked plasma or whole blood with 380 μL of cold dichloromethane (DCM) for 15 minutes, followed by centrifugation at $14X10^3$ rpm for 5 minutes. The organic layer was removed, dried and reconstituted in 1:1 ACN:water for analysis. A more complex LLE involved first denaturing 100 μL of spiked biological sample with 100 μL of perchloric acid ($HClO_4$) by vortexing for 15 minutes and centrifugation at $14X10^3$ rpm for 5 minutes. The supernatant of acid-treated sample was removed to a new microcentrifuge tube, to which 300 μL of 4M KOH was added followed by 1.0 mL of DCM or 10% methanol in DCM. The mixture was vortex for 15 minutes, centrifuged at $14X10^3$ rpm for 5 minutes. The organic layer was removed and the aqueous layer was extracted a second time under the same conditions. The organic layers were combined, tried under nitrogen in a 40°C water bath and reconstituted in 1:1 ACN:water for LCMS analysis.

After multiple optimizations the procedure that consistently allows for high recovery efficiencies from whole blood is as follows. Blood samples were prepared using solid phase extraction

method. 40 μL of the whole blood were spiked with 10 μL of **ADP109**-LNP of appropriate concentration and placed in a microcentrifuge tube with 10 μL of 0.4M potassium dichromate ($K_2Cr_2O_7$) and frozen at -80°C for at least 24hrs before sample workup. Frozen blood samples were thawed and kept on ice throughout workup preparation. 10 μL of internal standard (IS: **ADP107** at 10 μg/mL in ACN) were mixed with the blood samples, followed by addition of 100 μL methanol, vortex until well mixed and left on ice for 1 minute. 830 μL of 0.1M aqueous hydrochloric acid (HCl) were added to the mixture, vortexed, and centrifuged at $13.2X10^3$ rpm for 1 minute at room temperature. Supernatant of the sample were loaded onto a preconditioned mixed cationic exchange solid phase extraction (SPE) cartridge (Waters Oasis® MCX-SPE cartridge, Milford, MA). SPE procedures were as follows: the cartridges were conditioned with 1 mL MeOH followed by 1 mL 0.1N HCl before supernatant was loaded; the sample was washed with 1 mL deionized water (DI H_2O), then 2 mL of 50% MeOH in 0.48M aqueous formic acid (2.2% by mass), dried, and eluted with 100 μL 30% aqueous ammonium hydroxide followed by 900 μL 6:4 ACN:MeOH. The eluents were cooled on ice, centrifuged at $13.2X10^3$ rpm for 1.5 minute at room temperature before the supernatant were injected into LCMS for analysis.

Tissues collected from animal models: brain, liver, tumor infiltrated lymph nodes, and solid tumor, were homogenized at 1 gram of tissue per milliliter of 0.9% NaCl. 140 μL of tissue homogenate were aliquoted into 10 μL of IS, vortexed and kept on ice. 150 μL of 4N KOH were mixed with the homogenate sample, and extracted with 900 μL dichloromethane. The mixture was vortexed for 5 minutes, centrifuged at $1X10^4$ rpm for 5 minutes to collect the organic layer. The extraction process was repeated twice, dried under N_2 stream, and reconstituted in 500 μL of 30% $NH_4OH_{(aq)}$: ACN : MeOH (1:5.5:3.5).

Method Validation

Selectivity of the analytical method was studied by performing liquid-chromatography separation of the free compound **ADP109**, the internal standard **ADP107** independently and in combination. Extractions of **ADP109**-LNP spiked and blank whole blood were carried out to examine matrix effect in the monitored channels. Neat sample was prepared by first dilution with 50% of total volume of cold ACN, vortexed for 30 seconds, followed by addition of another 50% volume of water.

Linearity was defined over two orders of magnitude of concentration using 3 points ranging from 100 pg (10 ng/mL) to 10 ng (1000 ng/mL) on column.

Sensitivity of the assay was defined both in terms of lower limit of detection for neat compound and lower limit of quantification in case of blood-extracted sample. The limit of quantification was defined as the lowest concentration quantifiable on the standard curve in matrix based on an accuracy of 15%.

Accuracy of the assay was calculated as deviation of return value from theoretical value based on standard curve. Precision analysis of the standard curve was not reported due to only duplicate samples.

For standard curves, duplicate samples were run for intraday tests (n=2) and interday variation was studies with two set of samples from same stock run on two different days (n=2). Variation of less than 15% throughout the curve was accepted.

For quality control (QC) samples, independently diluted from the same **ADP109**-LNP stock, triplicate samples prepared independent were assayed (n=3). Accuracy was calculated using

intraday calibration curves and precision was reported as the coefficient of variance (%CV). Variation of up to 20% was accepted.

Recovery efficiency was estimated by comparing the peak area response (Equation 1) of **ADP109**-LNP from whole blood to that from neat sample of the same theoretical concentration at 100 ng/mL and 1000 ng/mL obtained from the same-day runs. Peak area vs. concentration standard curves with **ADP109**-LNP along were plotted to ensure linearity. Triplicate samples were prepared and efficiency (Equation 2) was reported as average ± S.D.

$$Peak\ Area\ Ratio = \frac{Peak\ Area\ (ADP109)}{Peak\ Area\ (ADP107)} \qquad \text{Equation 1}$$

$$Recovery\ Efficiency = \frac{Peak\ Area\ (whole\ blood)}{Peak\ Area\ Ratio\ (Neat)} \qquad \text{Equation 2}$$

Reproducibility of the assay was defined as the standard deviation of recovery efficiency calculated from three independently extracted samples. Value of less than 5% was acceptable.

Robustness was defined as the variation in recovery efficiency at two different concentrations, 100 ng/mL and 1000 ng/mL. Variation of up to 10% was accepted.

Reference

1. Lai, H. C.; Singh, N. P.; Sasaki, T., Development of artemisinin compounds for cancer treatment. *Investigational New Drugs* **2013,** *31* (1), 230-246.

2. Morris, C. A.; Duparc, S.; Borghini-Fuhrer, I.; Jung, D.; Shin, C. S.; Fleckenstein, L., Review of the clinical pharmacokinetics of artesunate and its active metabolite dihydroartemisinin following intravenous, intramuscular, oral or rectal administration. *Malaria Journal* **2011,** *10*, 17; Rath, K.; Taxis, K.; Walz, G.; Gleiter, C. H.; Li, S. M.; Heide, L., Pharmacokinetic study of artemisinin after oral intake of a traditional preparation of Artemisia annua L. (annual wormwood). *American Journal of Tropical Medicine and Hygiene* **2004,** *70* (2), 128-132.

3. Sun, W. C.; Han, J. X.; Yang, W. Y.; Deng, D. A.; Yue, X. F., Antitumor Activities of 4 Derivatives of Artemisic Acid and Artemisinin-B *in vitro*. *Acta Pharmacologica Sinica* **1992,** *13* (6), 541-543; Lai, H.; Singh, N. P., Selective Cancer Cell Cytotoxicity from Exposure to Dihydroartemisinin and Holotransferrin. *Cancer Letters* **1995,** *91* (1), 41-46; Woerdenbag, H. J.; Moskal, T. A.; Pras, N.; Malingre, T. M.; Elferaly, F. S.; Kampinga, H. H.; Konings, A. W. T., Cytotoxicity of Artemisinin-related Endoperoxides to Ehrlich Ascites Tumor-Cells. *Journal of Natural Products* **1993,** *56* (6), 849-856.

4. Posner, G. H.; Paik, I. H.; Sur, S.; McRiner, A. J.; Borstnik, K.; Xie, S. J.; Shapiro, T. A., Orally active, antimalarial, anticancer, artemisinin-derived trioxane dimers with high stability and efficacy. *Journal of Medicinal Chemistry* **2003,** *46* (6), 1060-1065; Singh, N. P.; Lai, H. C.; Park, J. S.; Gerhardt, T. E.; Kim, B. J.; Wang, S.; Sasaki, T., Effects of Artemisinin Dimers on Rat Breast Cancer Cells In Vitro and In Vivo. *Anticancer Research* **2011,** *31* (12), 4111-4114.

5. Zhang, Y. T. J.; Gallis, B.; Taya, M.; Wang, S. S.; Ho, R. J. Y.; Sasaki, T., pH-Responsive Artemisinin Derivatives and Lipid Nanoparticle Formulations Inhibit Growth of Breast Cancer Cells In Vitro and Induce Down-Regulation of HER Family Members. *Plos One* **2013,** *8* (3).

6. Zhang, Y. J.; Zhan, X.; Wang, L.; Ho, R. J. Y.; Sasaki, T., pH-Responsive Artemisinin dimer in lipid nanoparticles are effective against human breast cancer in a xenograft model. *Journal of Pharmaceutical Sciences*, **2015**, in press.

7. Karbwang, J.; NaBangchang, K.; Molunto, P.; Banmairuroi, V.; Congpuong, K., Determination of artemether and its major metabolite, dihydroartemisinin, in plasma using high-performance liquid chromatography with electrochemical detection. *Journal of Chromatography B* **1997,** *690* (1-2), 259-265.

8. Batty, K. T.; Davis, T. M. E.; Thu, L. T. A.; Binh, T. Q.; Anh, T. K.; Ilett, K. F., Selective high-performance liquid chromatographic determination of artesunate and alpha- and beta-dihydroartemisinin in patients with falciparum malaria. *Journal of Chromatography B-Biomedical Applications* **1996,** *677* (2), 345-350.

9. Lindegardh, N.; Hanpithakpong, W.; Kamanikom, B.; Pattayaso, J.; Singhasivanon, P.; White, N. J.; Day, N. P. J., Quantification of dihydroartemisinin, artesunate and artemisinin in human blood: overcoming the technical challenge of protecting the peroxide bridge. *Bioanalysis* **2011,** *3* (14), 1613-1624.

10. Huang, J.; Gautam, N.; Bathena, S. P. R.; Roy, U.; McMillan, J.; Gendelman, H. E.; Alnouti, Y., UPLC-MS/MS quantification of nanoformulated ritonavir, indinavir, atazanavir, and efavirenz in mouse serum and tissues. *Journal of Chromatography B-Analytical Technologies in the Biomedical and Life Sciences* **2011,** *879* (23), 2332-2338.

11. Prabhakar, K.; Afzal, S. M.; Kumar, P. U.; Rajanna, A.; Kishan, V., Brain delivery of transferrin coupled indinavir submicron lipid emulsions-Pharmacokinetics and tissue distribution. *Colloids and Surfaces B-Biointerfaces* **2011,** *86* (2), 305-313.

CHAPTER 7

Synthesis of pH-Responsive Artemisinin Dimer BODIPY Derivatives; Bovine Serum Albumin-bound Particle Preparation and Evaluation of Efficacy on Xenograft Model

Part of the content of this Chapter was submitted for publication as an original research article.

The manuscript was authored by:

Shusheng Wang, Yitong J. Zhang, Austin Le, Tomikazu Sasaki*

Department of Chemistry
University of Washington, Seattle, WA, 98195-1700, USA

Abstract

A fluorescence dye, BODIPY is used as the template for assembly of a novel class of artemisinin dimers (ART dimer BODIPY). The rigid BODIPY core is able to position two artemisinin groups in a well-defined geometry and the ART dimer BODIPYs show intense fluorescence enabling tracking of the molecules. In this chapter, synthesis of a number of ART dimer BODIPYs that possess polar side chains to enhance aqueous solubility is described. Hydrophobic ART dimer BODIPYs show potent cytotoxic activities when tested against two breast cancer cell lines, BT474 and MDA-MB-231. The IC_{50} values changed two orders of magnitudes when the structure of the aryl group at the *meso-position* was varied. Highest cytotoxic activity was observed when nitrogen-containing heterocycles were attached to the *meso*-position. For *in vivo* delivery of the most potent candidate ART dimer BODIPY derivative, ABPM, drug-bound bovine serum albumin (BSA) nanoparticles were prepared. The ABPM-BSA nanoparticles were shown to be effective in suppressing solid tumor growth in mice BT474 xenograft model.

Introduction

Artemisinin is a sesquiterpene lactone isolated from *Artemisia annua* L. in 1970's. Artemisinin contains an endoperoxide bridge that connects two quaternary carbons in the fused tricyclic core (**Figure. 1A**)[1]. Artemisinin (ART) and its derivatives, such as dihydroartemisinin (DHA), artemether, and sodium artesunate are widely used in human as the first-line antimalarial drugs, and have shown excellent safety profiles[2]. In addition to anti-malarial activity, artemisinin shows moderate cytotoxicity against cultured cancer cells. The cytotoxicity of ART is enhanced in the presence of iron salts or holotransferrin in the culture medium[3]. The reductive cleavage of the endoperoxide bond and subsequent generation of toxic radical species are believed to be responsible for the iron-dependent cytotoxicity of ART. Once activated, ART alkylates amino acid side chains such as Cys, Lys and His[4, 5]. The Heme group is also alkylated at the meso-position when incubated with the endoperoxide-containing sesquiterpene lactone[6]. Identity of the initial cellular target(s) of artemisinin is still a subject of active research although both the endoplasmic reticulum (ER) and mitochondria have been suggested to be the location where the natural product is activated[4, 7].

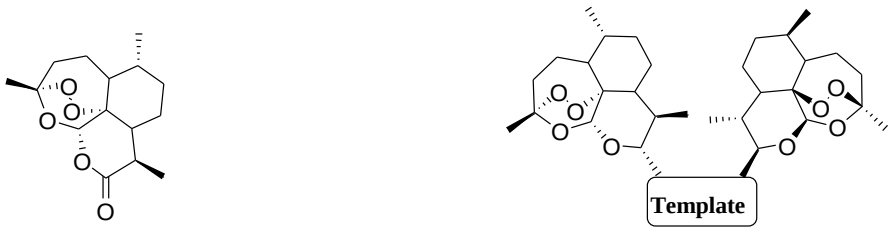

Figure 1. Structures of A) artemisinin, and B) artemisinin dimer.

Various analogs of ART have been synthesized, and some showed significantly higher cytotoxicity compared to the parent compound[8]. Among them, covalent dimers of artemisinin

(**Figure 1B**) show orders of magnitude higher activities than the natural product, and are an attractive class of compounds for further development as potential anti-cancer drug candidates[4, 9]. Specially, the class of highly potent C-10 carbon ART dimers cannot generate DHA by hydrolysis or metabolism. DHA has been linked to neurotoxicity that is observed in animal studies of some ART derivatives[10]. These promising results encouraged us to design a new series of C-10 Artemisinin dimers to explore their anticancer activity[11, 12].

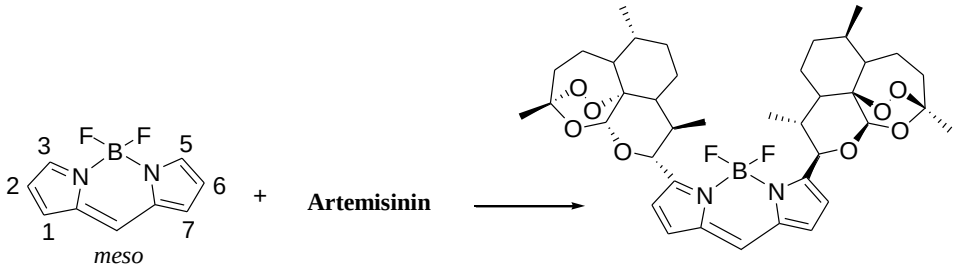

BODIPY core **ART dimer BODIPY**

Figure 2. Artemisinin dimers assembled on a BODIPY core (ART dimer BODIPY).

The C10 ART dimers reported in literature have flexible linkers covalently bonding the two pharmacophores, allowing the ART moieties to flop around and adopt the most favorable conformation depending on the immediate environment[11, 13]. However, few have reported a rigid linker that forces the two ART groups to be in fixed distance and conformation in ART dimer derivatives. 4, 4-Difluoro-4-bora-3a, 4a-diaza-s-indacene (BODIPY or difluoroboron dipyrromethane (**Figure 2**) is a class of highly fluorescent molecules widely used in bimolecular labeling[14]. The advantage of BODIPY is its amenability to structural modifications at the 3 and 5 positions. In addition, BODIPY dyes possess excellent photochemical properties such as prolonged photostability and high fluorescent quantum yield[15] that allow us to rack the molecule with fluorescence imaging after delivery. Furthermore, the dye is known for its biocompatibility

and relative stability under physiological conditions[14]. Thus, we speculated that BODIPY would serve as an attractive structural template for the assembly of new Artemisinin dimers.

As shown in **Figure 2**, ART dimer BODIPY derivatives are rigid and bulky compounds that possess highly hydrophobic moieties. ART dimer BODIPY derivatives are essentially insoluble in water. In drug development, hydrophobic drugs are often formulated with lipid, protein or polymers to enhance as a single phase suspension of drugs without need of organic solvents. One well-known example is the albumin-bound paclitaxel particle, Abraxane®, which was recently approved by the FDA. Thus, in development of the class of ART dimer BODIPY compounds for pre-clinical studies, we draw inspiration from Abraxane®[16, 17]. Serum albumin is the most abundant protein in blood and often serves as a hub for binding and transporting hydrophobic small molecules in the blood stream[18, 19]. From the success of Abraxane®, we infer that this versatile protein will also be able to deliver ART dimer BODIPY to biological systems without need of toxic organic solvents.

This chapter is adapted from a co-authored manuscript describing the design, synthesis and photochemical characterization of a number of ART dimers based on BODIPY core as an assembly template. Here, the synthesis focuses on a number of ART dimer BODIPY derivatives with polar side chains in attempt to increase aqueous solubility. We also demonstrate their cytotoxic activities against breast cancer cells both in vitro and in mice BT474 xenograft model using serum albumin nanoparticles of the most potent derivative.

Results and Discussion

Synthesis of ART dimer BODIPY Structural Motif

Scheme 1 illustrates the preparation of ART dimer BODIPYs starting from artemisinin α C10 pyrrole **1**, **1a** was synthesized in one step from dihydroartemisinin (DHA) by following the published procedure[20]. The ^{1}H NMR spectroscopy signal of H10 appears as a doublet at 4.49 ppm with a $J_{H10\text{-}H9}$ value of 10.8 Hz (NMR spectra see Chapter 9). This is indicative of a trans-trans diaxial relationship, giving artemisinin α C10 pyrrole as the product of reaction[20].

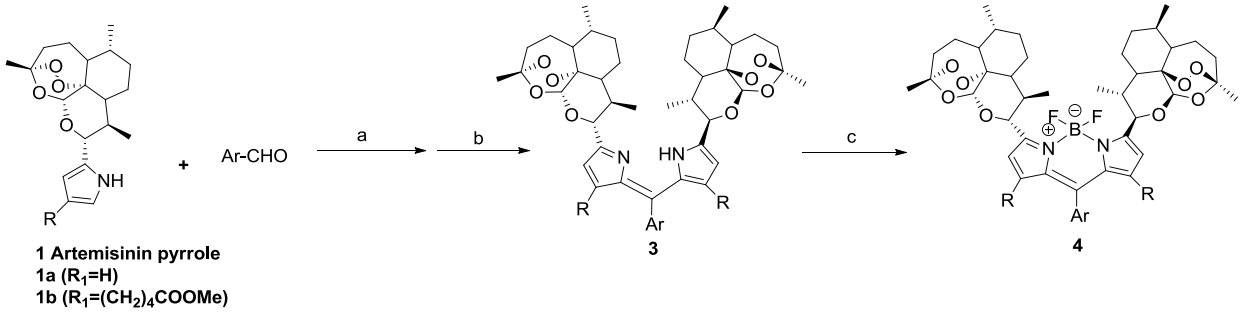

Scheme 1. Synthesis of ART dimer BODIPY **4a-c**. Reagents and conditions: (a) TFA, anhydrous DCM, rt; (b) DDQ, DCM, 30min, rt; (c) Boron trifluoride diethyl etherate, triethylamine, anhydrous DCM or anhydrous toluene, 0°C.

ART dimer BODIPYs with unsubstituted pyrrole and polar *meso* position side chains were prepared according to the published procedure of BODIPY synthesis[14]. Aryl aldehyde **2a** and **2b** were prepared via nucleophilic aromatic substitution on *para*-fluorobenzaldehyde (**Scheme 2**). Artemisinin α pyrrole **1a** was reacted with two different aryl aldehydes in the presence of 2 equivalence of trifluoroaceitic acid in dichloromethane followed by oxidation with 2, 3-Dichloro-5, 6-dicyano-1, 4-benzoquinone (DDQ) to give dipyrromethenes **3a** and **3b** in 19.4% and 10.5% yield respectively. Finally, the dipyrromethenes were coupled to boron trifluoride to afford the final fluorescent ART dimer BODIPYs **4a** in 84.2% and **4b** in 92% yield (**Figure 4**).

As a negative control, BODIPYs with identical meso position substitutions but no ART attachment **5a** and **5b** were prepared with the same procedure.

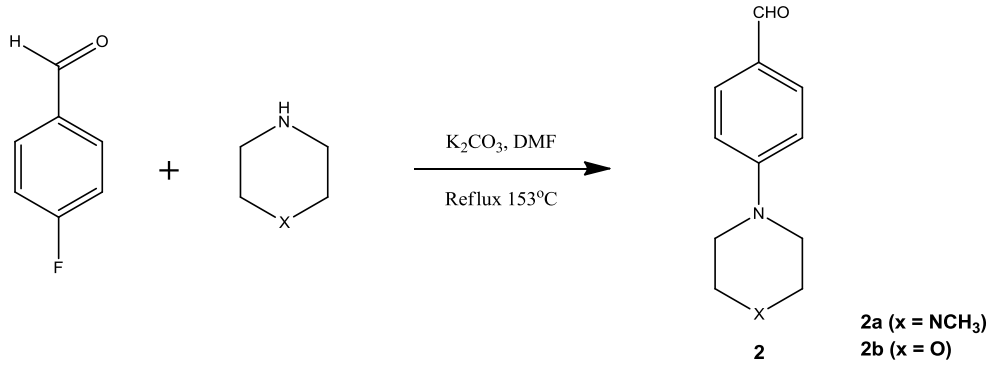

Scheme 2. Synthetic scheme for preparation of para-heterocycle substituted benzaldehydes **2a** and **2b**.

For installing polar side chains on the pyrrole, triisoproprylsilyl-protected pyrrole was used as the starting material, activated with n-bromosuccinimide, chain extended via lithium coupled halide exchange and finally converted to a carboxylic acid with Grignard Reaction. In the preparation of 2-ART-4-pentylcarboxy-pyrrole, **1b**, we protected the free carboxylic acid with methyl ester to prevent undesired reactivity due to active functional groups. The ART pyrrole **1b** was obtained in 6.8% yield in 7 steps (**Scheme 3**).

Next, ART pentylcarboxypyrrole **1b** was reacted with *p*-pyridylaldehyde to afford compound **3c**, followed by boron coupling to give **4c** in 35.6% overall yield. Due to the instability of the BODIPY core in presence of strong base, the methyl ester was then hydrolyzed with 10% (wt/v) hydrochloric acid to give ART dimer BODIPY **4d** with pentylcarboxylic acid side chains on the two pyrrole rings with complete conversion of the starting material. Compounds **4a-d** showed fluorescence when excited with long wavelengths UV light (**Figure 3**).

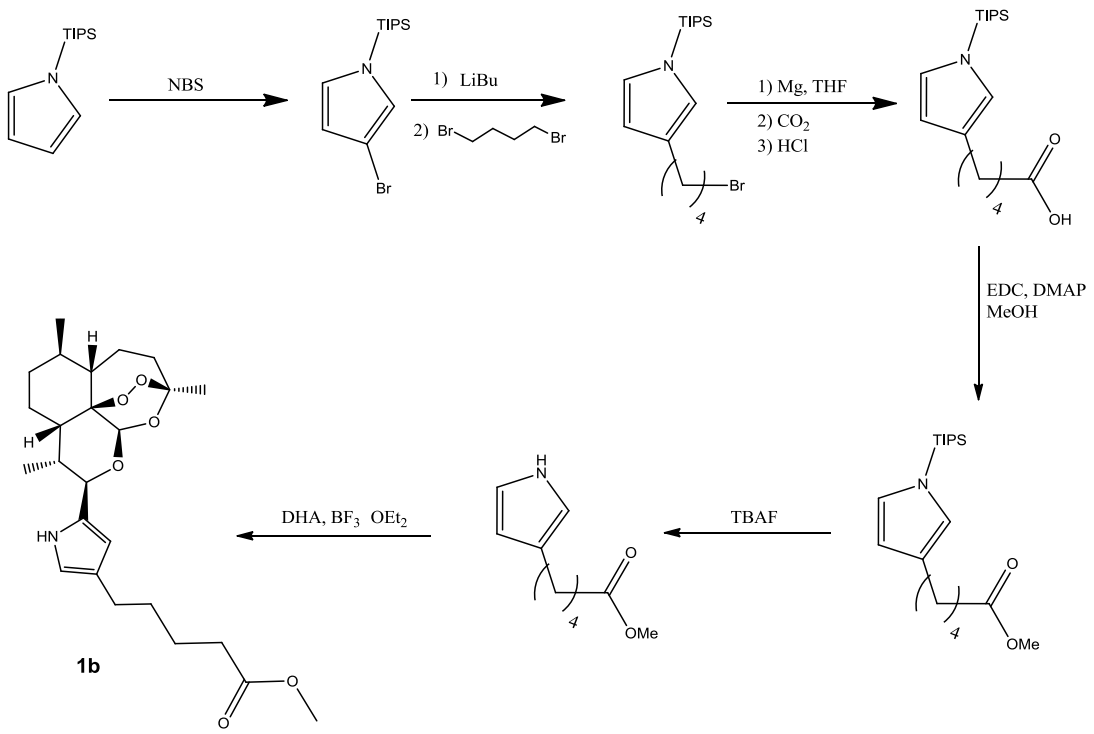

Scheme 3. Synthetic Scheme of Artemisinin pyrrole with polar side chains on pyrrole ring, compound **1b**.

Anti-proliferative Activity of ART dimer BODIPY on Human Breast Cancer Cell Lines

The Anti-proliferative activities ART dimer BODIPYs **4a-d**, as well as control compounds **5a** and **5b** were evaluated with the MTT assay on BT474 (HER^{2+}) and MDA-MB-231 (triple negative) human breast cancer cell lines. The IC_{50} values are summarized in **Table 1.** With BT474 cell line, all ART dimer BODIPYs **4a-d** showed significantly higher cytotoxicity compared to artemisinin pyrroles (IC_{50} = 86 ±13 μM). The cytotoxicity was strongly dependent on nature of the substituents at the *meso*-position of these ART dimer BODIPY derivatives. Nitrogen heterocycles at *meso*-position offer the highest potency with the most potent compound, **ABPM** (**Figure 4**), containing a pyrimidine ring at the *meso-position*, showed an IC_{50} value of 10 nM on BT474 cells. The MDA-MB-231 cells were less sensitive to the ART dimer BODIPY

derivatives compared to BT474 cells. The increased hydrophilicity of the ART dimer BODIPY resulted in compromised toxicity, likely due to the compound's decreased ability to cross membrane. BODIPY cores **5a** and **5b** were completely inactive against both cell lines.

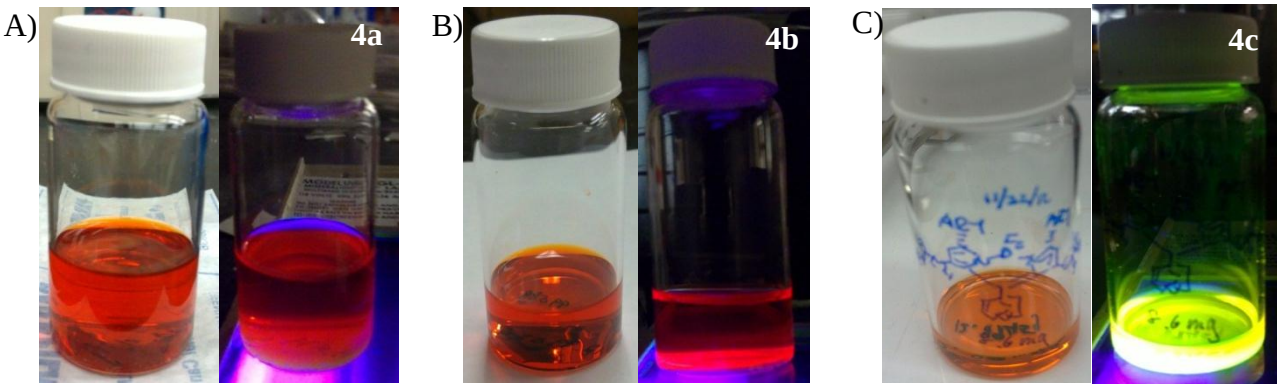

Figure 3. Photo of color and fluorescence behavior of ART dimer BODIPYs A) **4a**, B) **4b** and C) **4c** under natural light and UV lamp with wavelength of 366 nm.

Table 1. Cell cytotoxicity of ART dimer BODIPYs tested with MTT assay on BT474 human breast cancer cells with 48 hour incubation. Media contain 1% DMSO and 10% FBS. Values reported as average ± standard deviations of three independent experiments with each experiment run as triplicates.

Compound	BT474 IC_{50} (nM)
4a	Not Soluble
4b	Partially Soluble, 37 (±29)
4c	36 (±18)
4d	2250 (±1320)
ABPM	10 (±2.3)
ABPM-BSA NP	9 (±2.6)

Preparation of ART-BODIPY-Pyrimidine (ABPM) Albumin Nanoparticle

Of the class of ART dimer BODIPY, the derivative with *meso*-pyrimidine (**ABPM**), was selected as the lead compound for further development due to its high potency against the human breast cancer cell lines along with a high quantum yield (**Figure 4**). We formulated **ABPM** for *in vivo* studies in albumin-based nanoparticles. A similar formulation is used for commercialized product, Abraxane®[16, 19], where the insoluble paclitaxel is bound to the serum albumins in a drug-protein aggregate. When the albumin-based particles are injected and diluted in blood stream, the drug-protein aggregates fall apart and albumin-bound paclitaxel compounds behave in a similar way as traditional free-compound injections. In this study, bovine serum albumin was used as the delivery vehicle to suspend the hydrophobic compound.

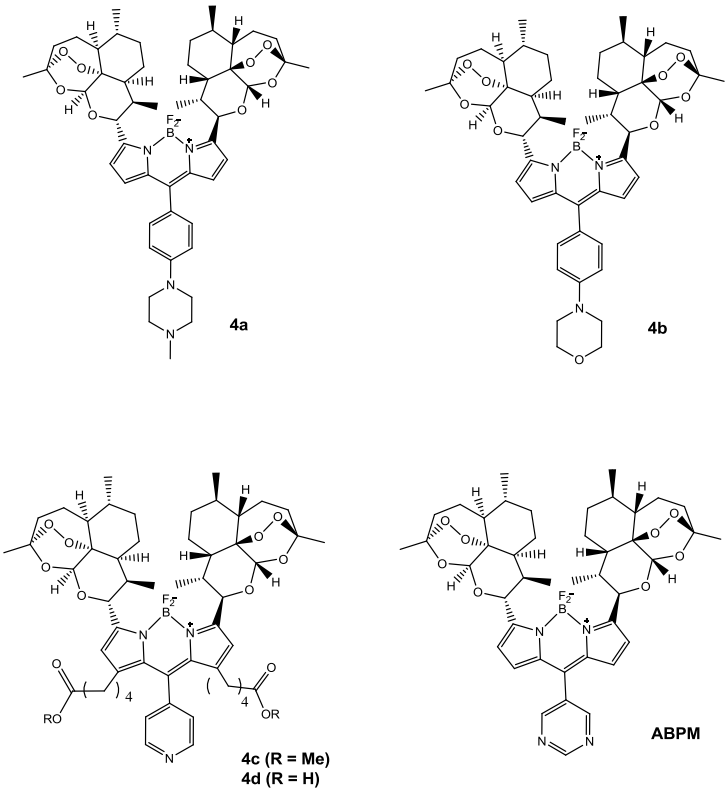

Figure 4. Chemical structures of ART dimer BODIPYs with polar side chains **4a-d**, and the most potent ART dimer BODIPY, **ABPM**, used for preparation of albumin-bound nanoparticles.

A number of different methods have been reported to prepare the protein aggregates[21]. In developing a preparation method for the albumin-bound **ABPM** protein aggregates with an average size of ~100 nm, we tried three different size reduction and drug-loading procedures (**Table 2**). After initial mixture of **ABPM**, dissolved in 1:9 EtOH:$CHCl_3$, a microemulsion was created by either vigorous vortex for 30 seconds, bath sonication for 30 seconds or 5 minutes. The organic solvents were then removed from the mixture by either rotary evaporation under reduced pressure or rapid stirring. It was found that 30 seconds vigorous vortexing after initial injection of organic solvents into the aqueous BSA solution followed by bath sonication for 5 minutes created a homogeneous microemulsion. The organic solvents were then evaporated to afford a translucent suspension after 4 hours of rapid stirring in a ventilated hood. After lyophilization and resuspension of the nanoparticle powder in 0.9% sodium chloride solution, the drug-protein aggregates showed relatively monodisperse population with average size of 80 (±10) nm and polydispersity index (PdI) ≈ 0.21 on dynamic light scattering measurements, where values less than 0.2 are acceptable as monodisperse populations.

With an preparation method developed, we next optimized the ABPM : BSA ratio to make microemulsions that will yield desirable size aggregates. To maximize the amount of hydrophobic drug loading, drug to BSA ratios were varied with fixed volumes of organic solvents in aqueous solution (**Table 2**). To ensure no denaturation of the protein, organic content was kept below 10% of the total volume of the mixture. At 10% (wt/v) BSA content in solution, we were able to suspend a maximum of 4 mg/mL ABPM, at drug to albumin ration of 2:5, with no visible precipitates and nanoparticle average size around 100 nm.

The exact concentration of ABPM was quantified using UV absorbance and the concentration ABPM-BSA particles used for *in vivo* was determined to be 4.28 (±0.03) mg/mL. Nanoparticle

ABPM-BSA NP was also active against BT474 cells *in vitro* with IC50 value of 9.0 (±2.6) nM, comparable to that of the free compound dissolved in DMSO. Given the high potency of the compound *in vitro*, this formulation was used for animal testing.

Table 2. Summary of method development of ABPM-BSA NP preparation. Optimizations of emulsification methods and drug to albumin ratio were conducted. Particle size reported as number average calculated based on NICOMP algorithm measured over 4 minutes on Particle Sizing Systems 380ZLS. Peaks with intensity over 1% are reported.

Size reduction – Solvent Evaporation Method Optimization						
Method	Sonicate 30 sec - Stir	Sonicate 10 min - Rotorvap			**Vortex 30 sec, sonicate 5 min - Stir**	
Size (nm)	22.5	98			**83**	
Drug to Protein Ratio Optimization						
ABPM:BSA ratio	1 : 0.15*	1 : 0.3*	1 : 1.25*	1 : 1.5	**1 : 2.5**	1 : 15
Size (nm)	118, 337	161, 728	27, 892	61.2	**84**	10, 17

* Visible aggregates that precipitate out of solution were observed in these preparations.
Optimal method and drug to protein ratio for final preparation of the particles are **bolded** in table.

Effect of ABPM-BSA nanoparticles on Human Breast Cancer Mice Xenograft Model

To examine the effect of the **ABPM-BSA** nanoparticles *in vivo*, we employed athymic nude mice carrying HER^{2+} human breast cancer solid tumor, BT474, as a xenograft model. Mice models were dosed at maximum tolerated dose of 0.8 mg/kg every other day for 14 days intravenously (I.V.). Positive and negative controls used were 10 mg/kg paclitaxel every 4 days for 4 doses and Blank BSA particles prepared in the same way as **ABPM-BSA** particles without the ART dimer respectively, both I.V. The results show that while mice in all groups showed no significant variation in body weight. Both **ABPM-BSA NP** and paclitaxel were able to suppress tumor growth with tumor size measurements significantly smaller than those in the Blank BSA group (**Figure 4**). At 0.8 mg/kg dosing regime, **ABPM-BSA NP** was able to control BT474

growth in these mice xenograft models with similar efficacy as first-line chemotherapeutic, paclitaxel. The demonstrated effectiveness and safety of **ABPM-BSA** nanoparticles warrant further investigation and development using this class of innately fluorescent ART dimer derivatives.

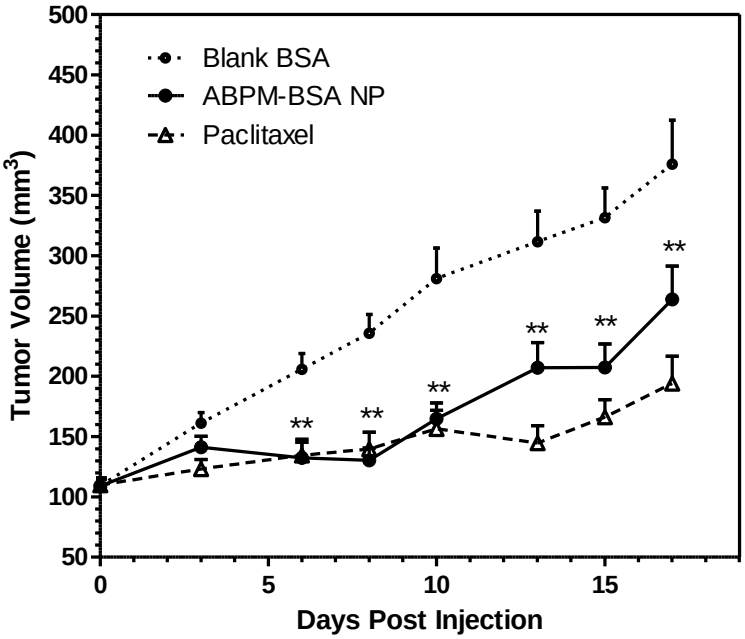

Figure 4. Average tumor volume in mice of **Blank BSA** (○) Control Group, **ABPM-BSA NP** (●) Test Group treated with 0.8 mg/kg I.V. (QOD X 14 days), and Paclitaxel (△) at 10 mg/kg I.V. (Q4 X 4) from Day 0 to Day 16. Day 0 is defined as 10 days after tumor implant. Values plotted as average with error bars as SEM of 15 animals in vehicle control and test groups and 13 animals in Paclitaxel group. Significant difference was defined by the *t*-test where $p < 0.05$: $^{**}p < 0.05$ between **Blank BSA** and **ABPM-BSA NP** groups. Paclitaxel group did not show significant difference compared with **BSA-ABPM NP** group.

Experimental Section

Material

Air-and moisture-sensitive reactions were carried out in oven-dried glassware sealed with rubber septa under a positive pressure of dry nitrogen. Similarly, air and moisture sensitive liquids and solutions were transferred via syringe. Anhydrous solvents were obtained from commercial sources. NMR spectra were measured on Bruker (300 MHz or 500 MHz) nuclear magnetic resonance spectrometers. Solvents are indicated in text. Mass spectra (MS) were measured by Bruker Esquire Ion Trap mass at chemistry department in University of Washington.

DMEM high glucose culture media, 0.25% Trypsin-EDTA solution, Dulbecco's phosphate buffered saline, 3-(4, 5-dimethylthiazol-2-yl)-2, 5-diphenyltetrazolium bromide (MTT) and Trypan blue (0.4%) solution were purchased from Sigma-Aldrich. Fetal bovine serum was obtained from Invitrogen Corp. Other chemicals and reagents for cell culture were obtained from Sigma-Aldrich. BT474 and MDA-MB-231 cells were obtained from the American Type Culture Collection (Manassas, VA).

Synthesis of ART-pyrrole Building Block

1a was prepared according to the published procedure[20].

1b: Artemisinin Pyrrole with methyl pentanoate side chain was prepared from N-TIPS-pyrrole in 7 steps as outlined in **Scheme 3**. 3g (13.4 mmol) of starting material pyrrole was brominated by reacting with 2.9 mg (16.1 mmol, 1.2 eq.) of N-bromoccucinamide in THF under inert N_2 atmosphere at -78°C for 2 hours. The reaction mixture was then warmed up to room temperature and stirred for another hour before quenched with addition of pyridine and side product precipitated with hexane and filtered through neutral alumina. The filtrate was concentrated on

rotary evaporator and the product was purified by flash chromatography using hexane as the mobile phase. The purified N-TIPS-3-bromo-pyrrole was obtained as a colorless oil.

In the next step, 0.95 g (3 mmol) of the previously functionalized pyrrole was added dropwisely into a solution of 2.5M nButyl lithium in hexane (2.52 mL, 6 mmol, 2 eq.) cooled to -78°C. The reaction was stirred for 30 minutes before 2.1 mL (18 mmol, 6 eq.) of 1,4-dibromobutane was added dropwisely into the reaction mixture and stirred at -78°C for another 30 minutes. The reaction was then warmed up to room temperature and let react for 2 hours before 5 mL of saturated $NaHCO_3$ was added dropwisely to quench the reaction. The mixture was extracted 3 times with DCM, the combined organic layers were concentrated and purified by flash chromatography with hexane to afford a colorless oil as the product (NMR shows contamination with 1,4-dibromobutane). ^{1}H NMR (300 MHz, $CDCl_3$) δ 6.69 (s, 1H), 6.52 (s, 1H), 6.14 (s, 1H), 2.62 – 2.42 (t, *J* = 6 Hz , 2H), 1.98 – 1.85 (m, 2H), 1.72 (d, *J* = 7.5 Hz, 2H), 1.48 – 1.31 (m, 2H), 1.08 (d, *J* = 7.4 Hz, 21H).

To functionalize the pyrrole with carboxylic acid, 1.0 g (2.8 mmol) of the product in the previous step was dissolved in 7 mL THF and added to a dried reflux apparatus containing 0.4 g of Mg turning and an I_2 crystal in 2.0 mL of THF at ~60°C, dropwisely. The reaction mixture was refluxed for 5 hours before cooled gradually down to room temperature, then 0°C. Dried CO_2 gas was bubbled into the reaction mixture as the mixture was warmed up to room temperature over 30 minutes to afford the carboxylate. The reaction was then quenched with 20 mL 0.5M HCl before extracted 3 times with DCM, concentrated and purified by flash column chromatography with 1:2 of ethyl acetate (EA) : hexane (H). It should be noted that the compound is heat sensitive and so should not be concentrated in a heated water bath. ^{1}H NMR (300 MHz, $CDCl_3$)

δ 6.69 (t, *J* = 2.3 Hz, 1H), 6.53 (s, 1H), 6.14 (d, *J* = 1.3 Hz, 1H), 2.51 (t, *J* = 6.9 Hz, 2H), 2.37 (dt, *J* = 7.5, 4.3 Hz, 2H), 1.70 – 1.56 (m, 2H), 1.40 (tt, *J* = 7.4, 5.3 Hz, 2H), 1.09 (d, *J* = 7.4 Hz, 21H).

Next the free acid was protected as a methyl ester. On a small scale, 16 mg (0.005 mmol) of the product from previous step and 3 mg (0.025 mmol, 5 eq.) of DMAP were dissolved in 0.5 mL of dry methanol. 8.5 mg (0.055 mmol, 11 eq.) of EDC was added to the solution and the reaction was stirred overnight at room temperature. The reaction mixture was filtered, concentrated, redissolved in 5 mL EA and extracted twice with 5 mL of water. The crude product was used directly for the next step, where TIPS protecting group was removed with reaction with 1 eq. of TBAF for 30 minutes at room temperature in THF. The deprotected pyrrole was purified by flash column chromatography using 1:3 EA:H to afford a colorless liquid as the product. ^{1}H NMR (300 MHz, $CDCl_3$) δ 6.64 (d, *J* = 26.0 Hz, 1H), 6.51 (s, 1H), 6.13 (s, 1H), 3.66 (s, 3H), 2.51 (d, *J* = 7.0 Hz, 2H), 2.32 (d, *J* = 7.2 Hz, 2H), 1.75 – 1.53 (m, 2H), 1.40 (dd, *J* = 14.8, 7.4 Hz, 2H), 1.08 (d, *J* = 7.3 Hz, 21H).

Finally, to couple artemisinin onto the pyrrole, 14 mg (0.05 mmol) and 10 μL (0.05 mmol) of the pyrrole from last step were dissolved in 1.0 mL DCM at -40°C. 8.2 μL (0.07 mmol, 1.3 eq.) of BF_3•OEt_2 was added slowly into the stirring solution, and let react for 1 hour. The reaction mixture was warmed up to -10-0°C and reacted for another 7 hours before quenched with 1 mL saturated $NaHCO_3$. The crude mixture was extracted 3 times with 2 mL DCM each, the combined organic layers were concentrated and purified by flash column chromatography with 3% EA in DCM to afford the final product as a white solid in 6.8% overall yield from N-TIPS-pyrrole starting material. ^{1}H NMR (300 MHz, $CDCl_3$) δ 8.25 (s, 1H), 6.51 (s, 1H), 5.87 (s, 1H), 5.37 (s, 1H), 4.41 (d, *J* = 10.6 Hz, 1H), 3.66 (s, 3H), 2.37 (dt, *J* = 14.2, 7.3 Hz, 6H including 2 m from ART), 2.10 – 0.58 (m, 21H).

*General Procedure for Synthesis of para heterocyclic substituted benzaldehydes **2a** and **2b***

To prepare the benzyaldehyde with *para*-substituted heterocyclic rings, *p*-fluorobenzaldehyde was reacted with N-methylpiperazine or morpholine via nucleophilic aromatic substitution. Specifically, *p*-fluorobenzaldehyde and the nucleophile were dissolved in dimethylformamide (DMF) with catalytic amount of potassium carbonate (K_2CO_3) and refluxed until complete consumption of starting material. The resulting product was purified via flash column chromatography to afford compounds **2a** and **2b**.

2a: 1.0 mL (9.3 mmol) of *p*-fluorobenzaldehyde and 2.5 mL (28 mmol, 3 eq.) of N-methylpiperazine were brought to reflux in 2 mL of DMF in presence of 0.77g (5.6 mmol, 0.6eq) of K_2CO_3 under N_2 atomosphere. The reaction mixture was kept under reflux overnight before cooled down to room temperature for work up. The reaction mixture was diluted with 25 mL of water and extracted twice with DCM. The combined organic layers were then extract 3 times with 20 mL of 0.1N Na_2CO_3, concentrated and purified by flash column chromatography with 1:1 EA:H containing 0.1% TEA. The purified product, a yellow solid, was prepared in 70.2% yield. ^{1}H NMR (500 MHz, $CDCl_3$) δ 9.78 (s, 1H), 7.75 (d, J = 8.9 Hz, 2H), 6.91 (d, J = 8.9 Hz, 2H), 3.56 – 3.37 (m, 4H), 2.71 – 2.51 (m, 4H), 2.35 (s, 3H).

2b: 1.0 mL (9.3 mmol) of *p*-fluorobenzaldehyde and 2.4 mL (28 mmol, 3 eq.) of morpholine were brought to reflux in 2mL of DMF in presence of 0.77g (5.6 mmol, 0.6 eq) of K_2CO_3 under N_2 atomosphere. The reaction mixture was kept under reflux overnight before cooled down to room temperature for work up. The reaction mixture was diluted with 25 mL of water and extracted twice with DCM. The combined organic layers were then extract 3 times with 20 mL of 0.1N Na_2CO_3, concentrated and purified by flash column chromatography with a gradient mobile phase from 1:3 EA:H to 2.5:1.5 EA:H, containing 0.1% TEA. The purified product, a

pale yellow solid, was prepared in 57.8% yield. ^{1}H NMR (300 MHz, $CDCl_3$) δ 9.71 (s, 1H), 7.72 – 7.67 (d, *J* = 8.9 Hz, 2H), 6.88 – 6.81 (d, *J* = 8.9 Hz, 2H), 3.80 – 3.74 (m, 4H), 3.29 – 3.23 (m, 4H).

*Synthesis of ART dimer dipyrromethanes **3a-c***

3a: Artemisinin pyrrole **1a** (84 mg, 0.25 mmol) was reacted with *p*-methylpiperazyl benzyaldehyde (27 mg, 0.125 mmol) and TFA (20 μL) as catalys in 3.0 mL dry DCM. The reaction was stirred for 30 minutes before 23 mg (0.125 mmol, 1 eq.) of DDQ was added and stirred for another 15 minutes. To quench the reaction, 0.2 g of anhydrous Na_2CO_3 was added to the reaction mixture and stirred briefly, the mixture was concentrated, redissolved in 10 mL EA with 5 mL 0.1N Na_2CO_3. The crude mixture was extracted twice with 10 mL EA and the product was purified on column with 5% methanol in EA with 0.1% TEA to afford product **3a** in 19.4% of yield as a red solid. ^{1}H NMR (300 MHz, Acetone) δ 7.45 (d, *J* = 7.6 Hz, 1H), 7.11 (d, *J* = 8.2 Hz, 1H), 6.61 (s, 1H), 6.47 (s, 1H), 5.49 (s, 1H), 4.72 (d, *J* = 10.7 Hz, 1H), 3.38 (d, *J* = 7.9 Hz, 2H), 2.62 (d, *J* = 21.9 Hz, 2H, including 1 multiplet from ART), 2.33 (s, 2.5H, including 1 multiplet from ART), 2.04 – 0.94 (m, 16.5H), 0.80 (d, *J* = 7.0 Hz, 3H).

3b: Artemisinin pyrrole **1a** (166.8 mg, 0.5 mmol) was reacted with *p*-morpholinyl benzyaldehyde (47.8 mg, 0.25 mmol) and TFA (3.3 μL) as catalys in 6 mL dry DCM. The reaction was stirred for 1 hour before 56.8 mg (0.25 mmol, 1 eq.) of DDQ was added and stirred for another 30 minutes. To quench the reaction, 5 mL of saturated $NaHCO_3$ was added to the reaction mixture and stirred briefly, the mixture was concentrated, redissolved in 10 mL EA with 5 mL Saturated $NaHCO_3$. The crude mixture was extracted 3 times with 10 mL EA and the product was purified on column with 10% EA in DCM with 0.1% TEA to afford product **3b** in

10.5% of yield as an orange solid. ^{1}H NMR (300 MHz, Acetone) δ 8.22 (d, *J* = 8.1 Hz, 1H), 7.88 (d, *J* = 7.5 Hz, 1H), 7.36 (s, 1H), 7.22 (s, 1H), 6.42 (s, 1H), 6.25 (s, 1H), 5.48 (d, *J* = 10.3 Hz, 1H), 4.62 (s, 2H), 4.08 (s, 2H), 3.62 (s, 5H), 3.21 (m, 2H, two types of protons), 2.77 – 1.48 (m, 25H).

3c: Artemisinin pyrrole **1b** (22.4 mg, 0.05 mmol, 2 eq.) was reacted with *p*-pyridylbenzaldehyde (2.3 μL, 0.025 mmol) and $ZnCl_2$ (25 μL, 1M in either, 0.025 mmol, 1 eq.) as catalyst in 2 mL of dry DCM. The reaction was stirred for overnight before addition of DDQ (5.7 mg, 0.025 mmol, 1 eq.). To quench the reaction, 1 mL of saturated $NaHCO_3$ was added to the reaction mixture and stirred briefly. The mixture was diluted with 5 mL EA and extracted 3 times with 5 mL EA and the crude product used for the synthesis of BODIPY core without further purification. ^{1}H NMR (500 MHz, $CDCl_3$) δ 8.71 (s, 1H), 7.34 (s, 1H), 6.18 (s, 1H), 5.37 (s, 1H), 4.54 (d, *J* = 10.6 Hz, 1H), 3.64 (s, 3H), 2.63 (s, 1H), 2.35 (s, 2H), 2.08 (m, 2H), 1.90 (s, 2H), 1.79 (d, *J* = 35.0 Hz, 3H), 1.68 – 0.69 (m, 33H).

*General Procedure for Synthesis of ART dimer BODIPYs **4a-c***

An anhydrous DCM solution of ART dimer dipyrromethanes **3a-c** was purged with nitrogen. To the solution was added 20 eq. of DIEA. The reaction solution was stirred at room temperature for 30 minutes before addition of 20 eq. of BF_3•OEt_2 dropwisely. The reaction was then stirred for an additional 30 minutes to overnight at room temperature before quenches with 5 mL of saturated $NaHCO_3$. The crude mixture was extracted twice with 5-10 mL EA, concentrated and purified by flash column chromatography to afford the desired products **4a-c**.

4a: ART dimer dipyrromethane **3a** (20 mg, 0.024 mmol) was coupled with BF_3•OEt_2 to afford **4a** as a purplish black solid in 84.2% chemical yield. Mobile phase for chromatography

purification was 10% methanol in EA with 0.1% TEA. ^{1}H NMR (300 MHz, $CDCl_3$) δ 7.45 (d, *J* = 7.4 Hz, 1H), 6.98 (d, *J* = 7.9 Hz, 1H), 6.92 (s, 1H), 6.77 (s, 1H), 5.49 (s, 1H), 5.13 (d, *J* = 11.6 Hz, 1H), 3.38 (s, 2H), 2.64 (s, 2H), 2.40 (s, 2.5H), 2.00 (s, 2H), 1.81 (d, *J* = 16.9 Hz, 3H), 1.78 – 0.65 (m, 27H).

4b: ART dimer dipyrromethane **3b** (22 mg, 0.026 mmol) was coupled with BF_3•OEt_2 to afford **4b** as a purplish black solid in 92% chemical yield. Mobile phase for chromatography purification was 5% EA in DCM with 0.1% TEA. ^{1}H NMR (300 MHz, $CDCl_3$) δ 7.37 (d, *J* = 7.4 Hz, 1H), 6.90 (d, *J* = 8.0 Hz, 1H), 6.82 (s, 1H), 6.67 (s, 1H), 5.39 (s, 1H), 5.04 (d, *J* = 10.7 Hz, 1H), 3.80 (s, 2H), 3.22 (s, 2H), 2.62 (s, 1H), 2.27 (d, *J* = 13.5 Hz, 2H), 2.16 – 1.03 (m, 25H), 0.90 (d, *J* = 5.1 Hz, 3H), 0.63 (d, *J* = 6.6 Hz, 3H).

4c: Crude ART dimer dipyrromethane **3c** (30 mg, ~0.03 mmol) was coupled with BF_3•OEt_2 to afford **4c** as a red solid in 35.6% chemical yield from ART pyrrole **1b**. Mobile phase for chromatography purification was 1:3 EA:DCM. ^{1}H NMR (500 MHz, $CDCl_3$) δ 8.80 (s, 1H), 7.33 (s, 1H), 6.53 (s, 1H), 5.46 (s, 1H), 5.10 (s, 1H), 3.65 (s, 3H), 2.67 (s, 1H), 2.38 (s, 2H), 2.15 (d, *J* = 5.9 Hz, 2H), 2.05 (s, 2H), 1.85 (s, 2H), 1.22-0.69 (m,33H).

*Synthesis of ART dimer BODIPY with free acid side chain **4d***

To synthesize the free acid side chains that may help increase aqueous solubility of the ART-dimer BODIPY derivatives, the methyl ester side chains of compound **4c** was hydrolyzed under acidic conditions to afford compound **4d**. 5 mg of compound 4c was dissolved in 0.4 mL dry THF, to which 250 μL of 3M HCl was added dropwisely. The reaction mixture was stirred for 3 days at room temperature before enough NaCl was added to condense out the aqueous layer. Crude product was extracted 3 times with DCM from saturated ammonium hydroxide solution

used to dilute the brine in reaction mixture. ^{1}H-NMR of the crude extracted sample showed pure compound with disappearance of the methyl ester peak. Yield was not calculated for this reaction. ^{1}H NMR (500 MHz, $CDCl_3$) δ 8.88 (s, 1H), 7.70 (s, 1H), 6.98 (s, 1H), 6.58 (s, 1H), 5.46 (s, 1H), 5.08 (d, *J* = 10.1 Hz, 1H), 5.01 (s, 1H), 3.25 – 2.85 (m, 6H), 2.72 (m, 1H), 2.37 (m, 2H), 2.12 (m, 2H), 1.91 (m, 4H), 1.69 – 0.63 (m, 35H).

*General Procedure for Synthesis of control BODIPY cores **5a** and **5b***

Following general procedure of Synthesis of ART dimer dipyrromethanes, 2,4-dimethylpyrrole (51.5 μL, 0.5 mmol, 2 eq.) was reacted with the respective benzaldehydes in DCM in presence of TFA, followed by oxidation with 1 eq. of DDQ to afford the dipyrrolmethenes. The condensation product was then coupled to 20 equivalent of boron trifluoride with 20 eq. of DIEA to give the final BODIPY core structure.

5a: 50.9 mg (0.25 mmol) of compound **2a** was reacted with 2,4-dimethylpyrrole in presence of 20 μL TFA for 20 minutes and oxidized to afford the corresponding dipyrromethene in 41.2% yield after purification with flash column chromatography using 10% methanol in EA with 0.1% TEA. The dipyrromethene was then coupled with BF_3•OEt_2 to afford **5a** as a red solid in 65.7% chemical yield. Mobile phase for chromatography purification was 1:2 EA:H with 0.1% TEA. ^{1}H NMR (300 MHz, $CDCl_3$) δ 7.23 – 6.77 (m, 4H), 5.69 (s, 1H), 5.35 (s, 1H), 3.20 (s, 4H), 2.58 (s, 4H), 2.35 (s, 3H), 2.14 (s, 6H), 1.82 (s, 6H).

5b: 47.9 mg (0.25 mmol) of compound **2b** was reacted with 2,4-dimethylpyrrole in presence of 1 μL TFA for 15 minutes and oxidized to afford the corresponding dipyrromethene in 13.2% yield after purification with flash column chromatography using 7% EA in DCM with 0.1% TEA. The dipyrromethene was then coupled with BF_3•OEt_2 to afford **5b** as a red solid in 55.7% chemical

yield. Mobile phase for chromatography purification was 5% EA in DCM with 0.1% TEA. ^{1}H NMR (300 MHz, $CDCl_3$) δ 7.21-6.84 (m, 4H), 5.70 (s, 1H), 5.36 (s, 1H), 3.86 (s, 4H), 3.15 (s, 4H), 2.15 (s, 6H), 1.82 (s, 6H).

Cell culture and MTT assay

BT474 cell and MDA-MB-231 cell were maintained in DMEM media supplemented with 10% v/v FBS. On reaching confluency (1×10^6 cells/ ml in a 25 mL flask), 1×10^6 cells were seeded in 25mL of fresh supplemented media. The cells were incubated under humidified air containing 5% CO_2 at 37 °C. Cell density was kept below 1×10^6 cells/ml to ensure exponential growth and to avoid differentiation. Cells were only used between passages 5 and 15 to prevent cell differentiation. Cell viability was above 95% for all experiments. The viable cell count was based on trypan blue exclusion from the cells and was performed in a hemocytometer using a light microscope. During experiments cells were exposed to drug stock solutions which were made up in 100% DMSO and the final solvent concentration was 1% v/v in each incubation. Each concentration in every experiment was carried out in triplicate.

BT474 (2000 cells/100 μl) or MDA-MB-231 cells (7500 cells/100 μl) were seeded on a 96 wells plate respectively, and incubated at 37 °C. After 24 h, the medium was removed. Serial dilutions of Artemisinin dimers and monomer stock solutions at 10 mM in DMSO will be made to 9 appropriate concentrations ranging from 10 nM to 100 μM in complete medium with 1% DMSO for BT474, respectively, and ranging from 100 nM to 100 μM for MDA-MB-231. 200 μL of the complete medium containing artemisinin derivatives was added every well, and every concentration of ART dimer BODIPY was set three parallels. The complete medium with 1% DMSO was used as negative control and positive control employed 100 μM ART dimer succinate. The cells were incubated for 48 h at 37 °C, the medium was removed, and replaced it

with 100 μL of fresh complete medium. 10 μL of 12 μM MTT stock solution (D-Hanks) was added to each well. After incubating for 3 h at 37 °C, Formosan crystals were solubilized in 50 uL of DMSO and absorbance was measured at 570 nm with BIO-RAD model 680 microplate reader. Dose response curves were plotted and IC_{50} values were determined with Graphpad Prism 5.

Preparation of ART-BODIPY-Pyrimidine (ABPM) Albumin Nanoparticles

To prepare ABPM-BSA nanoparticles, bovine serum albumin (Fraction V, Sigma Aldrich, St. Louis, MO) was suspended in injection grade sterile water (Baxter Healthcare Corporation, Deerfield, IL) at 1% (wt/v) and filtered through 0.2 μm cellulose acetate membrane (VWR International, Radnor, PA) to sterilize. **ABPM** stock was prepared by dissolving **ABPM** in 1:9 ethanol : chloroform at 40 mg/mL. In a screw-cap glass vial was added appropriate amount of BSA suspension and ABPM solution was injected into the aqueous suspension under gentle vortex with organic solvent volume not exceeding 10%. For instance, 500 μL of ABPM solution was added to 5 mL of BSA suspension in a 20 mL vial.

The mixture was then vortexed vigorously for 30 seconds and sonicated in a bath sonicator for 5 minutes at room temperature. The combination of vortex and sonication was repeated three times to give a homogenous emulsion. Organic solvents in the emulsion were evaporated in a fume hood under strong stirring at room temperature for 4 hours followed by lyophilization to remove all liquid. The particle powder was resuspended in sterile 0.9% sodium chloride solution for characterization and other assays. Precautions were taken to keep the process relatively sterile and blood agar culture was used to verify sterility of the samples.

Size of the resuspended particles was determined by dynamic light scattering (DLS) on a NICOMP^{TM} 380ZLS (90°scattering, Particle Sizing Systems, Santa Babara, CA). Exact concentration of the ABPM-BSA NP was determined by UV measurement. For sample preparation, 65 μL of particle suspension was crashed with 585 μL cold acetonitrile, vortexed for 30 seconds and centrifuged for 3 minutes at 14,000 rpm (Microfuge® 18 Centrifuge, Beckman Coulter, Indianapolis, IN). Supernatant of the centrifuged sample was taken for UV absorbance measurement at 495 nm on Victor^{2}D spectrometer (Perkin Elmer, Waltham, MA). Standard curves of ABPM were prepared with the same procedure using blank BSA extracted supernatant for dilution. Linear range was determined between 0.05 – 0.7 mg/mL with $R^2 > 0.99$.

Effect of ABPM-BSA Nanoparticles on Human Breast Cancer Mice Xenograft Model

Animal experiments were carried out by Washington Biotechnology, Inc. (Baltimore, MD) under IACUC approved protocol. Maximum tolerated dose was determined on healthy 6-8 weeks old female Swiss-Webster mice. Dose range study of single and multiple injections were done with 5 mice in each group intraveneously. Body-weight and clinical adverse reactions (piloerection, signs of distress) were monitored to determine the dose regimen for the efficacy study.

In the single dose efficacy study, 70 female athymic nude mice (Harlan Sprague-Dawley, Inc.), 5-6 weeks old, were implanted with $1x10^7$ BT474 cells (passage 15) in 30% Matrigel (BD Biosciences, San Jose, CA) subcutaneously in the right flank, and left to develop solid tumor for 10 days (Therapy Day -10 to Day 0). Additionally, each mouse was also implanted with a 0.72 mg 60-day time-release β-estradiol pellet (Innovative Research of America, Sarasota, FL) subcutaneously. Animals were grouped into three groups: Blank BSA Vehicle, ABPM-BSA NP and Paclitaxel Control. Starting from Day 0, mice were injected with 0.8 mg/kg drug of ABPM-BSA NP or Blank BSA equivalence intravenously every other day for 14 days, or 10 mg/kg

Paclitaxel (Hospira, Lake Forest, IL) intravenously every 4 days for 4 doses. All mice were weighed every Monday, Wednesday and Friday, and tumor sizes were estimated by calculating Tumor Volume according to **Eq. 6** below.

$$\text{Tumor Volume} = length \times width^2 \times \frac{1}{2}$$

Statistical comparison was evaluated by two-tail Student's *t* test. Data was presented as mean (±SEM) of 15 animals in Blank and ABPM-BSA NP groups and 13 animals for the Paclitaxel group. Extra animals were accounted for in each group in consideration of outliers and anomalies.

Reference

1. Dondorp, A. M.; Fanello, C. I.; Hendriksen, I. C. E.; Gomes, E.; Seni, A.; Chhaganlal, K. D.; Bojang, K.; Olaosebikan, R.; Anunobi, N.; Maitland, K.; Kivaya, E.; Agbenyega, T.; Nguah, S. B.; Evans, J.; Gesase, S.; Kahabuka, C.; Mtove, G.; Nadjm, B.; Deen, J.; Amumpaire, J. M.; Nansumba, M.; Karema, C.; Umulisa, N.; Uwimana, A.; Mokuolu, O. A.; Adedoyin, O. T.; Johnson, W. B. R.; Tshefu, A. K.; Onyamboko, M. A.; Sakulthaew, T.; Ngum, W. P.; Silamut, K.; Stepniewska, K.; Woodrow, C. J.; Bethell, D.; Wills, B.; Oneko, M.; Peto, T. E.; von Seidlein, L.; Day, N. P. J.; White, N. J.; Grp, A., Artesunate versus quinine in the treatment of severe falciparum malaria in African children (AQUAMAT): an open-label, randomised trial. *Lancet* 2010, *376* (9753), 1647-1657; Miller, L. H.; Su, X. Z., Artemisinin: Discovery from the Chinese Herbal Garden. *Cell* 2011, *146* (6), 855-858; White, N. J., Qinghaosu (Artemisinin): The price of success. *Science* 2008, *320* (5874), 330-334.

2. Taylor, W. R. J.; White, N. J., Antimalarial drug toxicity - A review. *Drug Safety* 2004, *27* (1), 25-61.

3. Lai, H.; Singh, N. P., Selective Cancer Cell Cytotoxicity From Exposure to Dihydroartemisinin and Holotransferrin. *Cancer Letters* 1995, *91* (1), 41-46; Singh, N. P.; Lai, H., Selective toxicity of dihydroartemisinin and holotransferrin toward human breast cancer cells. *Life Sciences* 2001, *70* (1), 49-56.

4. Stockwin, L. H.; Han, B. N.; Yu, S. X.; Hollingshead, M. G.; ElSohly, M. A.; Gul, W.; Slade, D.; Galal, A. M.; Newton, D. L., Artemisinin dimer anticancer activity correlates with heme-catalyzed reactive oxygen species generation and endoplasmic reticulum stress induction. *International Journal of Cancer* 2009, *125* (6), 1266-1275.

5. Witus, L. S.; Francis, M. B., Using Synthetically Modified Proteins to Make New Materials. *Accounts of Chemical Research* 2011, *44* (9), 774-783.

6. Zeng, Q.-P.; Zhang, P.-Z., Artesunate mitigates proliferation of tumor cells by alkylating heme-harboring nitric oxide synthase. *Nitric Oxide-Biology and Chemistry* 2011, *24* (2), 110-112; Meunier, B.; Robert, A., Heme as Trigger and Target for Trioxane-Containing Antimalarial Drugs. *Accounts of Chemical Research* 2010, *43* (11).

7. Mishina, Y. V.; Krishna, S.; Haynes, R. K.; Meade, J. C., Artemisinins inhibit Trypanosoma cruzi and Trypanosoma brucei rhodesiense in vitro growth. *Antimicrobial Agents and Chemotherapy* 2007, *51* (5), 1852-1854; Lu, M.; Sun, L.; Zhou, J.; Yang, J., Dihydroartemisinin induces apoptosis in colorectal cancer cells through the mitochondria-dependent pathway. *Tumor Biology* 2014, *35* (6), 5307-5314.

8. Efferth, T., Molecular pharmacology and pharmacogenomics of artemisinin and its derivatives in cancer cells. *Current Drug Targets* 2006, *7* (4), 407-421; Singh, N. P.; Lai, H. C., Artemisinin induces apoptosis in human cancer cells. *Anticancer Research* 2004, *24* (4), 2277-2280; Lai, H.; Sasaki, T.; Singh, N. P., Targeted treatment of cancer with artemisinin and artemisinin-tagged iron-carrying compounds. *Expert Opinion on Therapeutic Targets* 2005, *9* (5), 995-1007; Efferth, T.; Dunstan, H.; Sauerbrey, A.; Miyachi, H.; Chitambar, C. R., The anti-malarial artesunate is also active against cancer. *International Journal of Oncology* 2001, *18* (4), 767-773.

9. Lombard, M. C.; N'Da, D. D.; Breytenbach, J. C.; Kolesnikova, N. I.; Van Ba, C. T.; Wein, S.; Norman, J.; Denti, P.; Vial, H.; Wiesner, L., Antimalarial and anticancer activities of artemisinin-quinoline hybrid-dimers and pharmacokinetic properties in mice. *European Journal of Pharmaceutical Sciences* 2012, *47* (5), 834-841; Galal, A. M.; Gul, W.; Slade, D.; Ross, S. A.; Feng, S.; Hollingshead, M. G.; Alley, M. C.; Kaur, G.; ElSohly, M. A., Synthesis and evaluation of dihydroartemisinin and dihydroartemisitene acetal dimers showing anticancer and antiprotozoal activity. *Bioorganic & Medicinal Chemistry* 2009, *17* (2), 741-751; Jung, M.; Lee, S.; Ham, J.; Lee, K.; Kim, H.; Kim, S. K., Antitumor activity of novel deoxoartemisinin monomers, dimers, and trimer. *Journal of Medicinal Chemistry* 2003, *46* (6), 987-994; Jeyadevan, J. P.; Bray, P. G.; Chadwick, J.; Mercer, A. E.; Byrne, A.; Ward, S. A.; Park, B. K.; Williams, D. P.; Cosstick, R.; Davies, J.; Higson, A. P.; Irving, E.; Posner, G. H.; O'Neill, P. M., Antimalarial and antitumor evaluation of novel C-10 non-acetal dimers of 10 beta-(2-hydroxyethyl)deoxoartemisinin. *Journal of Medicinal Chemistry* 2004, *47* (5), 1290-1298.

10. Haynes, R. K., From artemisinin to new artemisinin antimalarials: Biosynthesis, extraction, old and new derivatives, stereochemistry and medicinal chemistry requirements. *Current Topics in Medicinal Chemistry* 2006, *6* (5), 509-537; Efferth, T.; Kaina, B., Toxicity of the antimalarial artemisinin and its dervatives. *Critical Reviews in Toxicology* 2010, *40* (5), 405-421.

11. Posner, G. H.; Northrop, J.; Paik, I. H.; Borstnik, K.; Dolan, P.; Kensler, T. W.; Xie, S.; Shapiro, T. A., New chemical and biological aspects of artemisinin-derived trioxane dimers. *Bioorganic & Medicinal Chemistry* 2002, *10* (1), 227-232.

12. Posner, G. H.; Paik, I. H.; Sur, S.; McRiner, A. J.; Borstnik, K.; Xie, S. J.; Shapiro, T. A., Orally active, antimalarial, anticancer, artemisinin-derived trioxane dimers with high stability and efficacy. *Journal of Medicinal Chemistry* 2003, *46* (6), 1060-1065; Posner, G. H.; McRiner, A. J.; Paik, I. H.; Sur, S.; Borstnik, K.; Xie, S. J.; Shapiro, T. A.; Alagbala, A.; Foster, B., Anticancer and antimalarial efficacy and safety of artemisinin-derived trioxane dimers in rodents. *Journal of Medicinal Chemistry* 2004, *47* (5), 1299-1301; Paik, I. H.; Xie, S. J.; Shapiro, T. A.; Labonte, T.; Sarjeant, A. A. N.; Baege, A. C.; Posner, G. H., Second generation, orally active, antimalarial, artemisinin-derived trioxane dimers with high stability, efficacy, and anticancer activity. *Journal of Medicinal Chemistry* 2006, *49* (9), 2731-2734; Chadwick, J.; Mercer, A. E.; Park, B. K.; Cosstick, R.; O'Neill, P. M., Synthesis and biological evaluation of extraordinarily potent C-10 carba artemisinin dimers against P-falciparum malaria parasites and HL-60 cancer cells. *Bioorganic & Medicinal Chemistry* 2009, *17* (3), 1325-1338.

13. Conyers, R. C.; Mazzone, J. R.; Siegler, M. A.; Tripathi, A. K.; Sullivan, D. J.; Mott, B. T.; Posner, G. H., The survival times of malaria-infected mice are prolonged more by several new two-carbon-linked artemisinin-derived dimer carbamates than by the trioxane antimalarial drug artemether. *Bioorganic & Medicinal Chemistry Letters* 2014, *24* (5), 1285-1289; He, R.; Forman, M.; Mott, B. T.; Venkatadri, R.; Posner, G. H.; Arav-Boger, R., Unique and Highly Selective Anticytomegalovirus Activities of Artemisinin-Derived Dimer Diphenyl Phosphate Stem from Combination of Dimer Unit and a Diphenyl Phosphate Moiety. *Antimicrobial Agents and Chemotherapy* 2013, *57* (9), 4208-4214.

14. Boens, N.; Leen, V.; Dehaen, W., Fluorescent indicators based on BODIPY. *Chemical Society Reviews* 2012, *41* (3), 1130-1172.

15. Loudet, A.; Burgess, K., BODIPY dyes and their derivatives: Syntheses and spectroscopic properties. *Chemical Reviews* 2007, *107* (11), 4891-4932; Ulrich, G.; Ziessel, R.; Harriman, A., The chemistry of fluorescent bodipy dyes: Versatility unsurpassed. *Angewandte Chemie-International Edition* 2008, *47* (7), 1184-1201.

16. Dawidczyk, C. M.; Kim, C.; Park, J. H.; Russell, L. M.; Lee, K. H.; Pomper, M. G.; Searson, P. C., State-of-the-art in design rules for drug delivery platforms: Lessons learned from FDA-approved nanomedicines. *Journal of Controlled Release* 2014, *187*, 133-144.

17. Hoy, S. M., Albumin-Bound Paclitaxel: A Review of Its Use for the First-Line Combination Treatment of Metastatic Pancreatic Cancer. *Drugs* 2014, *74* (15), 1757-1768.

18. Elsadek, B.; Kratz, F., Impact of albumin on drug delivery - New applications on the horizon. *Journal of Controlled Release* 2012, *157* (1), 4-28.

19. Kratz, F.; Elsadek, B., Clinical impact of serum proteins on drug delivery. *Journal of Controlled Release* 2012, *161* (2), 429-445.

20. Pacorel, B.; Leung, S. C.; Stachulski, A. V.; Davies, J.; Vivas, L.; Lander, H.; Ward, S. A.; Kaiser, M.; Brun, R.; O'Neill, P. M., Modular Synthesis and in Vitro and in Vivo Antimalarial Assessment of C-10 Pyrrole Mannich Base Derivatives of Artemisinin. *Journal of Medicinal Chemistry* 2010, *53* (2), 633-640.

21. Langer, K.; Balthasar, S.; Vogel, V.; Dinauer, N.; von Briesen, H.; Schubert, D., Optimization of the preparation process for human serum albumin (HSA) nanoparticles. *International Journal of Pharmaceutics* 2003, *257* (1-2), 169-180; Zhang, J. Y.; He, B.; Qu, W.; Cui, Z.; Wang, Y. B.; Zhang, H.; Wang, J. C.; Zhang, Q., Preparation of the albumin nanoparticle system loaded with both paclitaxel and sorafenib and its evaluation in vitro and in vivo. *Journal of Microencapsulation* 2011, *28* (6), 528-536; Kim, T. H.; Jiang, H. H.; Youn, Y. S.; Park, C. W.; Tak, K. K.; Lee, S.; Kim, H.; Jon, S.; Chen, X. Y.; Lee, K. C., Preparation and characterization of water-soluble albumin-bound curcumin nanoparticles with improved antitumor activity. *International Journal of Pharmaceutics* 2011, *403* (1-2), 285-291.

22. Magde, D.; Wong, R.; Seybold, P. G., Fluorescence quantum yields and their relation to lifetimes of rhodamine 6G and fluorescein in nine solvents: Improved absolute standards for quantum yields. *Photochemistry and Photobiology* 2002, *75* (4), 327-334.

CHAPTER 8

Conclusion and Future Directions

In conclusion, this project consisted of the numerous aspects of compound synthesis, formulation design, optimization and characterization, *in vitro* cell cytotoxicity assays, *in vivo* efficacy xenograft animal model studies and analytical method development for quantification of drug-lipid nanoparticles from biological tissue samples.

Synthesis of covalent dimers linked at artemisinin C10 position

Two series of pH-responsive artemisinin dimers were synthesized in this project. The first class was based on an isobutylene dimer first described by G. Posner et al (**ADP106-109**). The lead candidate, **ADP109**, showed 30-fold increase in aqueous solubility as pH of solution decreases from 7.4 to 4. A second class of dimers, artemisinin dimer BODIPY compounds, where the two pharmacophores are assembled on the structurally rigid fluorophore, BODIPY. The strong fluorescence signal would be able to track ART dimer in cell-based studies.

Lipid-based nanoparticle preparation, optimization and characterization

ADP109 was initially incorporated into EPC-based lipid nanoparticles as a proof of concept study, where 10% of the compound was able to associate with the particles. Then, to move the lipid-based formulation into *in vivo* studies with well-defined lipid compositions, we developed and characterized a pH-responsive artemisinin dimer in PEG-coated lipid formulation, **NP209**, with synthetic lipids of saturated fatty acid chain. The lipid composition was able to incorporate **ADP109** with near-complete efficiency and showed acid-induced drug released. Binding and insertion of **ADP109** into lipid membrane was confirmed by DPH depolarization studies, which showed a 3°C reduction in phase transition temperature due to drug incorporation. Furthermore, optimizations of formulation with various surface PEG concentration, cholesterol or mixture of synthetic lipids were also carried out. The maximum loading capability was found to be 10% **ADP109** for DPPC-based particles. A mixture of two synthetic phosphatidylcholines (PCs) with

symmetric saturated fatty acyl chains alluded to the potential enhanced stability of hydrophobic drug binding when binding pockets are introduced deep within the membrane.

Cell cytotoxicity and animal xenograft model studies

Our studies showed that ADP-NPs elicit a unique set of biological responses from breast cancer cells to ultimately induce cell death, potentially opening up new avenues for treatments of breast cancer. The **NP209** formulation was potent and selective against both HER2+ and Triple Negative Breast Cancer cell lines. Initial MDA-MB-231 mice xenograft studies validated the feasibility of **ADP109**-lipid nanoparticle formulations for *in vivo* delivery of artemisinin dimer derivatives as chemotherapeutic agents, inhibiting growth of the triple negative tumor cells that usually respond poorly to current drug therapies. **ADP109**-DPPC based formulation, **NP209**, was able to suppress drug resistant MDA-MB-231 cell growth beyond that achieved with paclitaxel in mice xenograft.

ART dimer BODIPYs showed potent cytotoxicity against two breast cancer cell lines, BT474 and MDA-MB-231. The albumin-based nanoparticle formulation was successfully used for the ART dimers, enabling the *in vivo* studies of these highly hydrophobic compounds. ART dimer-albumin nanoparticles were able to suppress tumor growth in a mice xenograft model implanted with BT474 cells. The efficacy was comparable to paclitaxel, a positive control. These data suggest that ART dimer BODIPYs are an attractive class of compounds for both clinical and biochemical investigations.

Fatty acyl (FA) domain drug binding pocket hypothesis and geometrical fit design model

We demonstrated that establishing binding pockets deep within the bilayer by using a mixture of lipids with different fatty acyl chain length could lead to a significant improvement in drug

loading and retention. The binding pocket was designed to complement the geometrical dimensions of the hydrophobic molecule of interest. For ADP109, a mixture of PCs consisting of 40% 14-carbon FA and 60% 18-carbon FA successfully retained >97% of the compound under physiological neutral while allowing release of the molecules under acidic pH. Our hypothesis was further validated with two other drug compounds, Darunavir and Curcumin.

Analytical method development for quantifying lipid-associated artemisinin dimer in various biological tissue samples: whole blood, liver, brain and tumor

The first sample preparation and LC-MS/MS techniques to extract an artemisinin dimer-piperazine conjugate drug candidate, ADP109, from whole blood, and quantify the drug concentration in whole blood and other tissue samples were described. Extraction of ADP109 was achieved by first stabilizing hemolysed blood with strong oxidizing reagent, potassium dichromate, followed by solid phase extraction using a mixed-cationic exchange cartridge. Tissue samples were prepared by a two-step liquid-liquid extraction. Separation of ADP109 from internal standard was performed on a BEH phenyl column with tandem mass spectrometry monitoring 782.4 m/z fragmented to 190.1 m/z for detection of ADP109. The analytical method reported above is versatile and robust, and can be adapted for future pharmacokinetics and tissue distribution studies.

Future directions

This thesis lays the foundation for a number of future studies that can be pursued in different areas of focus in more depth. Two structural motifs were explored to assemble artemisinin dimers here, of which the BODIPY based derivatives offer an advantage of molecule tracking

when delivered to cells. The high quantum yield as well as the versatility in fluorescence wavelengths, which can be manipulated by varying the *meso*-position substituent, can be further exploited to understand mechanisms of action of artemisinin derivatives in both malaria and cancer treatments. With the development of protein-drug aggregate nanoparticles that enable delivery of the fluorescent artemisinin dimers into animal models, we may be able to better understand the *in vivo* behavior and rationalize the observed enhancement in efficacy of these dimeric derivatives.

The analytical method developed as part of this work is an entry point into understanding the pharmacokinetic behaviors of dimeric artemisinin derivatives *in vivo*. Future pharmacokinetics and tissue distribution studies can be carried out to improve the current knowledge about mechanism of action, *in vivo* behavior as well as toxicity related to artemisinin dimer derivatives. With such knowledge, one can refine the compound structures to achieve improved specificity and efficacy of newly designed artemisinin derivatives in future synthetic endeavors. The sample preparation methods can also be adapted to other artemisinin dimeric or hydrophobic compounds with similar structural motifs.

Finally, the idea of leveraging the fatty acyl (FA) chain length different in common lipids (such as phosphatidylcholine) to allow formation of binding pockets where hydrophobic drug molecules can bind within a lipid membrane – the Drug Binding Pocket Hypothesis, was introduced for the first time. Interesting findings and the hypothesis were noted in a first disclosure manuscript and the hypothesis is actively being tested against other drug compounds that have presented challenge in developing lipid-nanoparticle formulations. Future biophysical studies and molecular dynamic simulations to provide further molecular insight and validate the presence of the drug binding pockets will strengthen the hypothesis. Leveraging understanding

of molecular geometry in choosing liposome composition simplifies the process of identifying optimal lipid formulation for hydrophobic compounds and thus expedites the chemotherapeutic development.

CHAPTER 9

Appendix

NMRs and Mass Spectrums

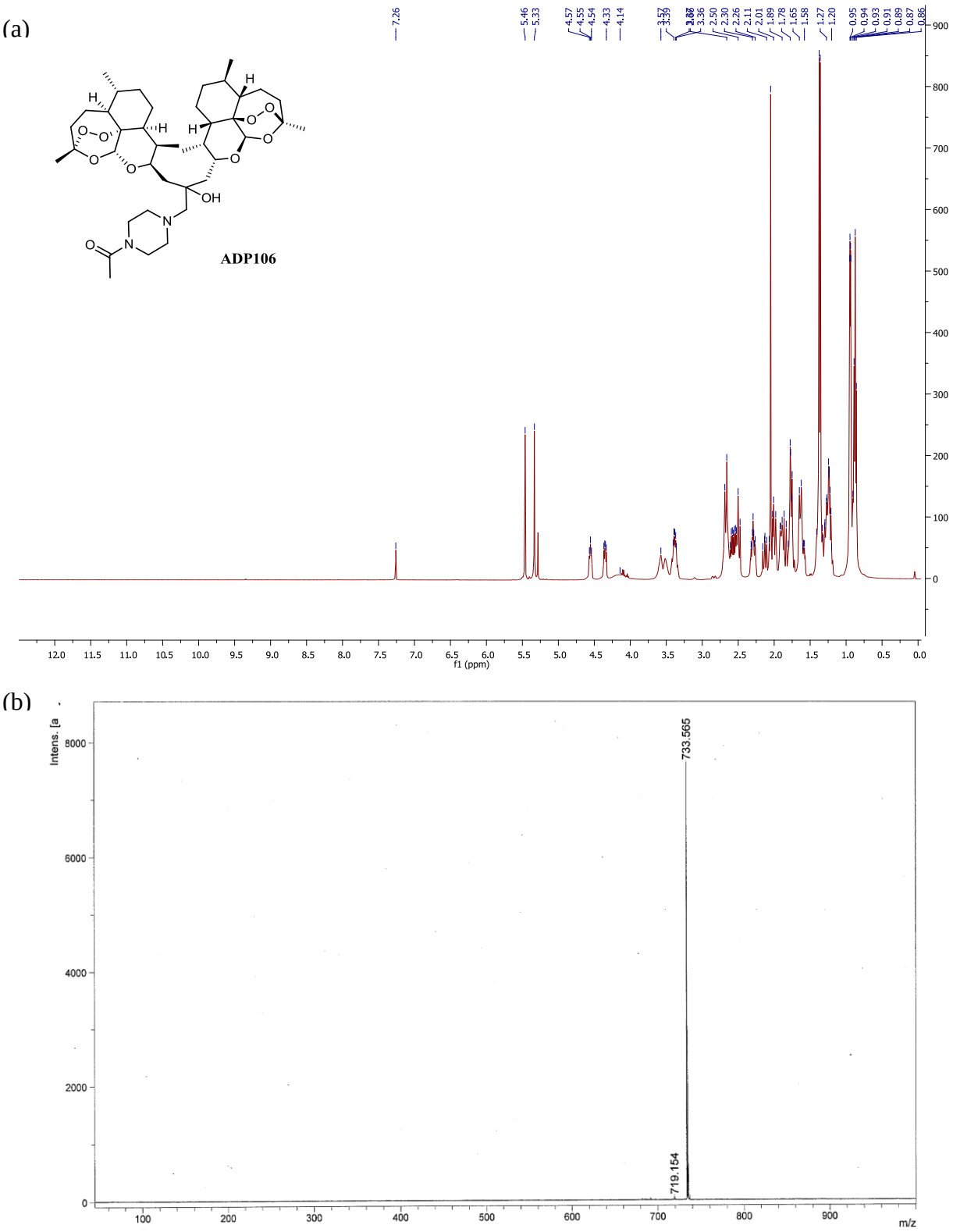

Figure S1. ^{1}H-NMR (a) and MALDI-TOF (b) of **ADP106.**

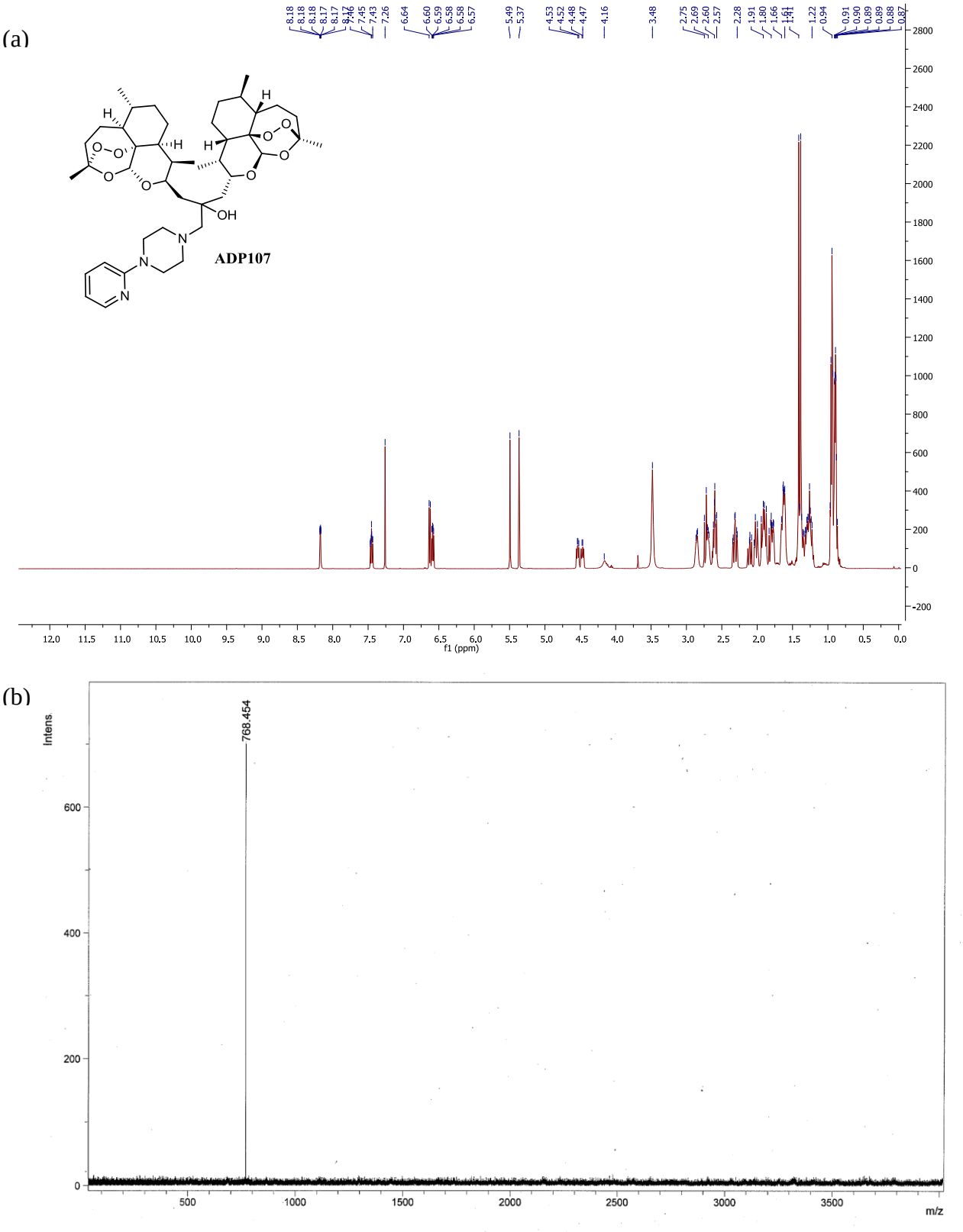

Figure S2. ^{1}H-NMR (a) and MALDI-TOF (b) of **ADP107.**

(a)

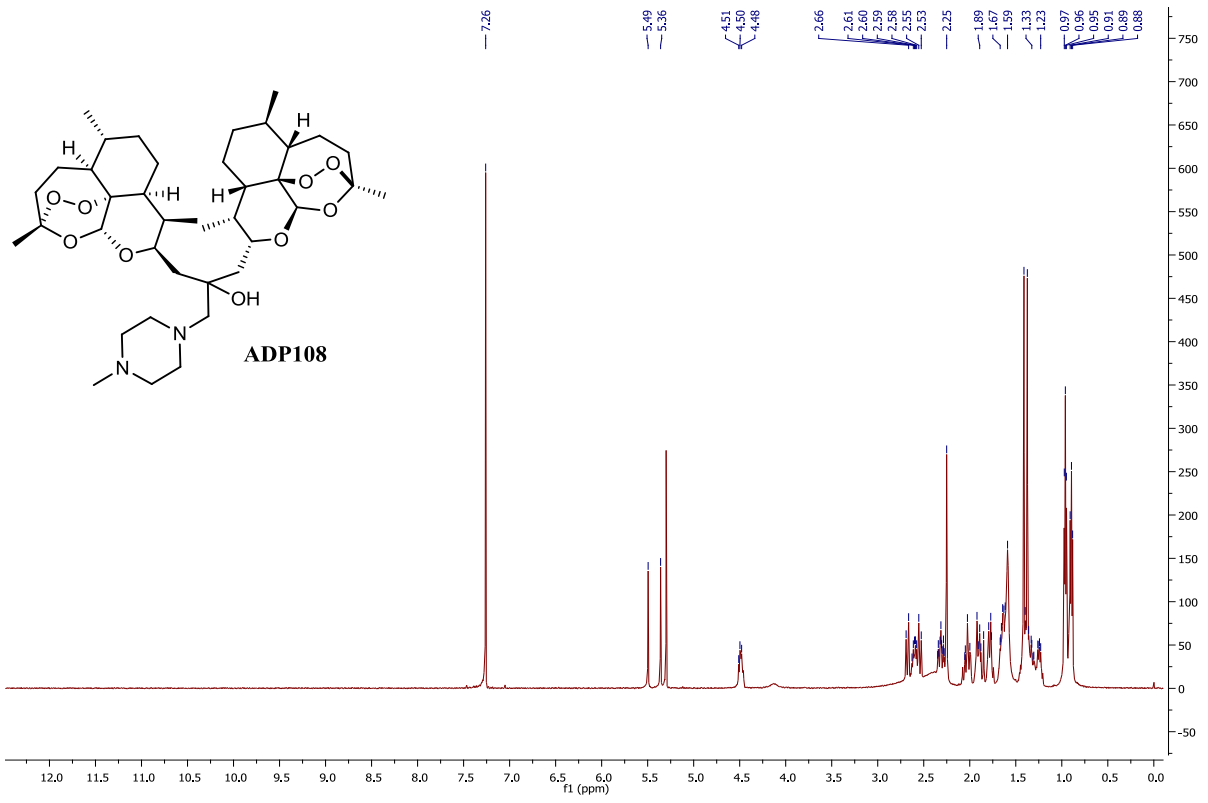

(b)

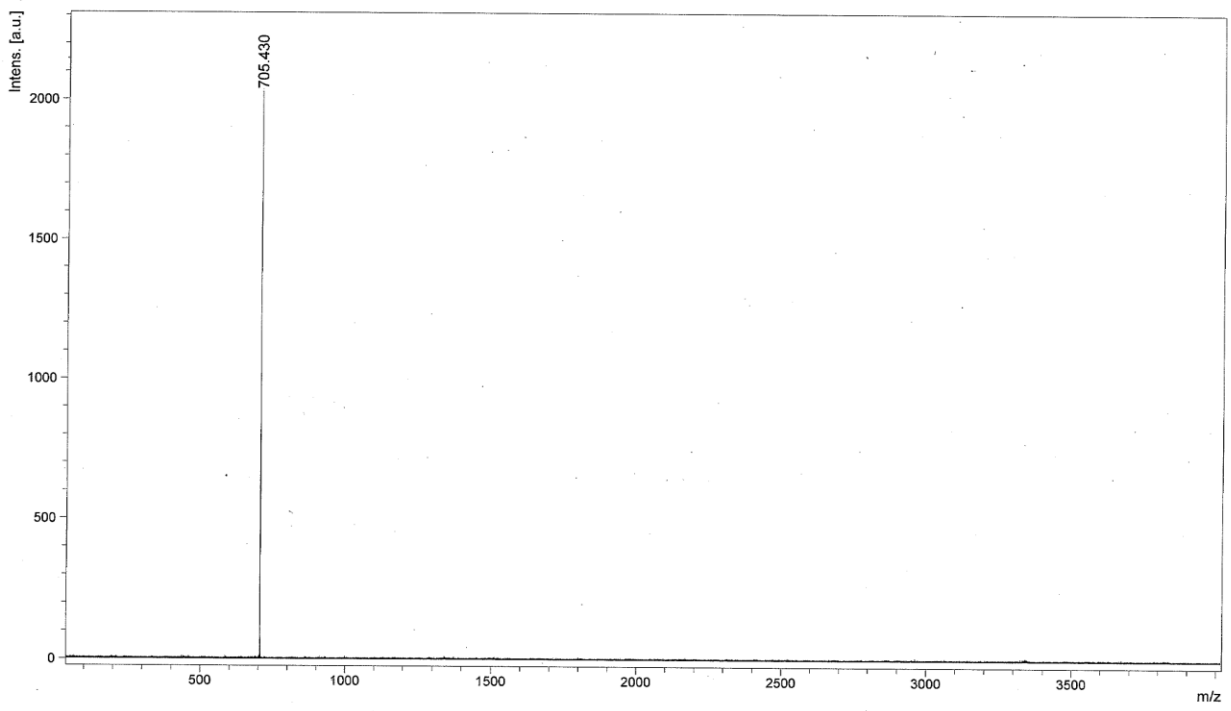

Figure S3. ^{1}H-NMR (a) and MALDI-TOF (b) of **ADP108.**

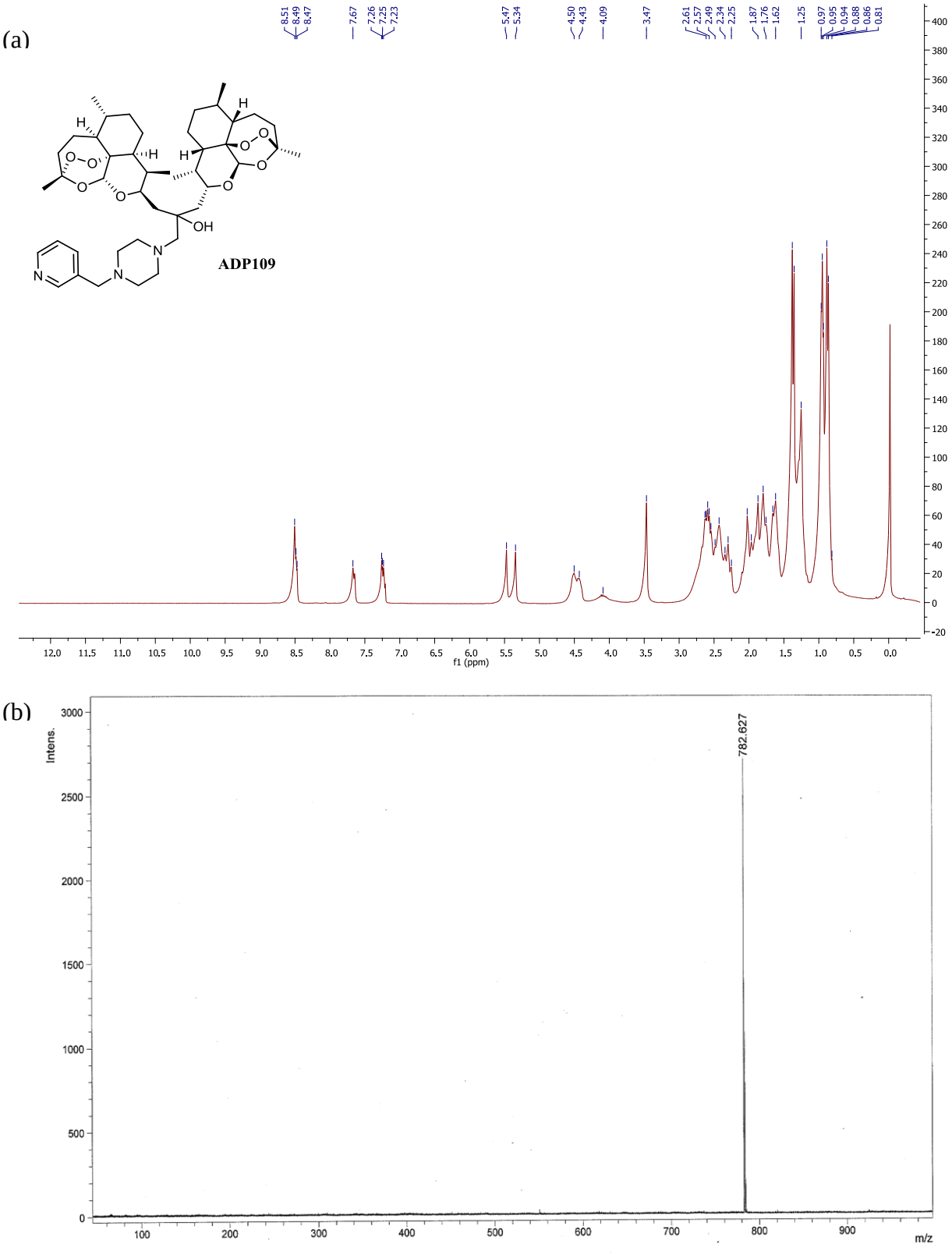

Figure S4. ^{1}H-NMR (a) and MALDI-TOF (b) of **ADP109.**

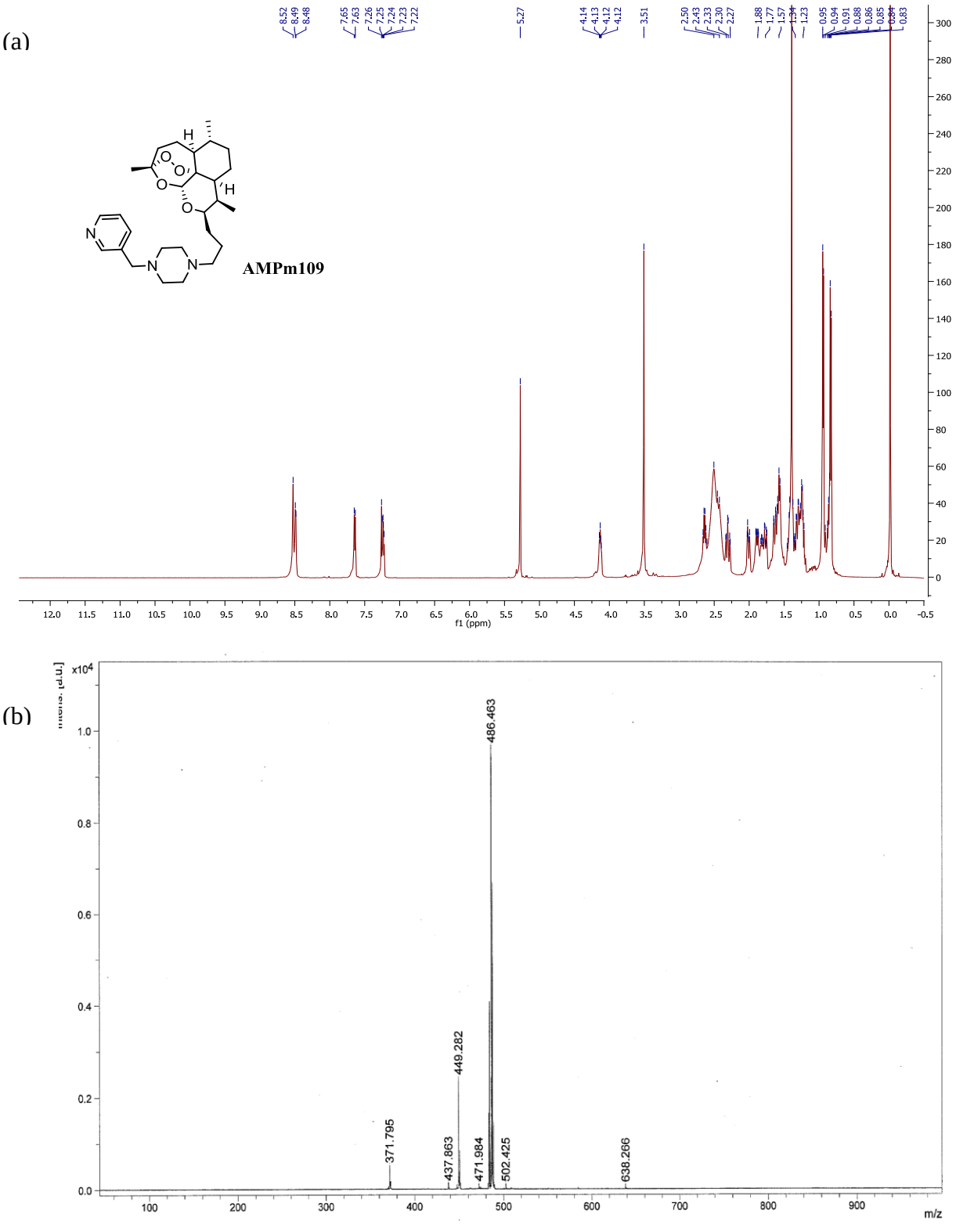

Figure S5. [1]H-NMR (a) and MALDI-TOF (b) of **AMPm109.**

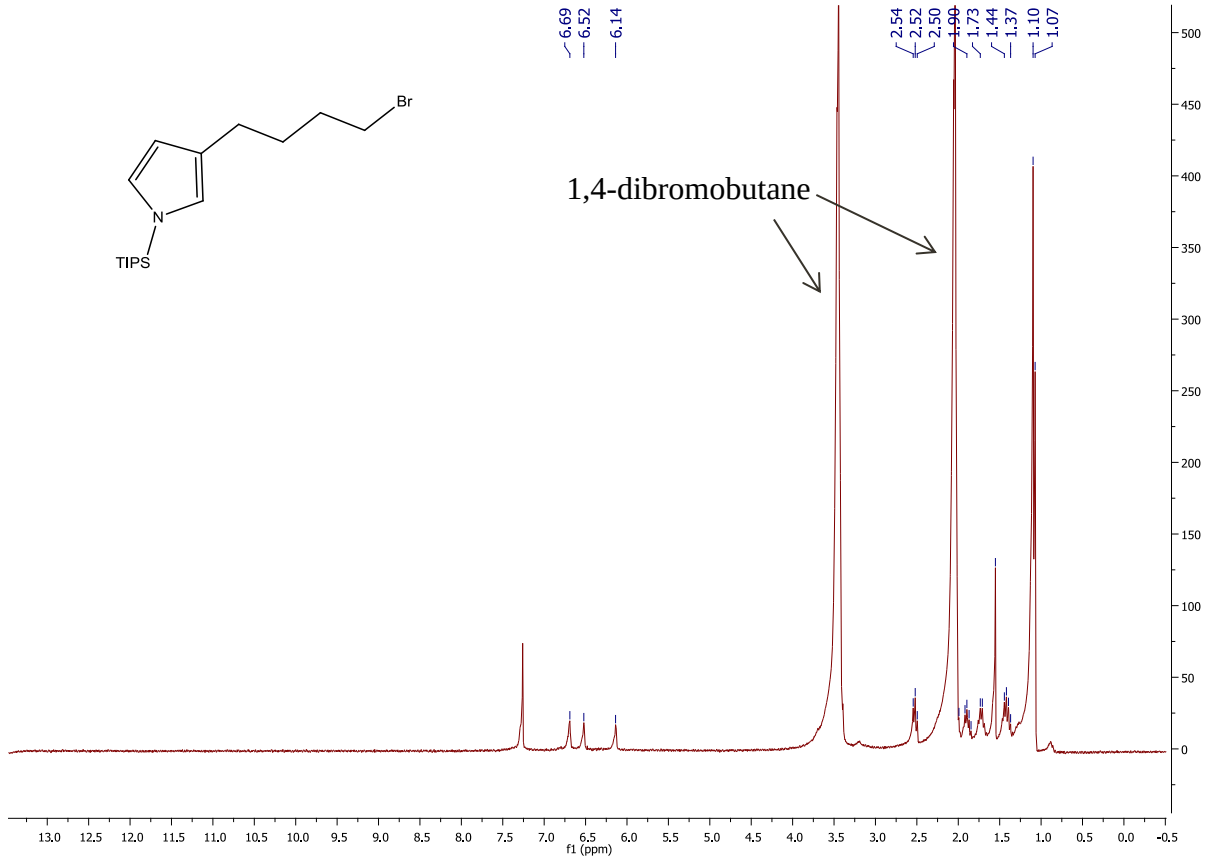

Figure S6. ^{1}H-NMR of N-TIPS-3-(4-bromobutyl)pyrrole. Preparation and peak annotation see Chapter 7. Contamination by 1,4-dibromobutane and small amount of water seen.

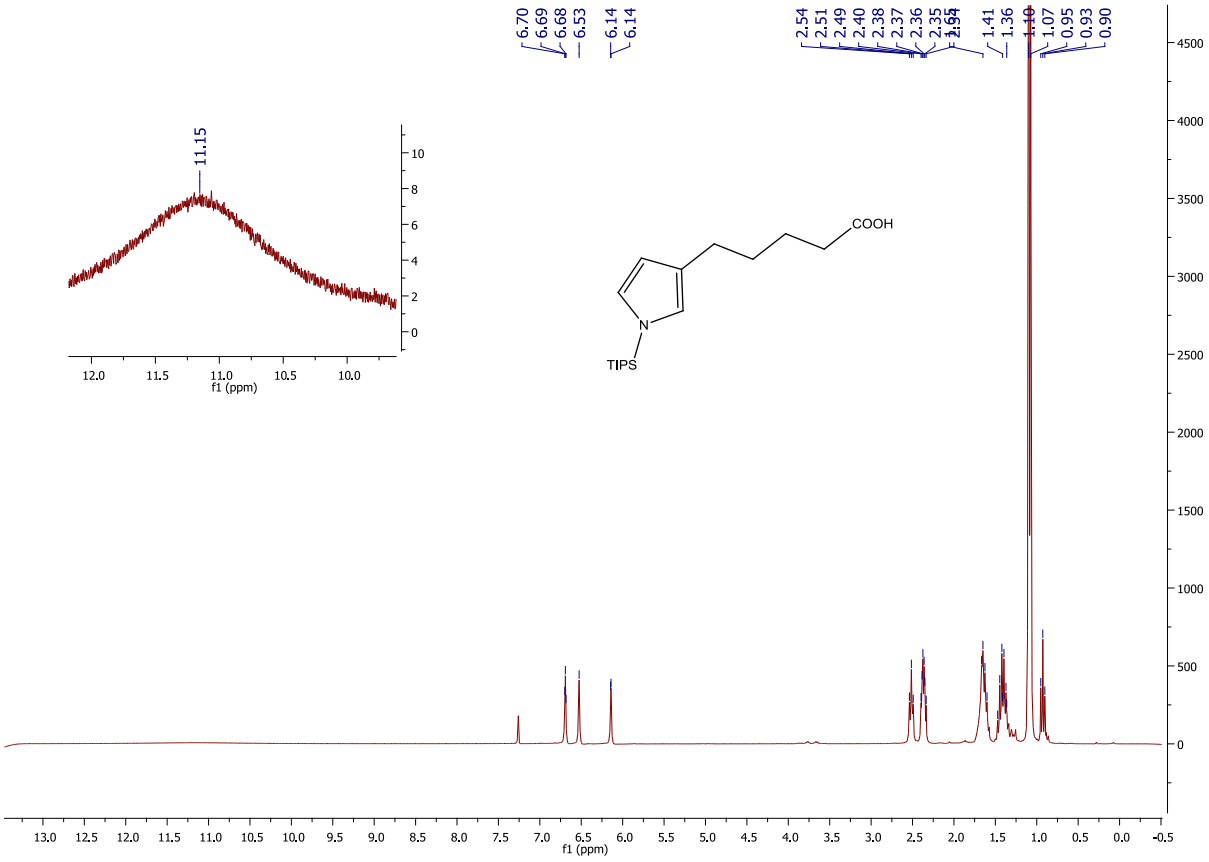

Figure S7. ^{1}H-NMR of N-TIPS pyrrole with pentanoic acid side chain. Preparation and peak annotation see Chapter 7.

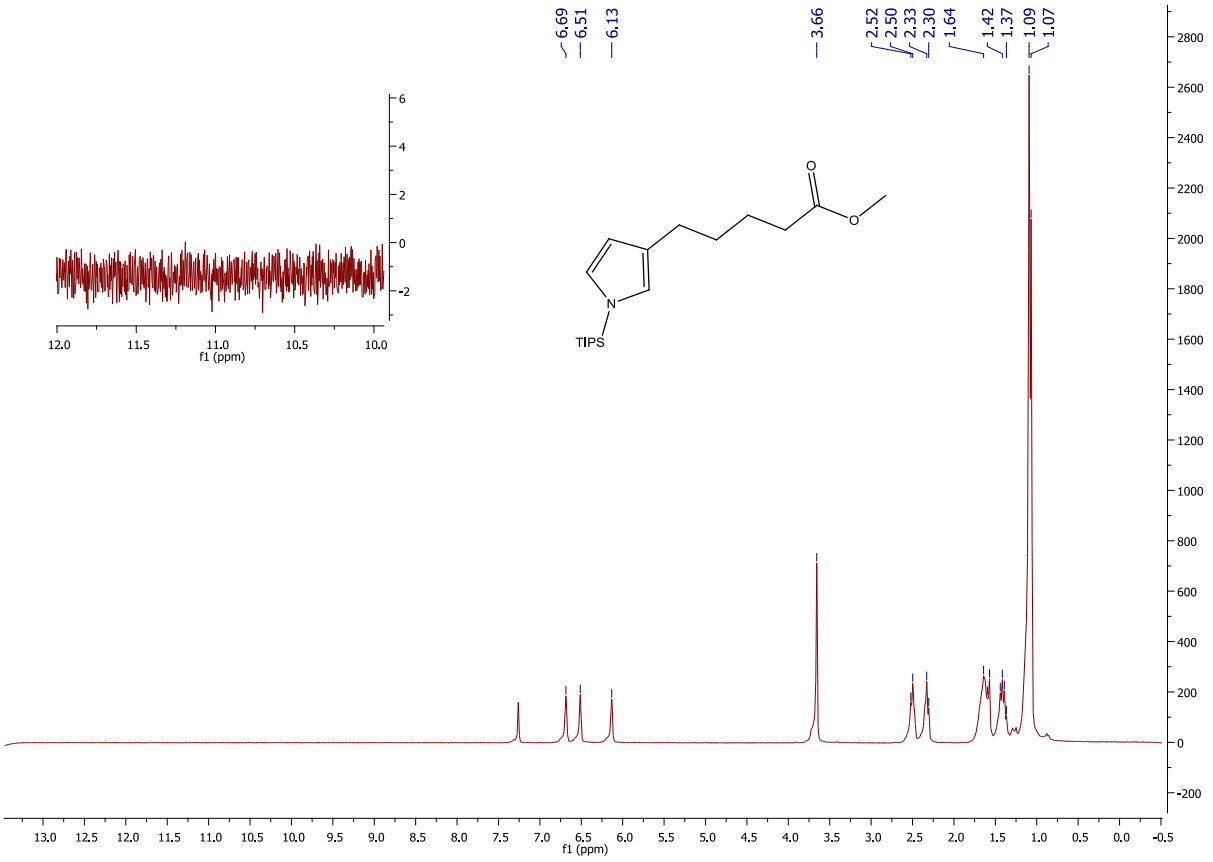

Figure S8. ^{1}H-NMR of N-TIPS pyrrole with methyl pentanoate side chain. Preparation and peak annotation see Chapter 7.

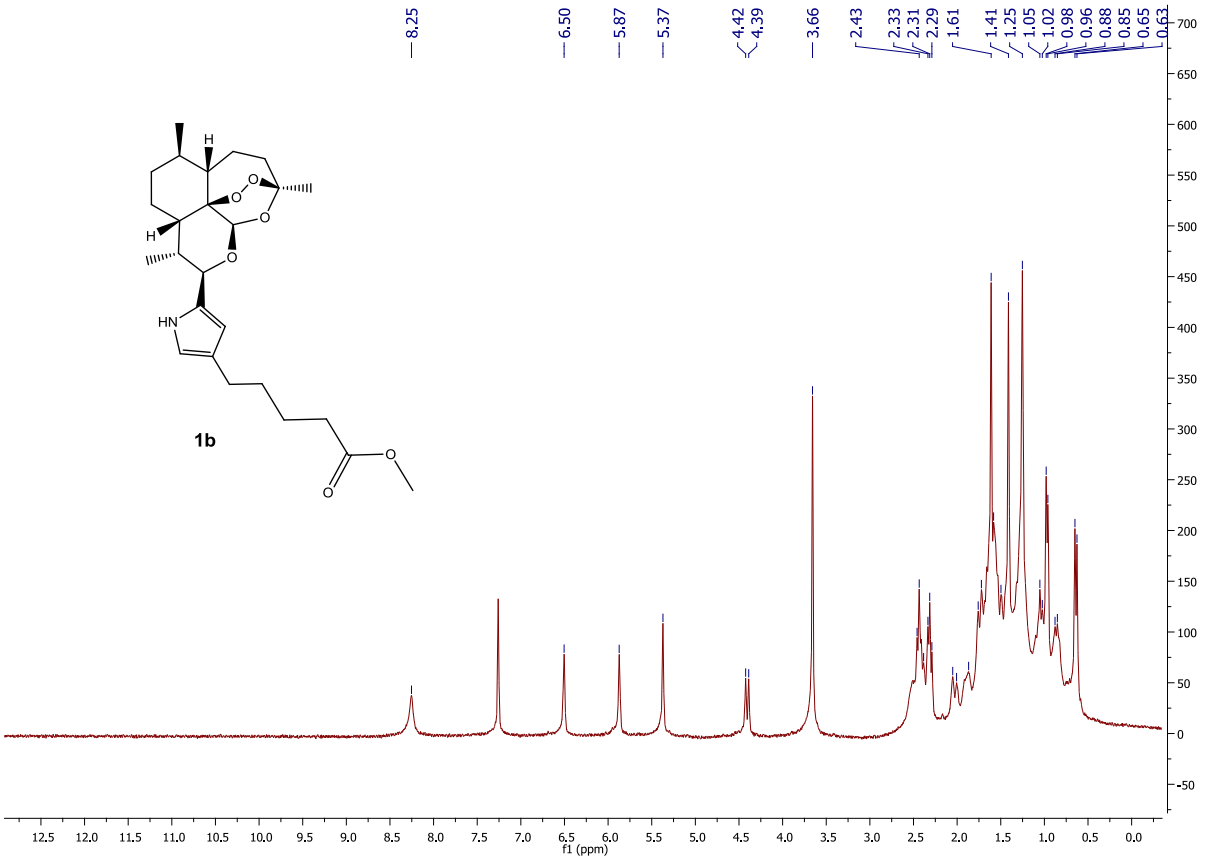

Figure S9. ^{1}H-NMR of Artemisinin-conjugated pyrrole with methyl pentanoate side chain. Preparation and peak annotation see Chapter 7, compound **1b**.

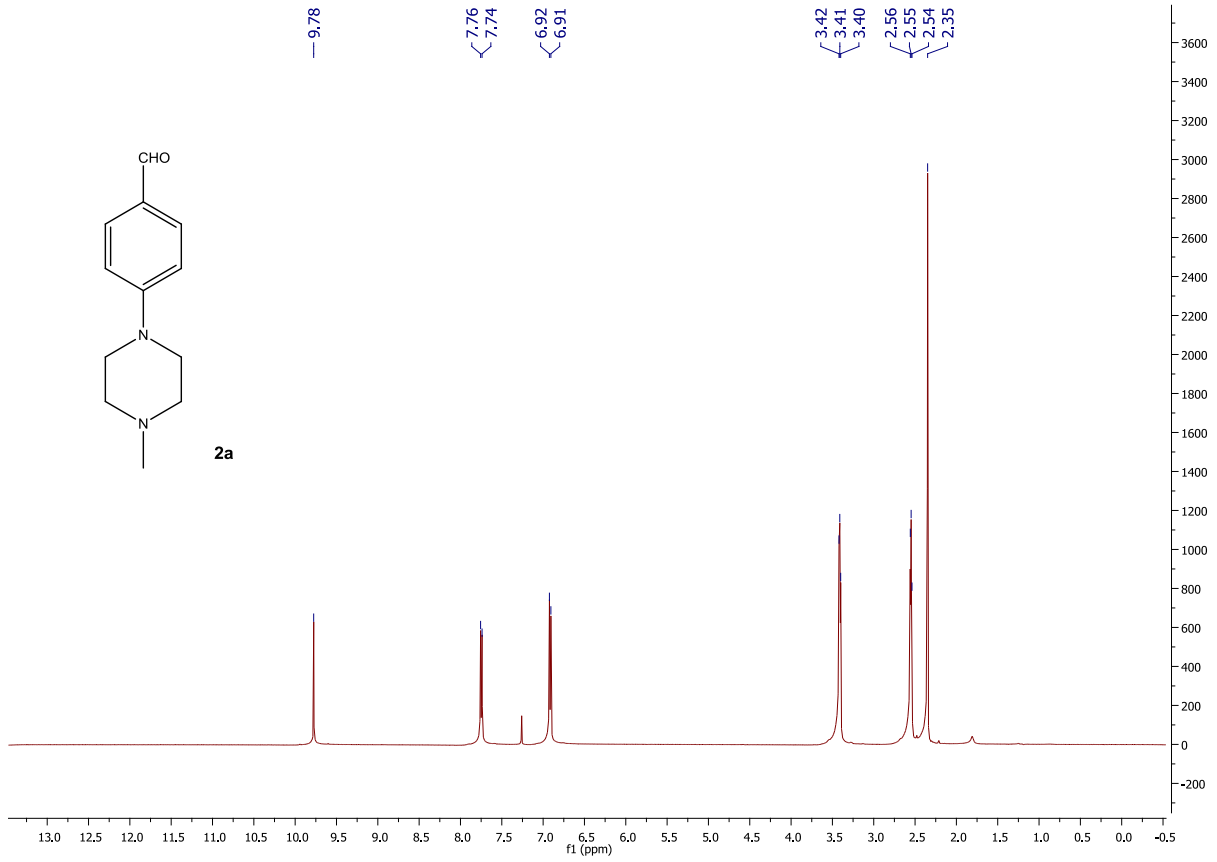

Figure S10. ^{1}H-NMR of 4-(N-methylpiperazyl)-benzaldehyde, compound **2a**. Preparation and peak annotation see Chapter 7.

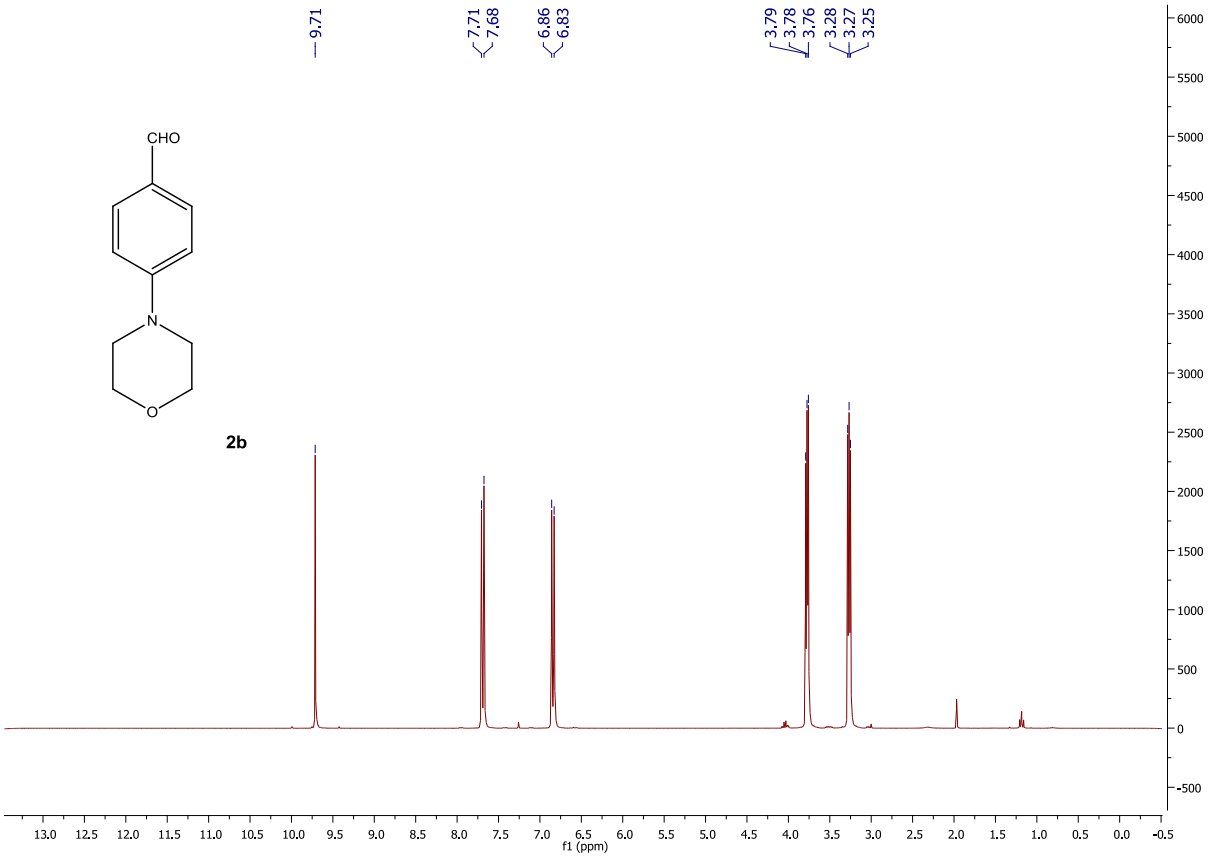

Figure S11. ^{1}H-NMR of 4-morpholinyl-benzaldehyde, compound **2a**. Preparation and peak annotation see Chapter 7.

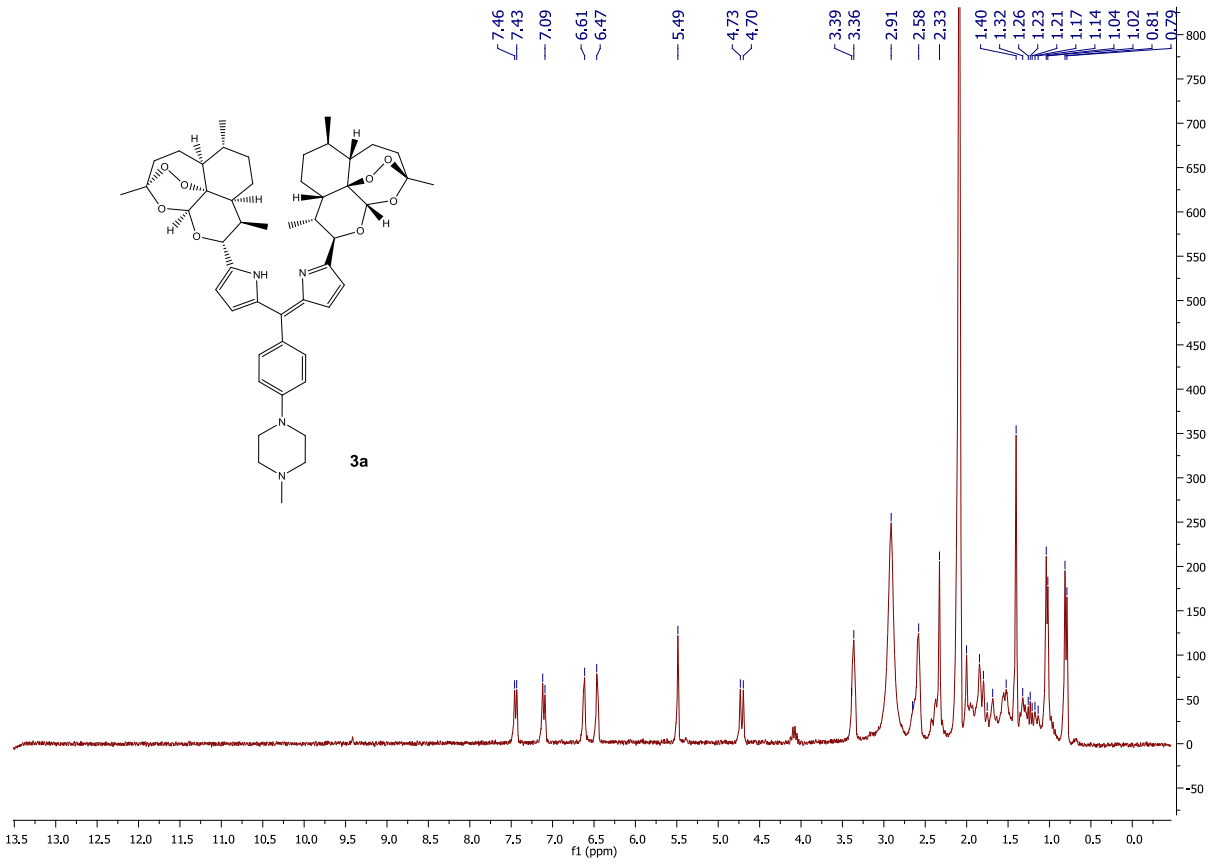

Figure S12. ^{1}H-NMR of BisART dipyrrolmethene compound **3a**. Preparation and peak annotation see Chapter 7. Water peak seen at 2.9 ppm.

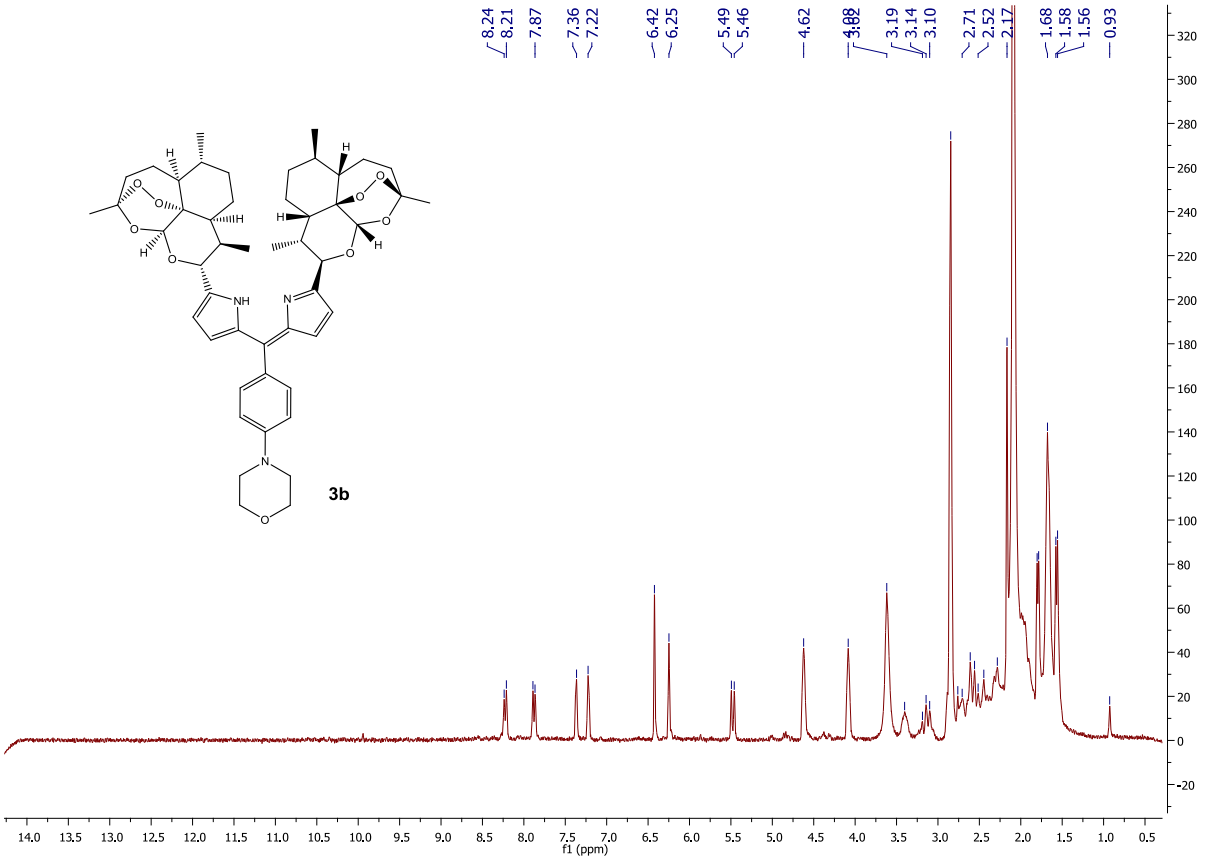

Figure S13. ^{1}H-NMR of BisART dipyrrolmethene compound **3b**. Preparation and peak annotation see Chapter 7.

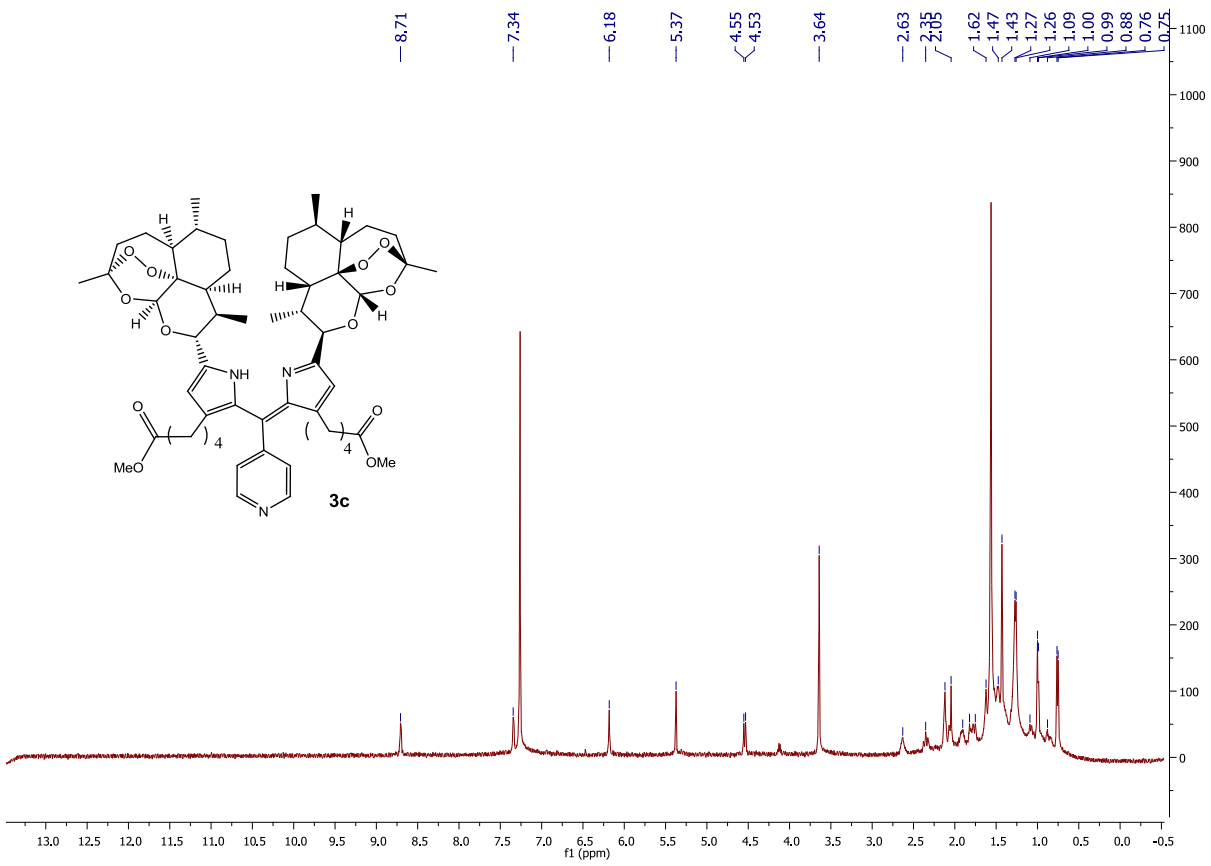

Figure S14. ^{1}H-NMR of BisART dipyrrolmethene compound **3c**. Preparation and peak annotation see Chapter 7.

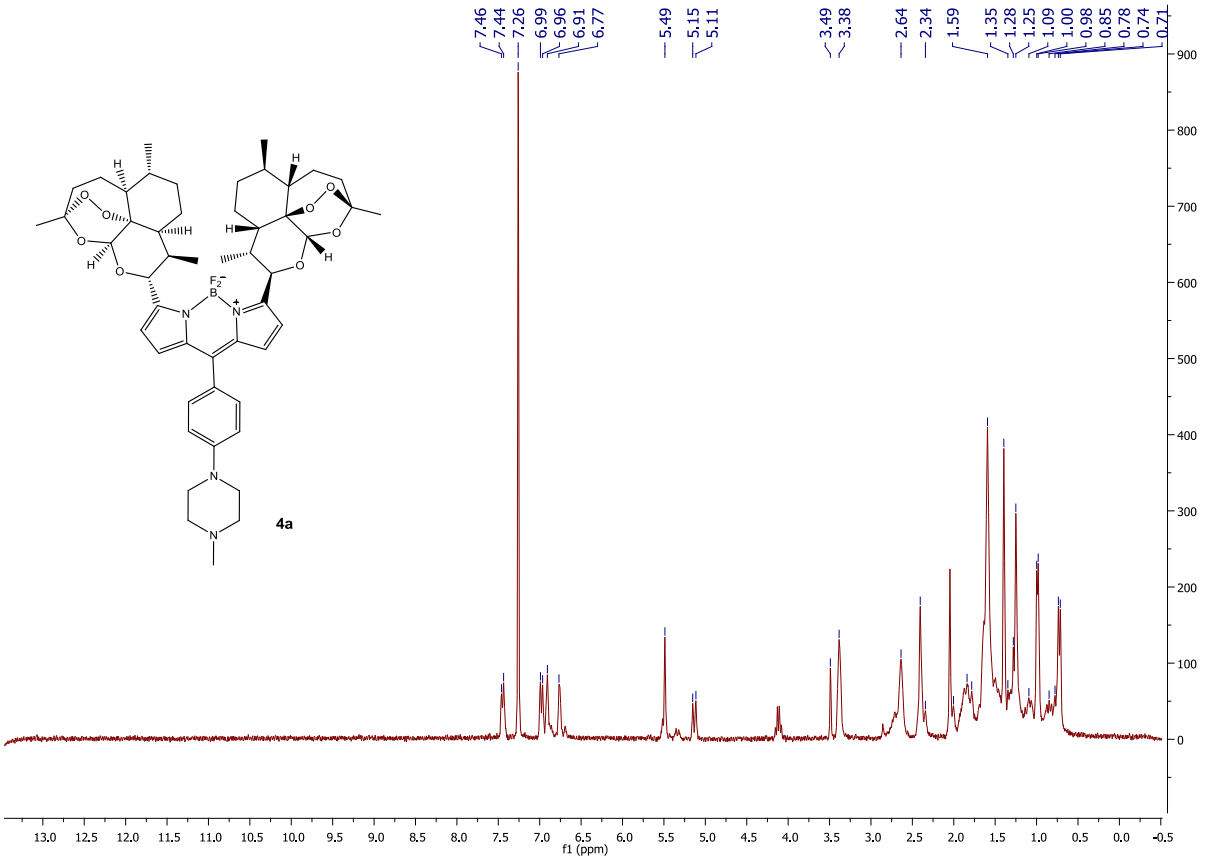

Figure S15. ^{1}H-NMR of BisART BODIPY compound **4a**. Preparation and peak annotation see Chapter 7.

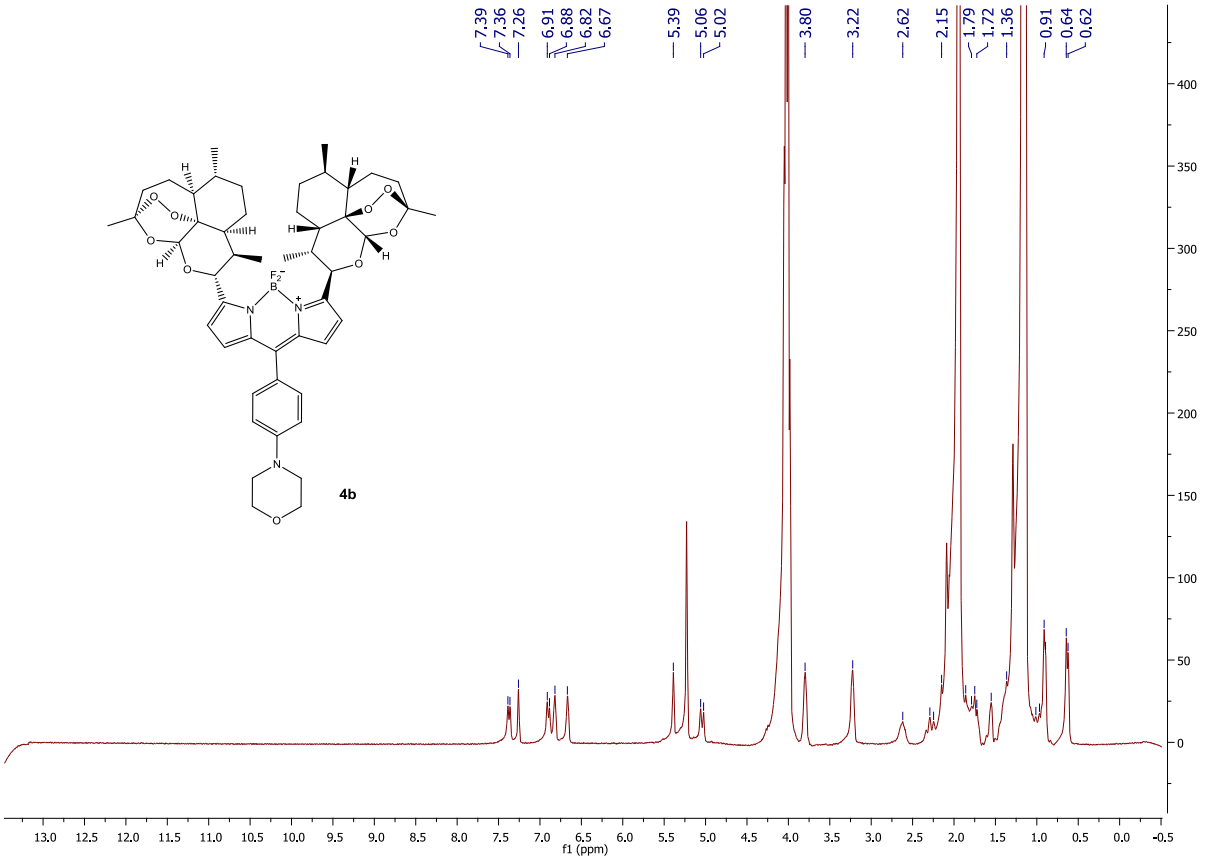

Figure S16. ^{1}H-NMR of BisART BODIPY compound **4b**. Preparation and peak annotation see Chapter 7. Sample was not dry and contained solvent peaks.

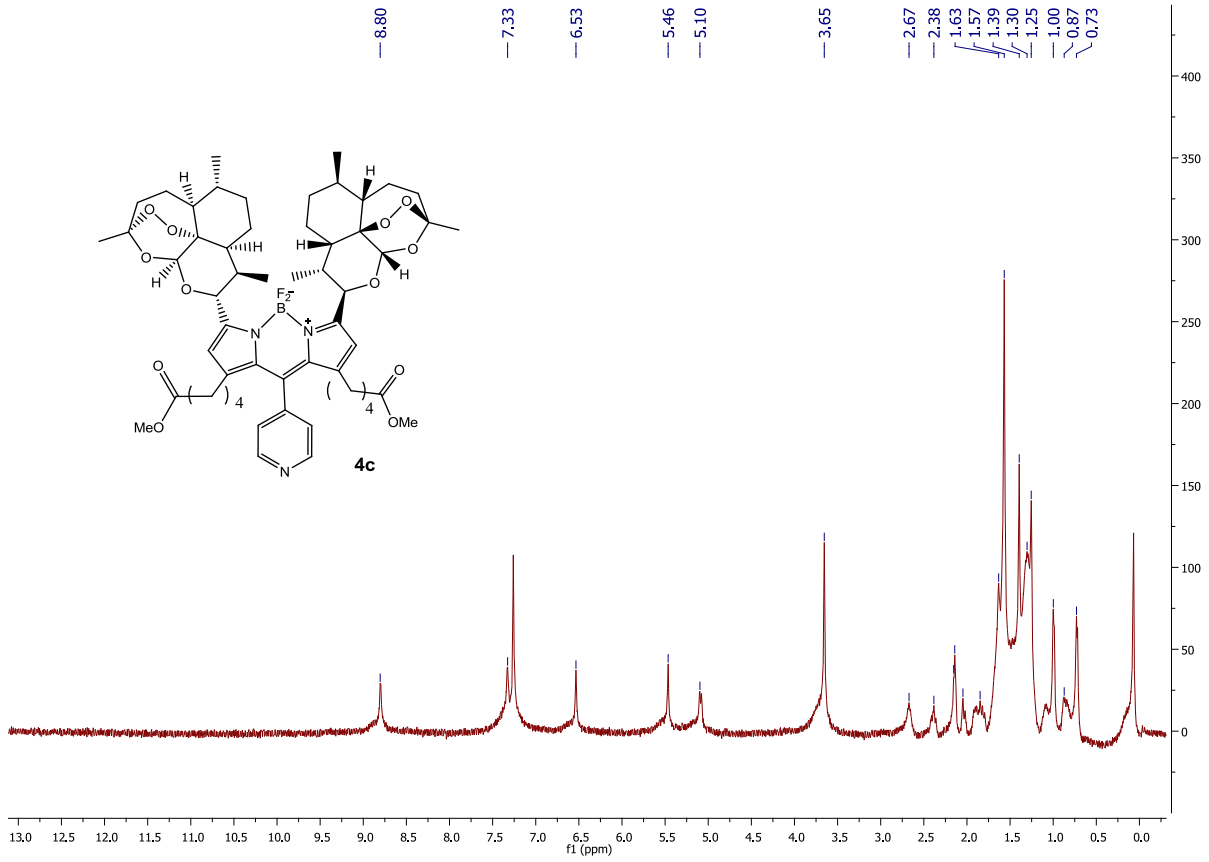

Figure S17. ^{1}H-NMR of BisART BODIPY compound **4c**. Preparation and peak annotation see Chapter 7.

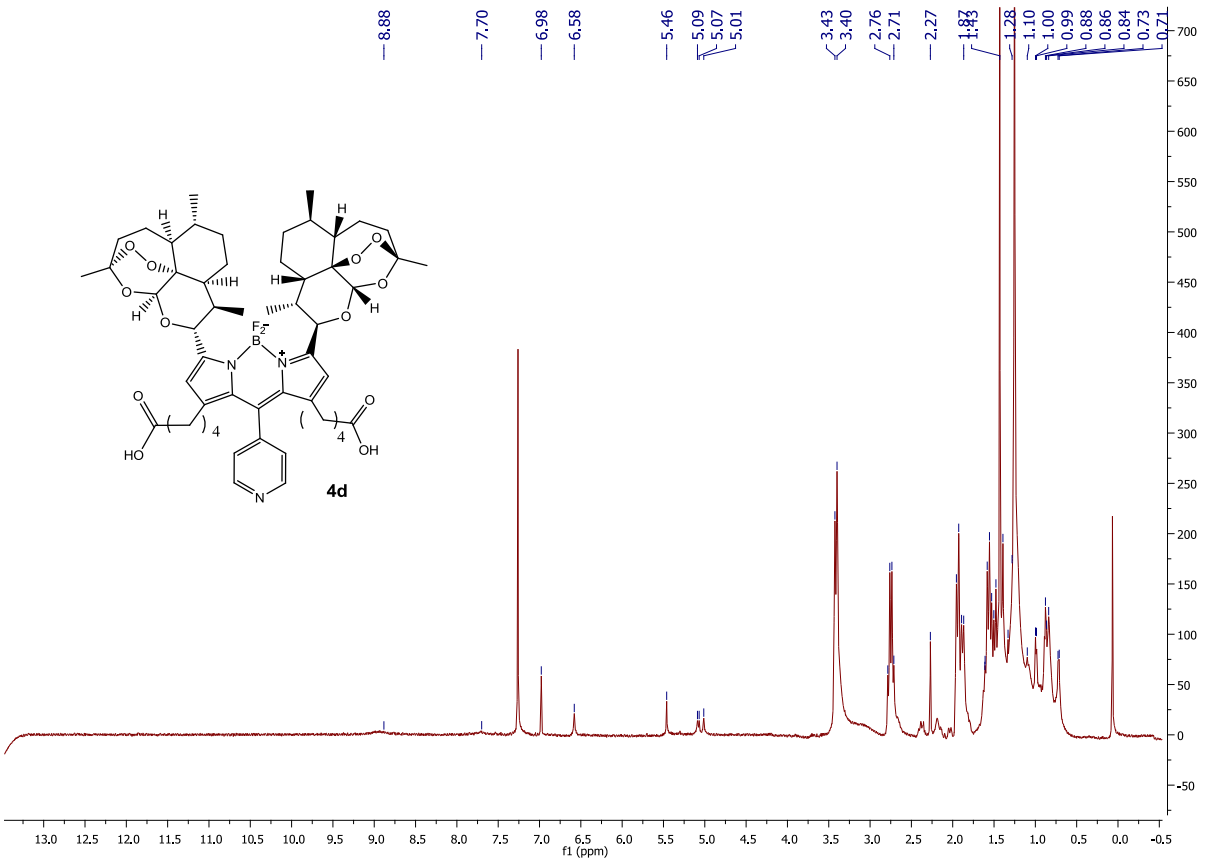

Figure S18. ^{1}H-NMR of BisART BODIPY compound **4d**. Preparation and peak annotation see Chapter 7. NMR taken on a crude sample, hydrolysis evident by disappearance of methyl group at 3.6ppm from spectrum shown in **Figure S17**.

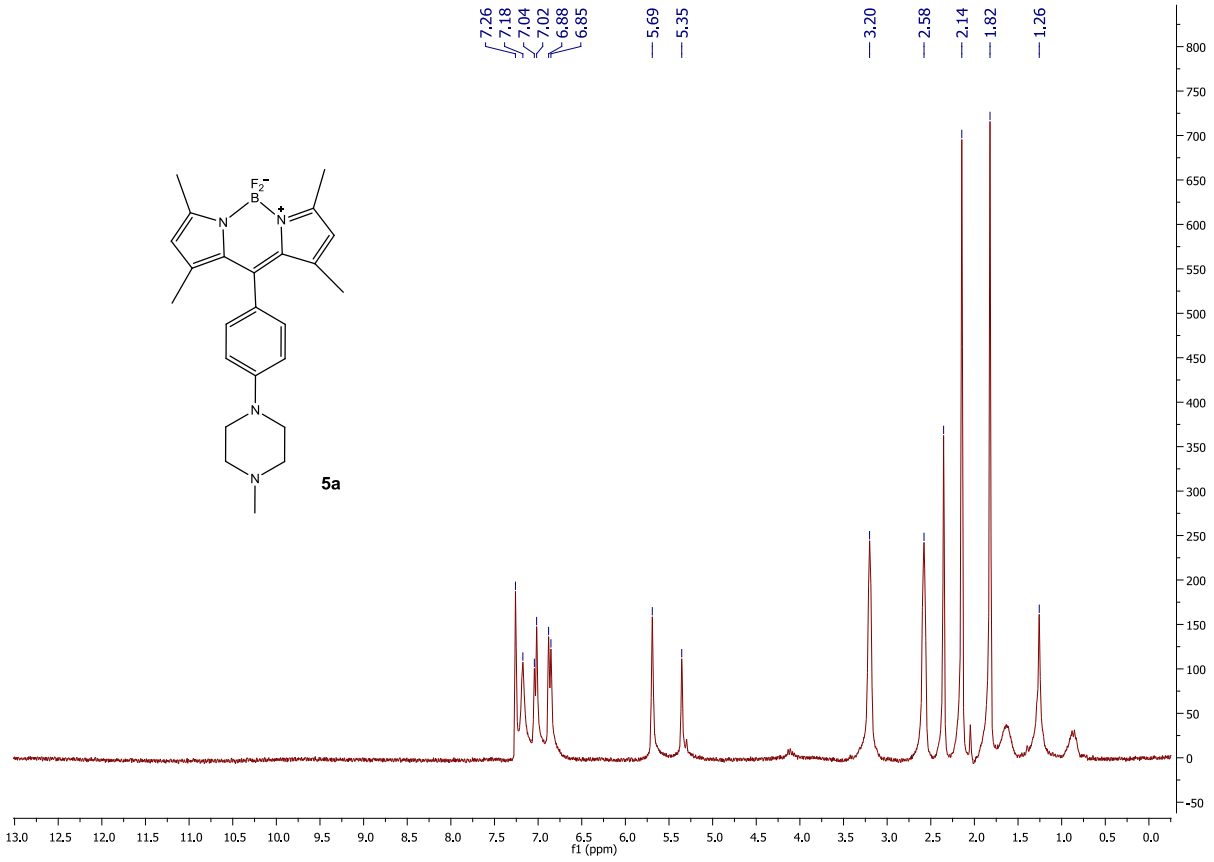

Figure S19. ^{1}H-NMR of BODIPY compound **5a**. Preparation and peak annotation see Chapter 7.

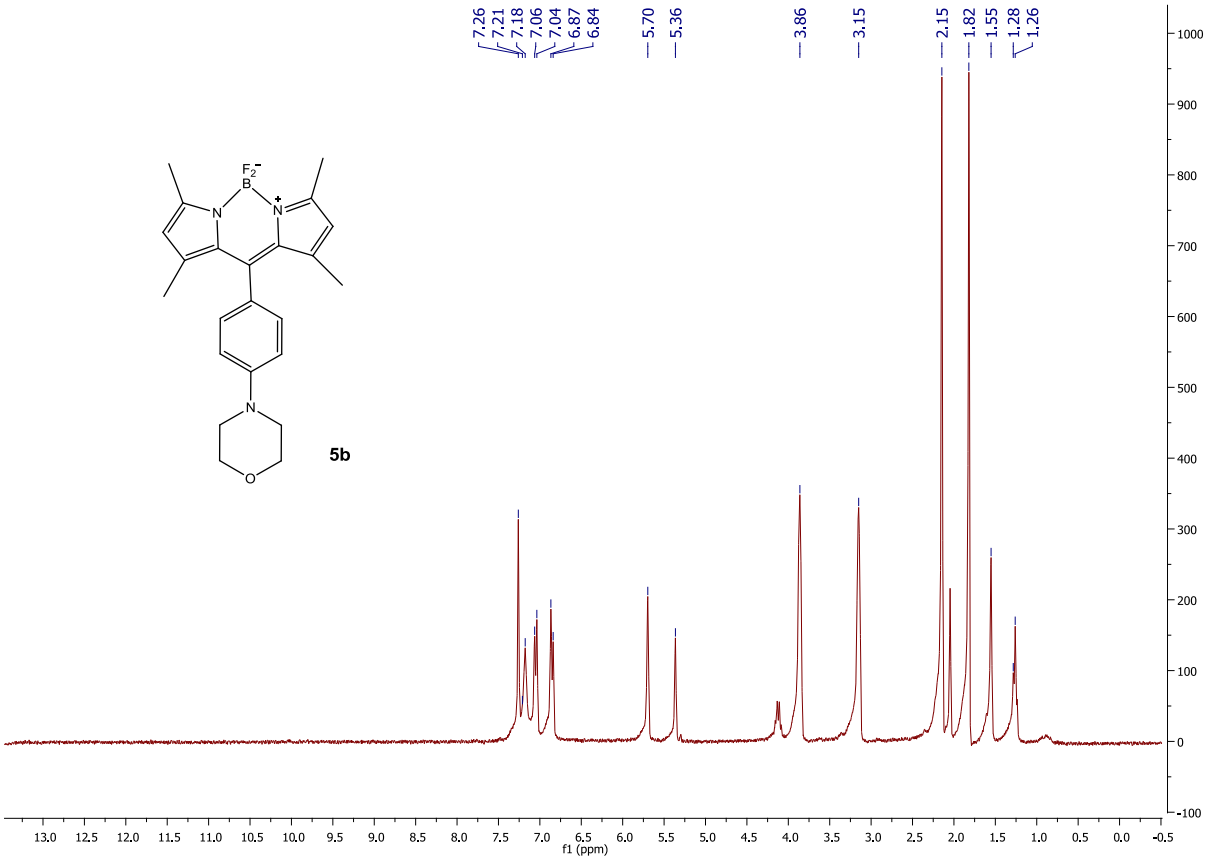

Figure S20. ^{1}H-NMR of BODIPY compound **5b**. Preparation and peak annotation see Chapter 7. Sample contained minor impurity peaks due to solvents.

ACKNOWLEDGEMENTS

First and foremost, I'd like to thank my lovely parents for raising me up to be curious and passionate. Without them and their support, I'd never be where I am today.

This dissertation would not have been made possible without the support and guidance of my adviser, Prof. Tomikazu Sasaki. I wish to express my highest respect to Prof. Sasaki for being a wise mentor, a knowledgeable teacher, a brilliant colleague, and a supporting friend. I'd also like to extend my highest respect to Prof. Rodney Ho, who have not only taught me to become more eloquent in expressing my ideas and research findings, but also acted as a role model and, at times, a caring father for me.

I wish to express my appreciation for the guidance and support of my supervisory committee: Prof. Daniel Chiu, Dr. AJ Boydston, Dr. Champak Chatterjee, Prof. Minoru Taya. I'd like to further thank Dr. Hong Shen and Prof. Niels Andersen, who also offered invaluable advice and helpful discussions as past members of examination committees.

I'd like to thank our collaborators, Dr. Dale Whittington, Dr. Byron Gallis, Prof. Henry Lai, Dr. Narendra Singh, Dr. Liguo Wang, Dr. Xi Zhan, for the many brainstorming sessions and discussions that helped to move the project forward.

Last but not least, I owe it to my past and present colleagues in both the Sasaki lab: Dr. Shusheng Wang, Michio Taya, Austin Le, Ji Hoon Hwang; and Ho lab: Dr. Jenny Freeling, Dr. Cuiling Shu, Dr. Yue Ding, Dr. Jinghua Duan, Jake Kraft, Bowen Li, Ziyao Wang; for being great lab-mates and friends to work with. Without them, I would probably not have enjoyed these few years as much as I have. I have been extremely fortunate to have met and gotten to know everyone mentioned and not mentioned here in the past years.